THE UNIVERSITY *of* EDINBURGH

THE HYDROTHERMAL STABILITY OF HIGH SILICA ZEOLITES

By

David Young

Thesis presented for the degree of

Doctor of Philosophy

University of Edinburgh

1988

To my parents, closest friends and the Scottish education system.

Acknowledgements

The research described in this thesis would not have been possible without funds, facilities and guidance. I'd like to thank the Science and Engineering Research Council for the provision of funds and both the University of Edinburgh and Imperial Chemical Industries PLC for the use of their facilities. Special thanks go to Dr B M Lowe for his guidance and discussion of ideas. I'd also like to acknowledge the help given by Dr H F Leach, Dr J L Casci (ICI) and Dr C Cundy (ICI) during the three years of my research.

Special thanks go to all members of the zeolite group, past and present, for discussion of results and ideas. Brian Hampson (for help with the catalytic work) and Dr C D Williams particularly deserve acknowledgement. Thanks also go to R J Plaisted (ICI) for discussions on solubility and stability studies.

Declaration

This thesis is of my own composition and is an accurate account of research carried out by myself at the University of Edinburgh between October 1984 and September 1987.

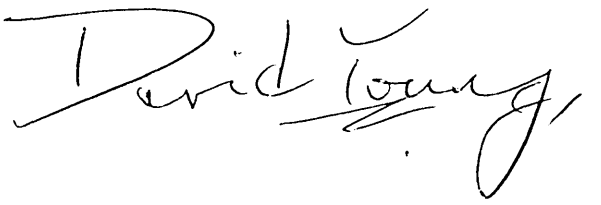

ABSTRACT

This thesis concerns the hydrothermal stability of two zeolite molecular sieves with the MFI structure, ZSM-5 and its 'aluminium free' form silicalite.

Silicalite was synthesised from low pH alkali metal free aqueous gels at 95°C and characterised by XRD, SEM, DTA and TG. ZSM-5 was crystallised from similar reaction mixtures but with the addition of aluminium salts. It was found that the incorporation of aluminium into the ZSM-5 framework was favoured by higher reaction temperatures (150°C) and the use of aluminium nitrate.

Solubilities were measured for silicalite, ZSM-5, ZSM-11, ZSM-39, ZSM-48 and EU-4 at temperatures up to 95°C. The solubilities were influenced by framework structure, the presence of template within the zeolite channels and the aluminium content of the lattice. Solubility measurements over a range of liquid/solid ratios showed that calcined silicalite was contaminated with about 1% amorphous silica.

Treatment with liquid water over the temperature range 95 to 230°C was used to remove amorphous silica and aluminosilicate species from silicalite and ZSM-5. This hydrothermal treatment had many other effects on the properties of these materials. The water uptake, orthorhombic to monoclinic symmetry transition, framework Si/Al ratio and thermal properties were all affected. SEM showed that the inside of the silicalite crystals was more soluble than the outer surface. The use of hydrothermally treated H-ZSM-5 as a catalyst for but-1-ene isomerisation showed that the treatment could have a marked effect on catalytic behaviour, and particularly on product selectivity.

Contents

CHAPTER 1

INTRODUCTION

1.1 Zeolites

Zeolites are a large group of aluminosilicates which have been studied for almost 250 years (1). The first zeolite to be discovered was Stilbite in 1756. Thirty-seven naturally occurring zeolites were identified by 1976. Zeolites are often present in the cracks and cavities of igneous rocks. The crystals are considered to have been formed from trapped solutions or fluids in the parent magma. The crystals nucleate and grow as the magma cools down. There is often more than one zeolite present in a cavity. This is not thought to be due to co-crystallisation but to successive growth as the composition of the trapped fluid changes. Zeolites have also been found in large quantities in sedimentary rocks. Their composition tends to reflect that of the rocks in which they are found.

The fundamental zeolite building blocks are tetrahedra of SiO_4 and AlO_4. Zeolites are formed by the linking of these tetrahedra. Each oxygen is shared between two tetrahedral centres; there are no unshared oxygen atoms within a perfectly formed framework. Hence zeolites are classified as tectosilicates. For every aluminium and silicon atom there are two oxygens. Furthermore, for every framework Si^{IV} which is replaced by Al^{III} a negative charge is formed, which is offset by an equivalent of cations. These sit in cavities and channels within the zeolite framework. In aluminous zeolites the void space usually contains water molecules, some of which solvate the cations. Both the cations and the water molecules tend to be mobile within the framework.

The 3-dimensional frameworks formed by linking the SiO_4 and AlO_4 tetrahedra are made up of a series of rings. There can be several different sizes of T-atom rings (T = Al or Si) in zeolite structures, as is summarised in Table 1.1 (2).

Table 1.1 Apertures Formed by Rings of

Tetrahedra in Zeolite Structures

No. of Tetrahedra in Ring	Maximum Free Dimension (Å)
4	1.6
5	1.5
6	2.8
8	4.3
10	6.3
12	8.0
18	15.0

The 18 T-atom window has not been observed for zeolite aluminosilicate molecular sieves. However, it has been demonstrated in the recently discovered aluminophosphate VPI-5 (3). This is the first molecular sieve to be discovered with rings that contain more than 12 T-atoms.

Zeolites are used as catalysts, sorbents and ion exchangers. Their application in catalysis and sorption is dependent on both the size and the layout of the zeolite channels. For sorption the pore volume, a measure of the total void space, is also important. It is related to the framework density, i.e. the number of T-atoms (Al or Si) per 1000 $Å^3$, the higher the framework density the lower the pore volume. Examples of some zeolite framework densities are shown in Table 1.2.

Table 1.2 Framework Density of Zeolites (4)

Zeolite	T/1000Å^3
Analcime	18.6
Mordenite	17.2
Stilbite	16.9
Sodalite	17.2
Natrolite	17.8
Ferrierite	17.7
Faujasite	12.7
Linde Type A	12.9
ZK-5	14.7
ZSM-5	17.9
ZSM-11	17.7

The sorption capacity for a particular sorbate is determined by factors other than the framework density and the total pore volume. Figure 1.1 shows a section through the Ferrierite channel system. There are wide channels (10 T-atom rings) and narrow channels (5 and 6 T-atom rings). From Table 1.1 above it is clear that larger molecules will only be able to enter the wider channels. For example water molecules cannot enter channels made up of 4 or 5 T-atom rings.

Cations within the zeolite channels also affect the pore volume. Exchange of sodium with potassium in analcime leads to a zeolite which is virtually anhydrous. A similar exchange of alkali metal cations in Ferrierite has a less significant effect. Such different effects are a direct consequence of the differing channel dimensions in the two zeolites, i.e. ten T-atom rings in Ferrierite but only six T-atom rings in analcime.

Since zeolites can be crystallised with different Si/Al ratios the number of cations within the channel system can be varied. Ion exchange can be used to introduce smaller or larger cations into the framework. The number of cations per unit cell may also be varied by exchange with cations of a different charge. For a particular zeolite, much can be done to alter its sieving properties. Diffusion and catalysis are similarly affected.

The application of zeolites in catalysis is dependent upon the size and shape of the reactant molecules as well as the properties of the zeolite itself. For most reactions catalytic activity is

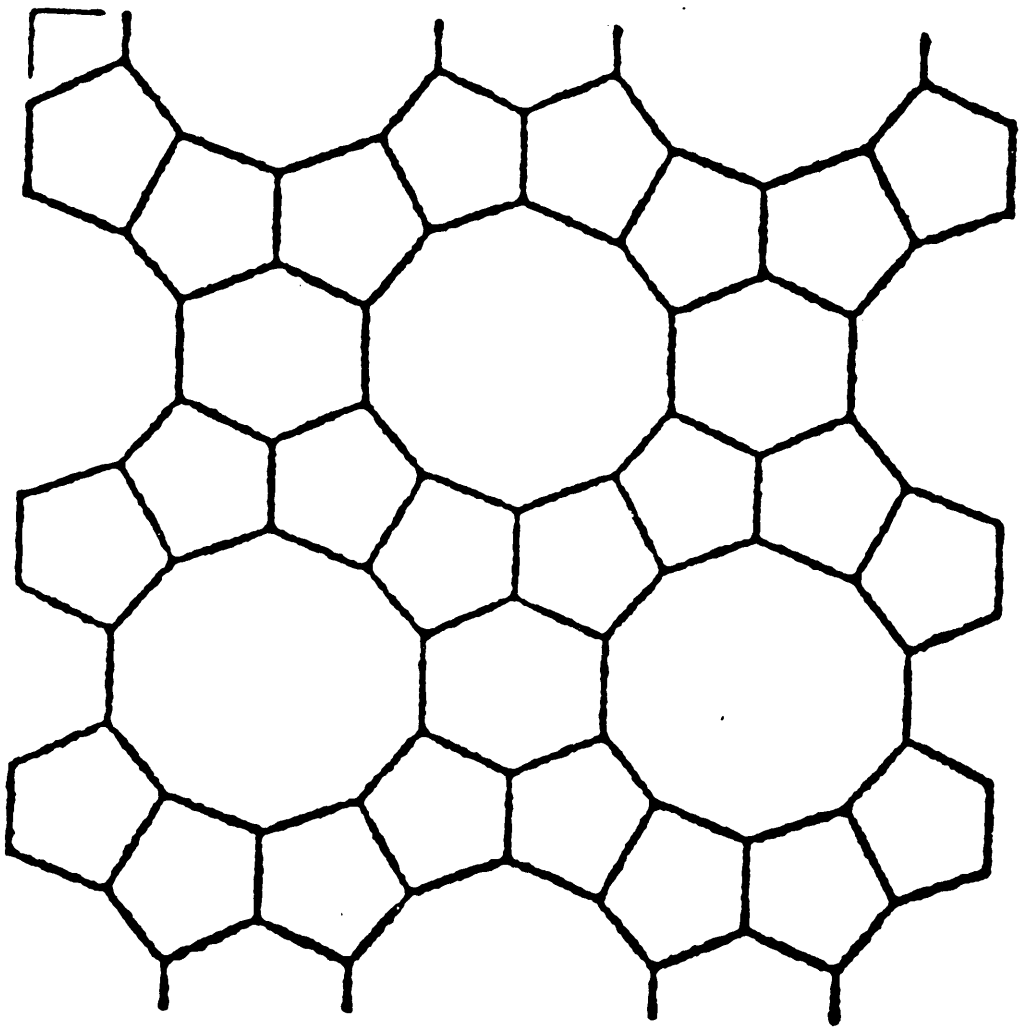

Figure 1.1 Framework projection along main channel of ferrierite

dependent upon the generation of acid sites within the zeolite cavities, but for others it is necessary to introduce clusters of a particular element (e.g. platinum) to provide a catalytically active surface. Some reactions require the zeolite to be in a basic form. For example, basic Na- or K-forms of zeolites X and Y favour the catalytic oxidation of H_2S by oxygen (5). When Bronsted acid sites are introduced (by replacement of the alkali metal cations by H^+) the oxidation rate declines.

Acid zeolites are very important for hydrocarbon conversion reactions, such as catalytic cracking or xylene isomerisation. These zeolites have Bronsted acid centres which act as strong acids able to generate carbocations, the key intermediates in the hydrocarbon reactions. At a Bronsted acid centre there is a silanol group close to a trivalent aluminium. The OH of the silanol in this situation is a strong proton donor with an acid strength which exceeds that of the OH groups in amorphous silica - alumina cracking catalysts.

Shape selectivity of products has been observed for many zeolitic catalysts. The methanol to gasoline (MTG) process converts the reactant to a range of hydrocarbons with a limited range of carbon atoms (6,7). During xylene isomerisation over ZSM-5, the smaller para-xylene product is favoured against the larger ortho- product. The differing diffusion characteristics of different products within the channel system also affects the selectivity of zeolite catalysts.

Zeolites are crystallised from aluminosilicate gels. These are usually formed by mixing aqueous solutions of soluble silicates and aluminates or their precursors (e.g. silica, alumina and an aqueous solution of an alkali metal hydroxide). Organic templates, e.g. amines or quaternary ammonium species, are used in the preparations of gels for the synthesis of high silica zeolites. At high pH values aqueous aluminium species exists as monomeric $Al(OH)_4^-$, whereas the silica may be monomeric, oligomeric or polymeric. When such solutions are mixed the aluminate and silicate anions react together and a gel is formed. The solid phase of the gel is amorphous aluminosilicate material, which gives a broad hump in its X-ray diffraction pattern. Aluminosilicate gels normally separate into a

solution phase and a gel solid. It has been suggested that the precursors which nucleate and maintain the growth of zeolite crystals may be oligomeric aluminosilicate anions (8). It is likely that only the smallest units are involved in zeolite crystallisation. The hydrous gel mixture is dissolved by alkali hydroxide and the growth of crystals proceeds via the solution phase.

Reaction mixture compositions are expressed in terms of mole ratios of oxides. For example a reaction mixture designed to synthesis silicalite may have the composition:

$3Na_2O\ 20SiO_2\ 2TPABr\ 1000H_2O$

The crystallisation conditions which are normally used (9,10) are:

[1] - Reactive amorphous solids.

[2] - High pH generated by alkali metal hydroxide.

[3] - Low temperatures (80-200°C).

[4] - Supersaturation of the solution phase, with respect to the zeolite, by amorphous gel components.

The final point, [4], should result in the nucleation of large numbers of crystals, and consequently the crystals of synthetic zeolites are usually very small (<5um). Alkali metal hydroxides readily form soluble aluminates and silicates, which are ideal for preparation of the reactive gel from which the zeolite crystallises. The gel composition and structure is related to the size and structure of the polymeric species. The rate at which crystallisation occurs is related to the gel reactivity and the concentration of hydroxide ions.

Between 1845 and 1937 a total of some 150 papers were published which reported the synthesis of zeolites. This work has been reviewed by Morey and Ingerson (11). Many of these results are very much in doubt since the products were characterised by chemical analysis and optical mineralogy only. The zeolites which were claimed to have been synthesised in this period include levynite, analcime, natrolite, chabazite, heulandite, scolecite, thomsonite,

faujasite, mordenite and phillipsite. Until the advent of X-ray diffraction the reliable characterisation of zeolite products was not possible. The first synthetic zeolites which were characterised by X-ray diffraction were mordenite (12) and analcime (13). The first to be crystallised which had no naturally occurring counterpart was zeolite A (15). Zeolites X and Y were discovered about the same time (16).

1.2 Classification and Nomenclature

All zeolites are framework aluminosilicates and their structures are three-dimensional and more difficult to describe than those of simple molecules. Since the advent of X-ray crystallography much confusion has been removed, as each zeolite gives a characteristic X-ray diffraction pattern.

If the IUPAC rules of nomenclature (which were based on unit cell compositions) are employed, then the naming of zeolites becomes confusing and unwieldy. Analcime has the unit cell composition:

$$Na_{16}(AlO_2)_{16}(SiO_2)_{32}.16H_2O$$

whereas jadeite has the unit cell composition $Na_4Al_4Si_8O_{24}$. When analcime and jadeite are anhydrous they both have the molar ratio $Na_2O:Al_2O_3:4SiO_2$.

Synthetic zeolites tend to be named (14) by:

(a) Letter(s) assigned by the original investigator, e.g. zeolite A (15), zeolite X (16), zeolite Y (17), ZK-5 (18).

(b) The letters designate the 'as synthesised' zeolite. Zeolite A has the composition $Na_{12}[(AlO_2)_{12}(SiO_2)_{12}].22H_2O$ when crystallised from a reaction mixture which contains Na_2O, Al_2O_3, SiO_2 and H_2O.

(c) Investigators have referred to synthetic zeolites by the name of a structurally similar mineral.

(d) Additional letters, for example the symbol of the main alkali metal within the zeolite, are also often used in the naming of materials, e.g. Li-A, Na-X. This may also apply to cation exchanged zeolites.

(e) Si/Al ratios or unit cell contents may also be added.

(f) The use of the letter N prior to a synthetic zeolite's name implies it was prepared with an alkylammonium base, e.g. N-A.

1.3 High Silica Zeolites and Organic Templates

The initial studies of zeolite crystallisation involved materials with Si/Al ratios less than ten. These were prepared by crystallisation from reactive aluminosilicate gels with alkali and alkaline earth metal hydroxides. The gels were normally of a high pH, greater than pH 13, and crystallised at 100°C or less. Zeolites A, X and Y come into this category. These highly aluminous materials are characterised by their hydrophilic surfaces, high ion-exchange capacity and relatively low hydrothermal stability.

In 1961 the use of the tetramethylammonium (TMA) cation in zeolite crystallisation was first reported (19). This has two main effects (20): (a) TMA has a structure directing effect which results in the synthesis of zeolites which contain small sodalite and gmelinite cages; (b) the presence of the TMA also fundamentally changes the gel chemistry and the crystallisation of more siliceous zeolites is promoted. These include zeolites N-A (21), α (22) and ZK-4 (23) which all have zeolite A type structures (but of higher Si/Al ratios). Zeolites prepared in the absence of TMA can have Si/Al ratios less than 5, whereas those made with TMA present have Si/Al ratios as high as 10 (24).

The synthesis of zeolite β was reported in 1967 from reaction mixtures which contained the tetraethylammonium (TEA) cation (25). Its Si/Al ratio was greater than 10. Shortly afterwards many high silica zeolites were reported in the literature, for example ZSM-5 (26), ZSM-8 (27) and ZSM-11 (28). Silicalite, a molecular sieve which is essentially free of aluminium, was reported in 1977 (29); it is isostructural with ZSM-5. Other pure silica molecular sieves include silica-ZSM-11 [or silicalite-2] (30) and silica-ZSM-48 (31). The organic and inorganic cations used in zeolite crystallisation have a strong structure directing effect; this is sometimes called templating. In early work with aluminous systems it was suggested that the alkali metal cations form a nucleus about which the secondary building units of zeolites are formed (32). It was considered that dehydrated sodium ion promoted the formation of

double four or six T-atom rings and that in its hydrated state it facilitated the formation of sodalite units. However because cations influence both the structure and the gel chemistry it is difficult to determine unequivocally their true role.

When a tetraalkylammonium cation is located at the centre of a cage, for example TMA in a sodalite unit, then the positively charged cation will have SiO_2 and AlO_2^- tetrahedra around it, with charged oxygen atoms pointing towards the TMA ion. Templating can then be related to both electrostatic interaction and the size and shape of the ion. Organic template cations may also fit into the channel space of zeolite molecular sieves. Tetraethylammonium (TEA), tetrapropylammonium (TPA) and tetrabutylammonium (TBA) can all act in this way, in zeolites such as ZSM-5 and ZSM-11, where there are channel intersections.

The presence of organic molecules can affect the gel chemistry in several ways. Some organic compounds, e.g. catechol, complex silica and therefore increase its solubility. Amines and quaternary ammonium hydroxides also increase silica solubility, but in this case by increasing the pH of the reaction mixture. Organic molecules may also form aluminosilicate species (33), e.g. TPA-aluminosilicates have been identified by ^{27}Al NMR spectroscopy (33).

Each of the above effects can influence the nucleation process and hence the growth of zeolite crystals. A review of the role of organic molecules in molecular sieve synthesis was published by Lok, Cannan and Messina in 1983 (34).

1.4 ZSM-5 and Molecular Sieves

Zeolite ZSM-5 (26,27) and its isostructural aluminium free analogue silicalite (29,35) were studied in the present work. The other materials which were studied include silica-ZSM-11 (36), silica-ZSM-39 (37), silica-ZSM-48 (38) and EU-4 (39).

ZSM-5 has been synthesised by the addition of a sodium aluminate solution to a solution of silica in tetrapropylammonium hydroxide (26). It has also been prepared from sodium silicate (waterglass), aluminium sulphate and tetrapropylammonium bromide (40). Sodium hydroxide was added in both cases to adjust the pH of the starting gel-solution mixture to between 10 and 11. The second synthetic method (40) was about six times faster than the first (26) at 120°C.

Morphology, crystal size and aluminium content are all affected by reaction mixture composition (41-47) since the nucleation and growth of the crystals are dependent on variables which in turn are dependent on the reactants and the synthesis conditions. Key variables in the nucleation and growth of ZSM-5 are pH, the nature of the organic template, the extent of stirring and the type of reaction vessel (48).

ZSM-5 has been crystallised from reaction mixtures which are alkali metal cation free. Bibby et al were the first to show that ZSM-5 could be obtained when the alkali metal hydroxide component of the gel is replaced by ammonium hydroxide (49). The crystallisation of zeolite TPA-ZSM-5 from reaction mixtures that contain TPA and with ammonium cations, has been studied by Ghamani and Sand (50). This reaction has the advantage of producing an alkali metal-free ZSM-5 which on calcination gives directly the acid catalyst H-ZSM-5.

ZSM-5 has been prepared in the absence of an organic template (51), from the Na_2O-Al_2O_3-SiO_2-H_2O system. ZSM-5 is formed in preference to mordenite at higher SiO_2/Al_2O_3 and lower Na_2O/SiO_2 ratios.

Aluminium is not homogeneously dispersed within the ZSM-5

framework (52) but is usually present in greater amounts on the outside of crystals (53). This suggests that the aluminium content of the solution phase is increased towards the end of the reaction. Aluminous gel solid is less easily depolymerised than siliceous material and hence is the last to dissolve and the last to be incorporated in the zeolite. This explanation implies crystal growth from the liquid phase.

Silicalite, which has the same framework topology as ZSM-5, was first reported in 1978 (54,55). Silicalite has been crystallised from many different reaction mixtures. These have contained fluoride (F^-) and tetrapropylammonium (TPA) cations (56,57), sodium hydroxide and TPA (58,59), ammonium hydroxide and TPA (60) and piperazine and TPA (61); along with a source of silica and water.

Several workers have crystallised silicalite from the system TPA_2O- SiO_2-water (50,54,55,62). However in this system TPAOH provides both the mineraliser (OH^-) and the template (TPA). This does not allow the variation of reaction mixture base content without a change in template concentration. Reaction mixtures in which each can be varied independently (e.g. ones with NaOH or an organic base and TPABr) are more informative (56-61). A reaction mixture which contains TPAOH and TPABr may be of interest as the TPA can be varied and the bromide ion does not participate in the reaction. Sodium hydroxide and TPA reaction mixtures are not ideal as both the Na^+ ion and the TPA ion participate in the reaction (58).

It has been shown for ZSM-5 that both nucleation and growth are affected by the choice of the organic template. The crystallisation of ZSM-5 is slower when tri-ethyl-n-propylammonium (TEPA) hydroxide is used rather than TPAOH (63). In the system wNa_2O-$x(TAA)_2O$-$ySiO_2$-zH_2O, where TAA is a tetraalkylammonium template, TPA gives the best result in terms of the degree of crystallinity of the silicalite (64). The other organic templates used in this study (64) were tetraethylammonium (TEA) and tetrabutylammonium (TBA) [which gave silica-ZSM-11 (silicalite-2) rather than silicalite-1]. Statistical methods have been used to establish the composition of the reaction mixture which gives the

largest crystals (65). Low concentration of sodium hydroxide and TPABr favoured the growth of large crystals (up to 400um). Crystal lengths were halved when the NaOH in the reaction mixtures was substituted with either KOH or CsOH. Product yields were, however, substantially increased (65).

The framework structure of ZSM-5, and hence silicalite, was first reported in 1978 (66). The three-dimensional channel system has straight channels which run parallel to the b-axis. Their 10 T-atom windows have a free diameter of 5.3 x 5.6 Å. The sinusoidal, or zig-zag, channels run parallel to the a-plane. They are more elliptical than the straight channels and have openings of 5.1 x 5.5 Å.

The channel system is represented in Figure 1.2. The structure can be derived from secondary building units which contain 12 T-atoms (67), as shown in Figure 1.2. Silicalite and ZSM-5 have orthorhombic (68,69) and monoclinic (69) crystal symmetries. The only significant change in the XRD pattern of the orthorhombic material on transition to the monoclinic form that is normally observed is the resolution of the 313/133 (hkl) lines between 24.3 and 24.5 2θ. Refinement of lattice parameters which were calculated from 'monoclinic' diffraction patterns showed that a increased by only 0.5% and α increased from 90° to 90.6° at most. As synthesised TPA-ZSM-5 and TPA-silicalite are always in the orthorhombic form. Kokotailo and co-workers reported the less apparent changes in the observed diffraction patterns upon the symmetry transition in 1979 (69). Both H-ZSM-5 and calcined silicalite exhibit the orthorhombic to monoclinic transition upon certain treatments, such as variations in humidity. The symmetry change is inhibited by framework aluminium. The change in position of the 10 0 0 and 0 10 0 (hkl) lines caused by the transition has been used quantitatively for aluminium determination (70). The symmetry change can be reversed by thermal treatment and also by the loading of the framework channels with ammonia (69).

The presence of the TPA template in the ZSM-5/silicalite channel system has been studied by thermal analysis (42,71-73) and ^{13}C MASNMR (magic angle spinning nuclear magnetic resonance spectroscopy)

(74,75). There are four TPA molecules per 96-T atom unit cell, each located at a channel intersection. The TPA-silicalite unit cell has the composition:

$$((C_3H_7)_4N)_4Si_{96}O_{192}(OH)_4$$

To preserve electroneutrality the TPA ion is associated with a broken siloxane bond, or possibly a hydroxide ion. When the TPA is removed by calcination or thermal degradation the lattice may heal.

Silica-ZSM-11 was used in the solubility studies of the present work. Its structure is closely similar to that of ZSM-5, but both of the intersecting channels are straight. The channel diameters are 5.3 x 5.4 Å (78). The organic template for this zeolite is commonly tetrabutylammonium (TBA) although other amines and quaternary ammonium ions have also been used (76,77). Like TPA in ZSM-5, TBA is also located at the channel intersections (75). As alkyl chains get longer, fewer molecules can be incorporated within the zeolite channels. The 80 Å channel length in the ZSM-11 unit cell can only be occupied by a maximum of 2.8 TBA ions. Since there are four intersections per ZSM-11 unit cell then not all of these sites can be occupied by TBA ions.

The structures of the other high silica zeolites used in the present work have been reported; ZSM-39 (ref 78, page 104), ZSM-48 (79) and EU-4 (ref 78, page 112) which has the nonasil structure. Silica-ZSM-39 and silica-EU-4 have cage structures which trap the template and make its removal very difficult. They are examples of clathrasils. ZSM-48 has a 1-dimensional channel system. The silica-ZSM-48 which was used in the present work was prepared with hexane-1,6-diamine (38) as the template whereas for the ZSM-39 preparation the template selected was piperazine (80).

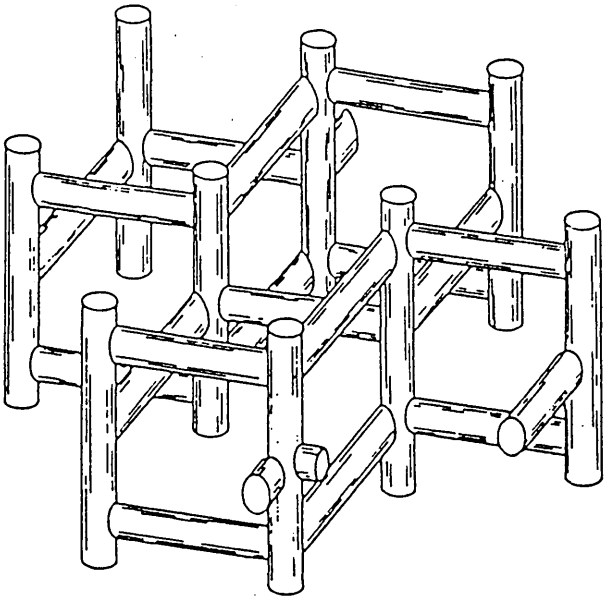

CHANNEL NETWORK

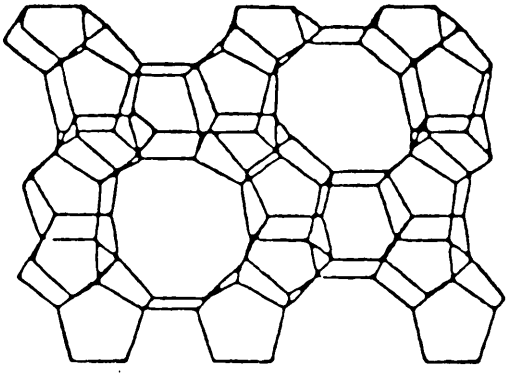

SKELETAL DIAGRAM OF THE (010) FACE

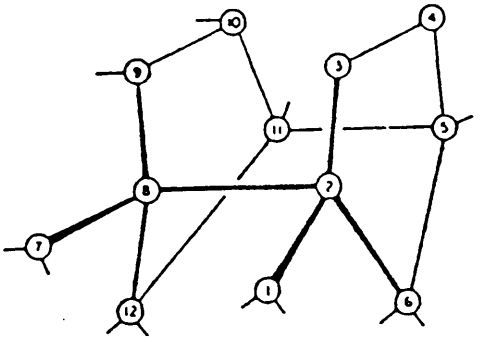

12 T-ATOM REPEAT UNIT

Figure 1.2 ZSM-5 structure (66)

1.5 Solubility

It is well established that aluminous zeolites are soluble in aqueous acidic media and siliceous ones are soluble in aqueous alkali. At a pH value of 7, neutral, the solubility of zeolitic materials is low. There have been few attempts to measure zeolite solubilities and reported studies of silica solubility have indicated that this apparently simple system is in fact rather complex.

The solubilities of amorphous silicas and quartz in water have been extensively reported (81,82) and a study of the solubility of amorphous silica in organic solvents has also recently appeared (99). In water at pH values greater than about 9 the solubility of amorphous silica greatly increases (ref 82, page 48) due to the formation of soluble silicates. The solubility of amorphous silica is also dependent on particle size (83).

In an aqueous environment amorphous or crystalline silica approaches, or is at, equilibrium:

$$SiO_2 \text{ (solid)} + 2H_2O \gtrless Si(OH)_4 \text{ (aq.)}$$

When $Si(OH)_4$, orthosilicic acid, in the aqueous solution is in equilibrium with the silica of the solid phase then the concentration of the orthosilicic acid is termed the solubility. The solubility of amorphous silica is greater than that of crystalline silica, and it is possible that in this case polysilicic acids are formed in the solution phase.

Under various conditions, many silicate ions will be present in the aqueous phase. Orthosilicic acid is a weak acid, and in alkali it readily dissociates to give $OSi(OH)_3^-$ or $O_2Si(OH)_2^{2-}$. It can also polymerise and in 1960 Kitahara reported that at 400°C the rate of polymerisation of silicic acid showed a maximum at a pH of 7.5 (84).

The presence of a variety of polysilicate species in aqueous sodium metasilicate solutions has been shown by ^{29}Si NMR spectroscopy (85). This technique revolutionised the identification of polymeric solution phase silica species. The condensation reactions of mono-,

di- and tri-silicic acids in aqueous solutions (silica concentration 0.5M, pH=2 and T=-2°C) have been investigated by ^{29}Si NMR. Monosilicic acid reacts to form di-, tri-, tetra-, cyclotetra-, bicyclohexasilicic and higher polymeric silicic acid species. In solutions of dimeric and trimeric silicic acid, hydrolysis to monomer occurs simultaneously with condensation reactions to higher products. After a reaction time of about 20 minutes the initial mono-, di- and tri-silicic acid solutions all contained the same reaction products (86). Further ^{29}Si NMR studies have shown that the rate of polymerisation of silicic acids produced from tetramethoxysilane, at pH 3.5 to 4.0 and -10°C, is very slow (87). Many polymeric silicate anions have been identified by ^{29}Si NMR (88-95), one of which (a double five ring silicate) is a possible precursor in the synthesis of ZSM-5 (96,97). This was suggested by the analysis of the ZSM-5 reaction mixture after the addition of organic solvents (methanol, ethanol or dimethyl sulphoxide), which reorganise the silicate structures present in solution. The double five-ring silicate was identified further by attenuated total reflection Fourier transform infrared spectroscopy and mass spectrometry. It was concluded that in the ZSM-5 reaction mixtures different silicate species are in equilibrium, and this probably plays a key role in the synthesis of the zeolite. It was suggested that during the formation of ZSM-5 from the double five-ring silicate, new rings are formed under the influence of the TPA cations. The silicate anions are provided by the dissolution of amorphous silica reactant by the OH^- mineraliser.

Zeolite synthesis and the dissolution of the reactants are closely linked by equilibria in the solution phase.

1.6 Hydrothermal Stability Considerations

The main aim of the present work was to determine the solubilities of high silica zeolites and investigate their hydrothermal stability. A knowledge of their solubility is essential for applications in which the zeolites are immersed for a prolonged time in water, e.g. when used to sorb low molecular weight organic molecules from aqueous solution (98). To prevent this dissolution zeolite molecular sieves have been impregnated with a water permeable organic polymer to reduce solubility (100-103). However this may not inhibit at least some framework attack and hence broken siloxane bonds. The generation of silanol groups will increase the hydrophilicity of the molecular sieve and hence reduce its organophilicity. This will significantly affect the capacity of the molecular sieve for the uptake of organic molecules from the aqueous environment. The contamination of molecular sieves by amorphous material will also affect their properties.

ZSM-5 catalysts are themselves affected by hydrothermal treatment with steam (104), so it is probable they would also be modified by treatment with liquid water. However this has never been investigated by previous workers, and it forms a major part of the present work. It was expected that such treatments would alter the catalytic and sorption properties. The acid exchange of catalysts, for the removal of framework alkali metal cations, is in itself a hydrothermal treatment. This may lead to some crystal dissolution and relocation of framework aluminium, which will affect catalyst activity and selectivity.

Knowledge of hydrothermal stability of the high silica zeolites is essential for their application and efficient use.

Chapter 1 References

[1] D.W. Breck

"Zeolite Molecular Sieves",

Wiley-Interscience (1974), page 188.

[2] R.M. Barrer

Chem. Ind., 1968, 1203.

[3] M.E. Davis, C. Saldarriaga, C. Montes,

J. Garces and C. Crowder

Nature, 1988, **331**, 698.

[4] W.M. Meier and D.H. Olson

"Atlas of Zeolite Structure Types",

International Zeolite Association, 1987.

[5] M. Ziolek and Z. Dudzik

Zeolites, 1981, **1**, 117.

[6] C.D. Chang and A.J. Silvestri

J. Catal., 1977, **47**, 249.

[7] W.W. Keading and S.A. Butler

J. Catal., 1980, **61**, 155.

[8] R.M. Barrer

Chemistry in Britain, 1966, 380.

[9] R.M. Barrer

"Hydrothermal Chemistry of Zeolites",

Academic Press, London, 1982.

[10] D.W. Breck

"Zeolite Molecular Sieves",

Wiley-Interscience (1974), page 250.

[11] G.W. Morey and E. Ingerson

Econ. Geol., 1937, **38**, 607.

[12] R.M. Barrer

J. Chem. Soc., 1948, 2158.

[13] R.M. Barrer and E.A.D. White

J. Chem. Soc., 1948, 1167.

[14] D.W. Breck

"Zeolite Molecular Sieves", Wiley-

Interscience, New York, 1974, page 23.

[15] R.M. Milton

U.S. Patent 2,882,243 (1959).

[16] R.M. Milton

U.S. Patent 2,882,244 (1959).

[17] D.W. Breck

U.S. Patent 3,130,007 (1964).

[18] G.T. Kerr

J. Inorg. Chem., 1966, **5**, 1539.

[19] R.M. Barrer and P.J. Denny

J. Chem. Soc., 1961, 971.

[20] E.M. Flanigen

Adv. Chem. Ser., 1973, **121**, 119.

[21] R.M. Barrer, P.J. Denny and E.M. Flanigen

U.S. Patent 3,306,922 (1967).

[22] G.T. Kerr

U.S. Patent 3,247,195 (1966).

[23] R.L. Walinger, E.J. Rosinski and C.J. Plank

U.S. Patent 3,375,205 (1968).

[24] E.M. Flanigen and E.B. Kellberg

U.S. Patent 4,241,036 (1968).

[25] R.L. Wadlinger, G.T. Kerr and E.J. Rosinski

U.S. Patent 3,308,069 (1967).

[26] R.J. Argauer and G.R. Landolt

U.S. Patent 3,702,886 (1972).

[27] Mobil Oil Corporation

Netherlands Patent 7,014,807 (1971).

[28] P. Chu

U.S. Patent 3,979,145 (1973).

[29] R.W. Grose and E.M. Flanigen

U.S. Patent 4,061,724 (1977).

[30] D.M. Bibby, N.B. Milestone and L.P. Aldridge

Nature, 1979, **280**, 664.

[31] P. Chu

European Patent Application 23,089 (1981).

[32] R.M. Barrer

Chem. Ind. London, 1968, 1203.

[33] E.G. Derouane, J.B. Nagy and Z. Gabelica

Zeolites, 1982, **2**, 299.

[34] B.M. Lok, T.R. Cannan and C.A. Messina

Zeolites, 1983, **3**, 282.

[35] E.M. Flanigen, J.M. Bennett, R.W. Grose, J.P.

Cohen, R.L. Patton, R.M. Kirchner and J.V. Smith

Nature, 1978, **271**, 512.

[36] M. Taramasso, G. Manara, V. Fattore

and B. Notari

G.B. Patent 2,024,790 (1980).

[37] D.M. Bibby and L.M. Parker

Zeolites, 1983, **3**, 11.

[38] A. Araya and B.M. Lowe

J. Catal., 1984, **85**, 135.

[39] J.L. Casci, B.M. Lowe and T.V. Whittam

European Patent Application, 63436 (1982).

[40] N.Y. Chen, J.N. Miale and N.Y. Reagen

U.S. Patent 4,112,056 (1978).

[41] B.P. Pelrine

U.S. Patent 4,100,262 (1978).

[42] M.A.M. Boersma and M.F.M. Post

European Patent Application 40,444 (1981).

[43] D.H. Olson

European Patent Application 26,963 (1980).

[44] D.H. Olson, L.D. Rollmann and E.W. Valyocsik

European Patent application 26,962 (1980).

[45] H. Nakamoto and H. Takahashi

Chem. Soc. Japan Chem. Lett., 1981, 1739.

[46] E.G. Derouane, S. Detremmeric, Z. Gabelica

and N. Blom

Applied Catalysis, 1981, **1**, 201.

[47] A. Nastro and L.B. Sand

Zeolites, 1983, **3**, 57.

[48] E.G. Derouane and Z. Gabelica

Journal of Solid State Chemistry, 1986, **64**, 296.

[49] D.M. Bibby, N.B. Milestone and L.P. Aldridge

Nature, 1980, **285**, 30.

[50] M. Ghamani and L.B. Sand

Zeolites, 1983, **3**, 155.

[51] R.W. Grose and E.M. Flanigen

U.S. Patent 4,257,885 (1981).

[52] E.G. Derouane, J.P. Gilson, Z. Gabelica,

C. Mousty-Desbuquoit and J. Verbist

J. Catal., 1981, **71**, 447.

[53] R. von Ballmoos and W.M. Meier

Nature, 1981, **289**, 782.

[54] E.M. Flanigen and R.L. Patton

U.S. Patent 4,073,865 (1978).

[55] E.M. Flanigen, J.M. Bennett, R.W. Grose, J.P.

Cohen, R.L. Patton, R.M. Kirchner and J.V. Smith

Nature, 1978, **271**, 512.

[56] G.D. Price, J.J. Pluth, J.V. Smith,

T. Araki and J.M. Bennett

Nature, 1981, **292**, 818.

[57] G.D. Smith, J.J. Pluth, J.V. Smith,

J.M. Bennett and R.L. Patton

J. Am. Chem. Soc., 1982, **104**, 5971.

[58] S.G. Fegan and B.M. Lowe

J. Chem. Soc. Chem. Commun., 1984, 437.

[59] S.G. Fegan and B.M. Lowe

J. Chem. Soc., Faraday Trans. 1, 1986, **82**, 785.

[60] R. von Ballmoos

"The O-Exchange Method in Zeolite

Chemistry" (Salle and Sauerlaender,

Frankfurter am Main, 1981), page 98.

[61] S.G. Fegan and B.M. Lowe

J. Chem. Soc., Faraday Trans. 1, 1986, **82**, 801.

[62] K.J. Chao, T.C. Tasai, M.-S. Chen and I. Wang

J. Chem. Soc., Faraday Trans. 1, 1981, **77**, 547.

[63] S.B. Kulkarni, V.P. Shiralker, A.N. Kotasthane,

R.B. Borade and P. Ratnasamy

Zeolites, 1982, **2**, 313.

[64] C.L. Huang, W.C. Yu and T.Y. Lee

Chemical Engineering Science, 1986, **41**, 625.

[65] D.T. Hayhurst and J.C. Lee

"Proceedings of the Seventh International

Zeolite Association Conference", Tokyo, 1986, 113.

[66] G.T. Kokotailo, S.L. Lawton, D.H. Olson and

W.M. Meier

Nature, 1978, **272**, 437.

[67] D.H. Olson, G.T. Kokotailo, S.L. Lawton and

W.M. Meier

J. Phys. Chem., 1981, **85**, 2238.

[68] R. von Ballmoos

"Collection of Simulated XRD Powder Patterns

for Zeolites", International Zeolite

Association, 1984, page 74.

[69] E.L. Wu, S.L. Lawton, D.H. Olson, A.C.

Rohrman Jr. and G.T. Kokotailo

J. Phys. Chem., 1979, **83**, 2777.

[70] D.M. Bibby, L.P. Aldridge and N.B. Milestone

J. Catal., 1981, **72**, 373.

[71] E.A. Hyde and D. Young

European Patent Application 108611 (1984).

[72] A.N. Kostathane and V.P. Shiralker

Thermochimica Acta, 1986, **102**, 37.

[73] K.R. Franklin and B.M. Lowe

Thermochimica Acta, 1988, **127**, 319.

[74] G. Boxhoorn, R.A. van Santen, W.A. van Erp,

G.R. Hays, R. Huis and D. Clague

J. Chem. Soc., Chem. Commun., 1982, 264.

[75] J.B. Nagy, Z. Gabelica and E.G. Derouane

Zeolites, 1983, **3**, 43.

[76] M.K. Rubin, C.J. Plank and E.J. Rosinski

European Patent Application 14,059 (1980).

[77] R.B. Calvert and L.D. Rollmann

European Patent Application 101,183 (1983).

[78] W.M. Meier and D.H. Olson

"Atlas of Zeolite Structure Types", International

Zeolite Association, 1987, page 94.

[79] J.L. Schlenker, W.J. Rohrbaugh, P. Chu,

E.W. Valyocsik and G.T. Kokotailo

Zeolites, 1985, **5**, 355.

[80] K.R. Franklin and B.M. Lowe

Zeolites, 1987, **7**, 433.

[81] S.A. Greenberg

J. Phys. Chem., 1957, **61**, 196.

[82] R.K. Iler

"The Chemistry of Silica", Wiley-Interscience,

New York, page 3.

[83] G.B. Alexander

J. Phys. Chem., 1957, **61**, 1563.

[84] S. Kitahara

Rev. Phys. Chem. of Japan. 1960, **30**, 131.

[85] R.O. Gould, B.M. Lowe and N.A. MacGilp

J. Chem. Soc., Chem. Commun., 1974, 721.

[86] D. Hoebbel, G. Garzo, G. Engelhardt and A. Till

Z. anorg. allg. Chem., 1979, **450**, 5.

[87] R.K. Harris, C.T.G. Knight, and D.N. Smith

J. Chem. Soc., Chem. Commun., 1980, 726.

[88] D. Hoebbel and W. Wieker

Z. anorg. allg. Chem., 1973, **400**, 148.

[89] D. Hoebbel, W. Wieker, P. Franke and A. Otto

Z. anorg. allg. Chem., 1975, **418**, 35.

[90] L.S. Dent Glasser, E.E. Lachowski, R.K. Harris

and J. Jones

J. Mol. Struct., 1979, **51**, 239.

[91] G. Engelhardt, D. Hoebbel, M. Tarmak, A.

Samoson and E. Lippmaa

Z. anorg. allg. Chem., 1982, **484**, 22.

[92] R.K. Harris and C.T.G. Knight

J. Mol. Struct., 1982, **78**, 273.

[93] K.J. Cavell, A.F. Masters and K.G. Wilshier

Zeolites, 1982, **2**, 244.

[94] L.S. Dent Glasser

"Proceedings of the Fifth International Zeolite

Association Conference", Naples, 1980, page 63.

[95] James S. Falcone, Jr. (Editor)

"Soluble Silicates", ACS Symposium Series

194, Washington, 1982, page 79.

[96] G. Boxhoorn, O. Sudmeijer and P.H.G.

van Kasteren

J. Chem. Soc., Chem. Commun., 1983, 1416.

[97] E.J.J. Groenen, A.G.T.G. Kortbeek, M. MacKay

and O. Sudmeijer

Zeolites, 1986, **6**, 403.

[98] G. Scott

Ph.D. Thesis, University of Edinburgh (1987).

[99] J.-L. Dandurand and J. Schott

Journal of Solution Chemistry, 1987, **16**, 237.

[100] S. Kulprathipanja and R.W. Neuzil

U.S. Patent 4,319,928 (1982).

[101] S. Kulprathipanja and H.S. Bloch

U.S. Patent 4,333,768 (1982).

[102] S. Kulprathipanja and R.W. Neuzil

U.S. Patent 4,333,769 (1982).

[103] S. Kulprathipanja

U.S. Patent 4,431,456 (1984).

[104] Y. Sendoda and Y. Ono

Zeolites, 1988, **8**, 101.

CHAPTER 2

ANALYTICAL AND EXPERIMENTAL EQUIPMENT AND PROCEDURES

2.1 Analytical Equipment

2.1.1 X-ray Diffraction

X-rays are diffracted by crystalline materials and this can be used as the basis for the qualitative and quantitative examination of powders (X-ray powder diffraction, XRD) and for structure determination using single crystals. In the present work only powder diffraction was used. Bragg related the wavelength [λ] of the X-rays, the diffraction angle [θ] and the distance between each set of atomic planes of the crystal lattice [d] (1), by the equation:

$$n\lambda=2d(\sin\theta)$$

Atoms on the crystal plane give the most intensely diffracted beam. Atoms halfway between crystal planes exert maximum destructive interference. Those in intermediate positions interfere either constructively or destructively, depending on their location. Therefore, from a knowledge of θ the value of d can be determined. The X-ray powder pattern, a plot of intensity as a function of 2θ or d, is characteristic of the crystalline material and may be used as a 'finger print'. Structural and symmetry changes, for example the transition of ZSM-5 from orthorhombic to monoclinic symmetry, can be detected by changes in the intensities and positions of the diffraction peaks.

The X-ray diffractometer used in the present work is shown in Plate 2.1. This instrument was manufactured by Philips Limited. It has a vertical goniometer and an automatic sample changer. It was fitted with a fine focus tube which generated CuK_α radiation (λ=1.5405 Å) and was operated at 40kV and 30mA. For most patterns a scan rate of $1^\circ 2\theta$ per minute, a chart speed of 1cm per minute, a time constant of 2 and range factors of 10^4 or $4x10^3$ were used. The accuracy of the instrument was regularly checked using a standard sample of microcrystalline quartz stone.

The samples were initially ground to a fine powder, and then packed into a sample holder. Care was taken to pack the sample holder uniformly and present a perfectly level surface to the X-ray

beam. It was possible to load several samples into a cassette so that they could be run consecutively.

Many of the X-ray diffraction patterns discussed in detail in this thesis were run on the equipment of ICI Chemical and Polymers Limited, at Wilton.

2.1.2 Scanning Electron Microscopy

This technique was used to determine the morphology and size of the zeolite crystals and for the examination of crystal surfaces. The instrument used was a Cambridge Instruments Limited Stereoscan S90B situated in the Edinburgh University Science Faculty SEM unit. Some samples were also examined with the SEM equipment of ICI Chemical and Polymers Limited, at Wilton.

Samples were prepared by putting a tiny amount of zeolite on a stub. A drop of acetone was placed on the tip of a microspatula, and the zeolite and acetone were then mixed on the face of the stub. Once the acetone had evaporated, the stub was placed in a vacuum and electroplated with gold; this enhances picture quality and dissipates charge build-up on samples (charging distorts the observed image). The stub was mounted in the instrument, which was then evacuated. The sample is then bombarded with high energy electrons. Some are reflected and others interact with the sample to produce secondary electrons which are emitted from the sample. Each electron type is detected by a photomultiplier, which creates an image of the sample.

The crystallisation of reaction mixtures was monitored by optical microscopy. The optical microscope was a Vickers Photoplan M41; this is shown in Plate 2.2.

2.1.3 Thermal Gravimetric Analysis

Thermal gravimetry (TG) is a technique in which the change in weight of a substance is recorded as a function of temperature [(2), and references therein]. Under normal circumstances a constant heating rate is used. In some cases the rate of change of weight is also recorded; this is known as differential thermal gravimetry (DTG). Only TG was used in the present work.

Plate 2.1 X-ray Diffractometer

Plate 2.2 Optical Microscope

The basic equipment is a precision electronic microbalance and a temperature programmed furnace. These are arranged so that the sample can be hung in the furnace from the balance arm by a stirrup pan. Plate 2.3 shows the Stanton Redcroft TG 770 used in this work. Plate 2.4 shows a close-up of the precision balance. Samples were hung in a stirrup pan on the hang-down wire, shown on the left of the print. Great care was taken to ensure that neither the the stirrup pan or the hang-down wire touched the sides of the raised furnace or the glass case of the balance.

The rate at which the sample is heated can affect the temperature at which the thermal events occur. If the heating rate is high then events occur at higher temperatures. This is also true for exothermic and endothermic events observed in differential thermal analysis (DTA). The nature of the atmosphere is also important. In this work all the samples were analysed by TG in a 15ml/minute flow of air at a heating rate of $10^{o}C$/minute.

2.1.4 Differential Thermal Analysis

In differential thermal analysis (DTA) both the sample to be tested and a reference alumina are placed symmetrically on separate thermocouples in a tubular furnace. The temperature of the furnace is raised at a constant rate and the difference in the temperature of the reference and test samples is monitored. There should be no temperature difference between the two materials unless a thermal event caused by a physical or chemical change occurs in the test sample. It is essential that the materials are arranged symmetrically within the furnace. Any misalignment of the samples in the furnace could result in them heating to slightly different temperatures and be observed as a drift in the base line.

If a reaction occurs in the test sample then there will be a temperature difference between the test sample and the reference alumina. If the thermal event is endothermic then the test sample temperature will be less than that of the reference material. When the sample temperature is greater than that of the reference material the event is exothermic. After either type of event the test sample and reference alumina return to the same temperature.

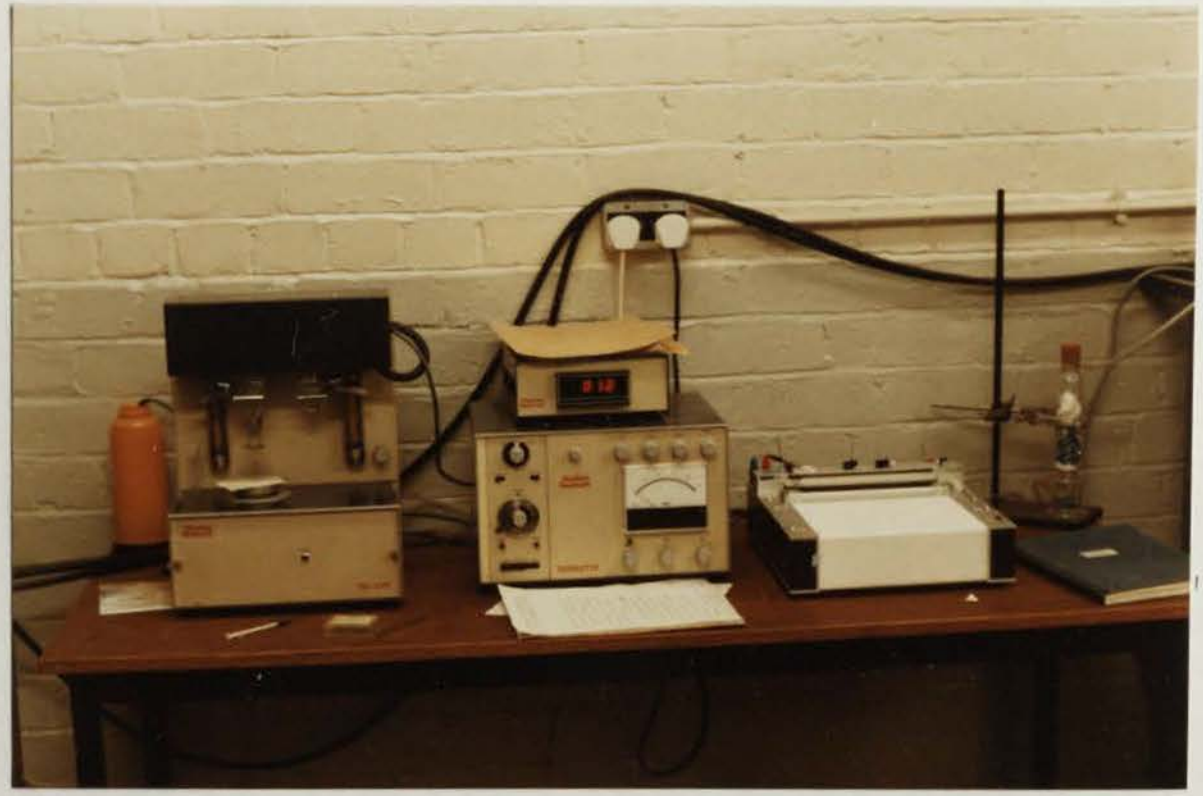

Plate 2.3 Thermal Gravimetric Analysis (TGA) Equipment

Plate 2.4 TGA Balance

During DTA a plot of the temperature difference of the two materials against temperature is recorded. The exact position of the peaks depends on the heating rate, sample size and the sample atmosphere (flowing or static, air or nitrogen). Peak shapes and sizes are easily interpreted for well understood systems, but for many it is necessary to obtain independent evidence (e.g. evolved gas analysis) before their origin can be identified. Physical and chemical events can be distinguished by the fact that the former do not exhibit a weight change in TG analysis. Physical changes are usually endothermic, whereas chemical changes are more often exothermic. For zeolites and related materials a broad endotherm at about 100°C signifies the loss of loosely bound water. At higher temperatures endotherms with a small associated weight loss often correspond to dehydroxylation. For TPA-silicalite in static air at a heating rate of 5°C/minute there is an exothermic peak at about 380°C. This peak is associated with the decomposition and combustion of the TPA template which is trapped within the channel system. With large samples this peak is often split because of oxygen starvation, especially if high heating rates are used (2).

Plate 2.5 shows the Stanton Redcroft differential thermal analysis equipment (DTA 674) used in this work. The furnace is to the top right of the print. Each sample was run in a static air atmosphere, at low heating rates (1 or 5°C per minute).

2.1.5 pH Measurements

The pH of samples taken from the reaction mixtures was monitored throughout the crystallisations [3]. The crystallisation of TPA-silicalite from reaction mixtures which have a high content of alkali metal hydroxide is accompanied by an increase in pH (4,5), whereas the crystallisation of TPA-silicalite from reaction mixtures which contain piperazine tend to show a decrease in pH (6). The measurement of pH is a quick and easy method to monitor zeolite crystallisation.

Plate 2.6 shows the Philips PW9422 pH meter used in this work. The instrument was calibrated with buffer solutions of pH values 7

and 9.2 on each day of use.

2.1.6 Colourimetry

A colourimetric method was used for the determination of monomeric silicic acid (7). A dilute molybdic acid solution was made up, portions of which were added to the solutions to be tested. After about two minutes the samples turned bright yellow (8). The absorbances of the samples were then measured at a wavelength of 410nm. The procedure is fully explained in Chapter 5.0.

The spectrophotometer used in this work was manufactured by Unicam Limited. It is shown in Plate 2.7.

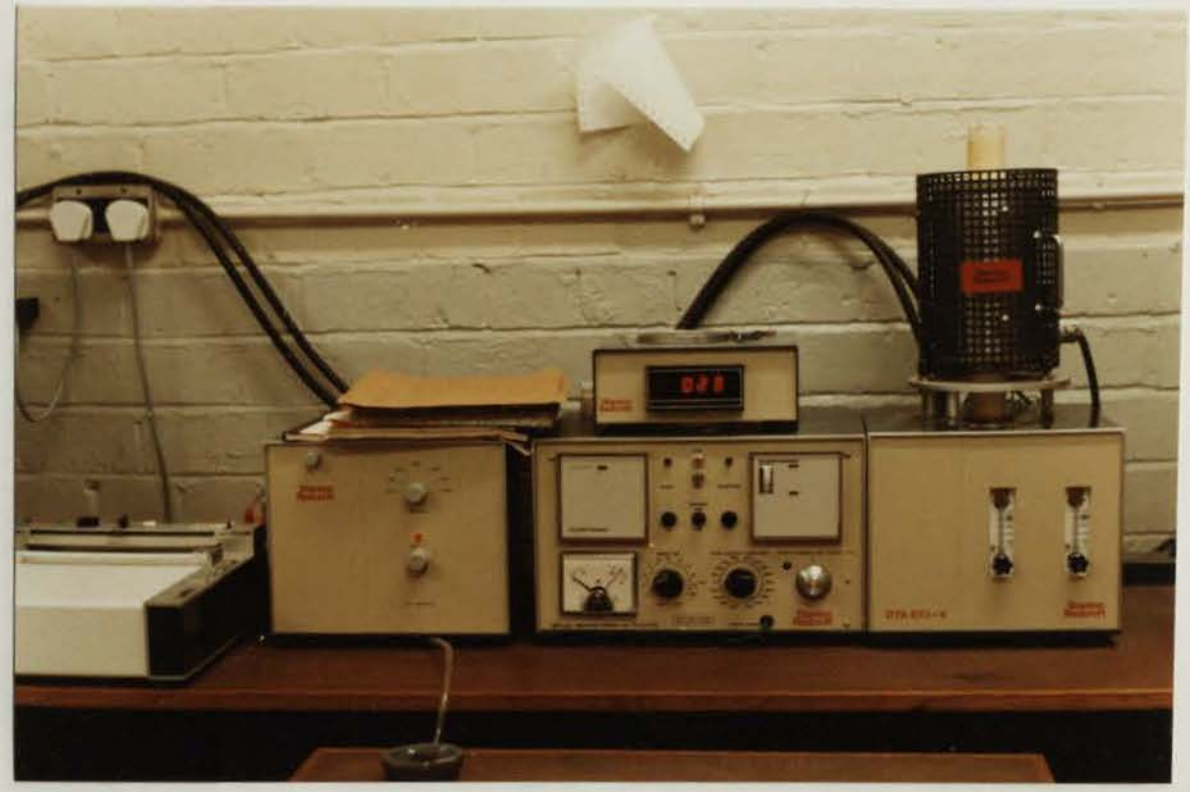

Plate 2.5 Differential Thermal Analysis (DTA) Equipment

Plate 2.6 pH Meter

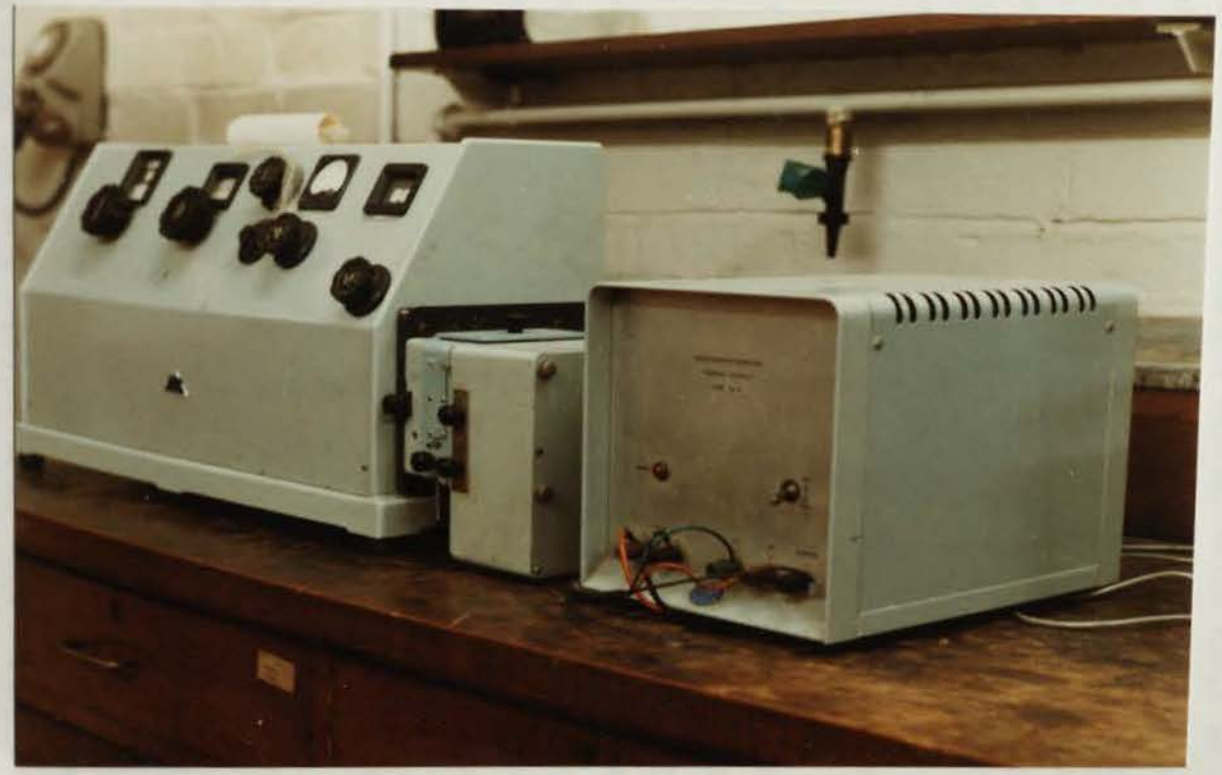

Plate 2.7 Spectrophotometer

2.2 Experimental Equipment

2.2.1 Reaction Vessels

Synthesis and hydrothermal stability work was conducted in autoclaves and in polypropylene bottles. The autoclaves were used for temperatures above 100°C. Plate 2.8 shows one of the 500ml autoclaves which was used. The heating mantle, which hangs at the base, surrounds the reaction vessel. The steel tube and tap which is at the front of the autoclave is for sampling the reaction mixtures. The motor at the top drives the paddle within the reaction mixture. The dismantled reaction vessel is shown in Plate 2.9. The reaction vessel is held to the body of the autoclave by six nuts, which are tightened in a sequence, using a torque wrench. The end of the sampling tube is to the right of the paddle, the temperature probe is to the left. An autoclave control panel is shown in Plate 2.10. The dial and meter on the left of the panel control the speed at which the autoclave contents were stirred, in this work at 300 revolutions per minute. The central gauge is the thermostat whilst the one on the bottom right is the temperature trip. The top right gauge monitors the current which is supplied to the heating unit. Synthesis and stability work at below 100°C was conducted with 1 litre polypropylene bottles in a 95°C thermostat bath. A plastic bottle and stirrer cap are shown in Plate 2.11. The shaft of the paddle is sealed at the top in order to prevent evaporation, as well as corrosion of the bearings. The glass stopper is used to seal the opening in the cap through which the reaction mixtures were sampled. The 95°C thermostat bath is shown in Plate 2.12. There are four immersed heating elements, one on each side of the bath. Each heater is separately fused and there are two temperature trips, on a platform on the top right of the bath. One of the plastic tubes on the right hand side of the bath supplies water to a constant head device and the other drains away the excess. This arrangement is essential to counteract the loss of water by evaporation. The motors on the gantry above the bath are used to stir reaction mixtures. Plastic balls were placed on the surface of the water, to reduce evaporation and heat loss. Plate 2.13 shows a polypropylene bottle

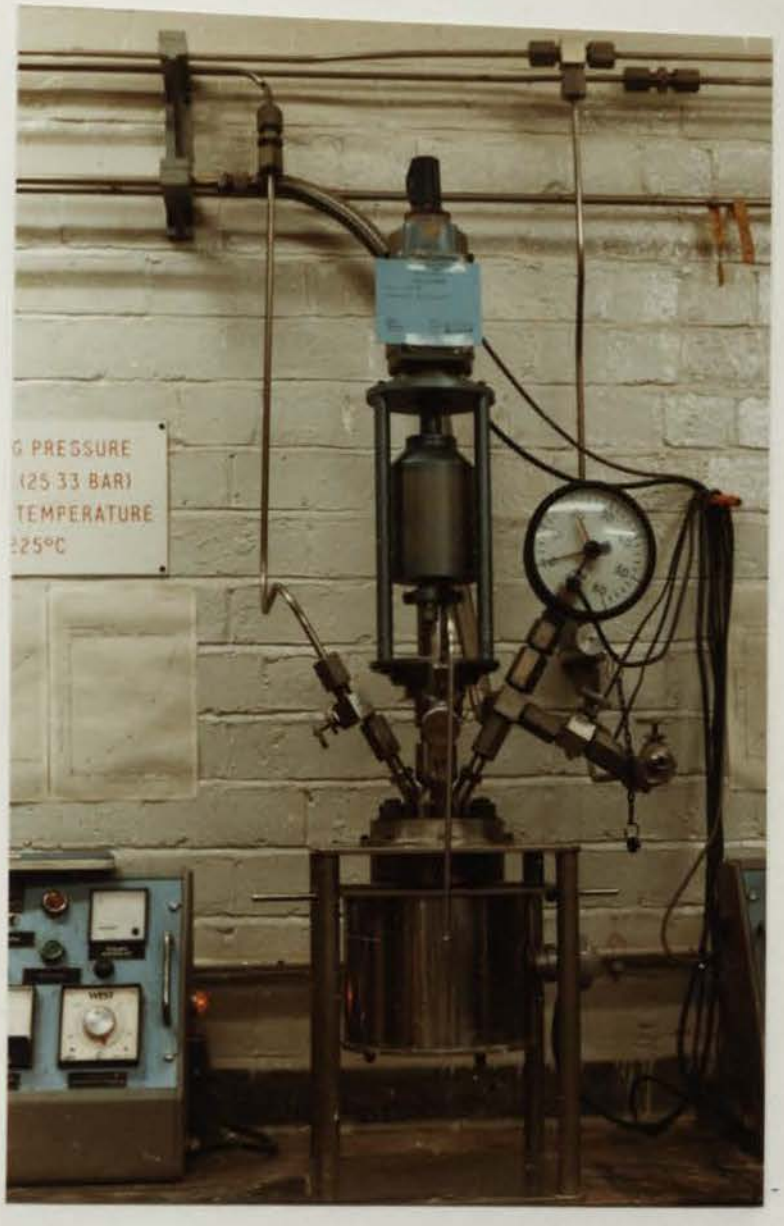

Plate 2.8 500ml Autoclave

Plate 2.9 Autoclave Reaction Vessel

Plate 2.10 Autoclave Control Panel

and stirrer cap fully assembled, attached to a stainless steel spindle from the drive motor and clamped to the side of the bath. The contents of the plastic bottles were always below the level of the water in the bath. The sampling port is clearly visible at the front of the stirrer cap.

2.2.3 Solubility Equilibration Equipment

Solubility studies at 25 and 40°C were conducted by attaching 30 or 60ml polypropylene bottles onto a rotary equilibrator, or 'hirly-gig'. An example of a small tumbling device is shown in Plate 2.14. Larger rotary equilibrators were also used; Plate 2.15 shows one immersed in a 25°C thermostat bath. The motor at the top of the device drives the tumbling framework through two sets of bevel gears. The motor and gear train were such that the samples were tumbled slowly. This prevents the occurence of concentration gradients within the solubility systems; in static systems concentration gradients are established and the equilibration is prolonged.

However static systems were used at 70 and 95°C. The rotary equilibrators could not be operated at these temperatures, and in any case diffusion and hence equilibration is much faster at these temperatures. The 70°C solubility studies were conducted in a thermostat bath filled with polyethyleneglycol. The 95°C work was done in the bath shown in Plate 2.12. Solubility systems were sealed in 30 or 60ml plastic bottles and then placed in a 1 litre bottle, which was filled with water and sealed. This was then completely immersed in either the 70 or 95°C thermostat baths. There were few problems with concentration gradients at these temperatures.

2.2.3 Catalytic Rig

The catalytic rig was one in which the reactant and product gases were repeatedly cycled over the same catalyst, and sampled at appropriate intervals for analysis by gas chromatography (GC).

The apparatus was constructed from Pyrex glassware and its general arrangement is shown in Figure 2.1. A "U" shaped reaction vessel, which incorporated a ground glass sinter of porosity 1, was attached to the apparatus by Quickfit swivel joints. The joints were

Plate 2.11 Polypropylene Bottle and Stirrer Cap

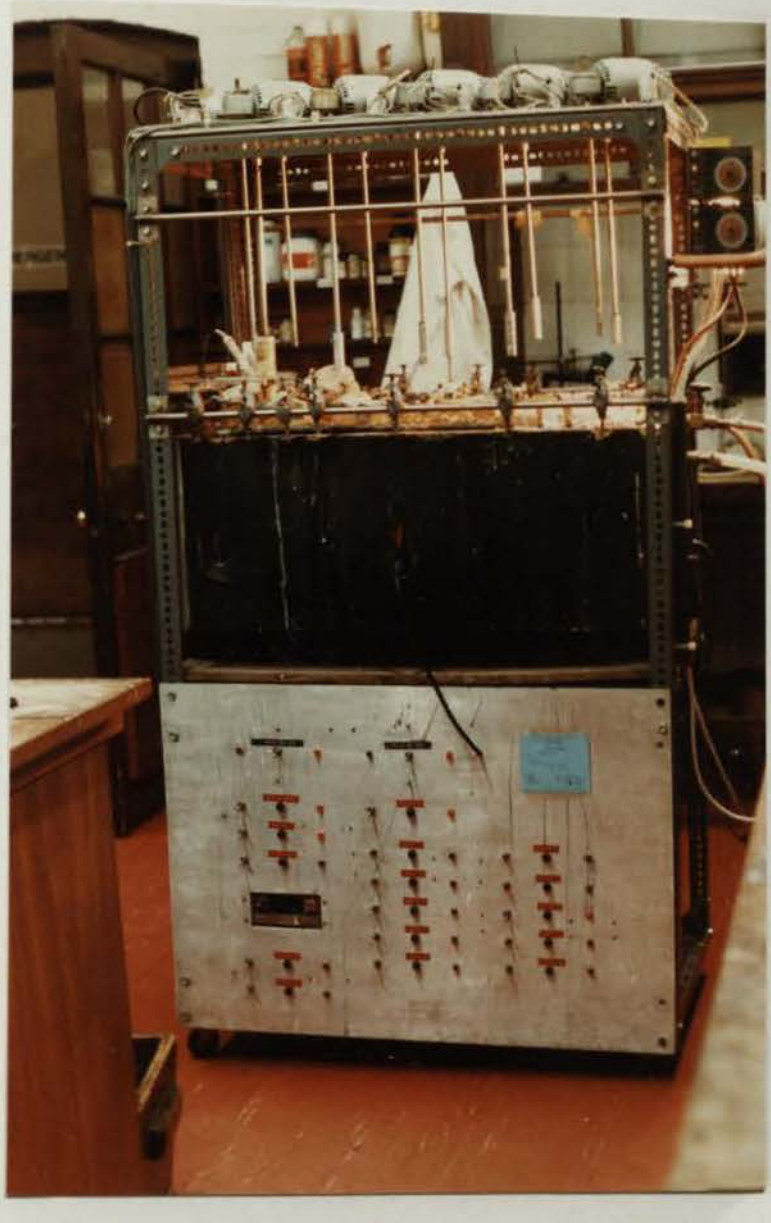

Plate 2.12 95°C Thermostat Bath

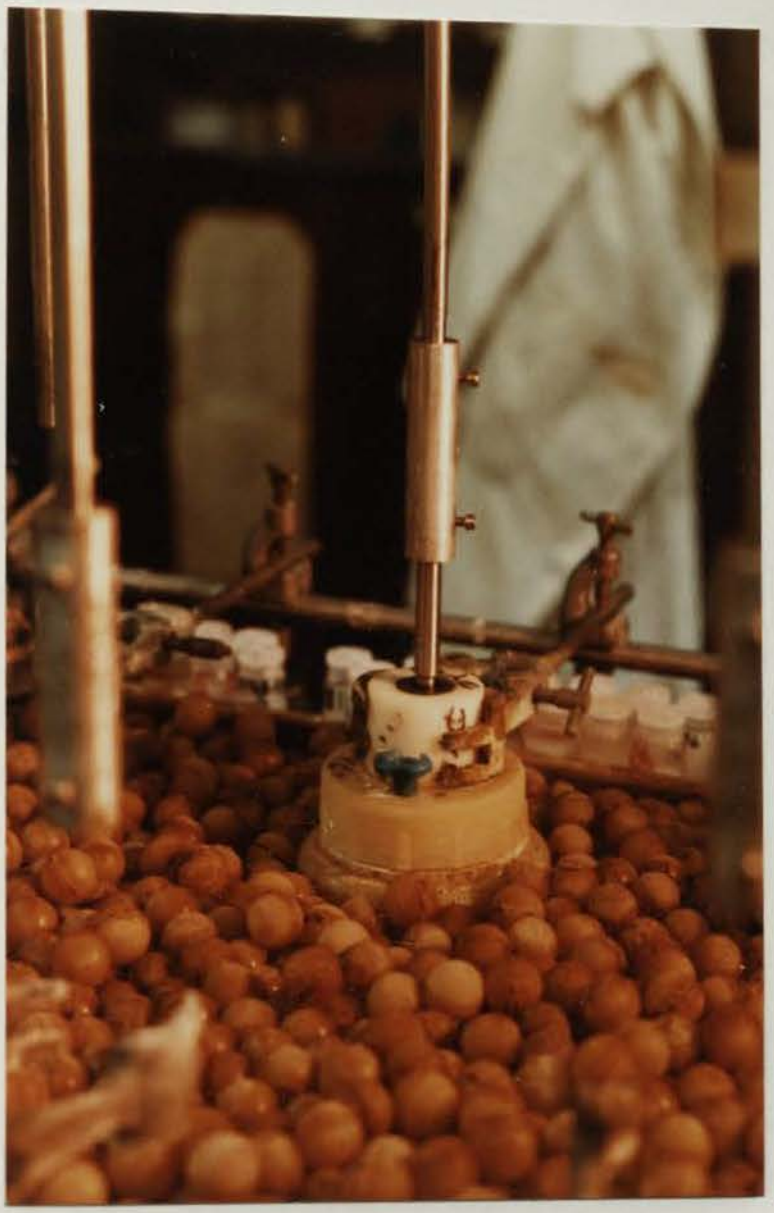

Plate 2.13 Reaction Vessel in the 95°C Bath

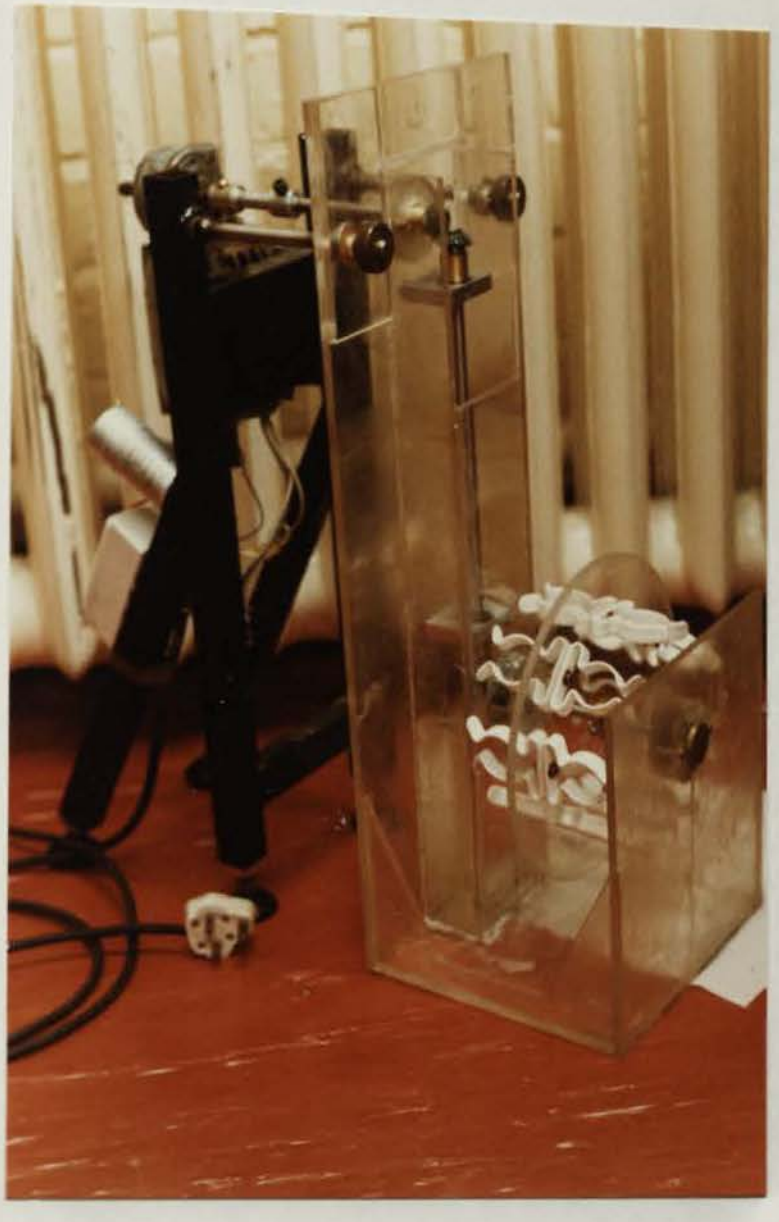

Plate 2.14 Rotary Equilibrator

Plate 2.15 Rotary Equilibrator in a 25°C Bath

lubricated with Apiezon "L" grease and air cooled.

Two mercury diffusion pumps could evacuate the equipment to about 10^{-6} torr (133 x 10^{-6} Nm^{-2}). The use of liquid nitrogen traps prevented contamination of the system from the mercury diffusion pumps. The ground glass joints were all sealed with Apiezon "L" grease in order to maintain a high vacuum. A McLeod gauge was used to check the high vacuum prior to each catalytic run. A mercury manometer was used to measure pressure in excess of 1 torr (133 Nm^{-2}).

A Metal Bellows Company MB-21E pump was used for the constant recirculation of the reactant and product gases through the catalytic bed. The flow rate was near identical for each run, but could be adjusted by variation of the voltage applied to the pump by a Variac. The flow rate was monitored with a meter in the cycling line.

Each catalyst was pelletted to 40-60 mesh (275-400um) by compressing a portion of ZSM-5 into a large pellet then breaking it up into smaller fragments, which were sifted to the above size range.

The ZSM-5 catalysts were heated in the reaction vessel by close fitting silica furnaces. The furnace temperature was controlled with a thermocouple wired to a Eurotherm temperature controller. Catalyst temperature was measured by another thermocouple which was placed down a pocket into the ZSM-5 catalyst bed, this was monitored with a Comark Digital Thermometer.

Once a run had been started, samples of the gas phase were withdrawn at certain time intervals with a three way tap, which was joined to a Carle Sampling Valve (which contained an evacuable sampling loop). Each sample was about 2% of the gas phase in the circulating system. The chromatographic column consisted of 4m of 0.32cm o.d. stainless steel tubing loaded with bis-methoxy ethyl adipate (13.5%) and di-2-ethyl hexyl sebacate on 80/100 mesh chromosorb P (9). The resolved butenes were eluted to a H_2/air flame ionisation detector. The signals were amplified with a Perkin Elmer amplifier and fed to a Servoscribe chart recorder and a Hewlett Packard 3373B Integrator (which converted the signals to a digital

form). The integrator printed the areas in microvolt seconds on pressure sensitive paper. Each catalytic run could then be quantitatively analysed.

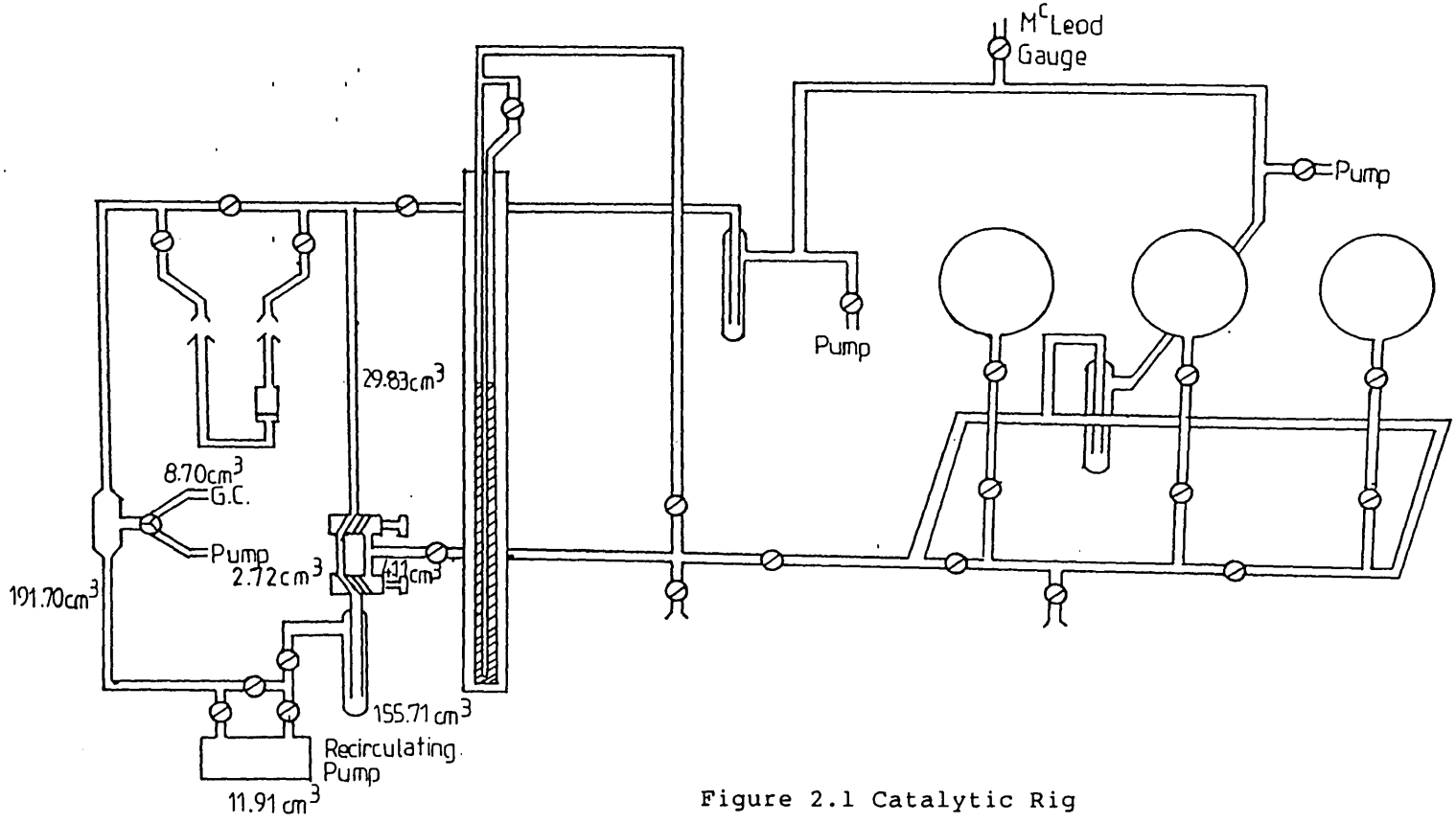

Figure 2.1 Catalytic Rig

Chapter 2 References

[1] L.S. Dent Glasser

"Crystallography and its Applications",

Van Nostrand Reinhold, New York, 1977, page 50.

[2] K.R. Franklin and B.M. Lowe,

Thermochimica Acta, 1988, **127**, 319.

[3] J.L. Casci and B.M. Lowe

Zeolites, 1983, **3**, 186.

[4] S.G. Fegan and B.M. Lowe

J. Chem. Soc. Faraday Trans. 1, 1986, **82**, 785.

[5] S.G. Fegan and B.M. Lowe

J. Chem. Soc. Chem. Commun., 1984, 437.

[6] S.G. Fegan and B.M. Lowe

J. Chem. Soc. Faraday Trans. 1, 1986, **82**, 801.

[7] R.K. Iler

"The Chemistry of Silica", Wiley,

New York, 1979, page 97.

[8] A.I. Vogel

"Textbook of Quantitative Inorganic

Analysis", 1979, page 757.

[9] J.A. Henderson

PhD Thesis, Edinburgh University (1986).

CHAPTER 3

SILICALITE SYNTHESIS IN THE PIPERAZINE -

PIPERAZINE.diHCl - TPABr - SiO_2 - H_2O SYSTEM

3.1 Introduction

Silicalite was first reported by Flanigen et al in 1978 (1). It is the aluminium free analogue of ZSM-5; the framework structure (2) is described in Chapter 1.

Silicalite is prepared by hydrothermal crystallisation at 90 to 210°C from alkaline reaction mixtures which consist of tetrapropylammonium (TPA) ions, amorphous silica and a source of hydroxide ions. The crystallised TPA-silicalite is calcined to give either the Na- or H-silicalite. When alkali metal bases are used, the products contain their cations. These are removed by acid exchange. Ideally, silicalite is pure silica although any aluminium present as an impurity in the reactants is incorporated into the framework (3). This effect tends to be small. Silicalite precursors are usually crystallised from reaction mixtures which contain alkali metal cations (4,5,6). The precursor is the crystallised material which contains the organic template or void filler; in this case TPA-silicalite. The composition of silicalite precursors is determined by the base content of reaction mixtures (7).

The products from reaction mixtures which contain alkali metal cations tend to have many broken siloxane bonds. Once the metal cations are removed by acid exchange then the silanol groups will increase the hydrophilicity and therefore decrease the organophilicity of the product. Calcination should help to heal the framework.

Alkali metal free silicalite has been synthesised (8) with tetrapropylammonium hydroxide (TPAOH) acting both as the base and the quaternary template. TPAOH tends to be expensive and alternatives are desirable. Von Ballmoos reported the crystallisation of silicalite with a combination of ammonium hydroxide (NH4OH) and TPAOH/TPABr (9).

Silicalite has also been synthesised with piperazine as the base and TPA as the template (10). Silicalite crystallised in an alkali metal free reaction mixture has fewer broken siloxane bonds,

therefore fewer silanols, greater hydrophobicity and greater organophilicity. On calcination, the silicalite does not need to be acid exchanged prior to use.

The aim of this work was to examine silicalite synthesis in low pH alkali metal free conditions at 95°C, using reaction mixtures in which piperazine acts as a base and piperazine.diHCl is used to suppress reaction mixture pH. The amount of piperazine was kept constant in each reaction mixture. The amount of HCl associated with the piperazine was varied.

Crystallisation at low pH should reduce nucleation and hence the product crystals should be larger (9). Low pH reaction mixtures, in which an alkali metal base was used, gave TPA-silicalite crystals of needle-like morphology (11). The organic base piperazine was used in the present work as it was considered that it would affect the crystal morphology.

3.2 Experimental

A series of reaction mixtures with the composition:

xPiperazine yPiperazine.diHCl 2TPABr $20SiO_2$ $1000H_2O$

were prepared.

The value of x ranged between 10 and 6, whilst y lay between 0 and 4. The sum of x and y equalled 10 for each preparation. The weights of the reagents for each reaction mixture were calculated with the BASIC program "MIXV3" on a BBC microcomputer. Each reaction mixture weighed 600 grams. The reactants were mixed by the following method. The organic compounds and water were weighed into a beaker which was then placed on a hot-plate. The warmed mixture was stirred until the piperazine and tetrapropylammonium bromide had dissolved then further heated to boiling. This hot solution was then added to amorphous fumed silica Cab-O-Sil M5 (BDH) which had been weighed into a 1 litre polypropylene bottle. The contents of the reaction container were then electrically blended to a homogeneous paste for three minutes. The stirrer cap was screwed onto the top of the bottle. The reaction vessel was then placed in a 95°C water bath and the paddle shaft clamped to the stirrer motor spindle. The equipment is described in Chapter 2.

Evaporation of water from the reaction container was checked every 46 to 50 hours. The level of the liquid in each 1 litre plastic bottle was detected by placing a light over the bath and a beaker against the side of the reaction container. The translucent polypropylene bottles had earlier been marked with a permanent pen to indicate the initial liquid level. Water could be added via the sampling port to bring the liquid level up to the mark.

Each synthesis mixture was periodically monitored by sampling. The samples were removed by means of a syringe to which was attached a plastic tube which could be inserted into the reaction mixture. Once crystallisation had occurred the pH of each sample was measured with a Philips PW 9422 pH meter (12). The solution phase of each

sample was removed by filtration. The unwashed solid phase was dried at 110°C for two hours.

All of the final products were examined by X-ray powder diffraction; in each case the product was silicalite. The crystallinity of each sample was determined by comparison of its X-ray powder diffraction pattern with a reference silicalite, adjudged 100% pure. Percentage crystallinities were based on the major peaks at 8.83, 23.07, 23.27, 23.69 and 24.36 2θ. The pH and crystallinity profiles of each synthesis are shown in Figures 3.1 and 3.2.

The polypropylene bottle which contained the reaction mixture A4 ruptured (after approximately 90 days) in the 95°C bath. This was before the synthesis had reached completion. Product material A4 was thus lost.

A portion of each product was calcined in a Gallenkamp size 1 box furnace. Each material was heated to 550°C and left at this temperature for about 16 hours in order to burn the TPA from the silicalite channel system. The furnace temperature was then increased to 800°C for 1 hour in order to remove any piperazine which may have been occluded into the silicalite framework during the synthesis.

3.3 Results and Discussion

The plots of pH and crystallinity against time are shown in Figures 3.1 and 3.2. The table below summarises the crystallisation data. Each synthesis mixture had the composition:

x(Piperazine) y(Piperazine.diHCl) 2TPABr $20SiO_2$ $1000H_2O$

Table 3.1 Synthesis Data for Low pH Preparations

Code	x	y	Initial pH	Final pH	pH Change	t(days) 100% Silicalite
A1	10	0	11.28	10.88	0.40	52
A2	9	1	10.55	9.90	0.65	63
A3	8	2	10.17	9.81	0.36	77
A4	7	3	9.79	9.44*	-	88*
A5	6	4	9.28	8.16*	-	111*

The values marked with an asterix (*) were taken at 80% crystallinity. Preparations A1 and A2 showed a steady decrease in pH as the TPA-silicalite crystallised. The syntheses A3, A4 and A5 each showed an inflection (arrowed on Figure 3.1) in their pH profiles at about pH values 10.10 (after 3-6 days), 9.70 (25-34 days) and 9.10 pH units (25-34 days) repectively. Optical microscopic observations indicated the formation of a globular amorphous gel in each preparation at these regions of inflection on the pH profiles. The crystallisation was observed to proceed via a different path for the three lowest pH syntheses in the series, with the formation of an intermediate gel phase prior to the crystallisation of TPA-silicalite from the reaction mixtures. In the higher pH syntheses (A1 and A2). crystallisation commenced without the formation of an extra intermediate gel phase. No inflection was observed in the pH profiles and no formation of globular amorphous spheres was seen by optical microscopy.

The first three samples during the the A5 synthesis were brown, but subsequent samples were white. This suggests that decomposition of some organic material occurred in the initial stages of the preparation, prior to the formation of the extra intermediate gel.

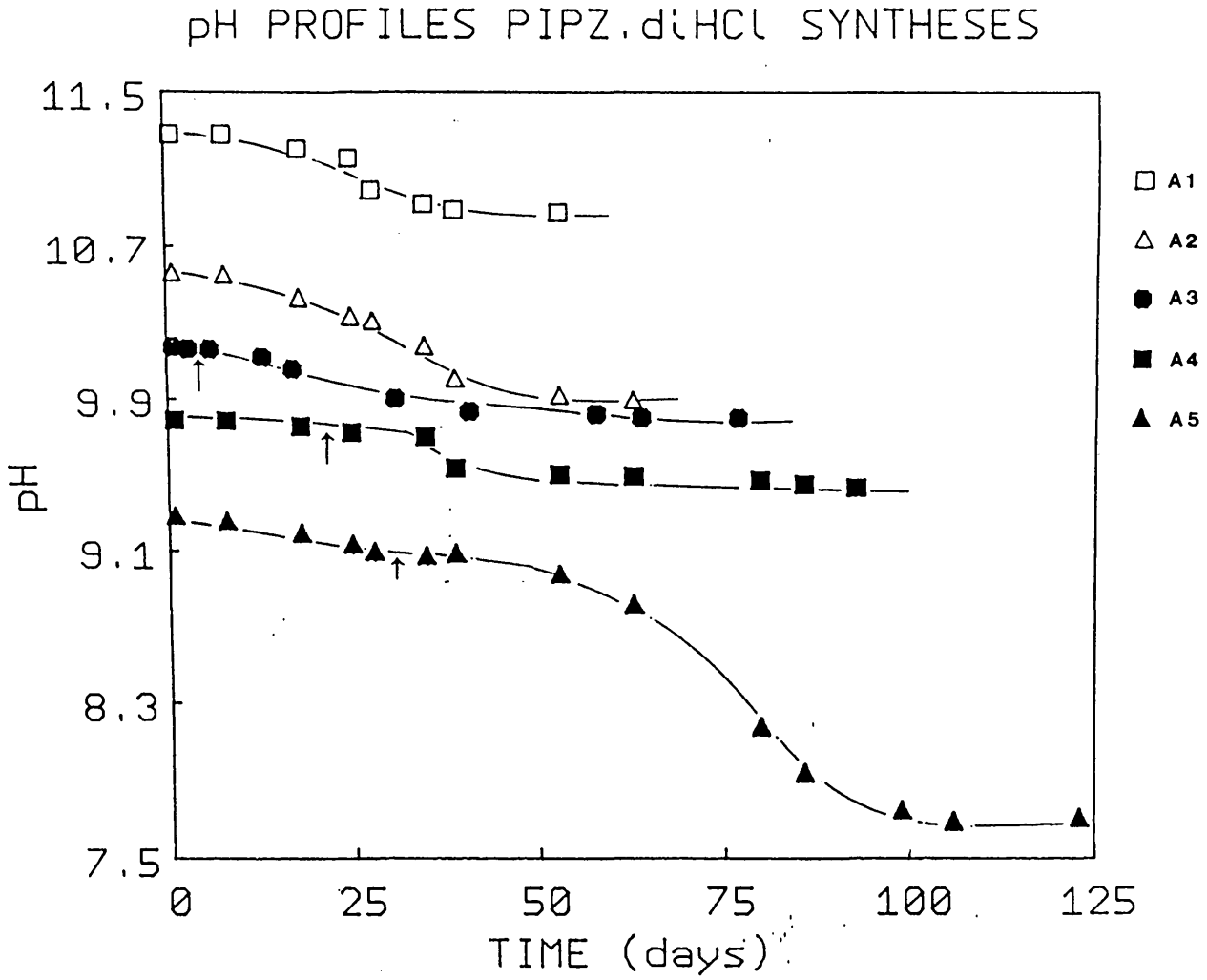

Figure 3.1 pH profiles silicalite syntheses

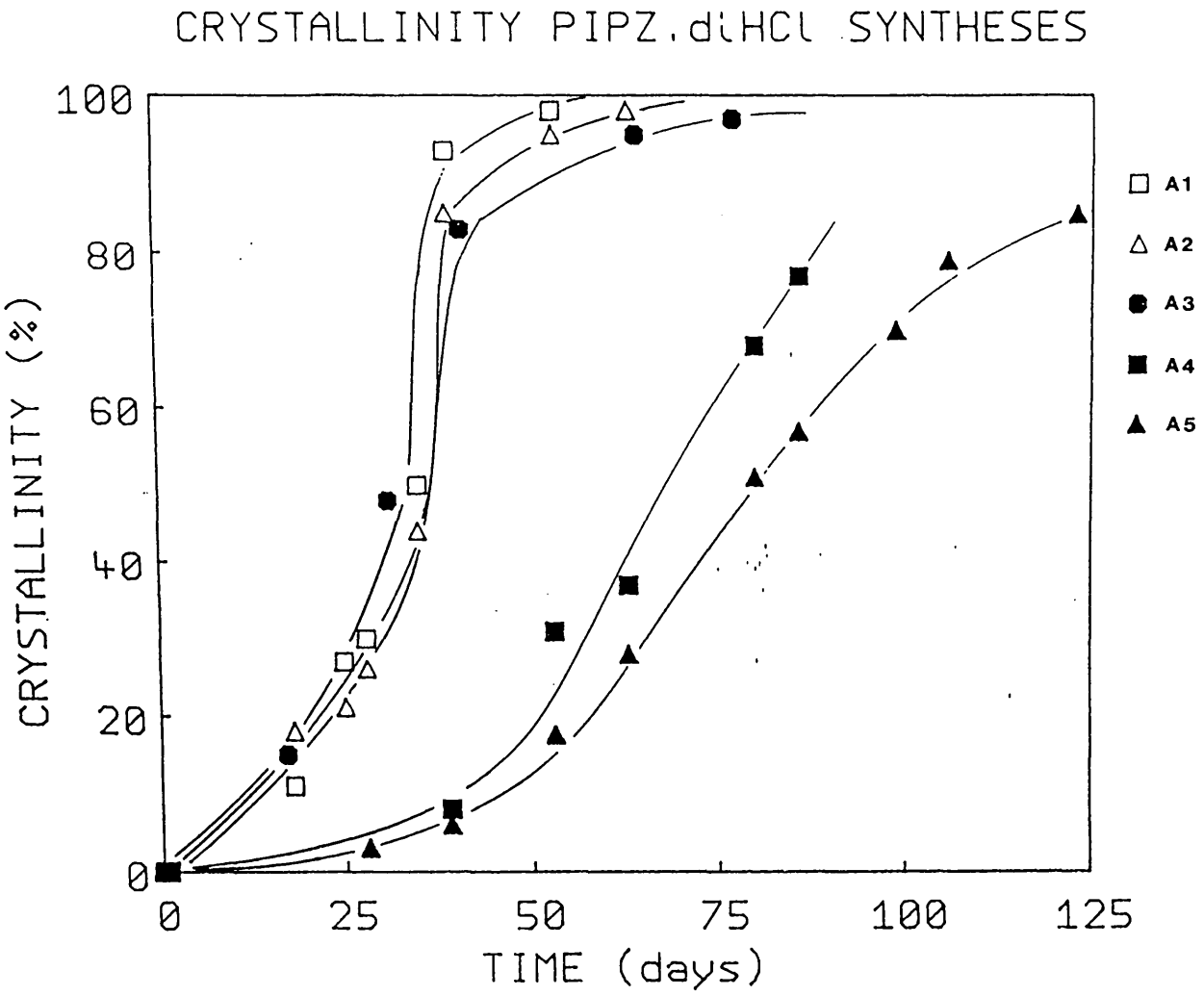

Figure 3.2 Crystallinity plots silicalite syntheses

Crystallisation ceased at around 80% after the reaction mixture pH had fallen to around 7.5. At this near neutral pH there is insufficient of the hydroxide mineraliser for the reaction to proceed.

X-ray diffraction (XRD) patterns of each uncalcined product material are shown in Figures 3.3 - 3.6. In all cases the only crystalline material present was TPA-silicalite. The XRD patterns of each calcined product H-silicalite are shown in Figures 3.7 - 3.10.

With the exception of that for A1, all of the XRD patterns showed slight preferred orientation. Preferred orientation is discussed in greater detail in Section 6.2. It is observed when crystals are either plates or needles and pack in a XRD sample holder in a particular way. In the case of silicalite enhancement of the peaks at 8.87, 17.80, 26.83, 36.04 and 45.50 2θ is observed.

Scanning electron microscopy (SEM) confirmed that the products which exhibited slight preferred orientation were plate-like in morphology. There was also a wide distribution of crystal sizes in the products of the preparations that contained piperazine.diHCl (Plate 3.1). Table 3.2 indicates which prints on Plate 3.1 correspond to each TPA-silicalite product.

Table 3.2 - SEM of TPA-silicalite products

TPA-silicalite	Print
A1	1
A2	2
A3	3
A5	4

TPA-silicalite A1 had mostly squat twinned crystals of 10-15 um. Material A2 had a crystal size distribution of 2-15 um; the crystals were plate-like and mostly untwinned. Product A3 had a crystal size distribution of 5-15 um; its crystals were thinner than those of material A2. TPA-silicalite A5 presented two morphologies, plates and rods. The crystal size varied between 2 and 15 um. As the reaction mixture pH decreased the product TPA-silicalite crystals

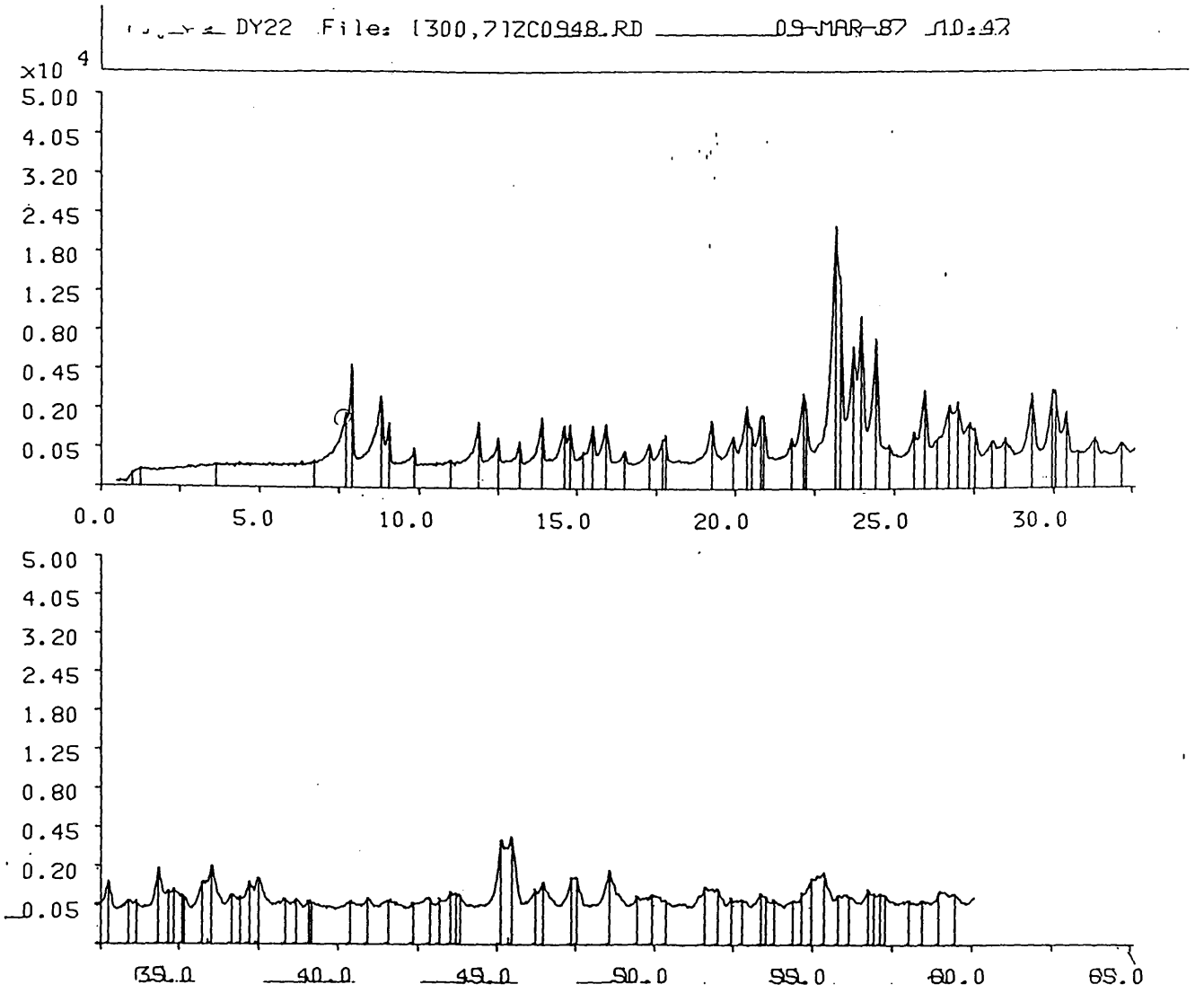

Figure 3.3 XRD pattern of TPA-silicalite Al

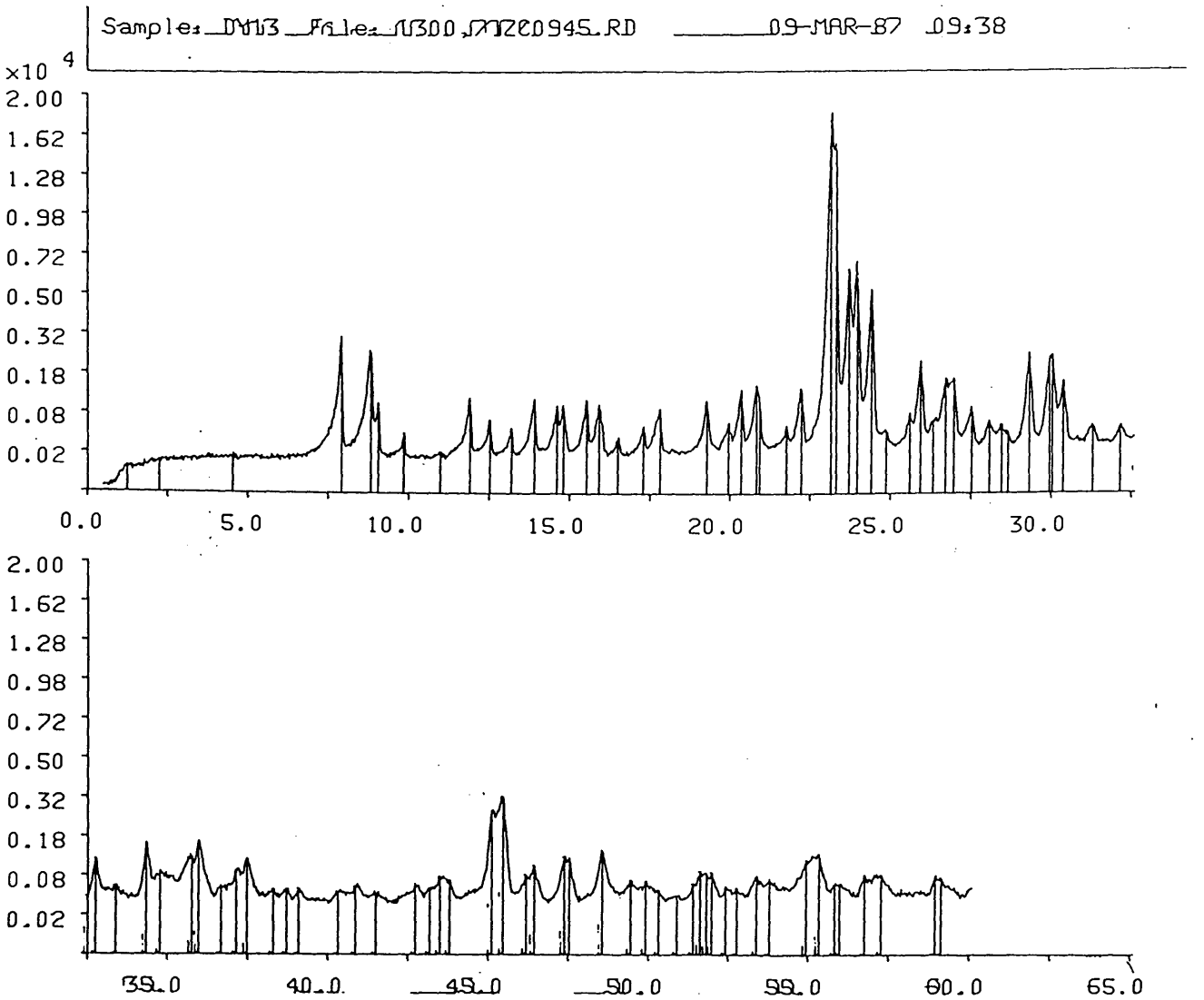

Figure 3.4 XRD pattern of TPA-silicalite A2

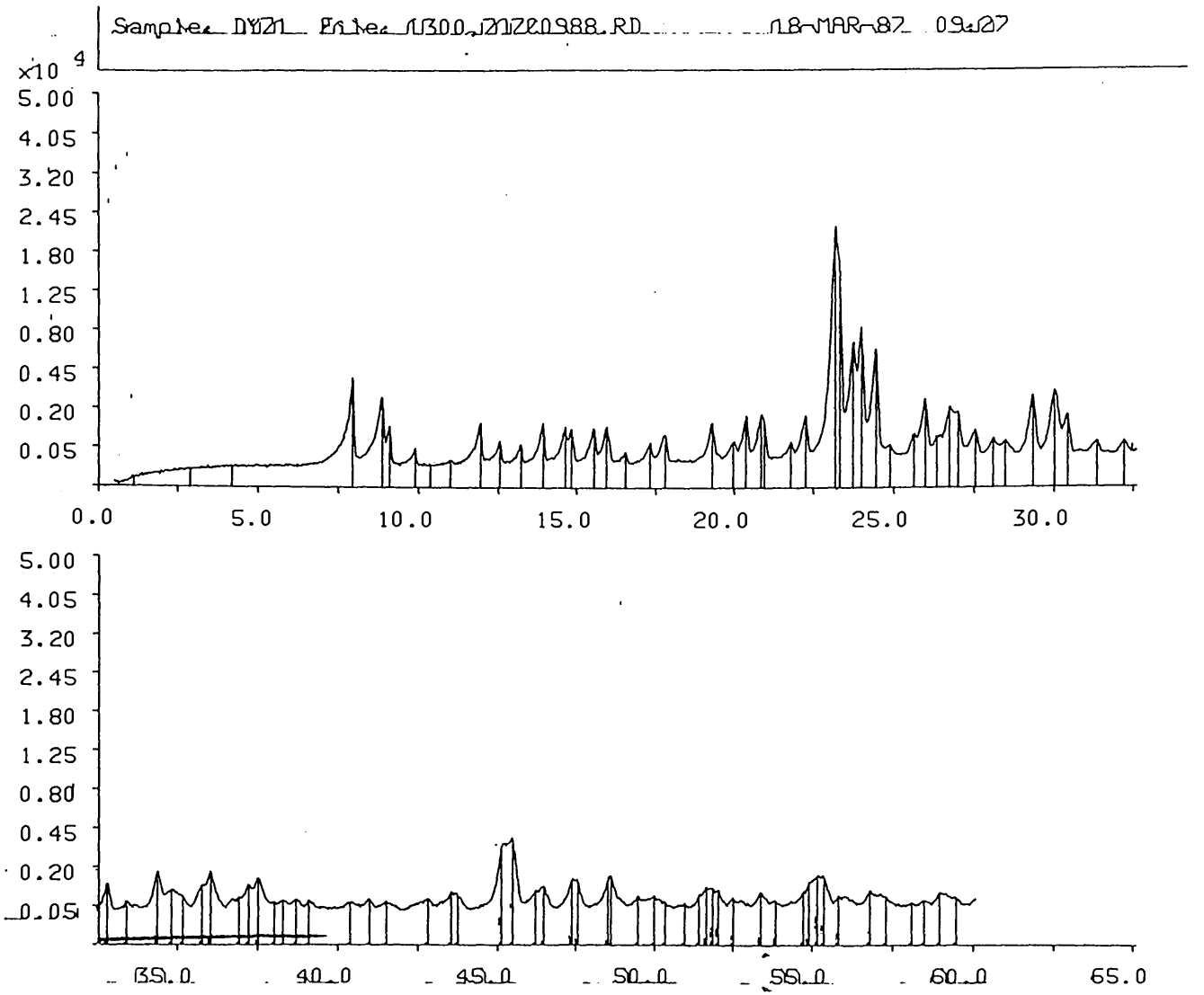

Figure 3.5 XRD pattern of TPA-silicalite A3

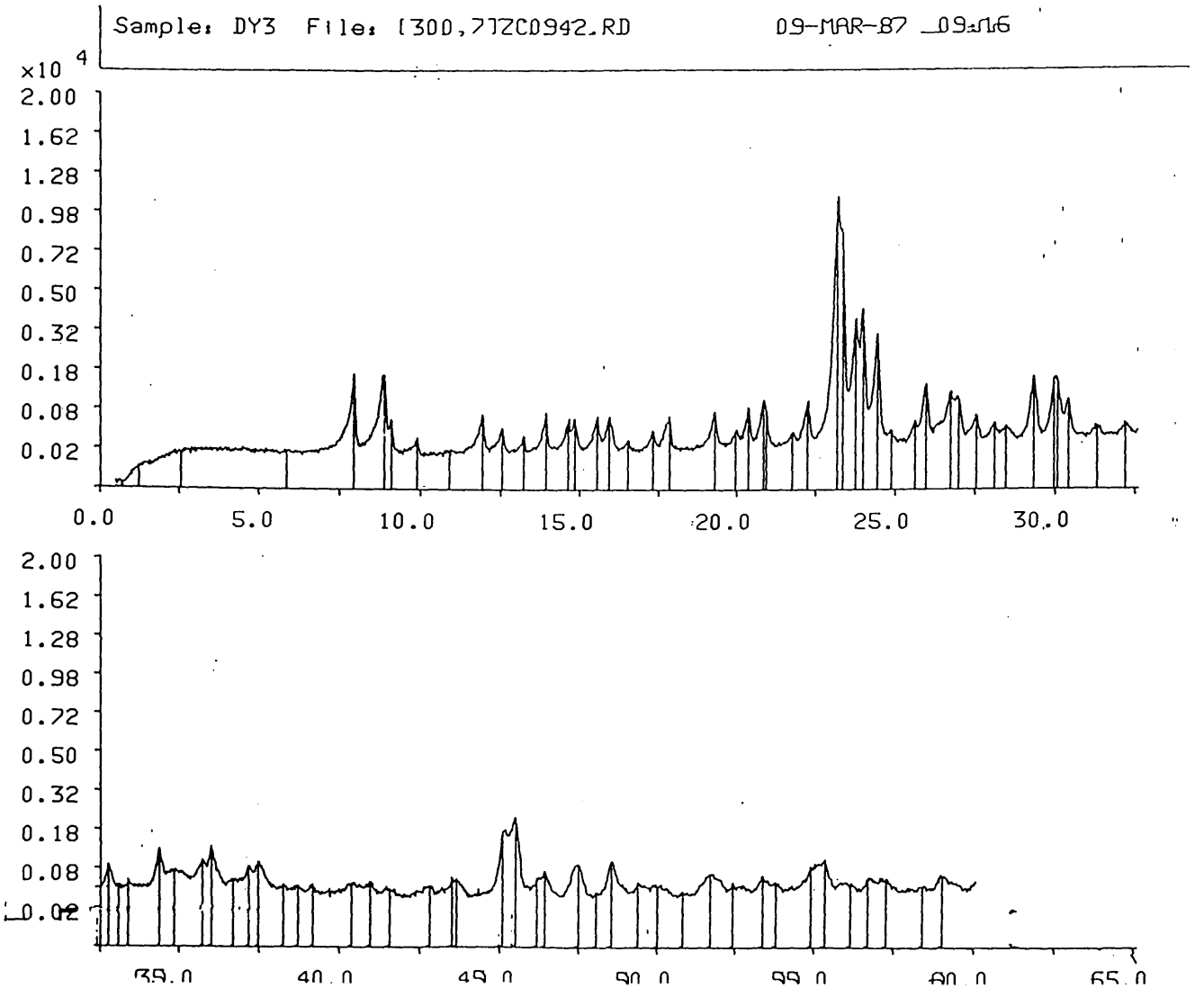

Figure 3.6 XRD pattern of TPA-silicalite A5

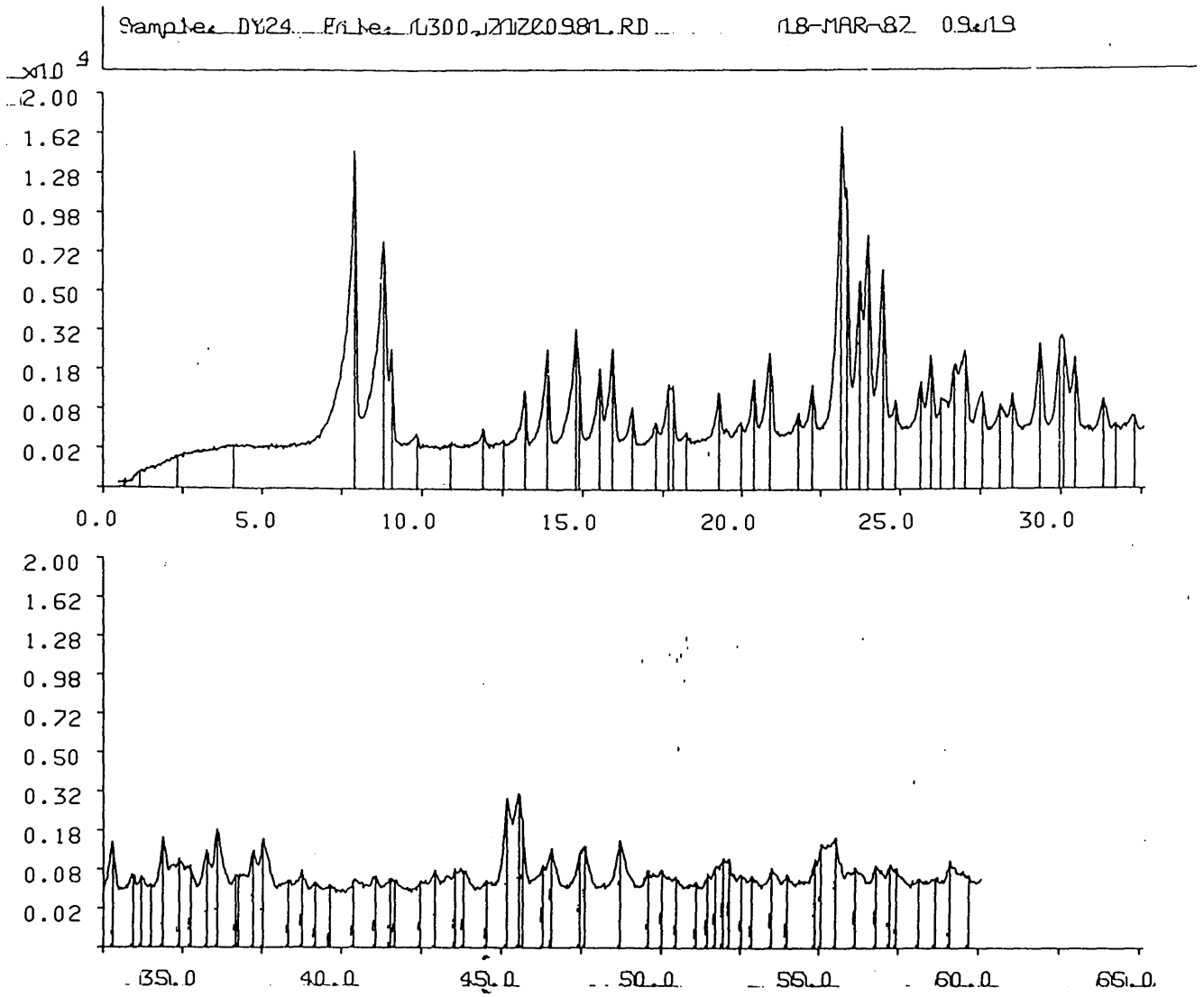

Figure 3.7 XRD pattern of H-silicalite A1

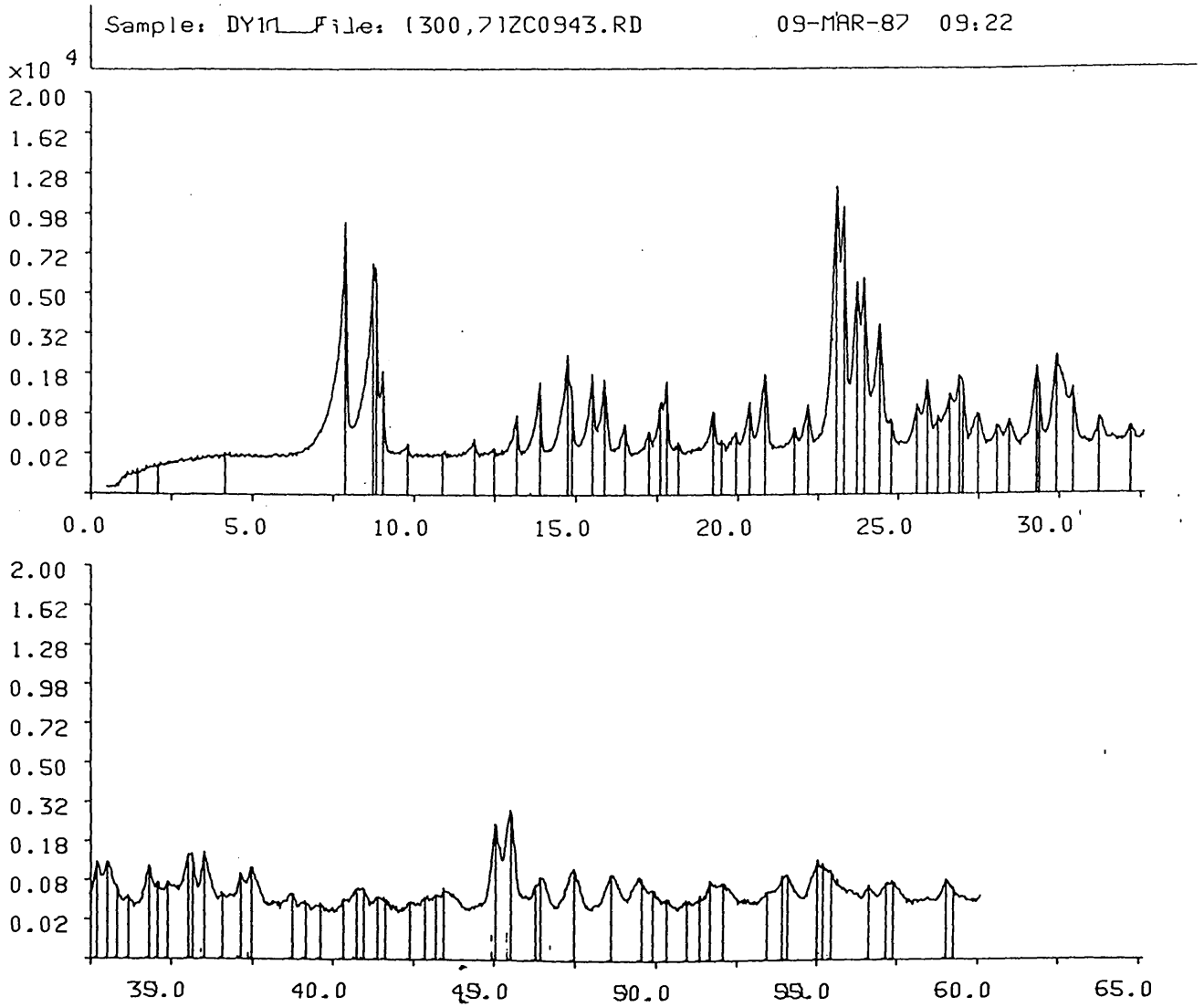

Figure 3.8 XRD pattern of H-silicalite A2

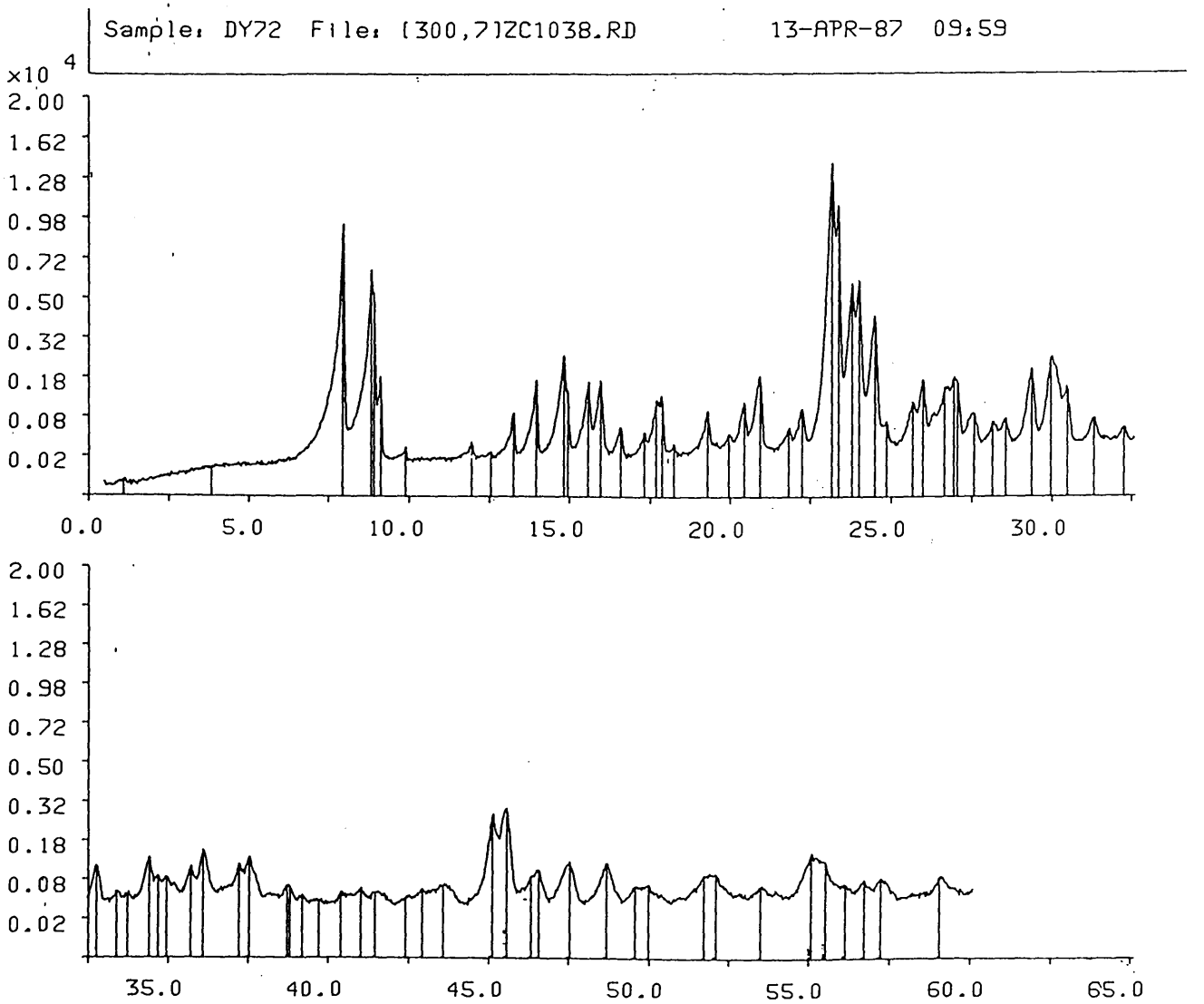

Figure 3.9 XRD pattern of H-silicalite A3

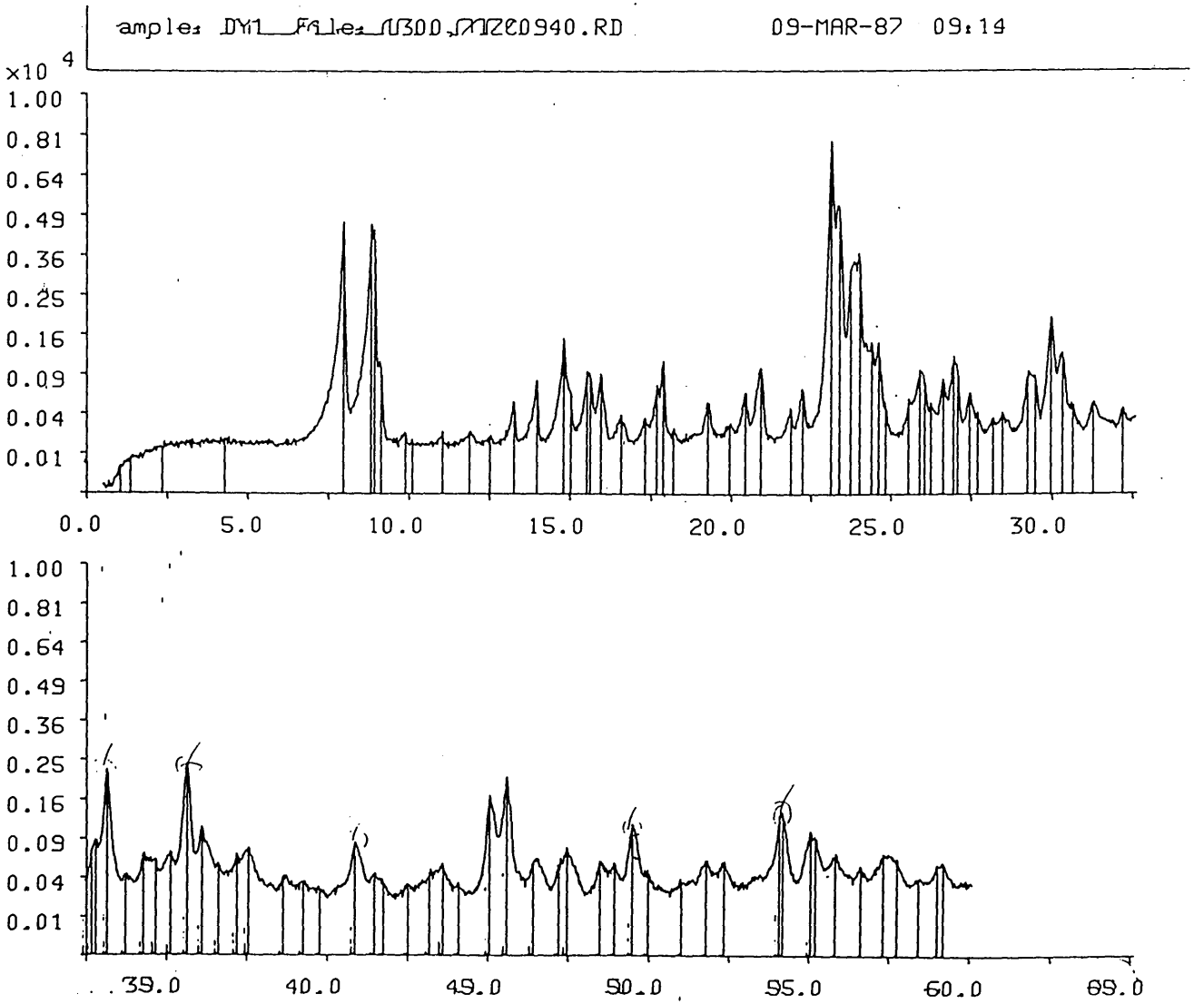

Figure 3.10 XRD pattern of H-silicalite A5

became thinner and a rod-like morphology started to emerge. The wide range of crystal size distributions evident in products A2 and A5 indicates that there may have been some secondary nucleation.

The product from reaction mixture A5 was brown. The X-ray diffraction pattern of calcined A5 showed extra Bragg reflections at 33.15, 35.62, 40.83, 49.42, 53.99 and 54.09 2θ. These peaks were absent in the uncalcined material. They were identified from the powder diffraction file (13) as those of Fe_2O_3 (Haematite), Table 3.3.

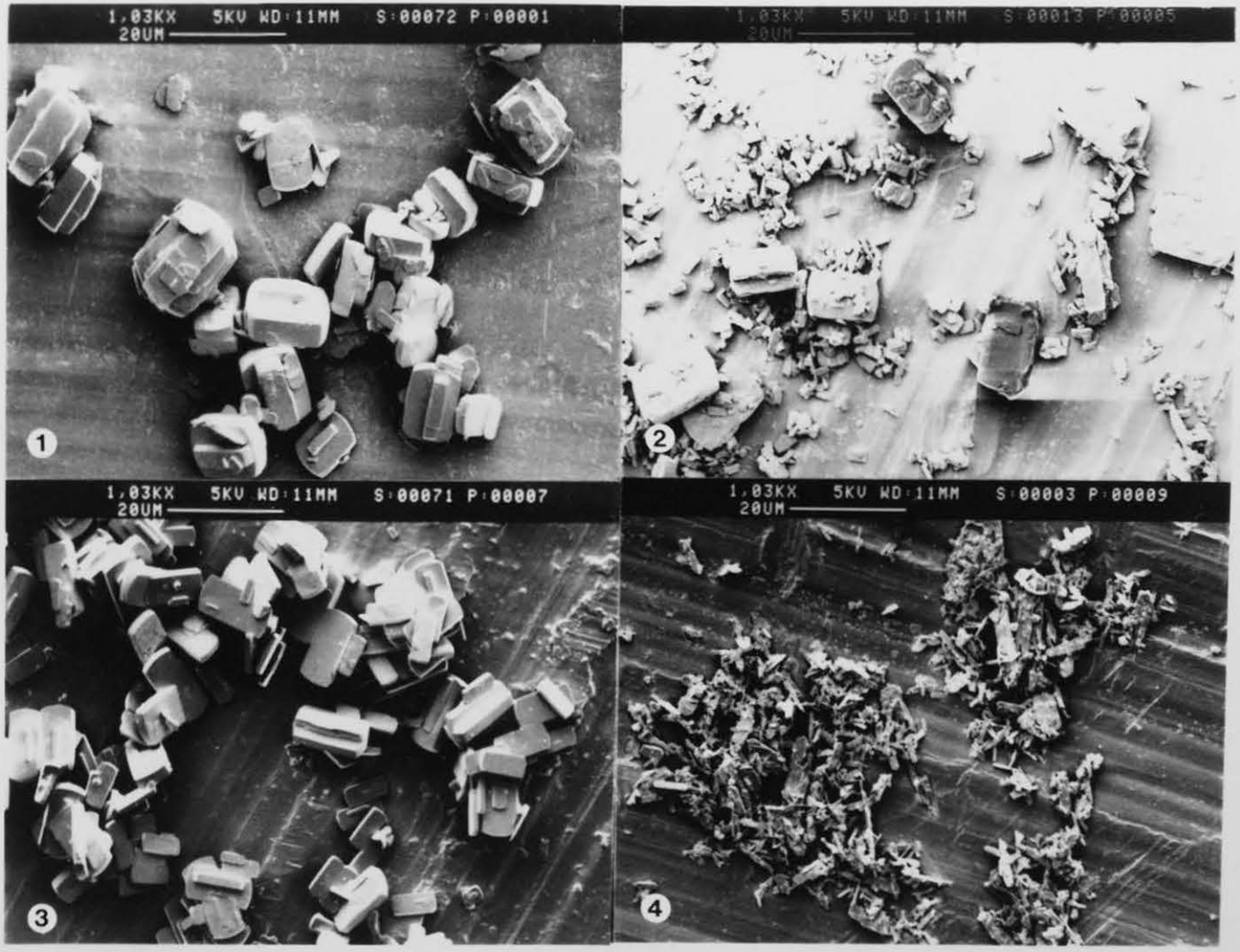
1,03KX 5KV WD:11MM S:00072 P:00001
20UM
1
1,03KX 5KV WD:11MM S:00013 P:00005
20UM
2
1,03KX 5KV WD:11MM S:00071 P:00007
20UM
3
1,03KX 5KV WD:11MM S:00003 P:00009
20UM
4

PLATE 3.1

Table 3.3 Bragg Reflection Positions of Fe_2O_3.

Observed 2θ	Calculated d-spacings	Literature d-spacings of Fe_2O_3 (Hematite) (ASTM 13-534)
33.15	2.70	2.69
35.62	2.52	2.51
40.83	2.21	
49.42	1.84	
53.99	1.70	
54.09	1.69	1.69

The origin of the iron oxide was found to be corrosion of the screws which held the stainless steel stirrer paddle to its stainless steel shaft. On calcination the amorphous hydrated iron oxide crystallised to give Fe_2O_3.

Thermal analysis of the products was also conducted. Differential thermal analysis (DTA) of each uncalcined product was performed at a heating rate of 1°C/minute from room temperature to 1200°C in a static air atmosphere. Each material was also analysed by thermal gravimetry (TG) at a heating rate of 10°C/minute from room temperature to 1200°C in a 15ml/minute flow of air. The samples for thermal gravimetry were about 5mg and those for differential thermal analysis about 40mg; in each case the sample size was kept constant for the whole experimental series.

The DTA peak positions are given in Table 3.4.

Table 3.4 DTA peak positions of TPA-silicalite

Sample	A1	A2	A3	A5
Temp (°C)	340	360	365	355

There was an insufficient quantity of material A4 for thermal analysis. The DTA traces for the final products are given in Figure 3.11.

Removal of the TPA template from the framework channels may occur by one of two mechanisms:-

(a) Oxygen diffuses into the pore system and reacts with the organic template within the framework.

(b) Heat decomposes the TPA to gaseous organic species which diffuse to the crystal surface where they react with oxygen.

Provided all the TPA molecules are in identical sites within the lattice all of the internal TPA should burn out in one thermal event, therefore one peak should have been observed on each DTA trace. This was not the case, the main DTA exothermic peak was often split (see Figure 3.11). This was thought not to be indicative of different TPA sites but an effect associated with the diffusion of oxygen into the channels. Diffusion of oxygen into the channel system, as well as the gaps between the crystals, is inhibited by the outward diffusion of combustion products from the framework. The effect is magnified by the relatively large samples used in the present work, and leads to a fall in the initial rate of combustion. This results in more than one peak in the DTA traces. In the present case because low heating rates were used the effect is not large; with higher heating rates multiple splitting of the main exotherm is observed (6). This is also discussed in more detail by Franklin and Lowe (14).

Material A5 showed a small endothermic peak at around 100°C which was associated with the removal of water from the material. This product also showed a distinct exothermic peak at 264°C which corresponds to TPAOH combustion. Both observations were consistent with the existence of amorphous gel in the sample. Earlier studies of the crystallinity of the product had indicated it was around 15-20% amorphous.

Thermal gravimetric analysis traces of the product TPA-silicalites are shown in Figure 3.12. Sample sizes were all about 4mg. Each as-made material gave weight losses of 14.0% (A1), 13.0% (A2), 12.8% (A3) and 10.1% (A5). TPA-silicalites A1-3 each gave a TG trace of similar shape which indicated one thermal event. Material A5 showed a small weight loss due to water and another probably due to TPAOH.

CHN analysis of the crystalline products revealed that the C/N

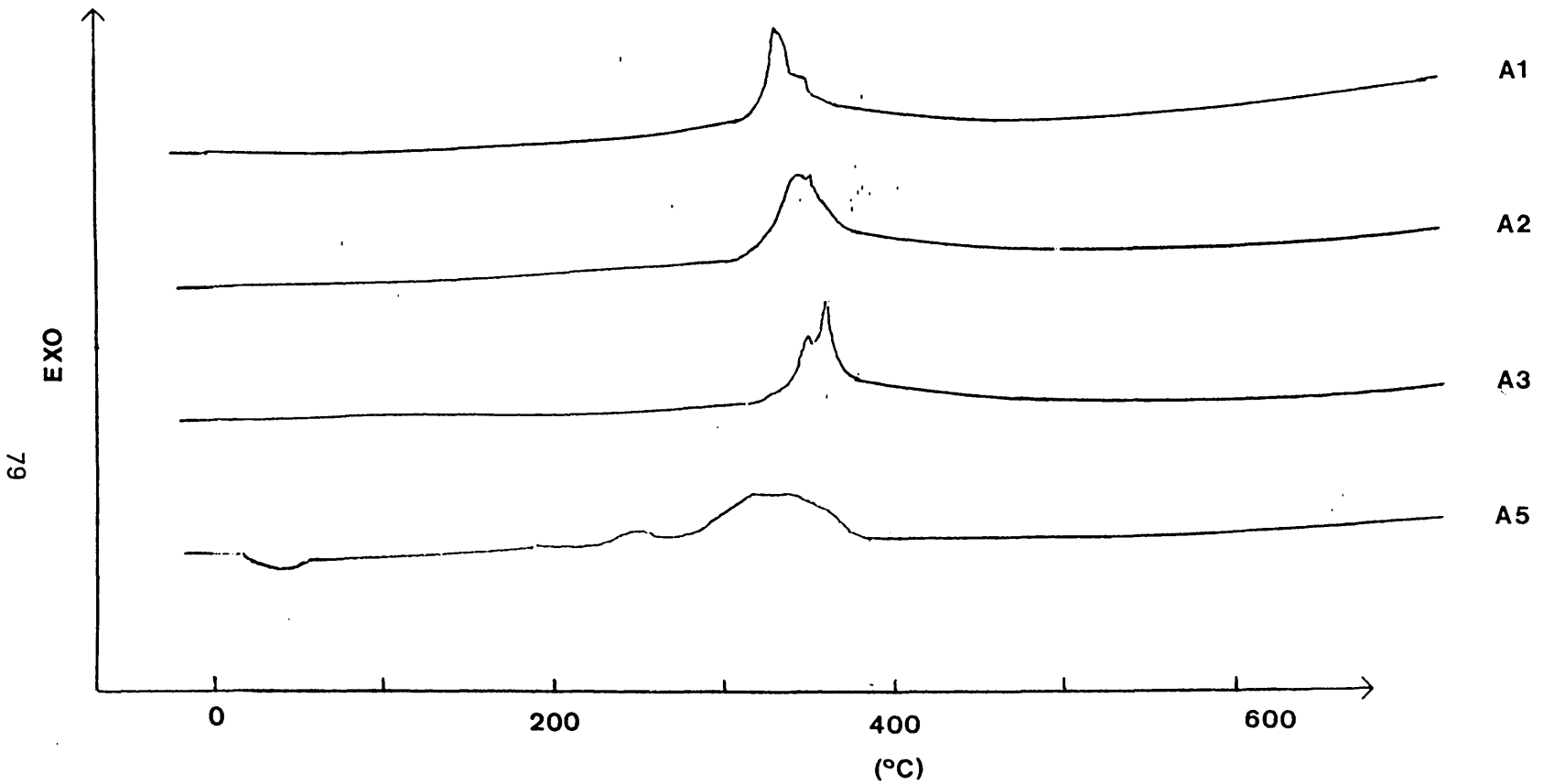

Figure 3.11 DTA traces silicalites A1,A2,A3 and A5

atom ratios were lower than the 12/1 expected for TPA, see Table 3.5.

Table 3.5 CHN analysis results for silicalites

Material	C (%)	H (%)	N (%)	C/N
A1	9.43	1.95	1.10	10.00
A2	9.77	1.98	1.10	10.36
A3	8.83	1.81	1.11	9.28
A5	9.81	1.98	1.66	6.89

The DTA of material A1 gave a shouldered exotherm, and product A3 had a split exotherm. These indicate either oxygen starvation (as discussed above) or, when the CHN results are considered, the presence of a second organic material within the channel system.

Materials A1 and A3 were submitted to ICI for ^{13}C magic angle spinning nuclear magnetic resonance (MASNMR). The resultant spectra are shown in Figures 3.13 and 3.14. These show that the product from A1 contained about 95% TPA and 5% piperazine. The peaks at chemical shift values 63.4, 16.9 and 11.6/10.7(twin) are characteristic of TPA (15). The peak at 44.8ppm is attributed to piperazine. The resonances at 113.5, 105.5 and 21.7ppm were assigned as side bands of the carbon resonance at 63.4ppm.

The figure of 5% piperazine is much less than would be expected from the CHN results for A1, one possibility is that the TPA was incompletely combusted by the CHN analysis, and hence less carbon was detected than actually present. The carbon residues remain in the pore system after the analysis. Other microporous silicas have also been found to give low C/N ratios (16). The MASNMR spectrum of A3 did not show any evidence of piperazine, and in this case either some breakdown of the TPA to tripropylamine has occurred or the CHN analysis is suspect. It is considered that the latter is the most likely.

Materials A2 and A5 were unsuitable for ^{13}C MASNMR as they were contaminated with iron, which is paramagnetic.

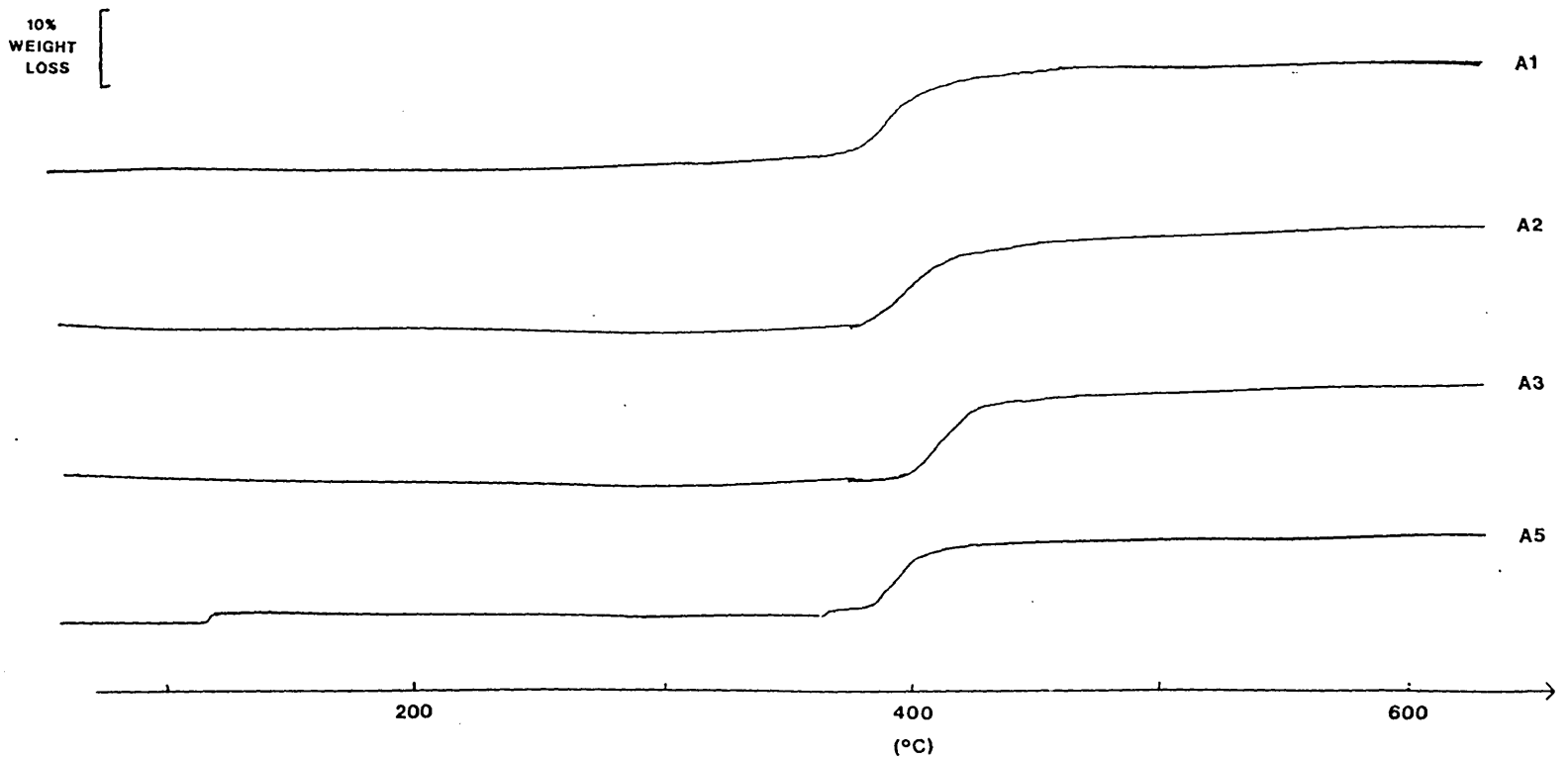

Figure 3.12 TG traces silicalites A1, A2, A3 and A5

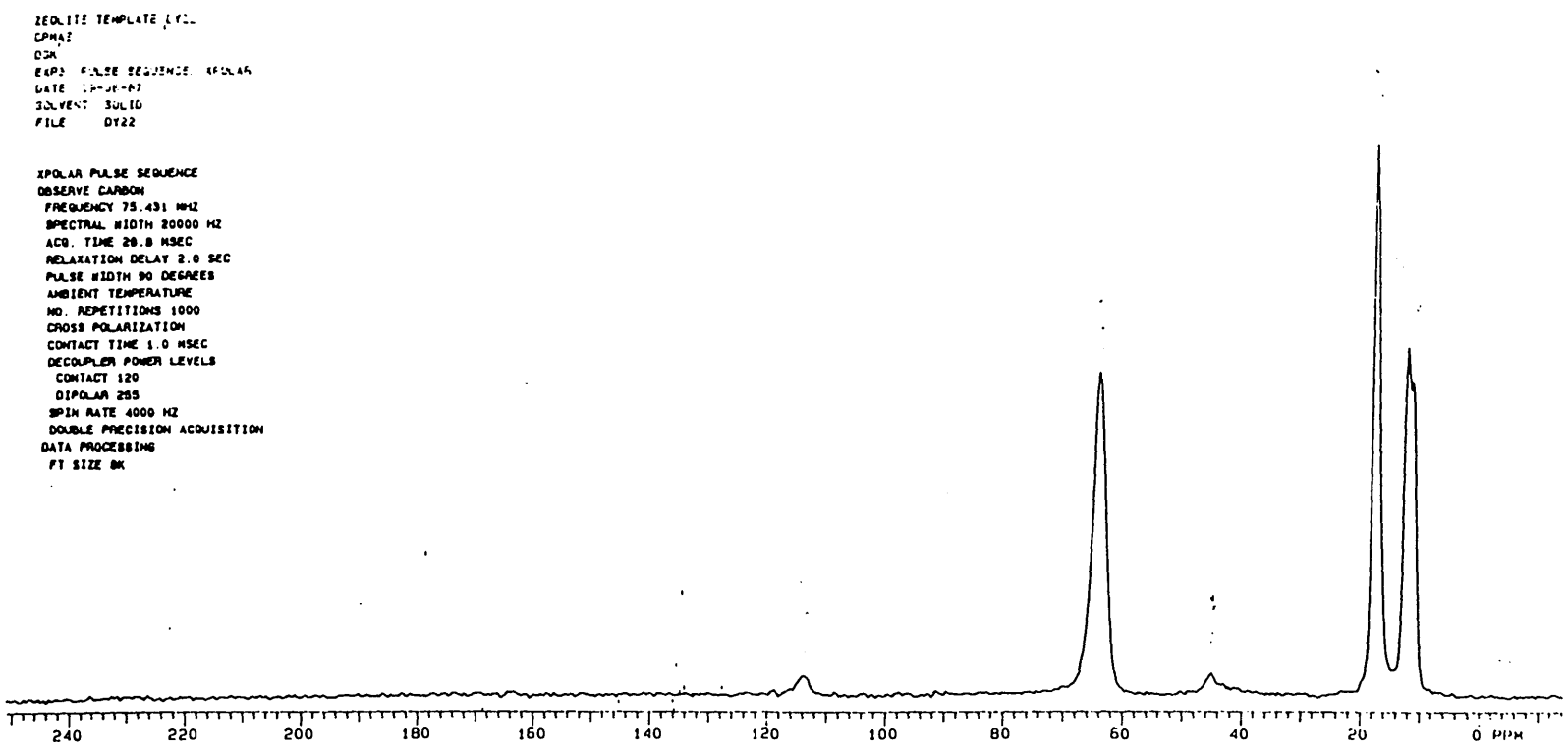

Figure 3.13 ^{13}C MASNMR silicalite Al

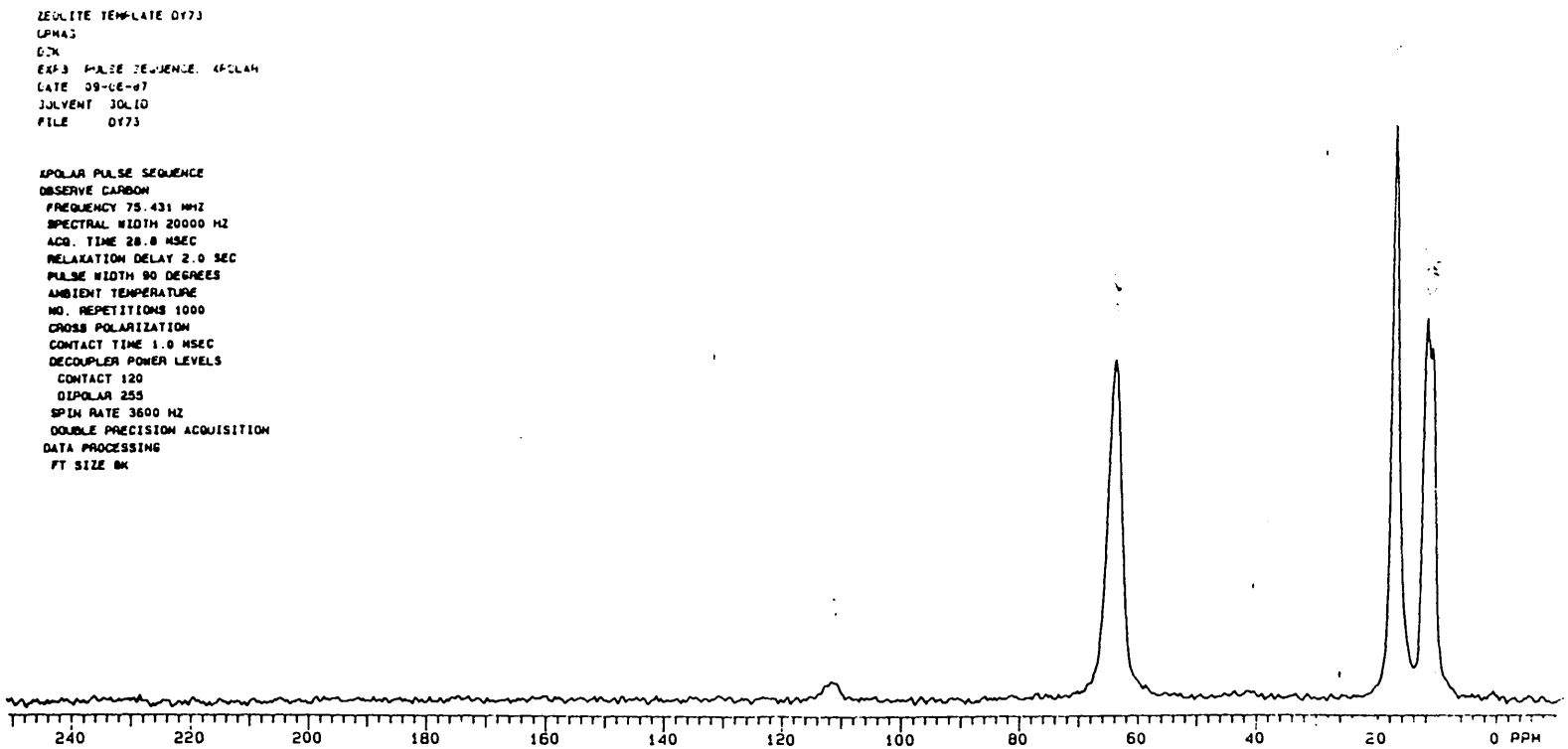

Figure 3.14 ^{13}C MASNMR silicalite A3

3.4 Conclusion

The low pH synthesis route had no advantages for the crystallisation of TPA-silicalite. As the reaction mixture pH was suppressed the morphology of the crystals became less uniform and their size also decreased. Rather than promoting the growth of large crystals through reduced primary nucleation, large deviations in crystal size were observed. This indicates the probable occurrence of secondary nucleation. The crystallisations were not carried out in completely sealed reaction containers; consequently water was lost through evaporation and had to be replenished every 48 hours. The removal and addition of water from the reaction mixture could have initiated some secondary nucleation which caused the large crystal size distribution. Use of a sealed system, for instance an autoclave, may remove this problem. The growth of large crystals and the suppression of nucleation in low pH systems may then be observed.

The time for apparent 100% crystallisation increased as the reaction mixture pH was reduced. Crystallisation ceased when the pH fell to near neutral, due to lack of hydroxide mineraliser.

The ^{13}C MASNMR spectrum of silicalite A1 showed that piperazine had been incorporated into its framework. The CHN analysis data gave C/N molar ratios which were lower than expected. This could not be accounted for simply by the incorporation of a second organic molecule, piperazine, into the framework along with TPA; since no piperazine was occluded into silicalite A3 yet its C/N ratio was 9.28 rather than the expected 12. The carbon within the TPA-silicalite samples which were submitted for CHN analyses was probably incompletely combusted relative to the nitrogen. This implies that the calcined materials were probably contaminated with carbon residues. Great care should be taken when zeolite precursors are submitted for CHN analysis, and special conditions may be required to obtain satisfactory results.

Chapter 3 References

[1] E.M. Flanigen, J.M. Bennett, R.W. Grose, J.P. Cohen, R.L. Patton, R.M. Kirchner and J.V. Smith
Nature, 1978, **271**, 512.

[2] G.T. Kokotailo, S.L. Lawton, D.H. Olsen and W.M. Meier
Nature, 1978, **272**, 437.

[3] C.A. Fyfe, G.C. Gobbi, J.Klinowski J.M. Thomas and S. Ramdas
Nature, 1982, **296**, 530.

[4] R.W. Grose and E.M. Flanigen
U.S. Patent 4,061,724 (1977).

[5] F.G. Dwyer and E.E. Jenkins
U.S. Patent 3,941,871 (1976).

[6] S.G. Fegan and B.M. Lowe
J.Chem.Soc., Faraday Trans. 1, 1986, **82**, 785.

[7] S.G. Fegan and B.M. Lowe
J.Chem.Soc., Chem. Commun., 1984, 437.

[8] H. Nakamoto and H. Takahasi
Chem. Lett., 1981, 1739.

[9] R. von Ballmoos
"The O-Exchange Method in Zeolite

Chemistry" (Salle and Sauerlaender,

Frankfurter am Main, 1981), page 98.

[10] S.G. Fegan and B.M. Lowe

J.Chem.Soc., Faraday Trans. 1, 1986, **82**, 801.

[11] G.H. Kuehl

European Patent Application, 93519 (1983).

[12] J.L. Casci and B.M. Lowe

Zeolites, 1983, **3**, 186.

[13] ASTM Powder Diffraction File

"Inorganic Phases" (1982), p. 403, 13-534.

[14] K.R. Franklin and B.M. Lowe

Thermochimica Acta, 1988, **127**, 319.

[15] G. Boxhoorn, R.A. van Santen, W.A. van Erp,

G.R. Hays, R. Huis and D. Clague

J.Chem.Soc., Chem. Commun., 1982, 264.

[16] K.R. Franklin

Personal Communication.

CHAPTER 4

SYNTHESIS OF

<TPA,PIPERAZINE>-ZSM-5

4.1 Introduction

Since the first ZSM-5 syntheses were described in the literature (1,2), there have been many improved recipes for its crystallisation (3-9). Much effort has been devoted to understanding the mechanism of its synthesis (10-21).

The vast majority of ZSM-5 preparations use alkali metal base as a component of the reaction mixtures, and most require the preparation of a sodium aluminate solution by dissolution of hydrated alumina in sodium hydroxide prior to incorporation with an amorphous silica to form the reactive gel.

Bibby et al found that the alkali metal hydroxide component of the gel can be replaced by ammonium hydroxide (22). This has the advantage of producing an alkali metal-free ZSM-5 which on calcination gives the acid catalyst H-ZSM-5. This procedure eliminates the need to acid-exchange alkali metal cations from the zeolite framework.

Silicalite, the aluminium free form of ZSM-5, has been crystallised from reaction mixtures which contain piperazine as an organic base, tetrapropylammonium bromide (TPABr) as the MFI structure directing template, amorphous silica and water, at temperatures between 95 and 150°C (23). The aim of the work now described (Section 4.2) was to extend this procedure to the preparation of alkali metal free ZSM-5. Aluminium sulphate and aluminium nitrate were used as the source of aluminium, since aluminate, aluminium metal or alumina all require the use of excess strong alkali. The weak organic base, piperazine, was used to make the reaction mixture alkaline. It was hoped that in this way it would be possible to make alkali metal free TPA-ZSM-5 which on calcination would give H-ZSM-5, without the need for acid exchange (21).

A major requirement for this work was a means of confirming that the aluminium was incorporated in the zeolite framework. Results in the literature (24-26) indicate that DTA can be used to show the

presence of framework aluminium. The greater the amount of framework aluminium present, the higher the peak temperature of the TPA combustion exotherm. Hence this was chosen as a technique for the qualitative study of the products from the ZSM-5 crystallisations.

4.2 Experimental

A series of reaction mixtures were prepared with the compositions:

10Piperazine 2TPABr x[$Al(NO_3)_3$] 20SiO_2 1000H_2O

and

10Piperazine 2TPABr y[$Al_2(SO_4)_3$] 20SiO_2 1000H_2O

The values of x and y were chosen for each set of preparations, to give Si/Al ratios of 20, 60, 180 and 540. The crystallisations with $Al(NO_3)_3$ were conducted at 95°C. The preparations which contained $Al_2(SO_4)_3$ were conducted at 95 and 150°C. All the reaction mixtures were stirred. The 150°C preparations were crystallised in a stainless steel autoclave and each reaction mixture weighed 300g. The 95°C preparations were crystallised in polypropylene bottles mounted in a thermostat bath. Each reaction mixture weighed 600g. The reaction vessels are described in Chapter 2.

Reaction mixture compositions were calculated with the "MIXV3" program on a BBC microcomputer. All the reaction mixtures were prepared by an identical procedure. The piperazine, tetrapropylammonium bromide, aluminium source and water were weighed into a beaker which was then placed on a hot-plate. A large clock glass was placed over the top of the beaker, to help reduce evaporation. The mixture was heated and gently boiled for 3 hours. The limited evaporation was countered by addition of water to bring up the level to a known mark on the side of the beaker, every 10-15 minutes. The gentle boiling was to dissolve as much aluminium as possible into the alkaline solution. It was anticipated that the aluminium would complex or at least ion-pair with the organic components, especially TPA, in the aqueous phase. This procedure also ensured that any of the precipitated aluminium hydroxide which did not re-dissolve was fully dispersed as fine colloidal particles. The final solutions of low aluminium nitrate content, i.e. those intended for the Si/Al=180 and 540 crystallisations, were clear. The

boiling sol, or solution, was then added to Cab-O-Sil M5 (BDH) which had already been weighed into a 1 litre polypropylene bottle. This was electrically blended for three minutes, by which time it appeared to be a homogeneous paste.

For each 95°C synthesis, a stirrer cap was screwed onto the top of the plastic bottle. The reaction vessel was then placed in a 95°C water bath and the paddle shaft clamped to the stirrer motor spindle. The equipment is described in Chapter 2. Evaporation of water from the reaction container was checked every 46 to 50 hours. The level of the liquid in each 1 litre plastic bottle was detected by placing a light over the bath and a beaker against the side of the reaction container. The translucent polypropylene bottles had earlier been marked with a permanent pen to indicate the initial liquid level. Water could be added via the sampling port to bring the liquid level up to the mark. Each synthesis was monitored by the withdrawal of samples at regular intervals. The samples were extracted with a syringe to which was attached a length of plastic tubing for insertion through the sampling port.

A second reaction mixture which contained aluminium nitrate to give Si/Al=60 was prepared by the above method. This was aged for one month prior to its insertion into the 95°C thermostat bath. The synthesis pH was monitored for comparison with its unaged counterpart crystallisation.

For the 150°C preparations, each blended reaction mixture was poured into the autoclave vessel, and the autoclave was immediately assembled. Each crystallisation was monitored by the discharge of a portion of the reaction mixture through the sampling tap.

On completion of each crystallisation the product was filtered at about 95°C, to avoid deposition of any amorphous material from the solution phase of the reaction mixture. The final material was washed with water and dried at 110°C for 16 hours. All of the final crystalline products were examined by X-ray powder diffraction; in each case the product was ZSM-5.

The pH of each liquid phase sample was measured with a Philips PW

9422 pH meter. The solution phase of certain samples was removed by filtration. The solid phase was dried at 110°C for two hours, and then equilibrated with water vapour prior to XRD analysis. Crystallinities were based on the major Bragg peaks at 8.83, 23.07, 23.27, 23.69 and 24.36 2θ.

A portion of each product was calcined in a Gallenkamp size 1 box furnace at 550°C overnight then for 1 hour at 800°C, to remove any piperazine that may have been present. The samples of H-ZSM-5 were analysed by XRD to confirm that their structures had not collapsed.

The uncalcined products were further characterised by scanning electron microscopy (SEM), differential thermal analysis (DTA) and thermal gravimetry (TG).

4.3 Results

4.3.1 Crystallisations

The reaction codes, Si/Al ratios, synthesis temperatures and aluminium sources are summarised in Table 4.1.

Table 4.1 ZSM-5 syntheses

Code	Reaction Mixture Si/Al	Synthesis Temperature (°C)	Aluminium Source
B1	-	95	Impurity
C1	540	95	Sulphate
C2	180	95	Sulphate
C3	60	95	Sulphate
C4	20	95	Sulphate
D1	540	150	Sulphate
D2	180	150	Sulphate
D3	60	150	Sulphate
D4	20	150	Sulphate
E1	540	95	Nitrate
E2	180	95	Nitrate
E3	60	95	Nitrate
E4	20	95	Nitrate
F1	60	95	Nitrate

The pH changes and time taken to obtain '100% crystalline' ZSM-5 are summarised in Table 4.2.

Table 4.2 Results for ZSM-5 Syntheses.

Code	Mixture Si/Al	Initial pH	Final pH	pH Change	t (days) 100% ZSM-5
B1	-	11.28	10.88	-0.40	52
C1	540	11.24	10.85	-0.39	25
C2	180	11.19	10.83	-0.36	25
C3	60	11.06	10.79	-0.27	25
C4	20	10.82	10.42	-0.40	25
D1	540	11.35	11.19	-0.16	1.75
D2	180	11.30	11.01	-0.29	1.75
D3	60	11.28	11.08	-0.20	3.92
D4	20	11.01	10.97	-0.04	*
E1	540	11.38	11.05	-0.33	26
E2	180	11.25	10.94	-0.31	26
E3	60	11.07	10.72	-0.35	35
E4	20	10.77	10.66	-0.11	*
F1	60	11.03	10.71	-0.32	21

The asterix in Table 4.2 indicates that the product was amorphous.

Reaction mixtures with Si/Al=540, 180 and 60 crystallised to ZSM-5 irrespective of aluminium source. The reaction mixture which contained aluminium sulphate at Si/Al=20 gave ZSM-5 at 95°C (C4) but not at 150°C (D4), where it remained amorphous. Examples of the XRD patterns of the as-made precursor TPA-ZSM-5 and the calcined H-ZSM-5 are in Figures 4.1 and 4.2. The aluminium nitrate preparation with Si/Al=20 at 95°C (E4) also failed to give ZSM-5 as product, but a transient crystalline phase (which could not be identified) was observed; this later collapsed and the final product was amorphous.

The pH profiles for the crystallisations with aluminium sulphate at 95°C (C1-4) are plotted along with a pH curve for a silicalite synthesis (B1), in Figure 4.3. The crystallisations which contained aluminium were all complete after 25 days; this was confirmed by the XRD patterns of samples taken during the syntheses. The silicalite synthesis took around 50 days.

The addition of aluminium to the preparations appeared to halve the crystallisation time, from about 7 to 3.5 weeks. The addition of aluminium sulphate decreased the pH of the initial reaction mixture,

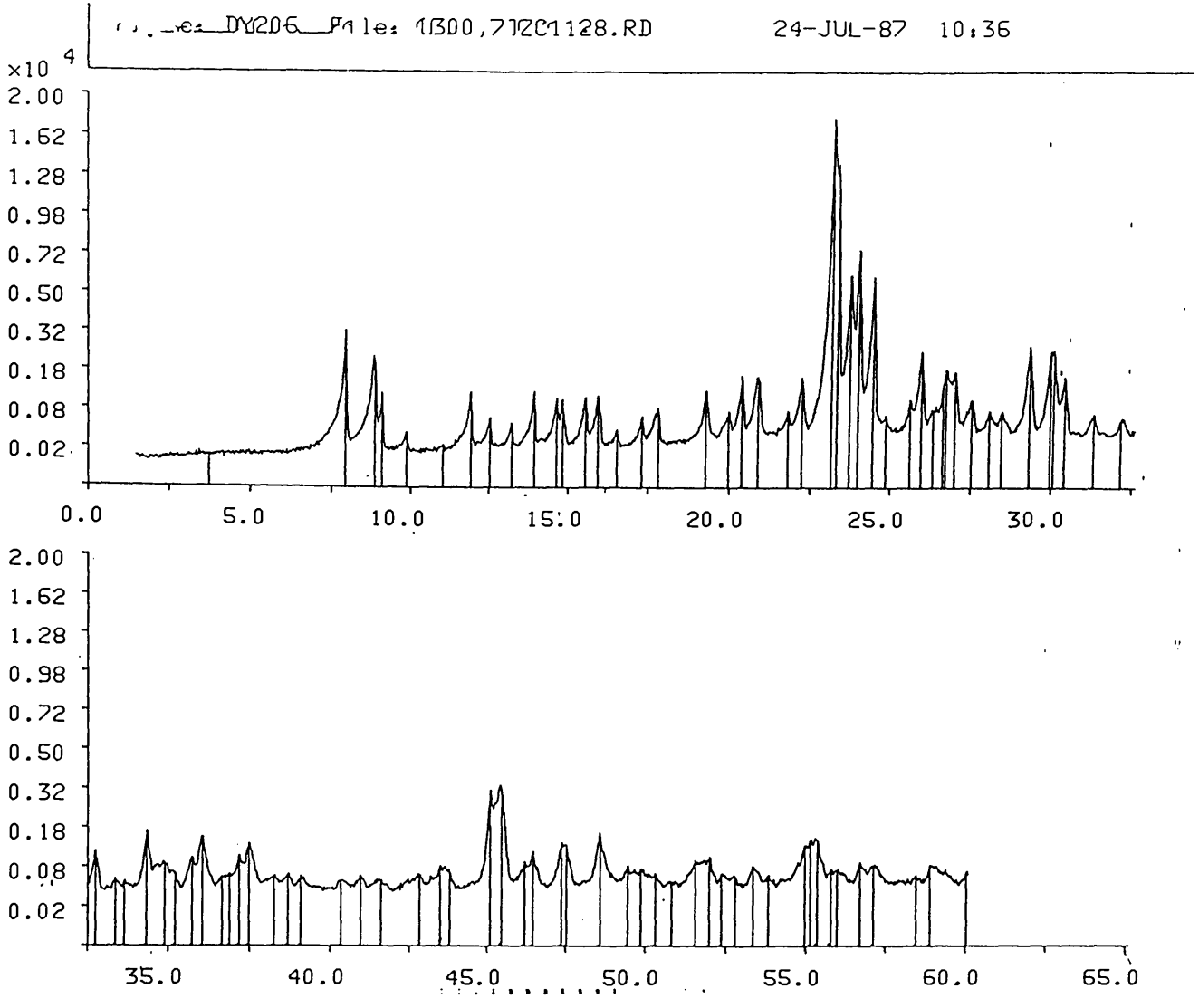

Figure 4.1 XRD pattern of TPA-ZSM-5 (C4)

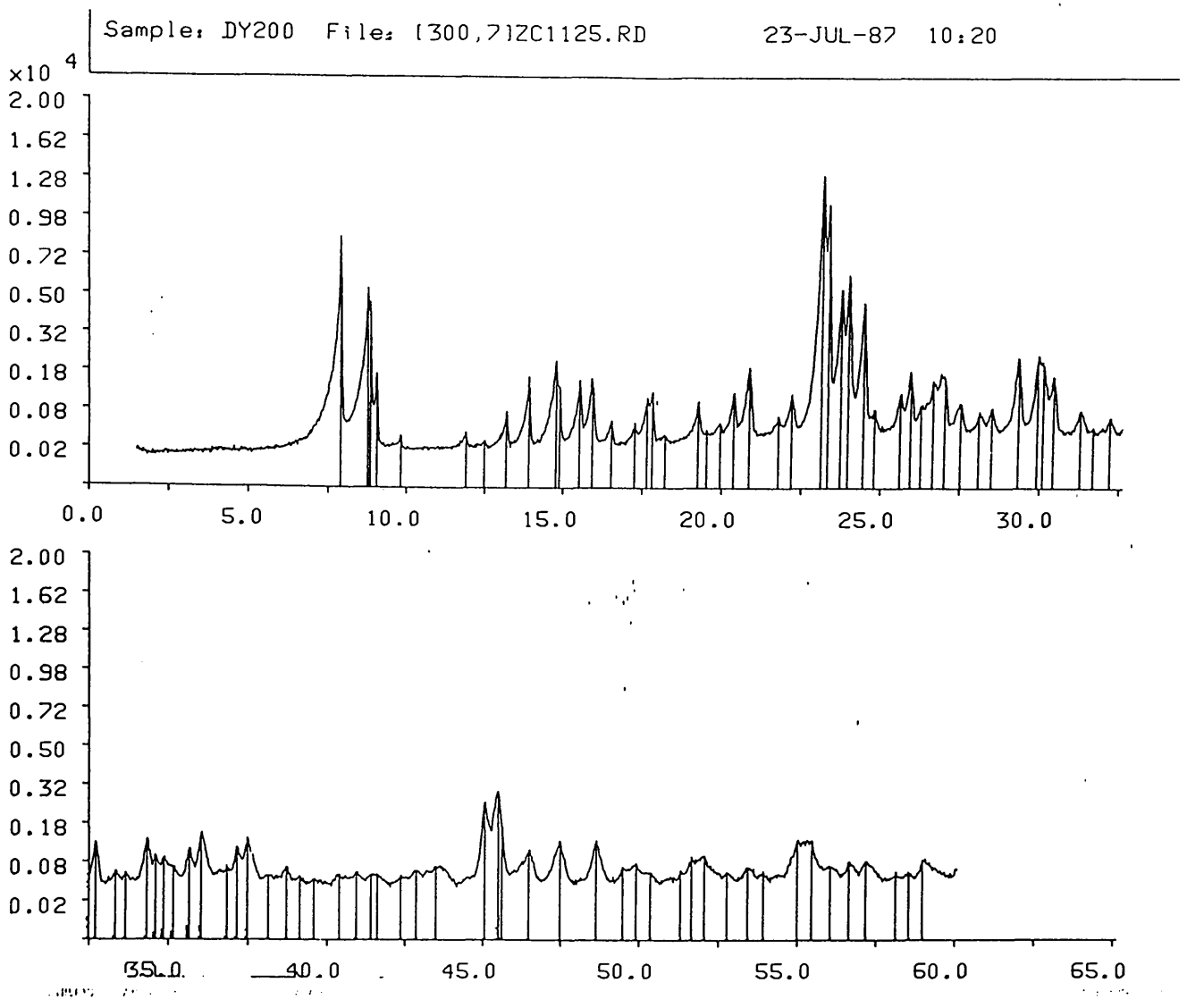

Figure 4.2 XRD pattern of H-ZSM-5 (C4)

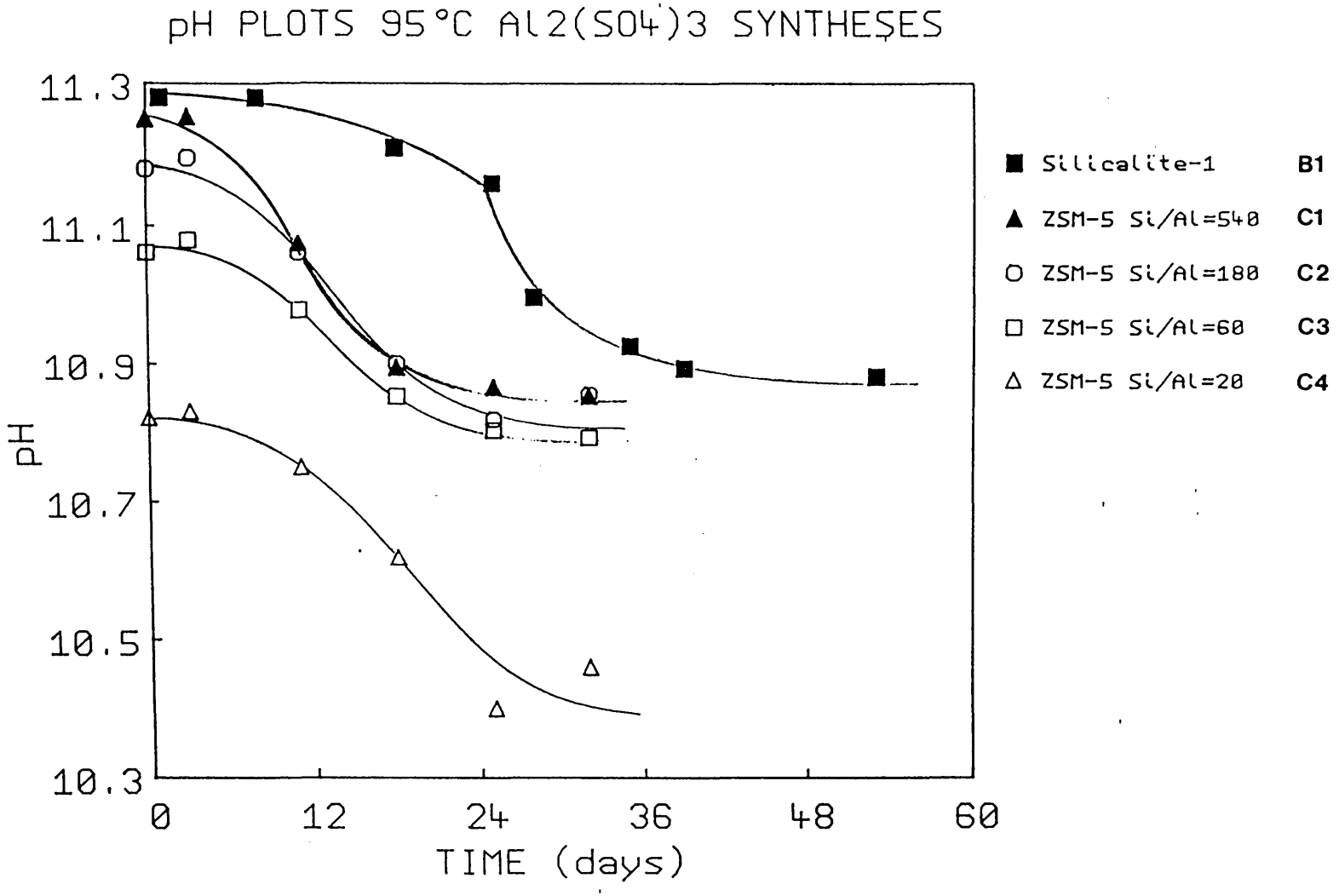

Figure 4.3 pH profiles for ZSM-5 syntheses (B1, C1-4)

but this did not seem to affect crystallisation times.

The 150°C reaction mixtures which contained aluminium sulphate gave ZSM-5 in three out of four preparations, D1 to D3. The Si/Al=20 (D4) synthesis was amorphous after 14 days. The Si/Al=540, 180 and 60 reaction mixtures were adjudged 100% crystalline, by XRD, after 40 (D1 and D2) and 90 (D3) hours. The pH profiles of the ZSM-5 crystallisations from the 150°C syntheses (D1-3) are in Figure 4.4. It is noteworthy that the most aluminous gel took about twice as long to crystallise. In contrast the 95°C Si/Al=60 preparation (C3) gave ZSM-5 in about the same time as the other crystallisations in its series (C1-4). These observations suggest that small amounts of aluminium decrease the crystallisation time, with respect to silicalite synthesis, but that with higher aluminium contents the crystallisations take longer or do not occur. The solubility of hydrated alumina increases with temperature, so the higher the synthesis temperature, the greater the amount of aluminium which can be incorporated in the gel. Hence for reaction mixtures of the same stoichiometry, those held at the higher temperature will have the most aluminous solid gel phase and be the slowest to crystallise.

As no sodium hydroxide was used in the preparation of the reaction mixtures, the counter ion for aluminate or silicoaluminate species in the solution phase of the gel must be the tetrapropylammonium ion or the piperazinium ion. However it is believed that most of the aluminium is present as a solid phase, either as hydrated alumina or silica-alumina solid gel phase.

The aluminium nitrate preparations with Si/Al=540, 180 and 60 crystallised at 95°C to ZSM-5 (E1-3). The reaction mixture which had Si/Al=20 (E4) was amorphous after 6 months. After 3 months a transient crystalline phase was observed by XRD, Figure 4.5. The Bragg reflections of this phase are in Table 4.3.

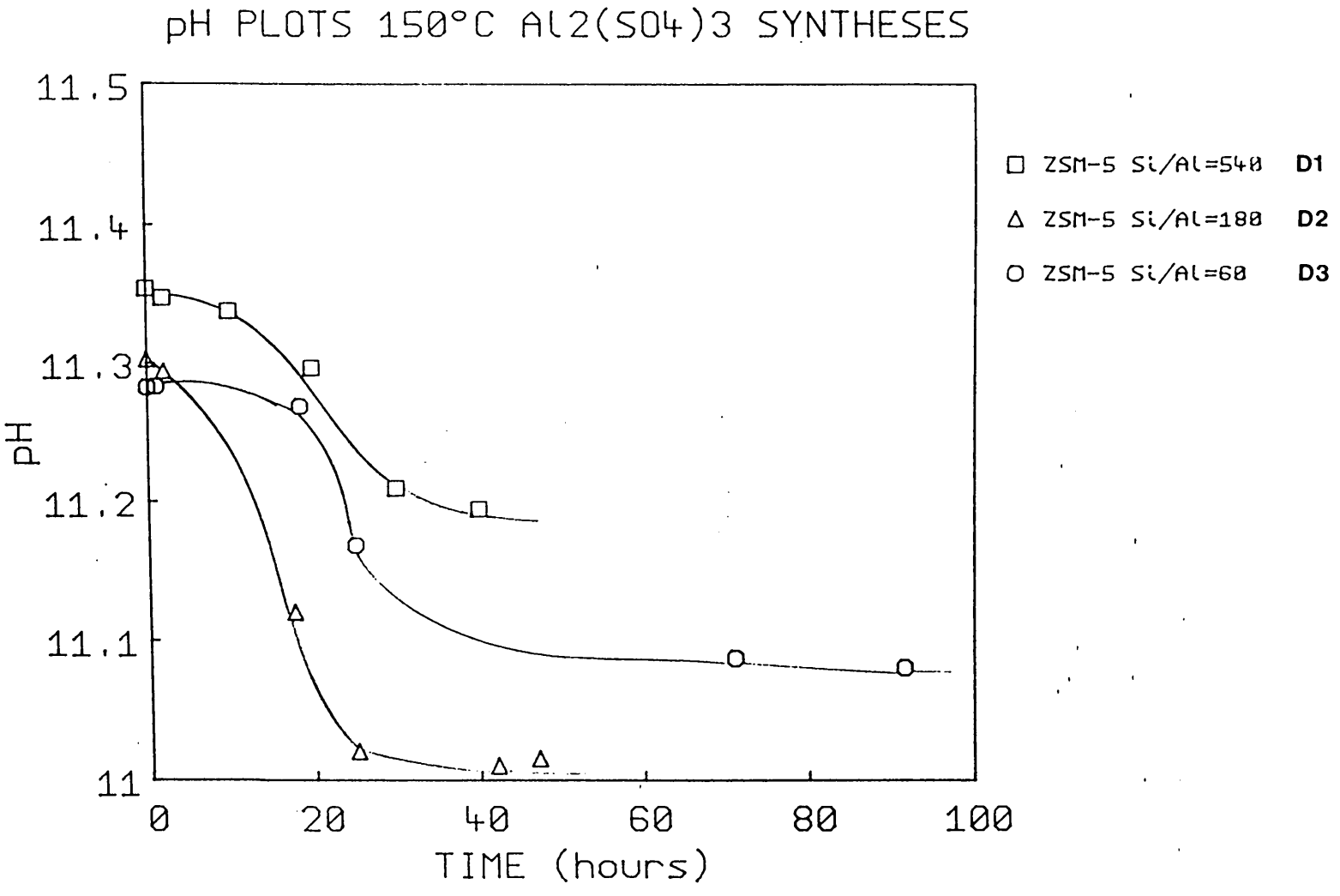

Figure 4.4 pH profiles for ZSM-5 syntheses (D1-3)

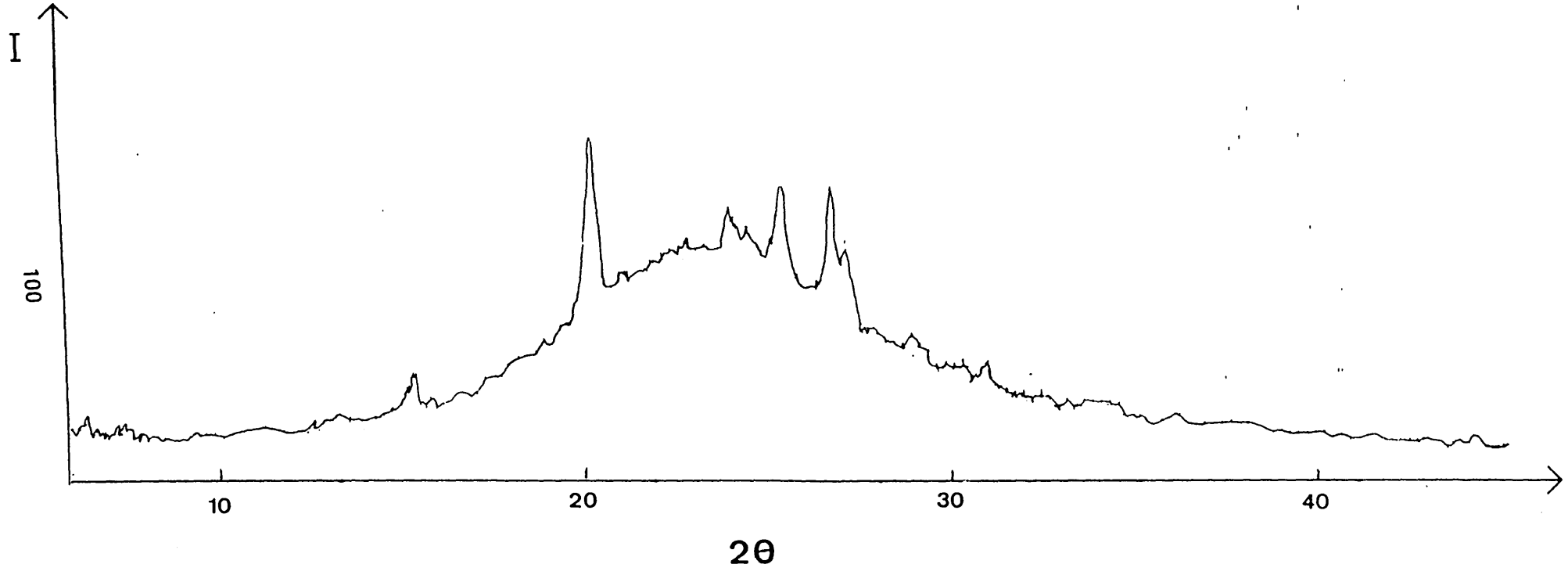

Figure 4.5 XRD pattern of transient phase (E4)

Table 4.3 Peak Positions of Transient Phase

2θ	d(Å)
15.6	5.68
20.9	4.24
23.2	3.83
25.6	3.47
26.0	3.42

This product was heavily contaminated with amorphous material, as shown by the broad hump between 20-30 2θ. The XRD pattern was run on the range $2x10^3$, a much more sensitive scale than that normally used.

The phase was analysed by thermal gravimetry (TG) and differential thermal analysis (DTA). TG indicated that the sample contained 12.4% water and 39.4% organic material (Figure 4.6). The DTA trace, Figure 4.7, showed three thermal events. The broad endotherm at 102°C corresponds to loss of water, the exotherm at 320°C is consistent with oxidative degradation of the organic material, which is possibly TPA. The second exotherm at 566°C is probably due to further organic removal, perhaps piperazine, followed by structure collapse. A literature search was conducted but no phase was found which fitted the analytical results. The experimental data suggest that the material is an organic silicate. Under the SEM the material resembled amorphous blobs, and it seems likely that the crystals were too small and too few to be detected in the amorphous matrix.

The pH profiles for the ZSM-5 crystallisations from the reaction mixtures which contained aluminium nitrate are shown in Figure 4.8 (E1-3). The preparations which had Si/Al ratios of 540 (E1) and 180 (E2) were both adjudged 100% crystalline after 26 days, about 1 day longer than for the comparative aluminium sulphate ZSM-5 syntheses. The Si/Al=60 mixture (E3) was 100% crystalline after around 35 days. This confirms the finding from the 150°C aluminium sulphate preparations, that the greater the amount of aluminium in the gel, the slower the ZSM-5 crystallisation.

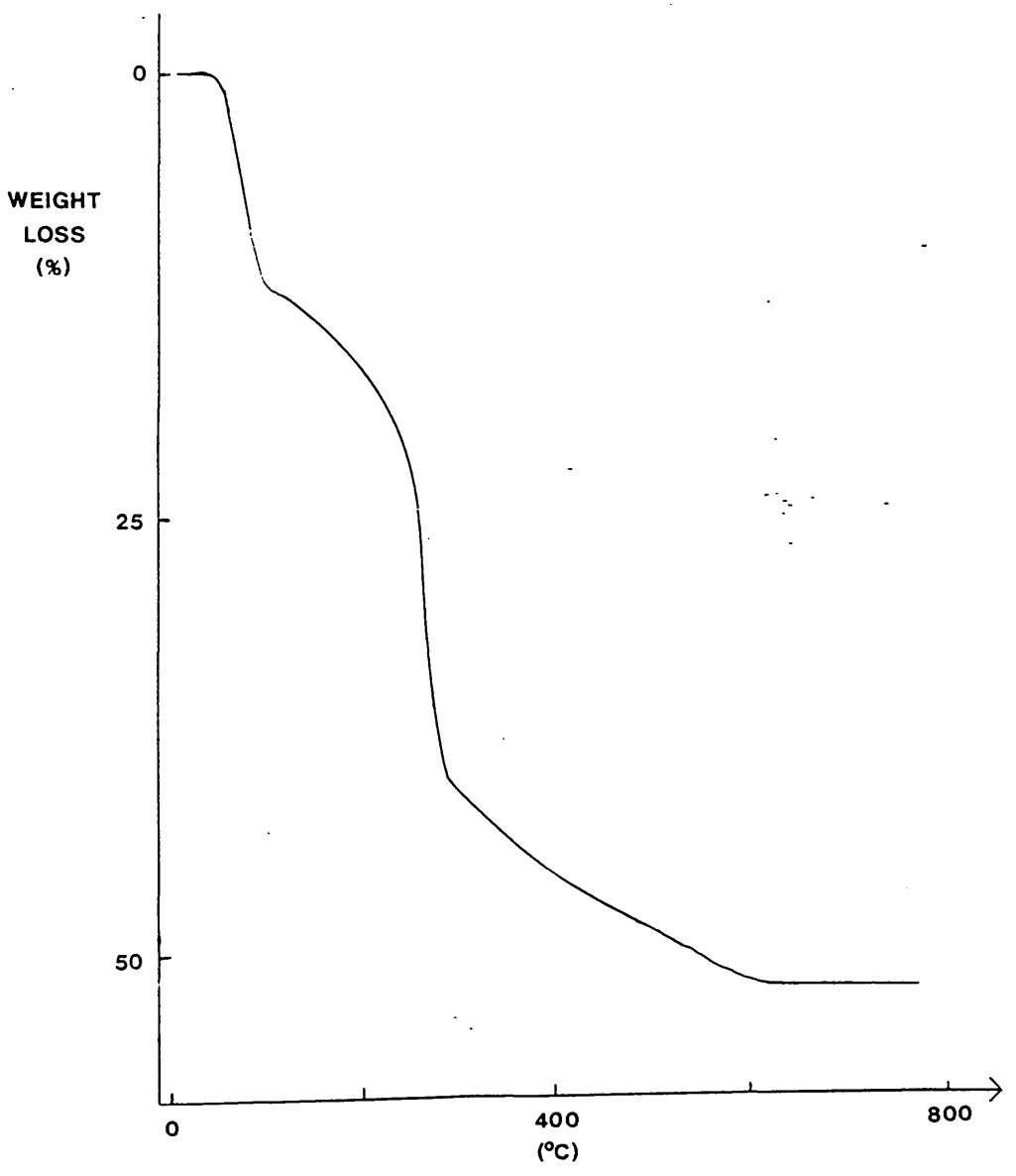

Figure 4.6 TG trace of transient phase (E4)

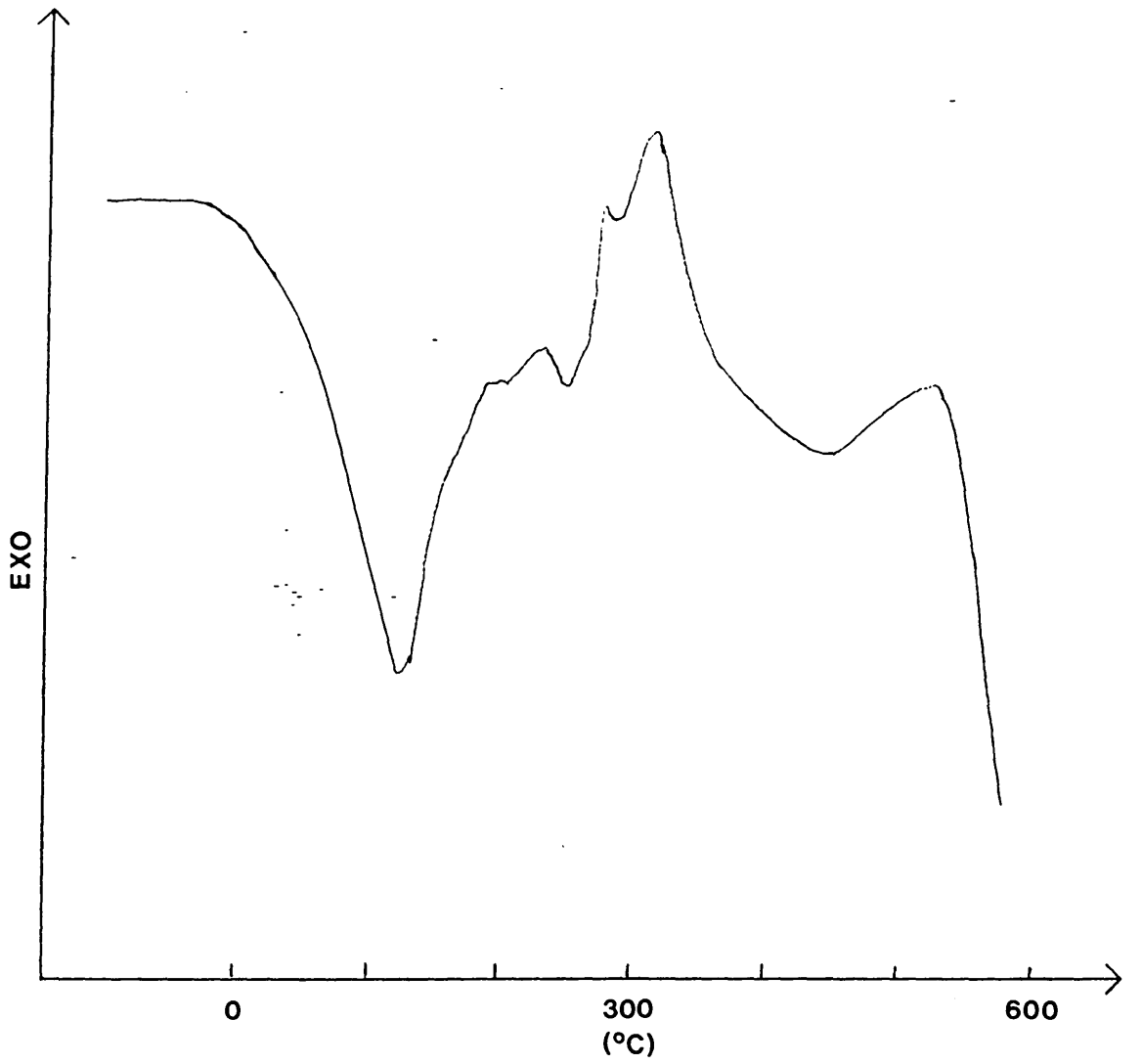

Figure 4.7 DTA trace of transient phase (E4)

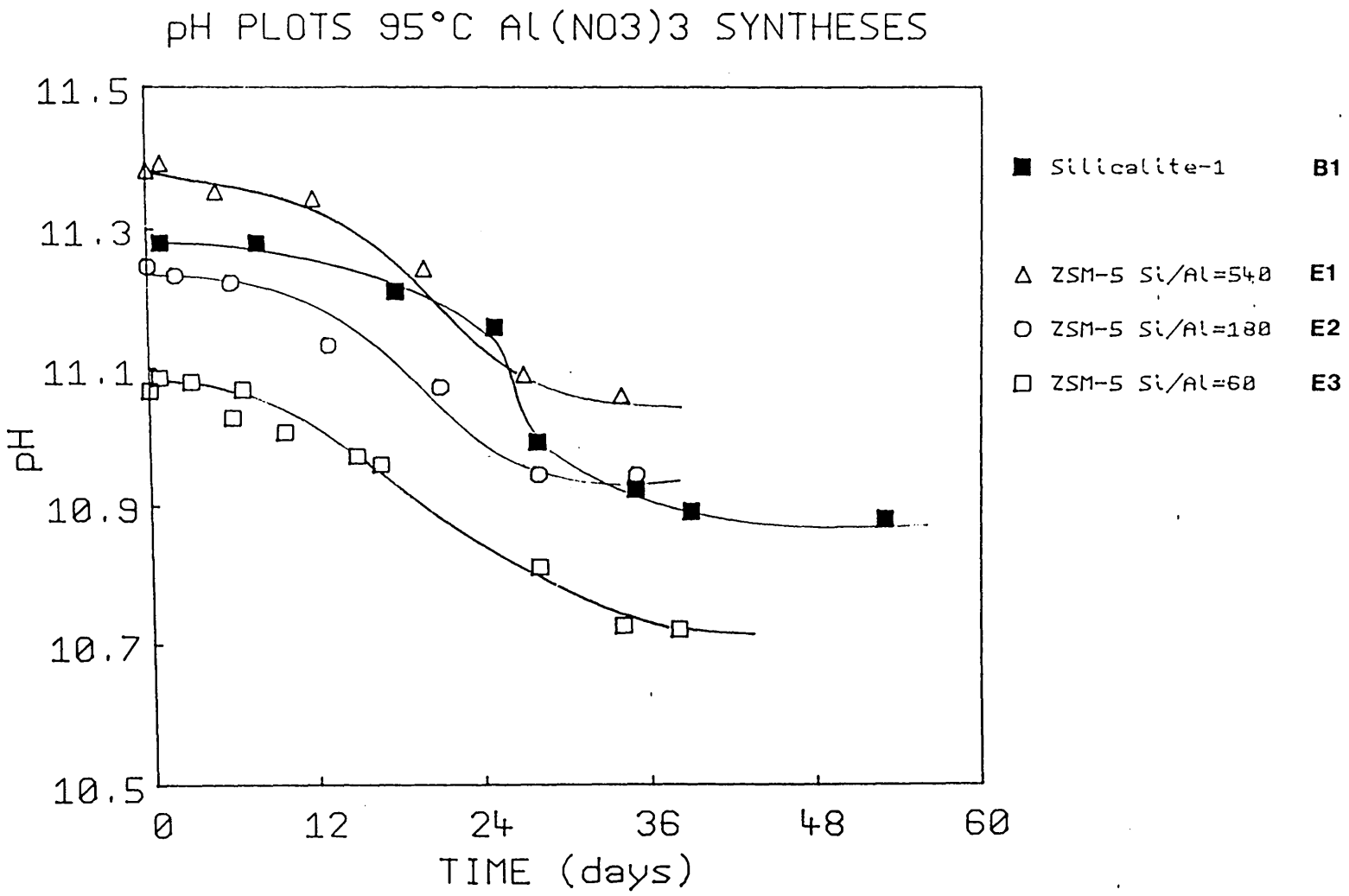

Figure 4.8 pH profiles for ZSM-5 syntheses (B1, E1-3)

A second crystallisation of ZSM-5 with aluminium nitrate to Si/Al=60 was conducted at 95°C after the reaction mixture had been aged for 1 month at room temperature (F1). The pH profile for this crystallisation is plotted with that of the unaged mixture (E3) in Figure 4.9. The initial and final pH values are almost the same for each synthesis. The crystallisation was much faster for the aged gel and was complete after 21 days, whereas 35 days were required for the unaged mixture. These results suggest that some primary nucleation occurs during the aging process and hence the crystallisation starts more rapidly.

The pH profiles of each of the unaged Si/Al=60 crystallisations (C3, D3 and E3) are compared in Figure 4.10. The 150°C mixture which contained aluminium sulphate (D3) was adjudged 100% crystalline after 90 hours. The same preparation at 95°C took 25 days (C3). The reaction mixture which contained aluminium nitrate at 95°C took 35 days (E3). Hence aging, aluminium source and reaction temperature have all been shown to influence crystallisation from the TPA/Piperazine systems.

4.3.2 Bulk Analysis

Bulk analyses of the products were carried out by ICI and the Si/Al ratios calculated from these results are given in Table 4.4. A silicalite sample, B1, is included in the table.

Table 4.4 Bulk Analysis of the ZSM-5 Products

Code	Reaction Mixture		ZSM-5 Product	
	Si/Al	Al/Si	Si/Al	Al/Si
B1	-	-	1193	0.00084
C1	540	0.00185	802	0.00125
C2	180	0.00555	302	0.00331
C3	60	0.01667	65	0.01530
C4	20	0.05000	30	0.03333
D1	540	0.00185	585	0.00171
D2	180	0.00555	189	0.00529
D3	60	0.01667	72	0.01390
E1	540	0.00185	882	0.00113
E2	180	0.00555	207	0.00483
E3	60	0.01667	52	0.01920

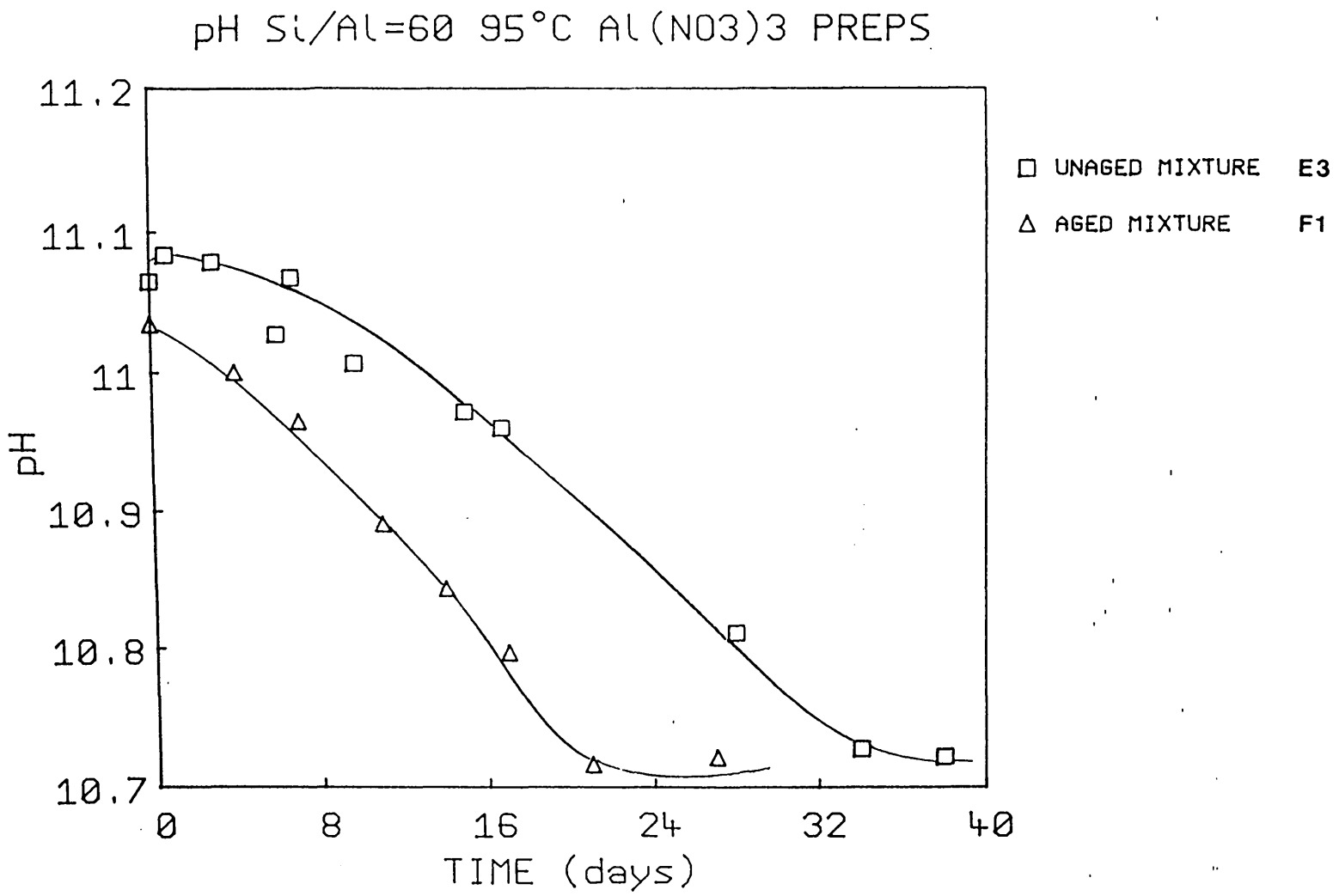

Figure 4.9 pH plots for aged (F1) and unaged (E3) syntheses

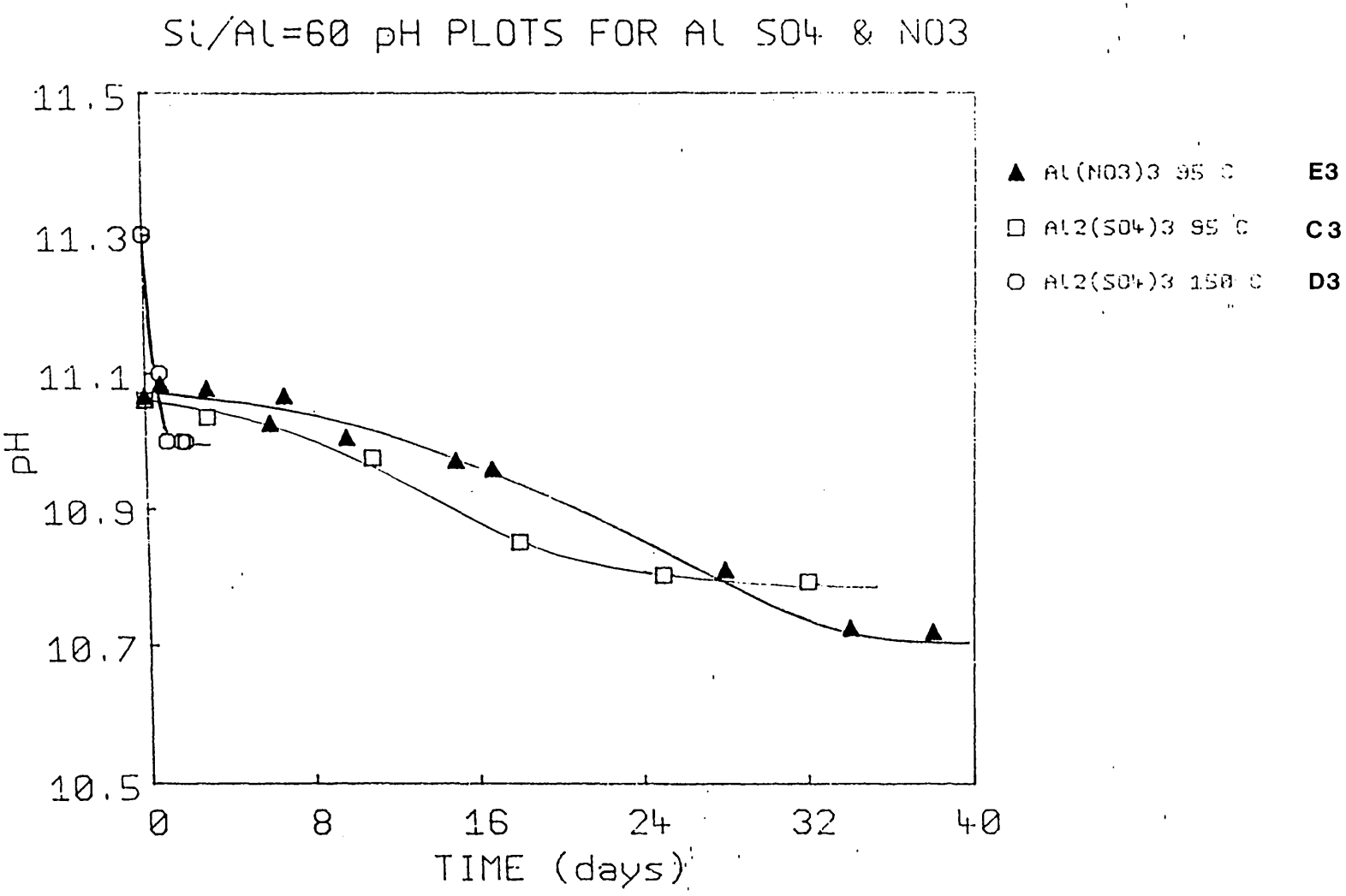

Figure 4.10 pH plots for crystallisation of ZSM-5 from unaged reaction mixtures with Si/Al=60 (C3, D3 and E3)

Figure 4.11 shows the Al/Si ratio of the product as a function of that for the reaction mixture. It can be seen that in most cases the product has a lower Al/Si ratio than that of the reaction mixture. This is in marked contrast to conventional ZSM-5 syntheses from inorganic base systems, which invariably give products with Al/Si ratios higher than that of the reaction mixtures. This is readily explained by the fact that much of the silica remains in the alkali rich solution phase. In systems with organic bases little silicon remains in the solution phase and the Si/Al ratios of the reaction mixtures and the bulk product are expected to be in close agreement. This is represented by the straight line in Figure 4.11. The maximum amount of aluminium that could be incorporated in an ideal TPA-ZSM-5 is given by the composition:

$(TPA)_4\ (AlO_2)_4\ (SiO_2)_{92}$

which corresponds to a Al/Si ratio of 0.043.

It is noteworthy that the product (C4) obtained from the reaction mixture with Al/Si=0.05 had a Al/Si less than the maximum possible value of 0.043.

It is important to recognise that the bulk analyses given in Table 4.4 do not necessarily represent the Al/Si ratios of the frameworks; both the Al and Si could be present as amorphous impurities external to the zeolite crystals and in the channel system.

The foregoing results tell us little about the quality of the ZSM-5 products. For this we must turn to thermal analysis. This indicates which ZSM-5 samples have most aluminium incorporated into their frameworks, and hence which preparations yield the products which are likely to be the best catalysts.

4.3.3 Thermal Analysis

Each ZSM-5 product was analysed by DTA and TG. The DTA of each sample was run with a heating rate of 5°C per minute, sample size of around 50mg and a chart recorder speed of 2mm per minute. The

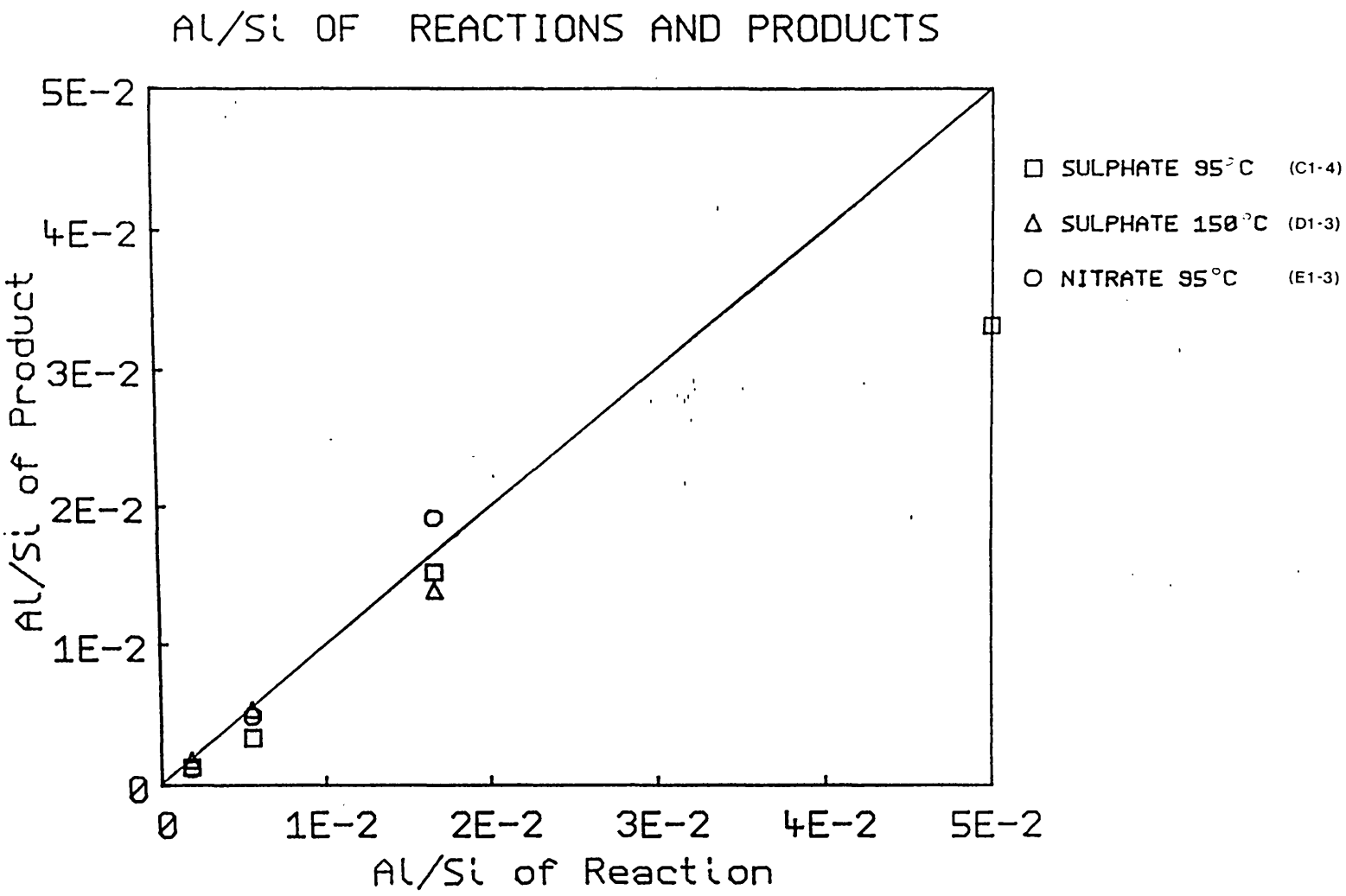

Figure 4.11 Comparison of the Al/Si ratios of reactions and ZSM-5 products

atmosphere was static air. TG analyses were run with about 5mg of material at a heating rate of 10°C per minute in a 15ml per minute flow of air.

DTA traces for the TPA-ZSM-5 products prepared from aluminium sulphate based reaction mixtures at 95 and 150°C are shown in Figures 4.12 and 4.13 respectively. The DTA traces of the ZSM-5 products crystallised at 95°C from reaction mixtures which contained aluminium nitrate are in Figure 4.14. The TG traces are shown in Figures 4.15-17.

For all the ZSM-5 samples there were two distinct thermal events. A major exotherm with a peak position which varied in the range 380-440°C. This peak was often split due to oxygen starvation. It is thought to be due to the oxidative degradation of the TPA ion and its peak temperature increases with the aluminium content of the product. It is also found in silicalite and hence it is ascribed to TPA associated primarily with hydroxide or broken siloxane bonds and to a lesser extent with framework aluminium. The other exotherm was observed as a shoulder or a broad peak centred at 460°C. This feature became more pronounced as the aluminium content increased and it is believed to be due to TPA specifically associated with framework aluminium. In summary then the two major thermal events are related to the environment of the TPA ion in the zeolite framework. Two extreme situations are recognised. TPA associated with broken siloxane bonds or silanols (type A) and TPA associated with aluminium (type B). For all the samples investigated type A sites are dominant, but the position of their exotherm varies with aluminium content which suggests that their nature is changed by the incorporation of aluminium. The peak temperature of the exotherm associated with the type B is independent of the aluminium content of the sample but its peak area increases. This shows that the nature of the type B site is independent of the aluminium content of the sample, but the number of type B sites increases with it. In principle it should be possible to deduce the framework Al/Si ratio from the peak position of the type A exotherm, or the peak area of the type B exotherm. The latter is difficult to measure for the samples with low aluminium content because for these it exists only

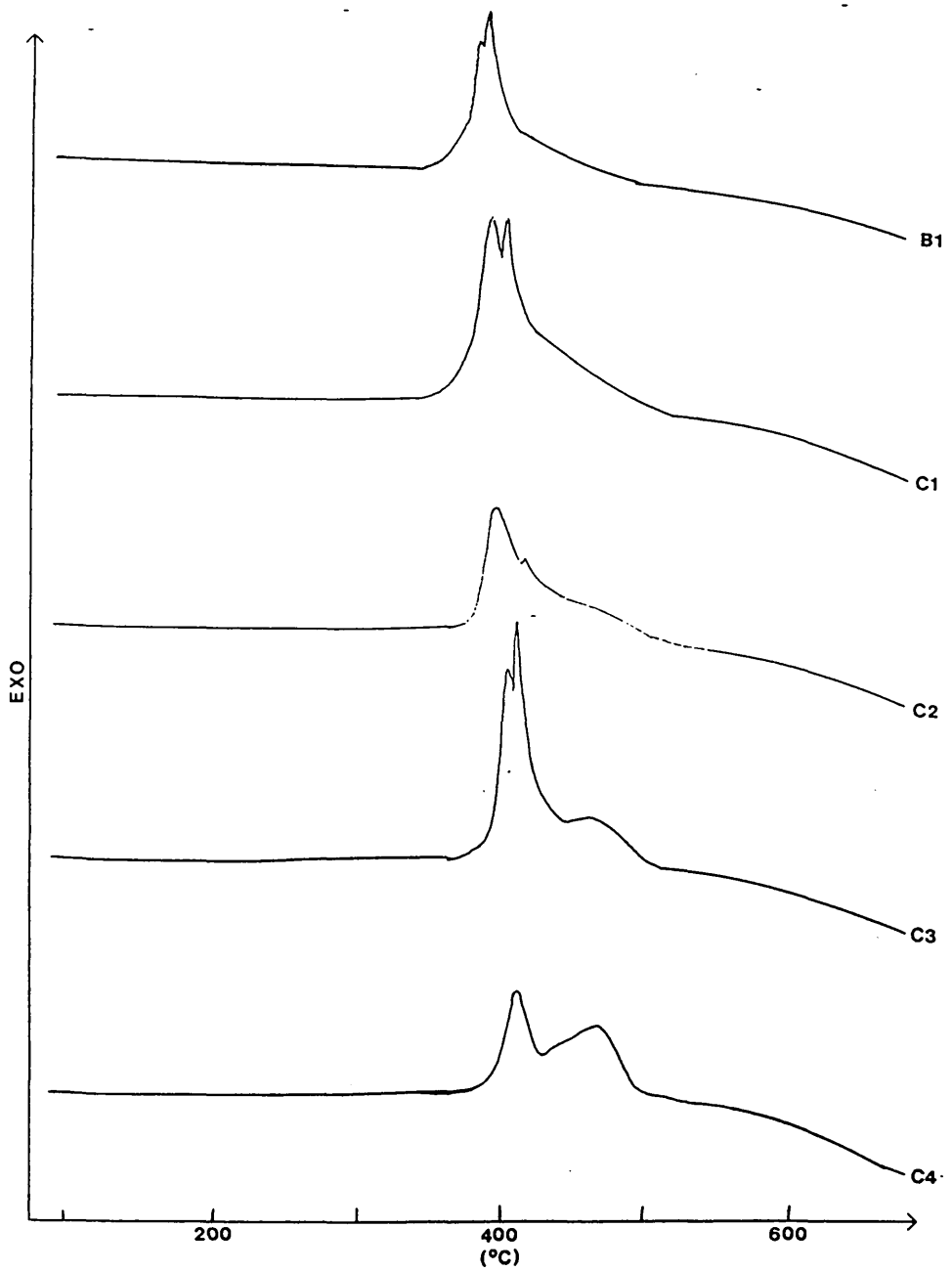

Figure 4.12 DTA traces for ZSM-5 products prepared at 95°C with $Al_2(SO_4)_3$ (C1-4) and silicalite (B1)

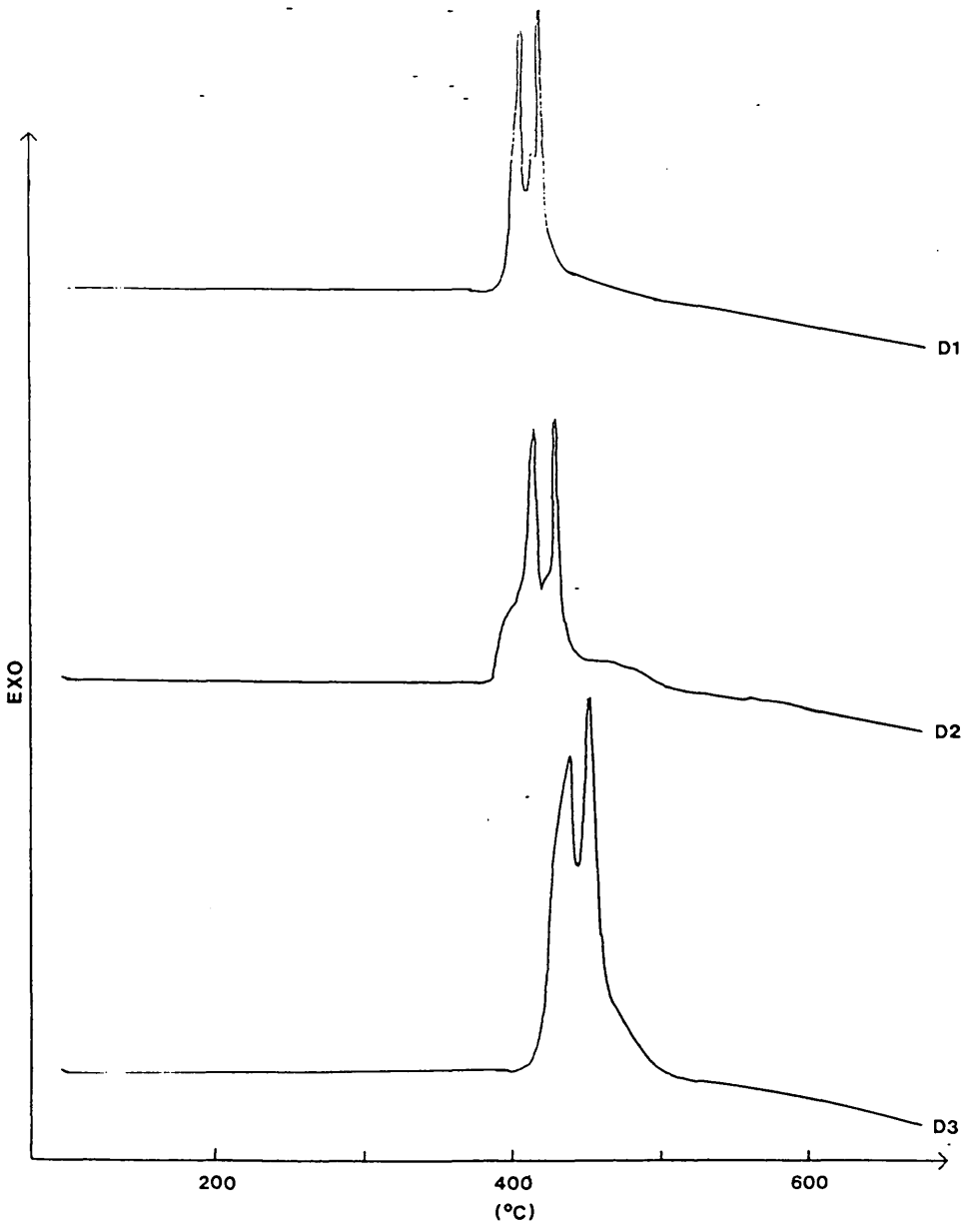

Figure 4.13 DTA traces for ZSM-5 products prepared at 150°C with $Al_2(SO_4)_3$ (D1-3)

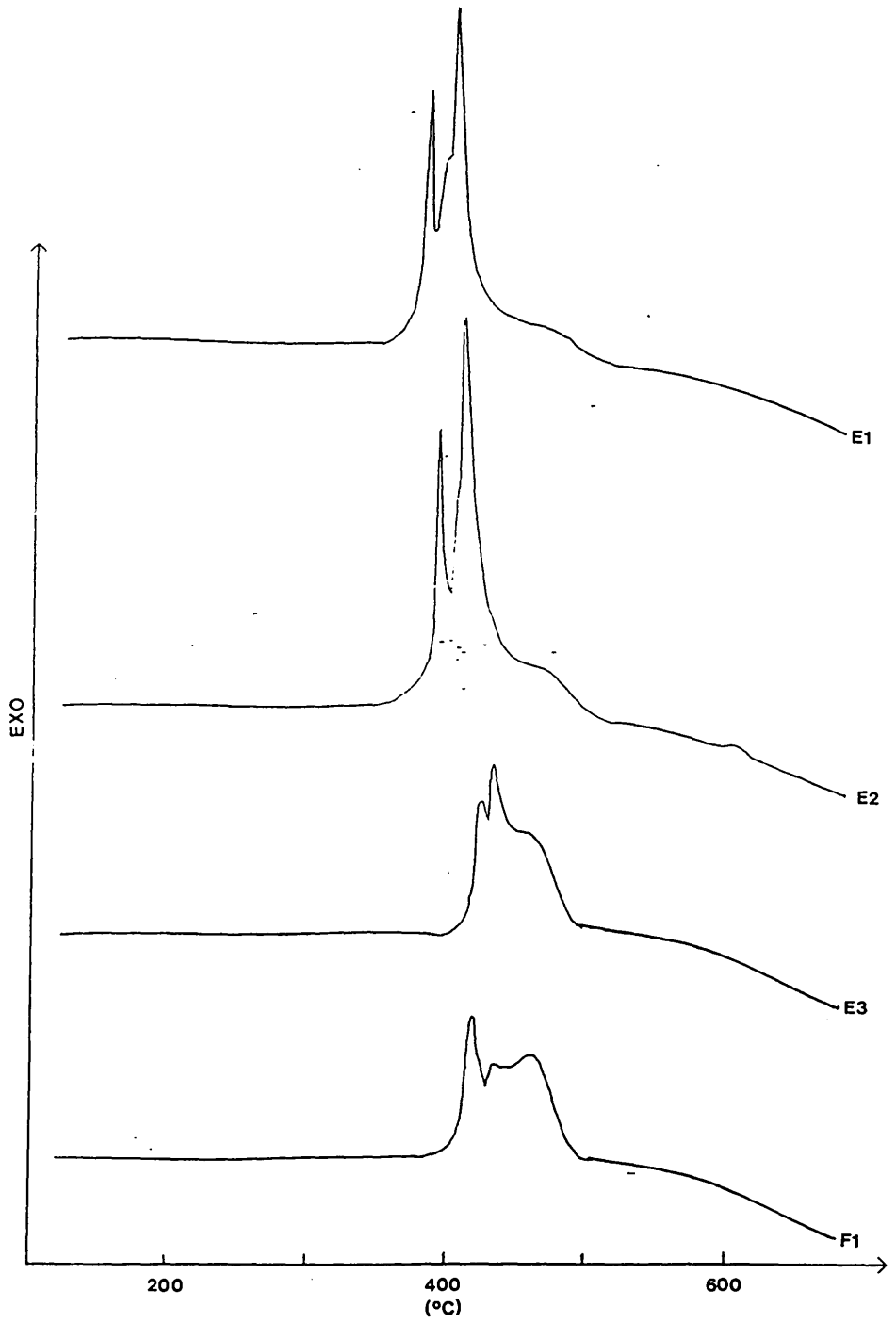

Figure 4.14 DTA traces for ZSM-5 products prepared at 95°C with $Al(NO_3)_3$ (E1-3, F1)

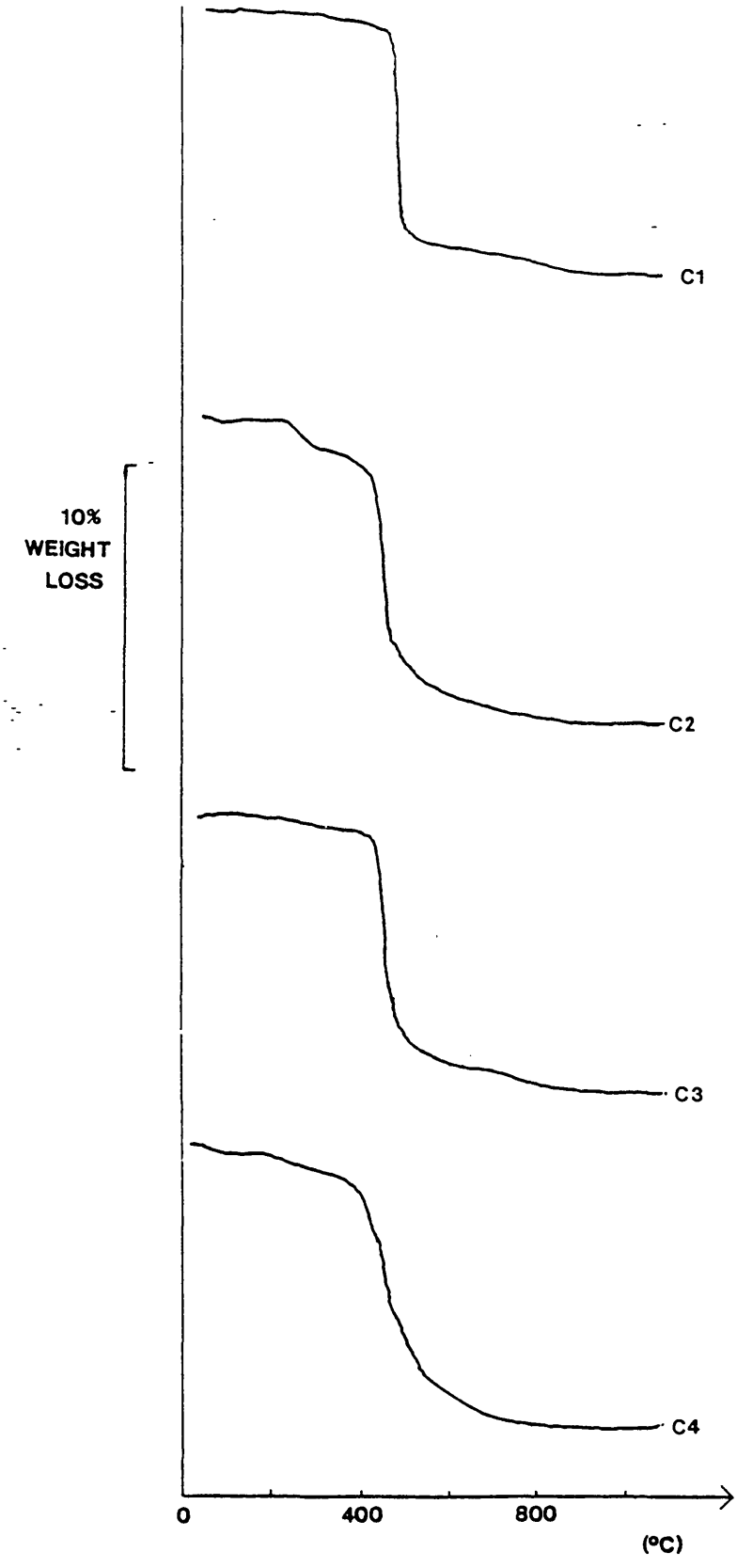

Figure 4.15 TG traces for ZSM-5 products prepared at 95^0C with $Al_2(SO_4)_3$ (C1-4)

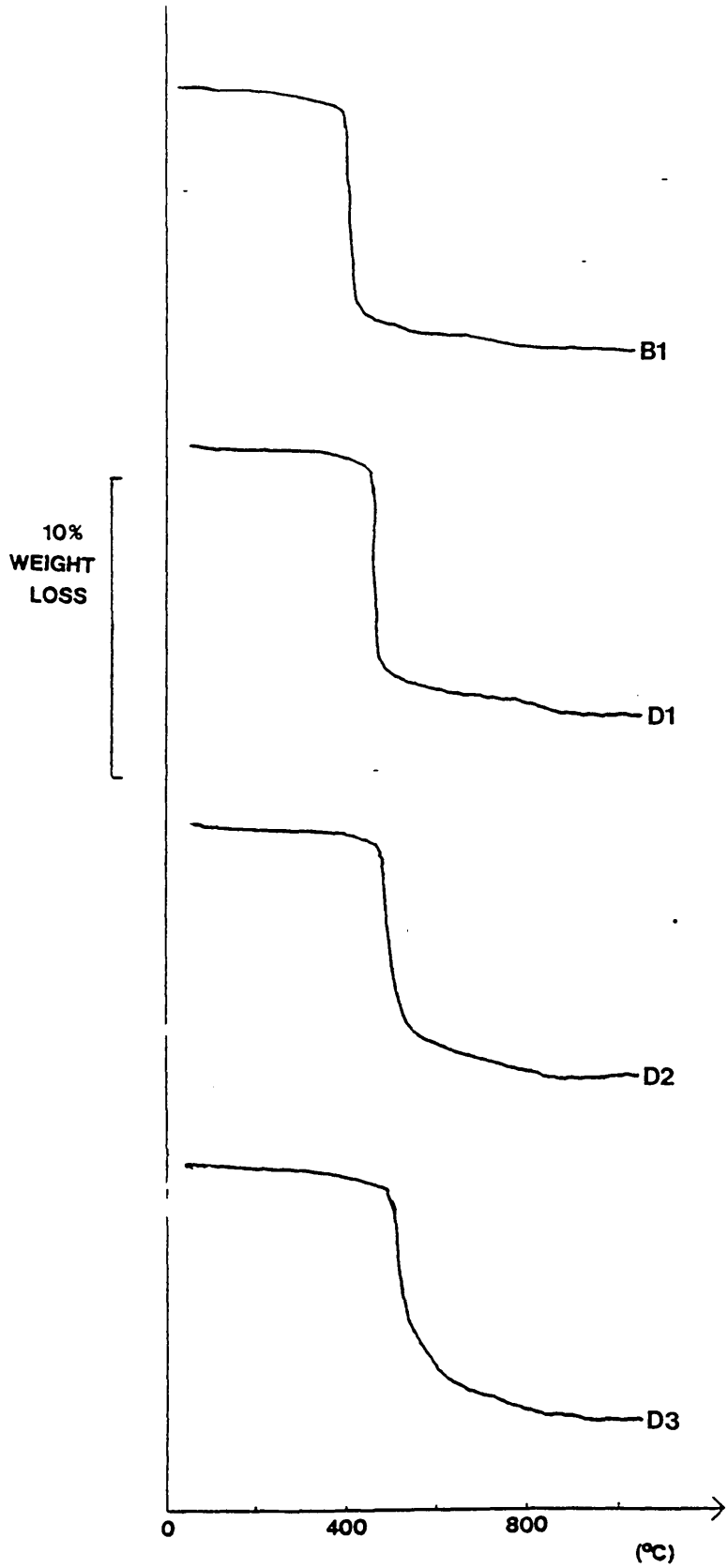

Figure 4.16 TG traces for ZSM-5 products prepared at 150°C with $Al_2(SO_4)_3$ (D1-3) and silicalite (B1)

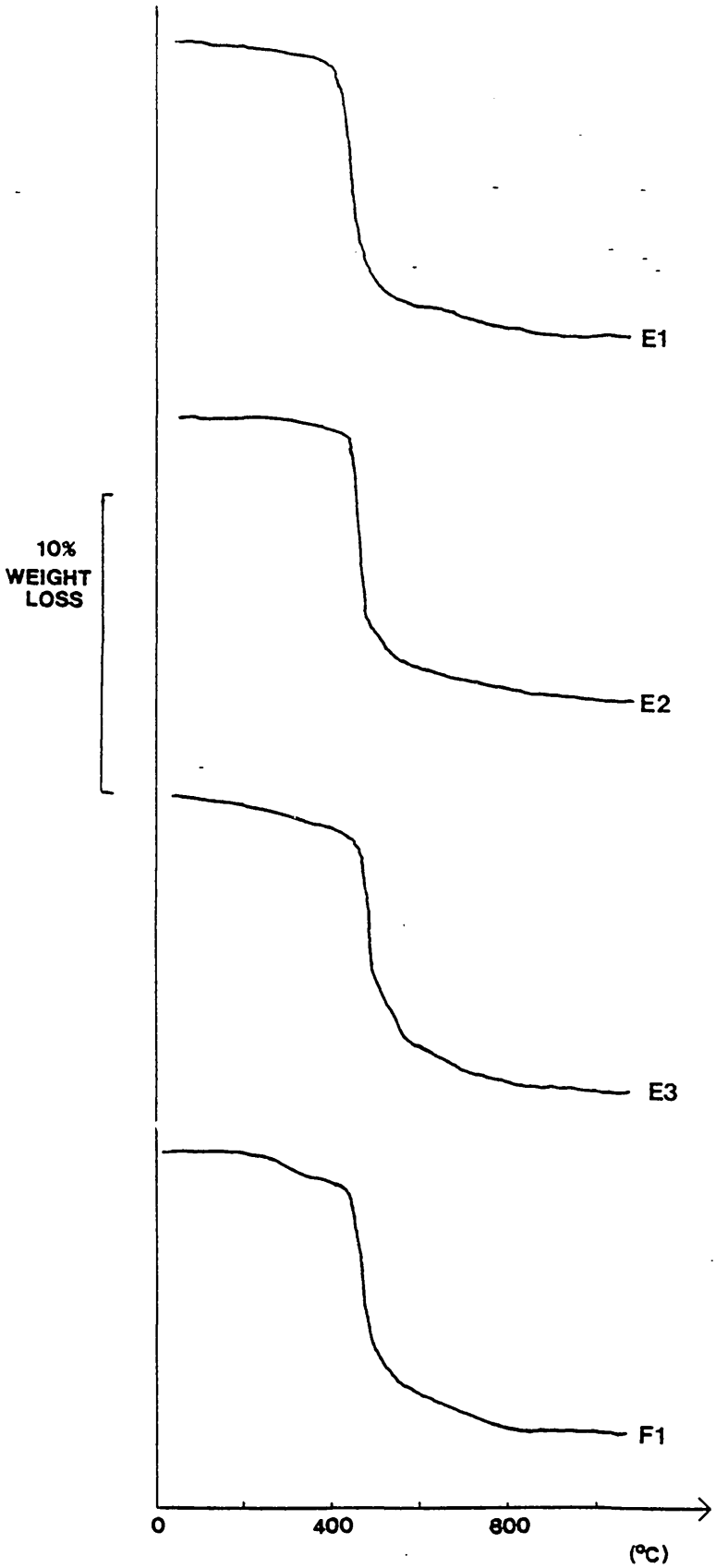

Figure 4.17 TG traces for ZSM-5 products prepared at 95°C with $Al(NO_3)_3$ (E1-3 and F1)

as a slight shoulder on the type A exotherm. This is unfortunate as it is only for the low aluminium content samples that there is a reasonable chance that all of the aluminium is incorporated in the lattice.

For each ZSM-5 sample the DTA exotherm, for the decomposition and combustion of TPA, appeared at a higher temperature than that for silicalite. The data are tabulated in Table 4.5 and are plotted for each synthesis type in Figure 4.18.

If we assume that for very low levels of aluminium, all is incorporated into the zeolite framework we can estimate the framework Al/Si ratios for other samples. This assumes that the peak temperature position varies linearly with Al/Si in the framework.

$$T=T_o+m(Al/Si) \quad [1]$$

where $T=T_o$ when the aluminium content of the framework is zero and Al/Si corresponds specifically to framework aluminium. For the silicalite B1 and for ZSM-5 sample D1 we shall assume that all the aluminium is in the framework, so we have:

Silicalite B1: T=380°C and Si/Al=1193.3

ZSM-5 D1: T=402°C and Si/Al=585

402-380=m[1/585-1/1193.5]

22=m[(1.709E-3)-(0.8379E-3)]

m=(22E3)/(1.709-0.838)=25258

The value of m and the Si/Al and thermal analysis data for the silicalite and ZSM-5 are then used to calculate To with Equation [1]. This is 359°C for each product. So we have:

T=359+25258(Al/Si) [2]

where Al/Si is specific to the framework and T is the peak temperature of the type A exotherm. Equation [2] was applied to the DTA data for each ZSM-5 product, and the results are shown in Table

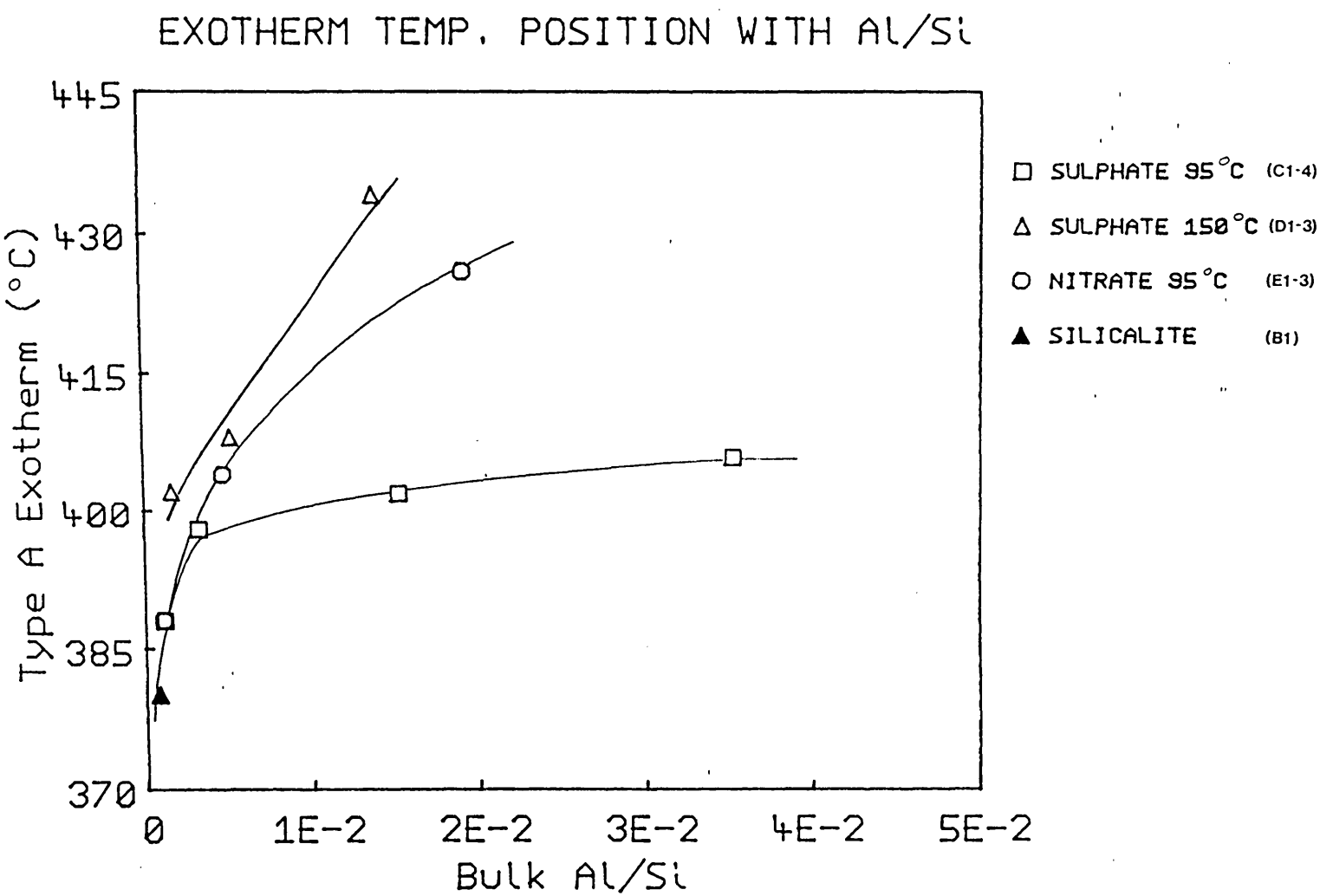

Figure 4.18 Peak temperature of type A exotherm as a function of bulk Al/Si ratio

4.5.

Table 4.5 Framework Aluminium in ZSM-5 Products

ZSM-5 Code	Bulk Al/Si	DTA T (°C)	Framework Al/Si
B1	0.00084	380	0.00084
C1	0.00125	388	0.00115
C2	0.00331	398	0.00154
C3	0.01530	402	0.00170
C4	0.03530	406	0.00186
D1	0.00171	402	0.00170
D2	0.00529	408	0.00194
D3	0.01390	434	0.00297
E1	0.00113	388	0.00115
E2	0.00483	404	0.00178
E3	0.01920	426	0.00265

The Al/Si ratio of the framework estimated with equation [2] is shown as a function of that for the bulk material in Figure 4.19. This shows that higher incorporations of aluminium are favoured by crystallisation at higher temperatures and by using nitrate in preference to sulphate. It is also instructive to consider the incorporation of aluminium in terms of the number of aluminium atoms per unit cell of 96 T-atoms. This is given by the equation:

$$(Al)f=[R/(1+R)]96$$

where R is the Al/Si ratio of the framework. The calculated values of aluminium in the framework are given with the aluminium content of the reaction mixtures, calculated on the same basis, in Table 4.6.

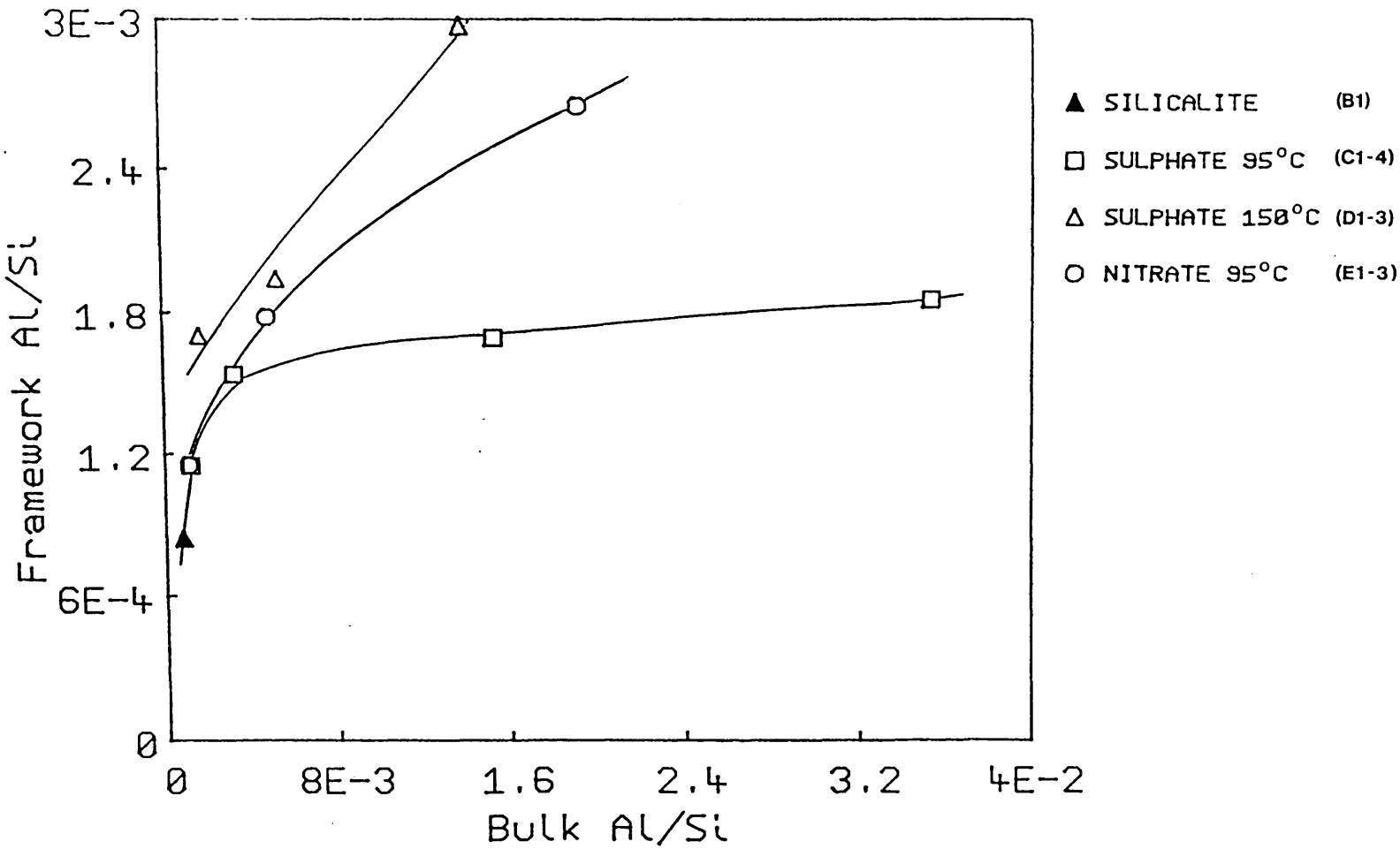

Figure 4.19 Incorporation of framework aluminium

Table 4.6 Aluminium Atoms per Unit Cell

ZSM-5 Code	Framework Aluminium	Reaction Aluminium
B1	0.08	-
C1	0.11	0.18
C2	0.15	0.53
C3	0.16	1.58
C4	0.18	4.57
D1	0.16	0.18
D2	0.19	0.53
D3	0.29	1.58
E1	0.11	0.18
E2	0.17	0.53
E3	0.25	1.58

It is significant that the values for framework aluminium are well below the theoretical value of four. In the case of the 95°C reactions with sulphate counter ion, it appears that the maximum incorporation of aluminium is less than 0.2 atoms per unit cell; although a maximum value of 0.4-0.5 can be estimated from Figure 4.20 for the other reactions. In practice crystallisation did not occur from the requisite aluminium rich reaction mixture.

Finally, it must be recognised that there is a considerable degree of uncertainty associated with the foregoing analysis. Because of oxygen starvation splitting the actual peak temperature, it is difficult to determine its position with certainty. However, the major error lies in the assumption that the peak temperature varies linearly with the framework Al/Si ratio. There is no evidence for this other than the linear relation between peak temperature and the bulk Al/Si ratios observed for the ZSM-5 products which contained least aluminium. The peak areas for the type B exotherms strongly suggest that the framework Al/Si ratios in Table 4.5 are under estimates. For example, for the DTA trace of ZSM-5 product C4 the peak areas for the type A and B exotherms are about the same, but the fraction of the Al estimated to be in the framework is about 5%. Furthermore, the results are inconsistent. The products obtained with aluminium sulphate at 150°C show little evidence of type B exotherms, yet the analysis of their type A exotherms suggests they incorporate the most framework aluminium. A better correlation is

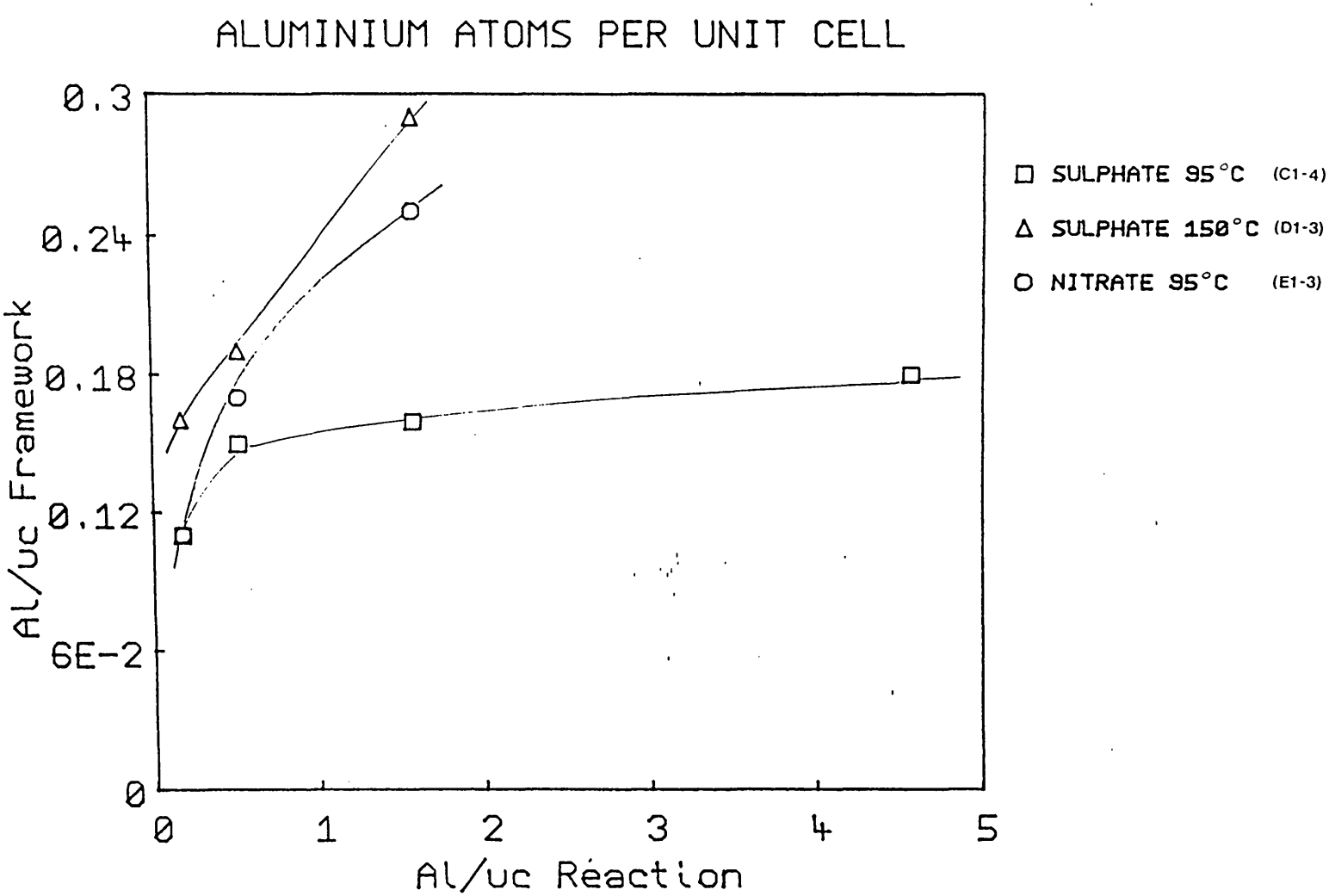

Figure 4.20 Aluminium atoms per unit cell

obtained in the other two cases, but the situation is far from satisfactory. The shape of the DTA trace may possibly depend on many other factors, for instance particle size/shape or packing density, besides the Al/Si ratio.

XPS (X-ray photoelectron spectroscopy) surface elemental analytical data were supplied by ICI Chemicals and Polymers Limited, Wilton. for two ZSM-5 products, C4 and E3. Table 4.7 summarises the bulk and surface Al/Si ratios for each product.

Table 4.7 XPS and Bulk Analysis Al/Si

Ratios for Materials C4 and E3.

ZSM-5 Code	Surface Al/Si	Bulk Al/Si	Framework Al/Si
C4	0.163	0.0353	0.00186
E3	0.095	0.0192	0.00265

For each product, the Al/Si ratio at the surface was about five times greater than that of the bulk product. It is clear that there was an uneven distribution of aluminium in the product crystals and that their surfaces were aluminium rich.

4.3.4 Scanning Electron Microscopy

The size of the ZSM-5 crystals decreased as the amount of aluminium in the reaction mixture was increased. Table 4.8 outlines which products correspond to the prints on Plates 4.1 to 4.4.

Table 4.8 Scanning Electron Micrographs

of ZSM-5 Products.

Code	Plate	Print
C1	4.1	1
C2	4.1	2
C3	4.1	3
C4	4.1	4
*	4.2	1
D1	4.2	2
D2	4.2	3
D3	4.2	4
B1	4.3	1
E1	4.3	2
E2	4.3	3
E3	4.3	4
E3	4.4	1
F1	4.4	2

The material which is marked with an asterix was a silicalite synthesised at 150°C. The ZSM-5 products C1-C4 can be compared with the scanning electron micrograph of silicalite B1 shown in Plate 4.3.

Plate 4.4 shows the affect of gel aging on crystal size. The crystal size decreased after the gel was aged for 1 month (at room temperature). However, this led to little change in the amount of framework aluminium in the product; its DTA peak position was almost identical to that of the ZSM-5 product derived from the unaged reaction mixture. The aging appeared to promote primary nucleation which resulted in the formation of smaller crystals.

The addition of aluminium to the reaction mixtures appears to promote nucleation, to decrease the crystallisation time (Section 4.3.1) and to promote the formation of smaller crystals.

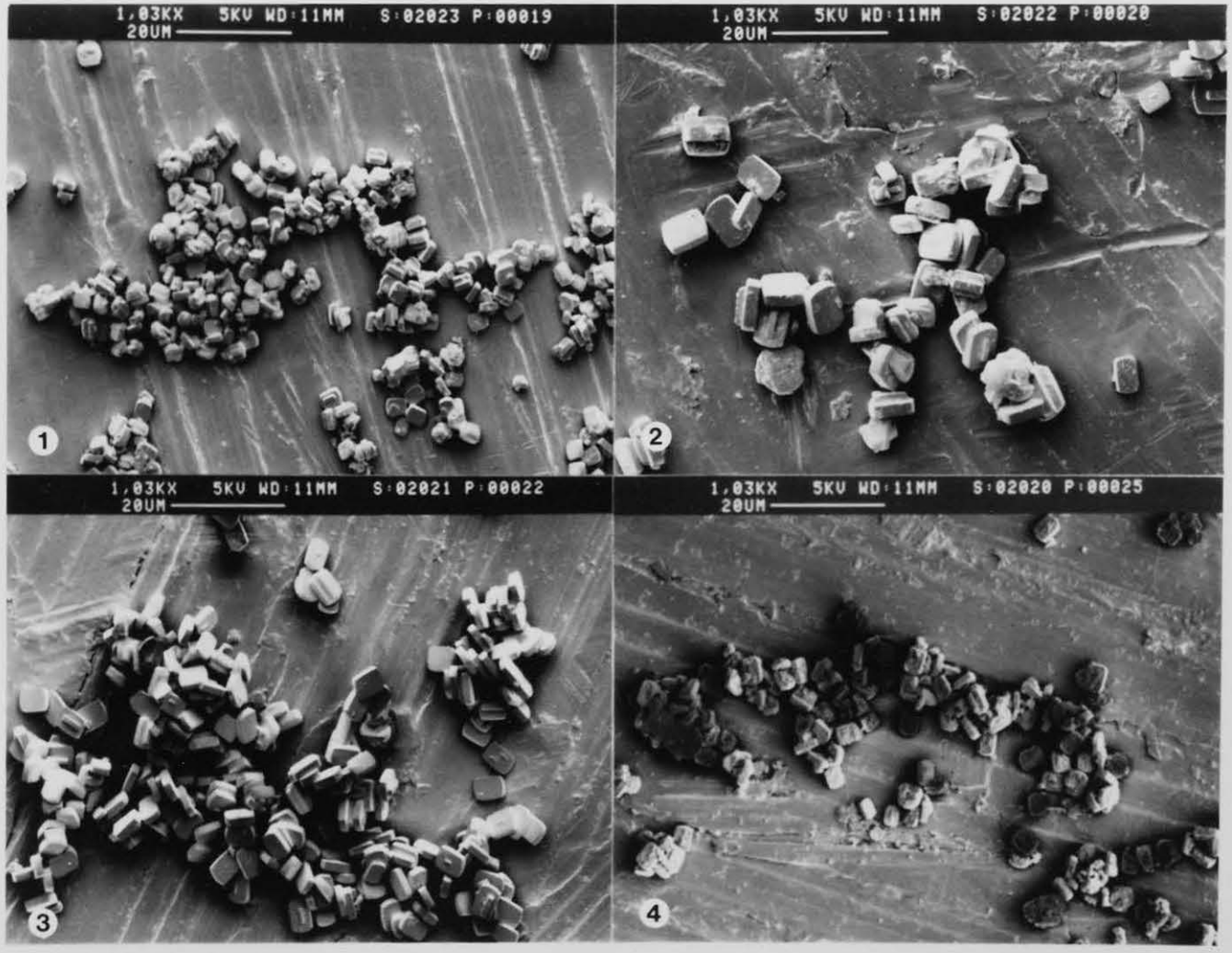
1,03KX 5KV WD:11MM S:02023 P:00019
20UM
1
1,03KX 5KV WD:11MM S:02022 P:00020
20UM
2
1,03KX 5KV WD:11MM S:02021 P:00022
20UM
3
1,03KX 5KV WD:11MM S:02020 P:00025
20UM
4

PLATE 4.1


1,05KX 5KV WD 11MM S:07100 P:00035
20UM
1
1,03KX 5KV WD:11MM S:03200 P:00013
20UM
2
3
1,03KX 5KV WD:11MM S:03000 P:00016
20UM
4

PLATE 4.2

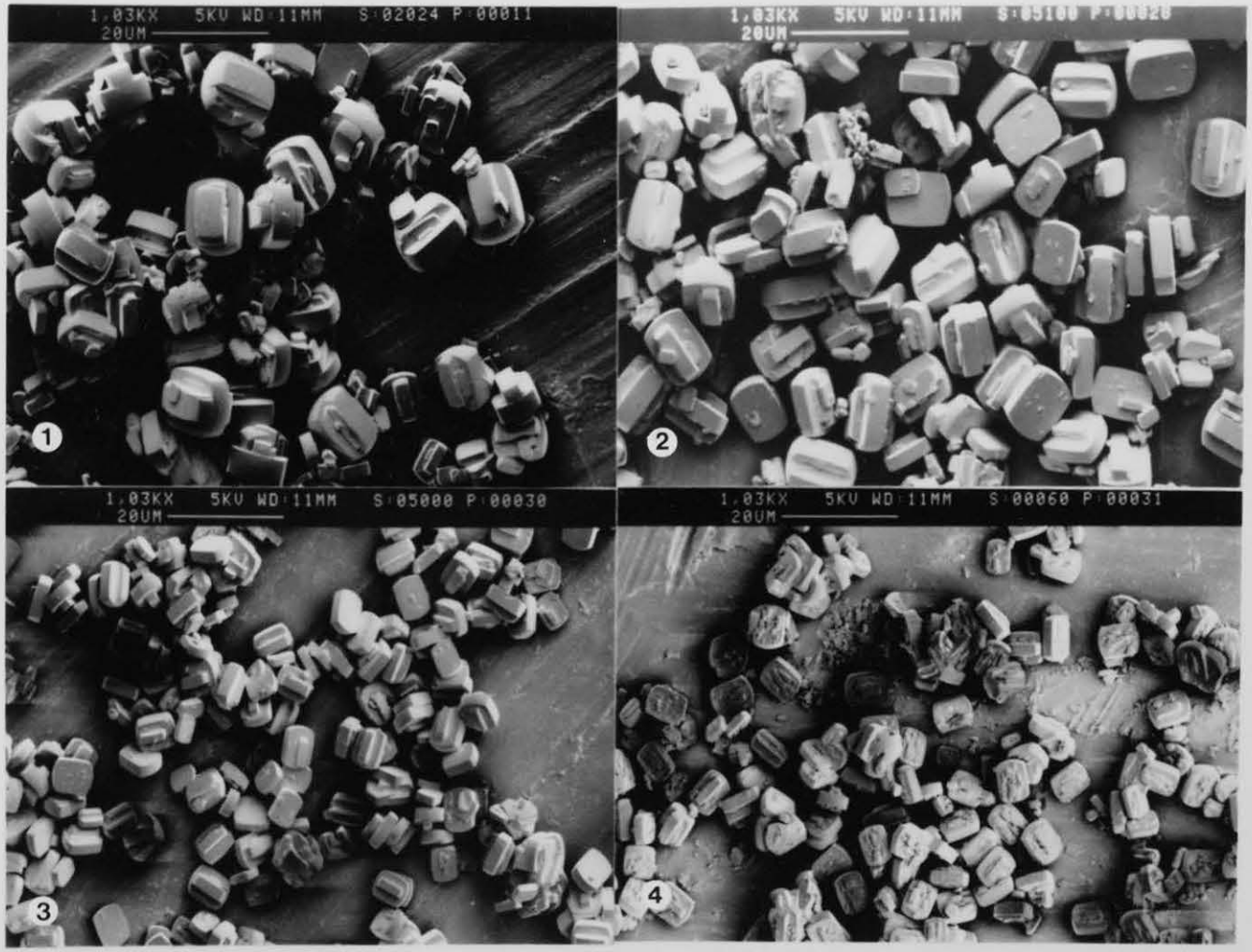
1,03KX 5KV WD 11MM S 02024 P 00011
20UM
1
1,03KX 5KV WD 11MM S 05100 P 00020
20UM
2
1,03KX 5KV WD 11MM S 05000 P 00030
20UM
3
1,03KX 5KV WD 11MM S 00060 P 00031
20UM
4

PLATE 4.3


1,03KX 5KV WD:11MM S:00060 P:00031
20UM
1
1,03KX 5KV WD:11MM S:06050 P:00034
20UM
2

PLATE 4.4

4.4 Conclusions

Several parameters affected the crystallisation of ZSM-5 from the TPA/piperazine system. The source of aluminium was crucial. Reaction mixtures which contained aluminium nitrate gave a higher quality ZSM-5 product at 95°C than with aluminium sulphate. Too much aluminium in the intermediate gel stopped the formation of the ZSM-5 product.

Aging also affected the crystallisation time but lead to a product which had slightly less aluminium incorporated into its framework. Crystallisation temperature affected both the time for ZSM-5 product formation and the degree of aluminium incorporation into the zeolite framework. The 150°C synthesis temperature favoured faster crystallisation and greater incorporation of aluminium. The SEM of the products showed that crystal size decreased as aluminium content of the products increased. There was, however, an uneven distribution of aluminium between the bulk and the surface of the ZSM-5 crystals.

There are some advantages to this synthesis procedure. The products are highly crystalline and there was little evidence of any impurities. The products are readily converted into their catalytically active hydrogen form by calcination, and there is no need to carry out hydrogen ion exchange. The product crystals are of uniform morphology.

Chapter 4 References

[1] Mobil Oil Corporation

Netherlands Patent 1,014,807 (1971).

[2] R.J. Argauer and G.R. Landolt,

U.S. Patent 3,702,886 (1972).

[3] B.P. Pelrine

U.S. Patent 4,100,262 (1978).

[4] D.H. Olson, L.D. Rollmann and E.W. Valyocsik

European Patent 26,962 (1981).

[5] D.H. Olson and E.W. Valyocsik

European Patent 26,963 (1981).

[6] M.A.M. Boersma and M.F.M. Post

European Patent 40,444 (1981).

[7] R.B. Calvert and L.D. Rollmann

European Patent 59,540 (1982).

[8] R.B. Calvert and L.D. Rollmann

European Patent 101,183 (1984).

[9] H. Nakamoto and H. Takahashi

Chem. Lett., 1981, 1739.

[10] R.M. Barrer

"Hydrothermal Chemistry of Zeolites",

Academic Press, London (1982).

[11] F. Janowski and K.M. Bergk

Z. Chem., 1982, **22**, 277.

[12] T. Inui

J. Catal. Soc. Japan, 1983, **25**, 261.

[13] B.M. Lok, T.R. Cannan and L.A. Messina

Zeolites, 1983, **3**, 282.

[14] Kh.M. Minachev and D.A. Kondrat'ev

Russ. Chem. Rev., 1983, **52**, 1113.

[15] H. Lechert

Stud. Surf. Sci. Catal., 1984, **18**, 107.

[16] E.W. Valyocsik and L.D. Rollmann

Zeolites, 1985, **5**, 123.

[17] S.B. Kulkarni, V.P. Shiralkar, R.B.

Borade and P. Ratnasamy.

Zeolites, 1982, **2**, 313.

[18] A. Araya and B.M. Lowe

Zeolites, 1986, **6**, 111.

[19] D.M. Bibby

Chemistry in N.Z., 1986, **50**, 5.

[20] R. Mostowicz and L.B. Sand

Zeolites, 1983, **3**, 219.

[21] E.G. Derouane and Z. Gabelica

J. Solid State Chem., 1986, **64**, 296.

[22] D.M. Bibby, N.B. Milestone and L.P. Aldridge

Nature, 1980, **285**, 30.

[23] S.G. Fegan and B.M. Lowe

J. Chem. Soc., Faraday Trans. 1, 1986, **82**, 801.

[24] Z. Gabelica, J.B. Nagy, P. Bodart

and A. Nastro

Thermochimica Acta, 1985, **93**, 749.

[25] V.R. Choudhary and S.G. Pataskar

Thermochimica Acta, 1986, **97**, 1.

[26] A.N. Kotasthane and V.P. Shiralkar

Thermochimica Acta, 1986, **102**, 37.

CHAPTER 5

SOLUBILITY AND DISSOLUTION OF HIGH SILICA ZEOLITES

5.1 Introduction

The solubility and dissolution of amorphous and crystalline silicas has been extensively studied (1-3). Particle size has been shown to affect the solubility of amorphous silica in water; the smaller the particles, the higher the surface area the greater solubility. The number of silanol groups in the amorphous silica and the presence of metal impurities also control the solubility (4). Dissolution of silica is both temperature and pH dependent. This has also been shown for glass apparatus (5), which emphasises the need to avoid glassware in silica solubility studies. Plastic equipment should be used at all times.

Guth and co-workers reported that aluminosilicates are soluble in dilute alkaline solutions (6). Initial studies involved pH measurements but further work used conductimetry (7) and Raman spectroscopy (8). This work was related to the growth of zeolite Na-A from dilute aluminosilicate solutions (9). Guth and co-workers further studied the solubility of zeolites Na-A and Na-X. The effect of temperature and the concentration of sodium ions in the liquid phase were studied; equilibration was found to take up to 60 days (10). The Si/Al ratio of the solution phase, at equilibrium, varied with the initial liquid/solid (L/S) ratio of the system. Thermodynamic parameters for the dissolution of zeolites Na-A and Na-X were also evaluated (12).

Barrer (13) pioneered the theory that zeolite nucleation results from the condensation of silicate, aluminate and other complex ions in the aqueous phase. Growth is assured by a continuous supply of soluble species, from the dissolution of the amorphous solid phase of the aluminosilicate reaction mixture. Zhdanov established the influence which the composition of the liquid phase has on the nature of the product zeolite (14). Many studies have confirmed Barrer's theory (15-19). This formed the basis on which Guth et al approached their work (20). Dissolution studies are a means of studying crystal growth in reverse, and solubility measurements provide information about the thermodynamics of crystallisation.

The ion exchange, hydrolysis and resultant degradation of zeolite A in water has also been reported (21,22), with particular emphasis on the environmental impact of zeolite detergents. Knowledge of zeolite solubility is important for their use in ion exchange (23,24) or the sorption of organic substances from aqueous solution; for example removal of caffeine from coffee extract by zeolite Y (25,26). In these applications, there is an undesirable tendency for the zeolite to dissolve in the aqueous solution. To counteract this zeolites have been impregnated with binder material, a water permeable organic polymer, which reduces dissolution (27-30).

Preliminary work on the solubility of Na-silicalite and (Na,TPA)-silicalite in water and dilute solutions of sodium hydroxide at 25°C was carried out prior to the present investigation (31). The presence of the sodium in the silicalite probably increased its solubility to values well above those of the pure silica form. The tetrapropylammonium (TPA) ion is known to form solutions with up to sixteen different silicate anions when it is reacted in alkaline solution with amorphous silica (32). These oligosilicates will interfere with the analysis of aqueous silica in solubility studies of uncalcined TPA-silicalite, and may have invalidated the preliminary study (31).

The method of analysis which is used in the present work relies on the reaction between monosilicic acid species and molybdic acid (33). This spectrophotometric analytical method has been extensively studied (34-37). It is also possible to use gravimetric methods (37) but the colourimetric method is superior at low aqueous silica concentrations.

The molybdic acid only reacts with monomeric silicon species. There are, however, in most silicon containing solutions many polymeric species (39,40). This has been shown by ^{29}Si nuclear magnetic resonance studies of silicate anions (41-43). Silica species are depolymerised by the addition of excess sodium hydroxide (44), and this is a necessary preliminary step in the spectrophotometric analysis (33).

There are no data in the literature for the solubility of silica molecular sieves. The aim of the present work was to obtain fundamental data for the dissolution of high silica zeolites in water, over a range of temperatures.

It has been shown by a theoretical treatment that solubility data can be used to predict the pH changes which occur during the crystallisation of high silica zeolites (45). One aim of the present work was to obtain data that could be applied in this equilibrium model.

5.2 Experimental

Mixtures of water and high silica zeolites were prepared at various liquid/solid (L/S) ratios, by weight. The materials were carefully weighed into polypropylene bottles, which were fitted with screw caps and sealed with film prior to immersion in a thermostat bath. The bottle size was either 30 or 60ml; some early studies were conducted in 1 litre bottles. The mixtures were tumbled at temperatures up to 40°C, those at 70 and 95°C were static. All of the mixtures were equilibrated in thermostat baths which were at a temperature constant to within 0.1°C. The tumbling was carried out on rotary equilibrators.

Some initial solubility studies were conducted in static systems at 25°C. This was found to be unsuitable since a silica concentration gradient built up from the solid at the bottom of the bottles to the surface of the system. This effect did not noticeably occur at 70 and 95°C. Stirred vessels were also used in the initial studies. These were unsuitable since the magnetic stirrer bars ground the solid phase into the base of the polypropylene bottles. Such a mechanical effect is undesirable, and occasionally led to the rupture of the bottom of the plastic bottles.

Once the mixtures had been equilibrated they were taken off and centrifuged at 1,800 revolutions per minute for 20 minutes, in order to separate the liquid phase from the solid phase. A 5ml portion of the liquid phase was drawn off with a plastic pipette, and immediately placed in another 30 or 60ml plastic bottle together with 0.5ml of 10M sodium hydroxide. This was added to depolymerise the silica species in the aqueous phase. Portions of 1ml were taken from the mixtures at 70 and 95°C and diluted to 5ml prior to the addition of caustic soda. This brought their aqueous silica concentrations to within the calibration plot. This plot (Figure 5.1) was determined from absorbance measurements on standard solutions (which were made up from a stock standard solution supplied by Koch Light Limited). Standards were run whenever samples were analysed.

The spectrophotometric molybdosilicic acid method was used for the determination of silica in the aqueous phase (33). The molybdate reagent was prepared as follows:

Reagent (A) - 41.0ml of 95.5% H_2SO_4 was diluted to 1 litre.

Reagent (B) - 10g of $(NH_4)_6Mo_7O_{24}.4H_2O$ (mol. wt. 1235.9) was dissolved in 90ml water, 4.7ml concentrated NH4OH solution was added, and this solution was then diluted to 100ml.

Reagent (C) - 200ml of (A) was added to the 100ml of (B) and diluted to 800ml.

Reagent (C) had a pH of about 1.2 and was 0.0707M with respect to the molybdate anion. Reagents (B) and (C) were made up on each day of use, since they both had a life of about one week.

A portion of 20ml of reagent (C) was added to each 5.5ml standard and test solution. Each was analysed at a wavelength of 410nm five minutes after the addition of reagent (C); by this time the yellow colour of the samples was fully developed. Aqueous silica concentrations were then determined from the absorbance calibration graph, in which the absorbance values were plotted as a function of the silica concentrations in the standard solutions. The analytical technique was accurate to within $\pm$3%.

Once the time for complete equilibration had been established, the variation of solubility with temperature was studied.

Solubility studies were conducted with silicalite (silica-ZSM-5), silica-ZSM-11 and silica-ZSM-48 in their hydrogen forms. Attempts were also made to determine the solubility of TPA-silicalite. The template cannot be removed from ZSM-39 and EU-4 and hence these were studied in their 'as made' form. The dissolution of aqueous silica from ZSM-5 at 25°C was also determined. The initial solubility studies involved amorphous and crystalline silica.

The effect of treating silica-ZSM-48, ZSM-39 and EU-4 with water at 180°C was also studied. Samples were treated for 3 hours in an autoclave at a L/S ratio of 200. They were then filtered and dried

in an oven at 110°C for 2 hours. The treated materials were then examined by X-ray powder diffraction and scanning electron microscopy. Chapters 6.0 and 7.0 describe similar hydrothermal treatment studies of silicalite and ZSM-5.

5.3 Solubility Results

5.3.1 Amorphous Silica and Quartz

The solubilities of quartz and two amorphous silicas in water at 25°C were determined. The quartz was synthesised from the reaction mixture:

$5Na_2O\ 60SiO_2\ 3000H_2O$

Sodium hydroxide was dissolved in the required amount of water and then added to the amorphous silica, Cab-O-Sil (BDH), which had been weighed into a polypropylene bottle. The mixture was blended to a homogeneous paste with a glass rod and was then transferred to an autoclave. The reaction mixture was stirred at 300rpm and thermostatted at 180°C. The crystallisation of the quartz was complete after 6 days, as determined by X-ray diffraction, optical microscopy and the rapid sedimentation of the product. The pH increased during the reaction by 1.0 units.

Several solubility mixtures were prepared for the quartz and for two amorphous silicas; a fumed silica (Cab-O-Sil from BDH) and a precipitated granular silica (from Koch-Light). The solubility mixtures each had a liquid/solid (L/S) ratio of 1000. Initial studies showed that the equilibration took about 12 days. After 14 days the aqueous phase was analysed by the spectrophotometric method. A typical calibration plot is shown in Figure 5.1. This was plotted using the absorbances measured for solutions of a known monomeric silica concentration prepared from a stock solution supplied by Koch-Light. The measured solubilities of the three silicas are given in Table 5.1. The dissolution of silica is a chemical reaction and involves reaction with water:

$$2H_2O + SiO_2\ (solid) = Si(OH)_4\ (aqueous)$$

In some cases, e.g. with amorphous silica, polymeric silicic acids may be formed. The solubilities in this thesis are expressed in terms of ppm SiO_2 (aq); this is equivalent to mg of SiO_2 per litre.

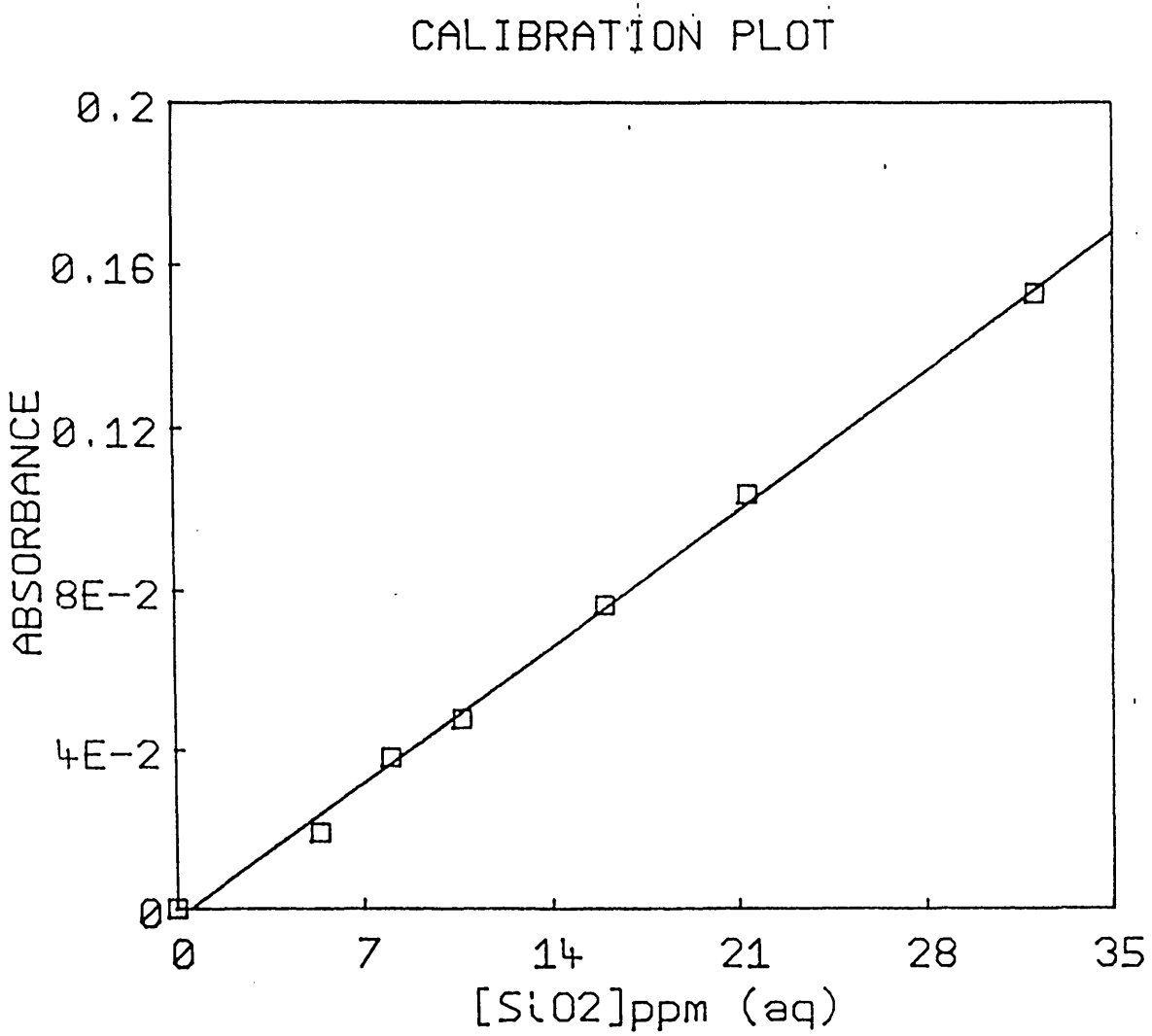

Figure 5.1 Calibration plot for silica analysis

Table 5.1 Solubility of Silica at 25°C in Water

Silica	Equilibrium $[SiO_2]$ppm (aq)
Fumed silica	161.8
Precipitated silica	138.7
Quartz	14.1

Each solubility value is accurate to within ±3%. The very fine fumed silica (Cab-O-Sil) has a higher solubility than the coarse precipitated amorphous silica. The solubility of the crystalline silica (quartz) is about ten times less than the value measured for the amorphous material.

For crystallisation from reaction mixtures that contain amorphous solids, changes in thermodynamic quantities can be calculated from the solubilites of the amorphous and crystalline material, $K_{s,gel}$ and $K_{s,cryst}$. The free energy change ΔG is related to the solubility of the gel and the crystalline product by the equation (45):

$$\Delta G = -RT \ln(K_{s,gel}/K_{s,cryst})$$

The pH change is given by:

$$\Delta pH = -F \log(K_{s,cryst}/K_{s,gel})$$

where F is a factor in the range 1 to 0.5. Using the solubilities obtained for quartz and amorphous silica, the pH change for the crystallisation of quartz from Cab-O-Sil is predicted to be between 1.06 and 0.53 pH units. This is compatible with the observed value of 1.0 pH units stated above.

In summary, solubility data can be applied to predict certain thermodynamic characteristics of zeolite crystallisation. The quartz synthesis considered here is a crystallisation from a simple reaction system. There is no template involved in the crystallisation and hence many complications to the theoretical treatment are avoided (45).

5.3.2 Silicalite and Silica-ZSM-11

The solubility of H-silicalite was measured at 25°C at various liquid/solid (L/S) ratios. Low L/S values always gave results which were similar to the solubility of amorphous silica, whereas high L/S ratios gave results which were similar to those expected for a crystalline silica. Sometimes the observed solubility values were between these limiting values, but this only occurred for a certain range of L/S ratios. This is shown in Table 5.2, for the observed solubility of a calcined H-silicalite (B1).

Table 5.2 Variation in observed solubility with L/S ratio

Liquid/Solid Ratio	$[SiO_2]$ppm (aq)
50	154.3
100	69.0
500	25.3
1000	17.6
5000	16.5

The solubility of pure materials should not vary with liquid/solid (L/S) ratio. In solubility systems of a low L/S ratio there is a greater amount of solid present than in those of a high L/S ratio, and the effects of highly soluble impurities will be magnified. Since the solubility of amorphous silica is about ten times that of crystalline silica, any amorphous silica in the test silicalite samples will have a major affect on observed solubility values for systems with low L/S ratios. This effect will be reduced as the amount of solid in the solubility systems is decreased since less amorphous silica will be present to contribute to the aqueous phase silica.

At low L/S ratios the observed solubility values were always similar to those which had been measured for amorphous silica in the initial studies. At high L/S ratios the observed solubilities were similar to those noted for crystalline silica. The solubility of H-silicalite at 25°C in water was 16.5ppm aqueous silica, that for the amorphous silica impurity contained within the test samples was 154.3ppm aqueous silica. In order to calculate the effect of the L/S

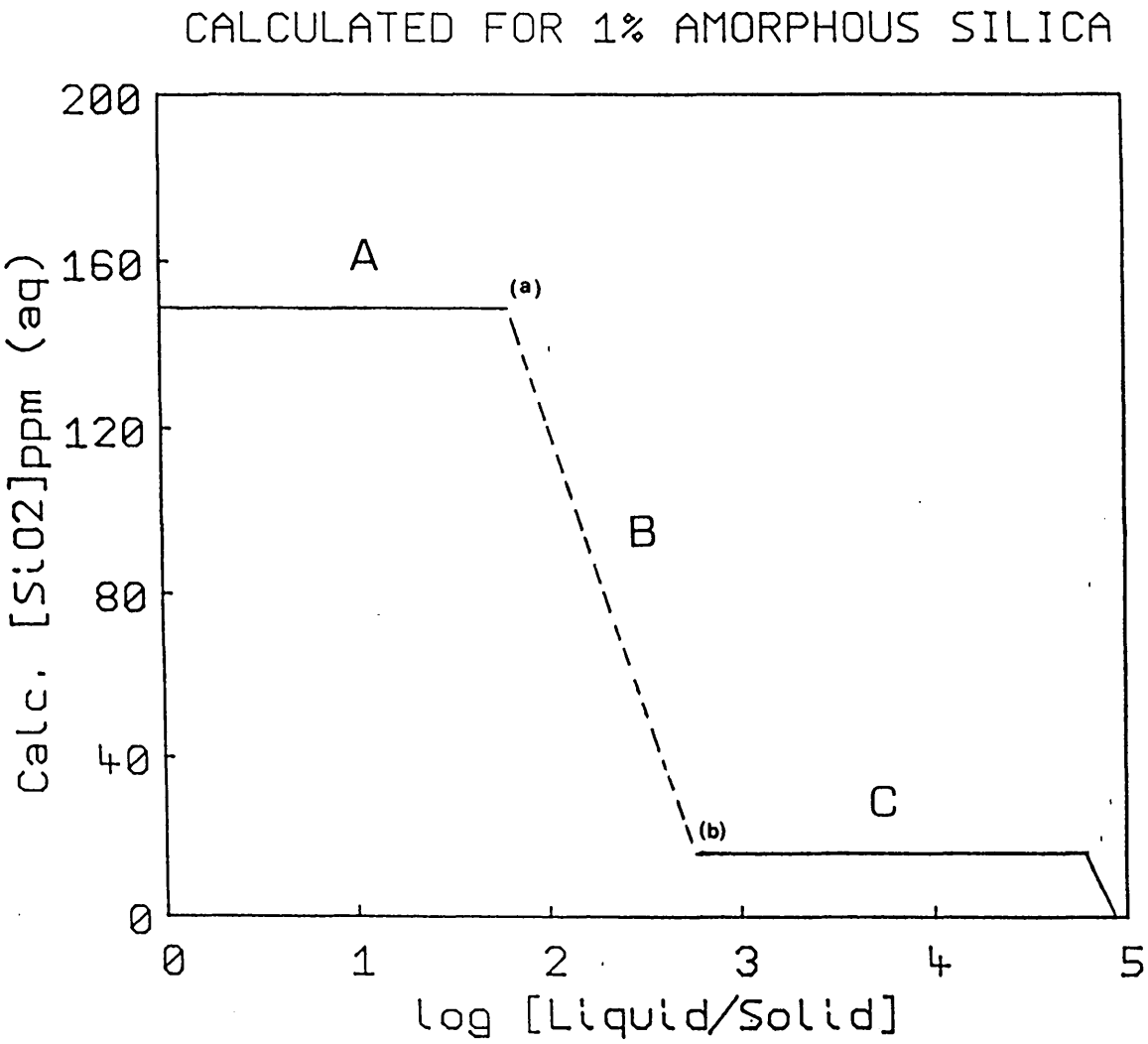

Figure 5.2 Calculated variation of observed solubility of impure silicalite in water at 25°C, for a 1% level of amorphous impurity

ratio on the observed solubility values it was assumed that there is one type of amorphous silica present and that the silicalite is a homogeneous phase. Figure 5.2 shows how the observed solubility would vary with L/S ratio if 1% of the total silica was an amorphous impurity. In region A there is still some amorphous silica present in admixture with the H-silicalite. The concentration of silica in solution is the solubility of the amorphous silica. In region B there is insufficient amorphous silica present to saturate the solution; at equilibrium the solid phase is H-silicalite. In region C all of the amorphous silica dissolves to give an aqueous silica concentration less than that for the true solubility of silicalite. The dissolution of silicalite then controls the equilibrium aqueous silica concentration. This region corresponds to the true solubility of silicalite. Points (a) and (b) were arrived at as follows:

Let

W_L = Weight of water

W_S = Weight of impure silicalite

W_Z = Weight of pure silicalite in solid phase

W_A = Weight of amorphous silica in solid phase

$W_S = W_Z+W_A$

X_Z = Weight fraction of silicalite in solid phase

X_A = Weight fraction of amorphous silica in solid phase

$$X_Z=W_Z/(W_A+W_Z)=W_Z/W_S$$

$$X_A=W_A/(W_A+W_Z)=W_A/W_S$$

$$X_Z+X_A=1$$

Weights refer to the start of the experiment. At point (a) all of the amorphous silica has just dissolved.

$$W_A=W_L.S_A$$

Where S_A is the solubility of the amorphous silica in grams per gram

of water. The L/S ratio at point (a) is then given by:

$$W_L/W_S=(W_A/S_A).(1/W_S)=X_A.(1/S_A)$$

The calculation for point (b) is more complicated. At this point all the amorphous silica originally present is just sufficient to provide all the silica required to saturate the solution with respect to the silicalite.

$$W_A=S_Z.W_L$$

Where S_Z is the solubility of the zeolite. At this point the solution phase is saturated with respect to silica but all the silica has come from the amorphous phase. The L/S ratio that gives rise to point (b) is given by the equation:

$$W_L/W_S=(W_A/S_Z).(1/W_S)=X_A/S_Z$$

The value of S_A is 154.3ppm, that of S_Z is 16.5ppm aqueous silica. The equations were applied to determine the positions of points (a) and (b) for 1% amorphous contamination of an H-silicalite sample, X_A = 0.01. The L/S ratio calculated for point (a) was 64.81, and that for point (b) was 606.06. This is represented in Figure 5.2. The x-axis is plotted as a log scale so as to accommodate the range of the L/S ratios. These results indicate that to measure the solubility of high silica zeolites it is essential to use high L/S ratios. This is especially important if the materials contain a substantial proportion of amorphous contaminants. It is important to recognise that this is only an approximate treatment, since the silica species which enter the solution from the amorphous silica are not necessarily the same as those that enter from the crystalline material. For example the amorphous silica is more likely to give rise to oligosilicic acids and the crystalline silica probably dissolves as monosilicic acid. Hence it is not possible to make an exact estimate of the amount of amorphous impurity from the results in Table 5.2. However the results suggest an impurity level in the 0.7 to 1.5% range.

An estimate of the time required for equilibration of silicalite with its aqueous solution was determined by measuring the solution

phase concentration at regular time intervals. For these measurements a silicalite (A4) which had been synthesised at 95°C and calcined to the H-form was used. A L/S ratio of 1000 was chosen which should be adequate for 1.5% amorphous impurity. The equilibration time at 25°C was judged to be about 8 days, as can be seen in Figure 5.3. The solubility was about 22ppm aqueous silica, which is somewhat higher than expected. This probably indicates that the framework was silanol rich and hence more soluble than a defect free material.

Solubility systems were set up at 15, 25, 40, 70 and 95°C for two silicalite samples (P2 and Q1) and one silica-ZSM-11 material, which was supplied by Dr. K.R. Franklin. Each material was in its hydrogen form. A L/S ratio of 1000 was chosen for each mixture.

The results are given in Table 5.3 and plotted together in Figure 5.4.

Table 5.3 Solubility of silicalite and silica-ZSM-11

in water at 25°C.

Temperature	Solubility [SiO_2]ppm (aq.)		
(°C)	Silicalite (P2)	Silicalite (Q1)	Silica-ZSM-11
15	13.7	16.3	22.8
25	15.0	17.6	28.6
40	22.8	28.0	46.1
70	63.9	70.4	79.1
95	119.1	153.7	167.7

These results show that the silicalite synthesised at 150°C (P2) was less soluble than the one which was prepared at 180°C (Q1) even though each product was prepared from the same reaction mixture (10Piperazine, 2TPABr, 20SiO_2, 1000H_2O). The difference is small, and may simply reflect a greater level of broken siloxane bonds or some other structural defect in the material synthesised at 180°C. The silica-ZSM-11 is significantly more soluble than either of the H-silicalite samples. The ZSM-11 framework (MEL) is more strained than that of silicalite. Although each of their unit cells contains 96-T atoms, the silicalite unit cell contains only eight 4-T atom

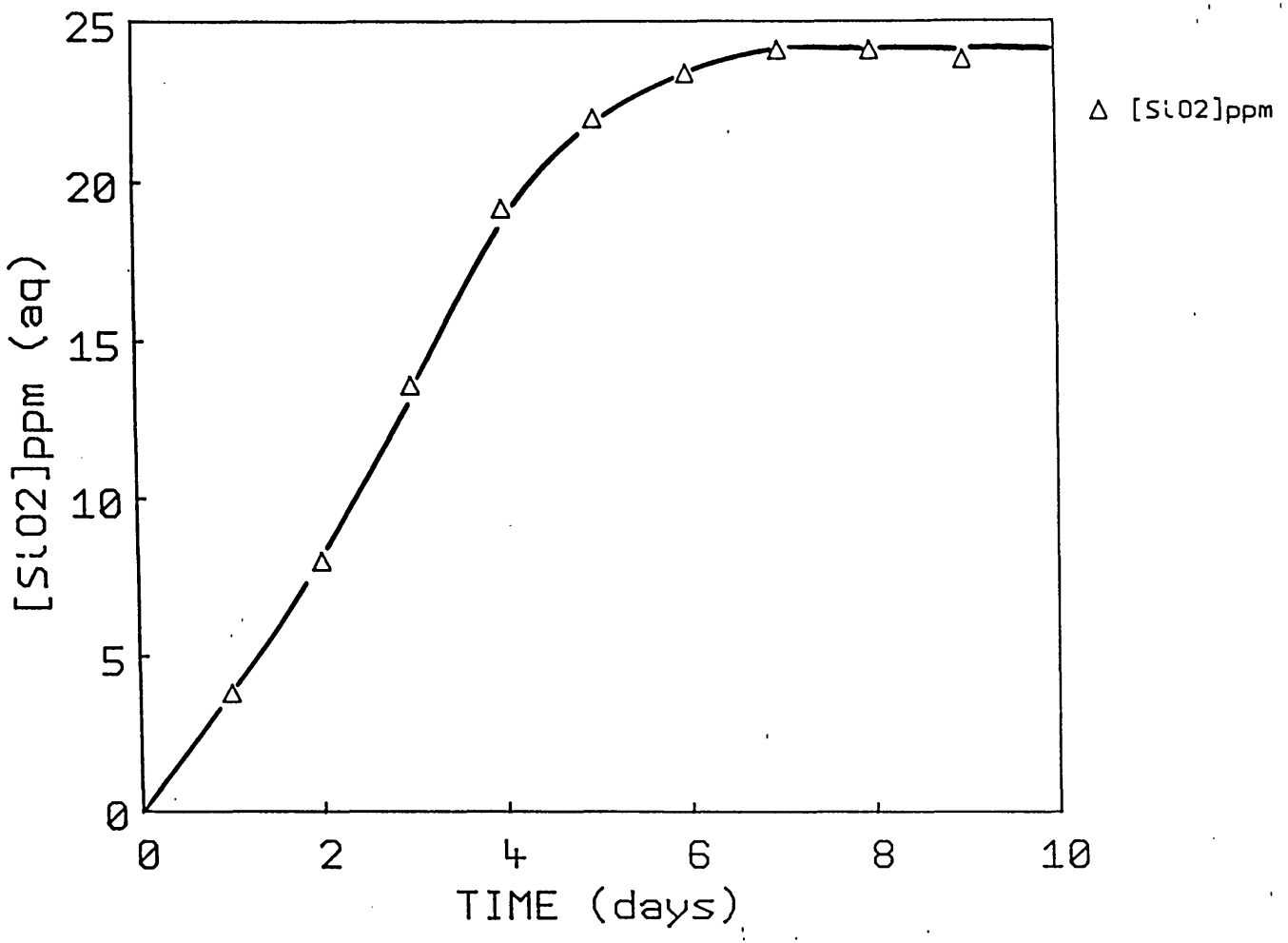

Figure 5.3 Equilibration time for a H-silicalite in water at 25°C

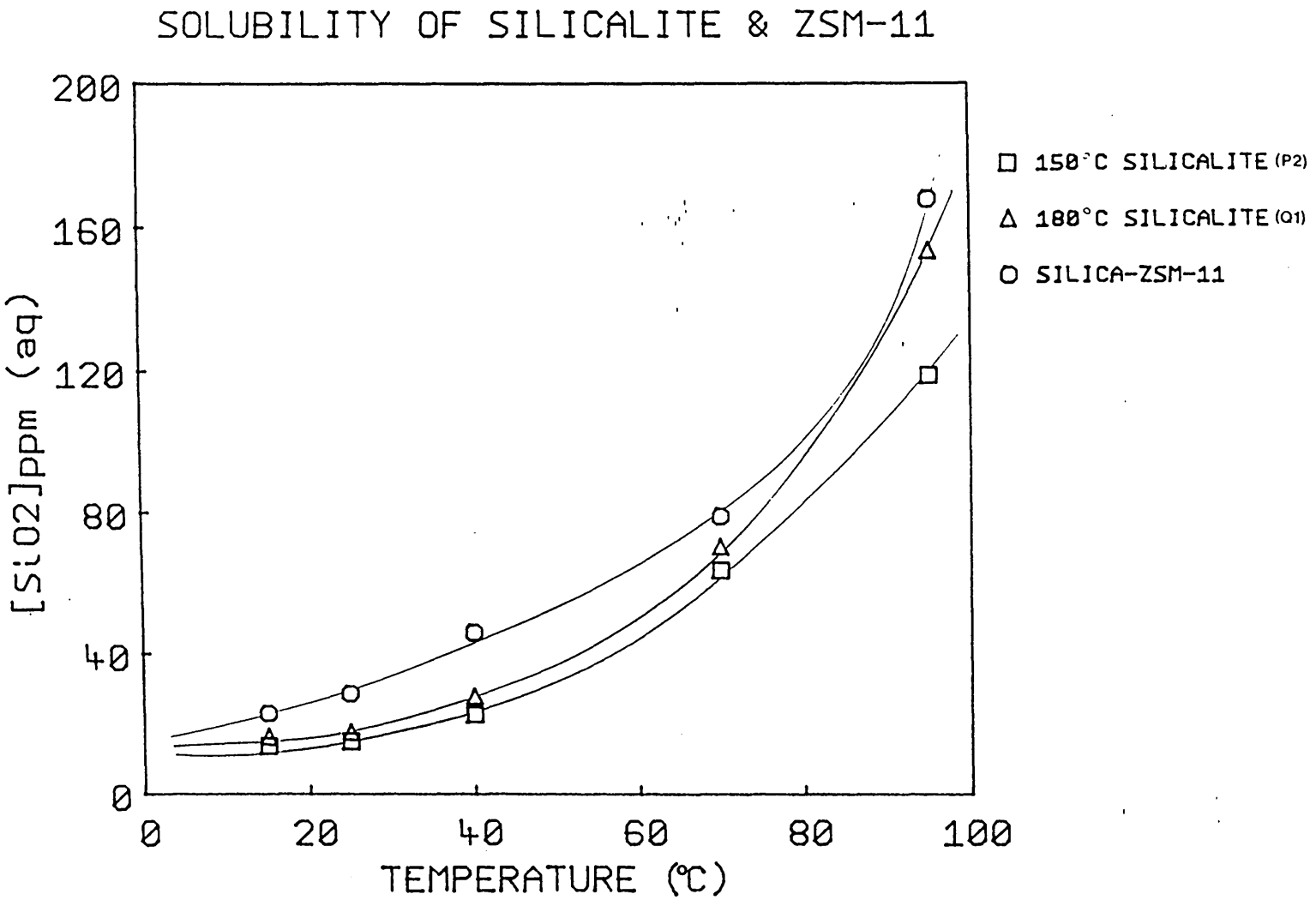

Figure 5.4 Solubility of H-silicalite and H-silica-ZSM-11 in water

rings, whereas that of silica-ZSM-11 has thirty 4-T atom rings. The consequent increased framework strain will make ZSM-11 less stable and hence more soluble. There is also less likelihood of complete ring closure in more highly strained frameworks. Thus silica ZSM-11 is likely to have more framework silanol groups than silicalite and these will promote the dissolution process.

The heat of solution of the three molecular sieves can be calculated from the van't Hoff equation.

$$d(\ln K)/d(1/T) = -\Delta H/R$$

If ln(K/ppm) is plotted against 1/T then the slope is $-\Delta H/R$, where T is in degrees Kelvin and K is the solubility of the molecular sieve. Multiplication of the gradient by the gas constant R gives the heat of solution. A plot of lnK versus 1/T for both silicalites and the silica-ZSM-11 is shown in Figure 5.5. The gradients were calculated with a least squares program and the heats of solution are given in Table 5.4.

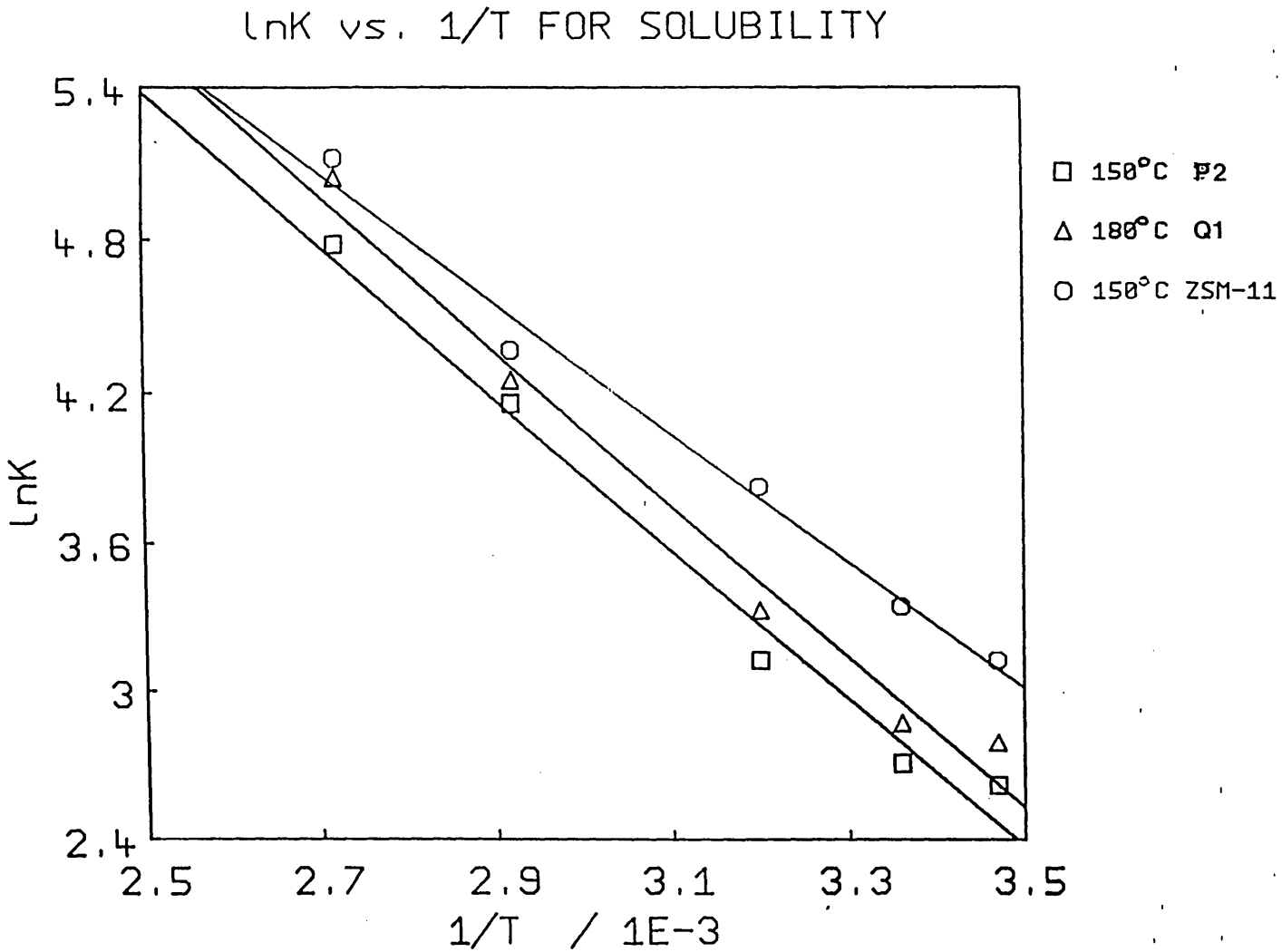

Figure 5.5 Van't Hoff plot for H-silicalite and H-silica-ZSM-11

Table 5.4 Heats of Solution for Silicalite and silica-ZSM-11

Material	Synthesis T (°C)	Heat of Solution (kJ mol^{-1})
Silicalite (P2)	150	25.1
Silicalite (Q1)	180	25.5
Silica-ZSM-11	150	21.3

It can be seen from Figure 5.5 that the plots are not perfectly linear, and hence the exact values of ΔH given in Table 5.4 may be unreliable. However the difference between the values obtained for silicalite and silica-ZSM-11 is considered to be significant. The values are close to that reported (ref.1, p.31) for quartz (22.2 kJ mol^{-1}).

In summary, the presence of trace amounts of amorphous impurity can affect solubility results for the high silica zeolites. It is essential that high L/S ratios are used for solubility determinations. The effect of the amorphous silica impurity on the solubility may be used to predict the extent to which the materials are contaminated by amorphous impurities. However, this approach is based on the assumption that the crystalline product and the amorphous impurity are likely to be distinct homogeneous phases. This is not always the case. The silicalite framework will itself contain many silanol groups which may be formed by incomplete ring closure during crystallisation or be generated during calcination. These, in effect, constitute regions of imperfect crystallinity, and might tend to behave like amorphous impurities. The hydrothermal treatment of silicalite is further studied in Chapter 6.0.

The solubility of a TPA-silicalite (B1) was found to be 7.5 ppm aqueous silica at 25°C. Hence the presence of the template suppresses the solubility of silicalite.

The presence of aluminium also suppresed the dissolution of silica from the framework. The solubility of a H-ZSM-5, synthesis code E3 (Chapter 4.0), was measured as 13.2ppm aqueous silica at

25°C, in contrast to a value of 16.5 ppm for H-silicalite.

5.3.3 Silica-ZSM-48

Silica-ZSM-48 (46-49) was crystallised from the reaction mixture:

10Hexane-1,6-diamine $20SiO_2$ $1000H_2O$

The mixture was stirred in an autoclave at 180°C and crystallisation was complete after about 36 hours. The product resembled hollow spheres of interwoven fibrous ZSM-48, see print 1 on Plate 5.1.

Half of the product was calcined at 550°C for 16 hours. The uncalcined and calcined ZSM-48 were both hydrothermally treated at 180°C in an autoclave for 3 hours. The L/S ratio of each treatment was 200. The X-ray powder diffraction traces of each pair of untreated and treated materials are shown in Figures 5.6-7. The scanning electron micrographs of the untreated (print 1) and treated (print 2) calcined H-ZSM-48 samples are in Plate 5.1.

The SEM clearly show the break-up of the hollow spheres to a fibrous material under the influence of the hydrothermal treatment. This may account for the changes in the XRD patterns, since the treated samples are more densely packed in sample holders. Calcination changed certain line intensities; this is due to the removal of the template from the ZSM-48 framework. The main low angle peak in calcined H-ZSM-48 is significantly increased in area after the hydrothermal treatment. This may be due to the removal of amorphous material from the zeolite framework.

The solubility of calcined silica-ZSM-48 was studied in the same manner as for other high silica zeolites. Figure 5.8 shows a plot of solubility against temperature for this material. The values obtained at 25, 40, 70 and 95°C were 18.2, 20.3, 74.7 and 168.3 ppm aqueous silica respectively. Thus the solubility increases with temperature to a value higher than that determined for silicalite. From a plot of ln(K/ppm) versus 1/T, Figure 5.9, the heat of solution was calculated as 27.8kJ mol^{-1}. This is between the values for

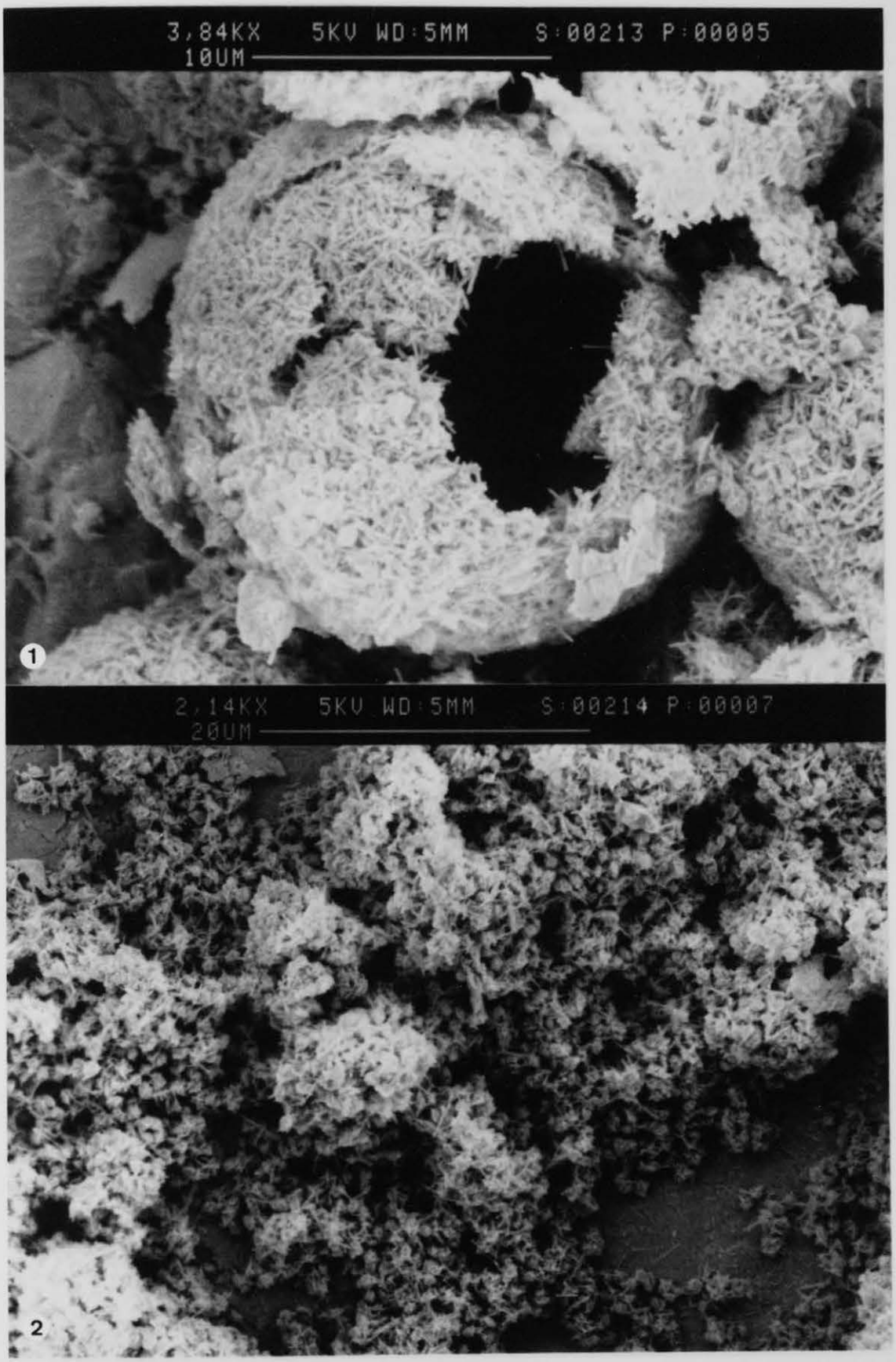
3,84KX 5KV WD:5MM S:00213 P:00005
10UM
1
2,14KX 5KV WD:5MM S:00214 P:00007
20UM
2

PLATE 5.1

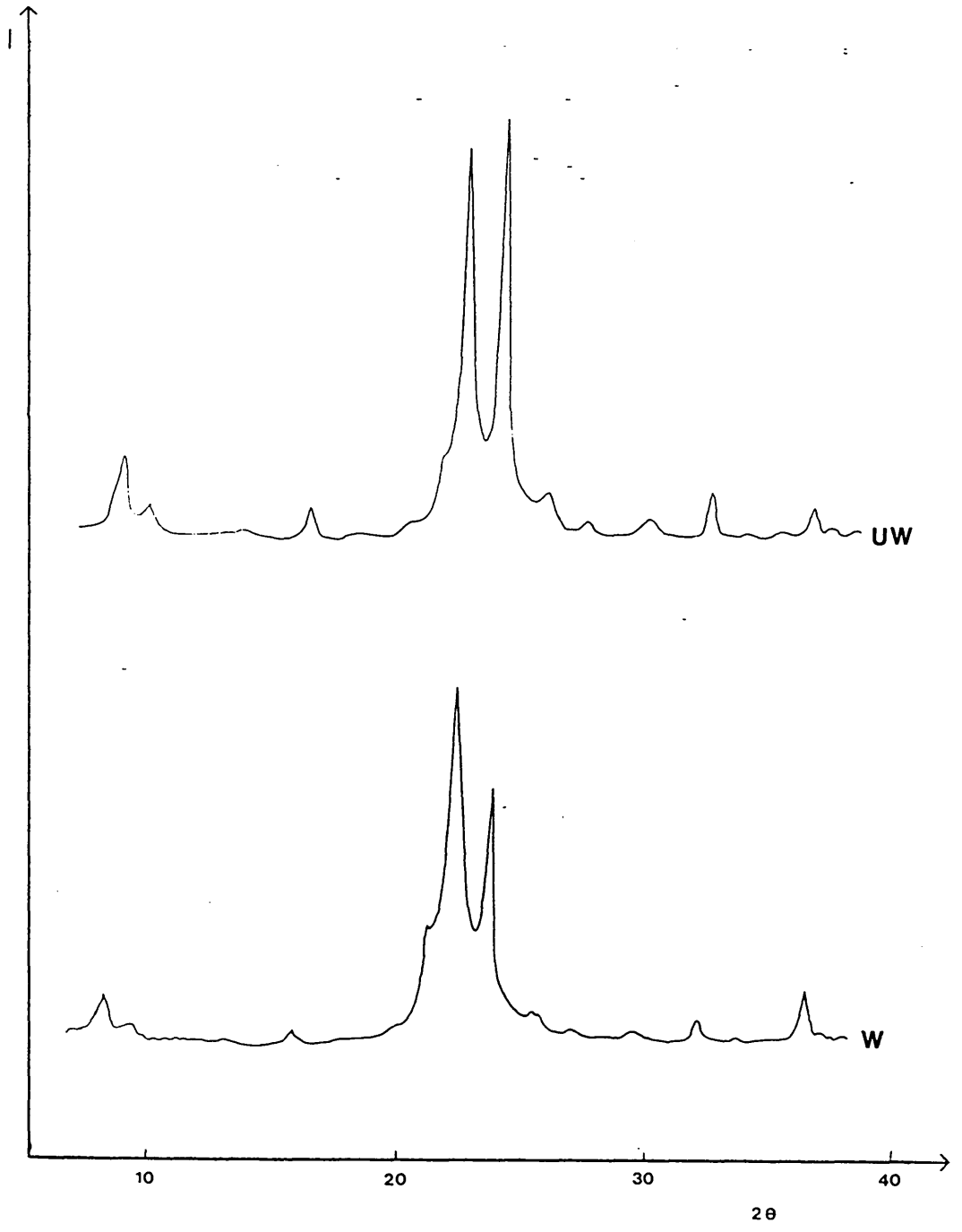

Figure 5.6 XRD patterns of untreated (UW) and treated (W) uncalcined silica-ZSM-48

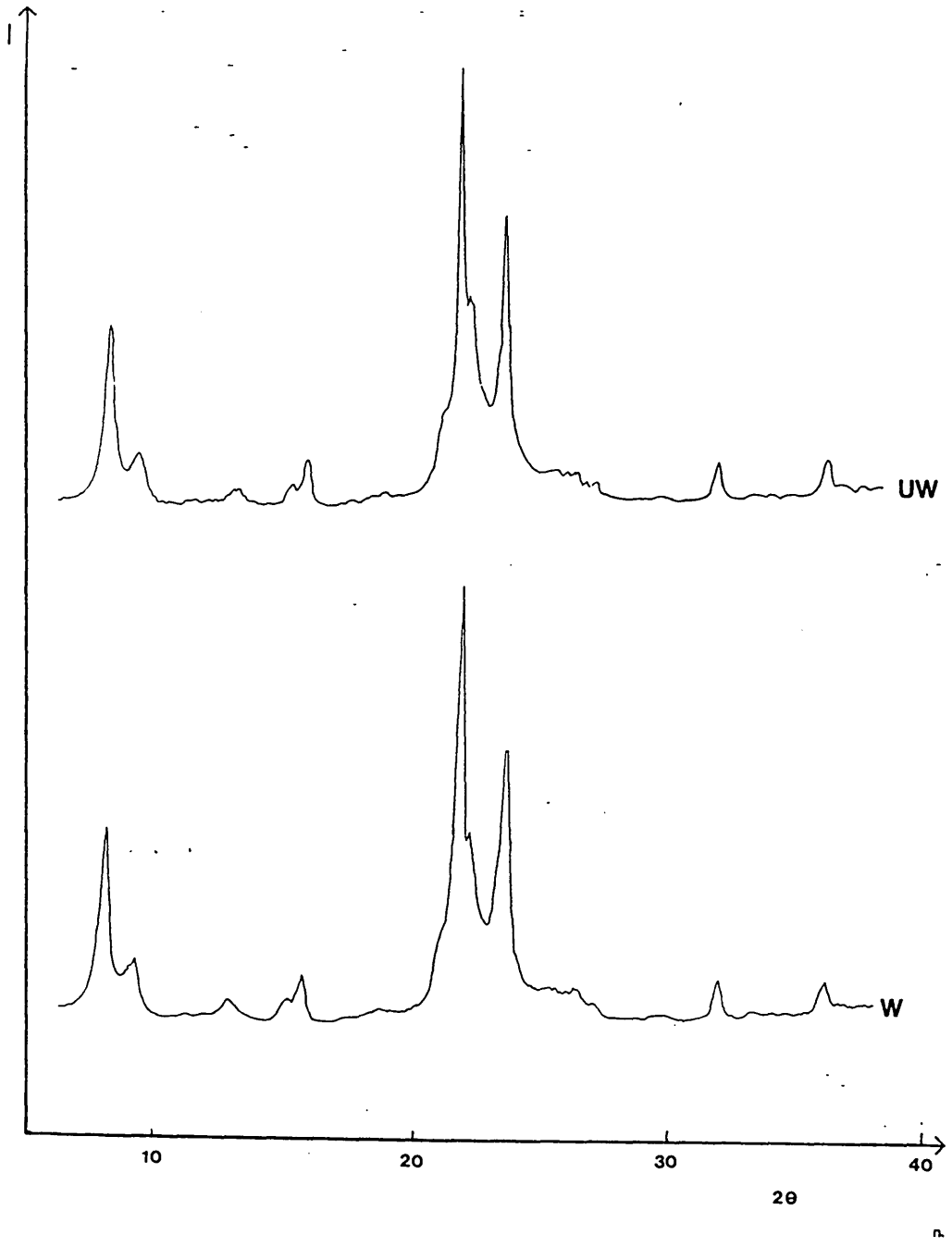

Figure 5.7 XRD patterns of untreated (UW) and treated (W) calcined H-silica-ZSM-48

quartz (3) and silicalite. The solubility of ZSM-48 also appears to be intermediate between the two.

5.3.4 ZSM-39 and EU-4

Samples of ZSM-39 (50) and EU-4 (51) were synthesised and supplied by Dr K.R. Franklin. The organic void fillers (piperazine for ZSM-39 and aminocyclohexane for EU-4) cannot be removed from these frameworks by calcination. The materials were each hydrothermally treated at 180°C at a L/S ratio of 200 for 3 hours. Thereafter the X-ray powder diffraction patterns and the scannning electron micrographs of the treated and the initial 'as made' materials were obtained. The solubilities of ZSM-39 and EU-4 in water were then studied over a range of temperatures.

The XRD patterns of untreated (UW) and treated (W) ZSM-39 and EU-4 are shown in Figures 5.10-11. There were only minor changes in the powder patterns. The SEM of the ZSM-39 samples are in Plate 5.2 and those of the EU-4 materials are in Plate 5.3. The prints which are numbered 1 are for the untreated samples, those numbered 2 are for the treated materials. The two high silica zeolites dissolve by quite distinct routes. The edges of the ZSM-39 crystals become smoother and there is little evidence of pitting of the surfaces. In contrast EU-4 appears to dissolve by pitting at the edges and the crystal faces.

The solubility plots of ZSM-39 and EU-4 are in Figure 5.12. For ZSM-39 the solubilities were 4.9, 5.3, 35.5 and 71.9 ppm at 25, 40, 70 and 95°C, and those for EU-4 were 7.5, 9.2, 32.9 and 60.7 respectively. Thus ZSM-39 was less soluble than EU-4 at 25 and 40°C, but was more soluble at 70 and 95°C. The solubilites obtained at 25°C for ZSM-39 and EU-4 are less than that obtained for quartz (14.1 ppm) in the present work, and emphasise the stabilising effect of the organic guest molecule. The heat of solution for each material was calculated from a plot of ln(K/ppm) versus 1/T, Figure 5.13. The value for ZSM-39 was 36.6 kJ mol^{-1}, which is larger than the values reported for quartz [30.7 kJ mol^{-1} (3), 22.2 kJ mol^{-1}, ref (1) page 31]. EU-4 had a heat of solution of 29.0 kJ mol^{-1}.

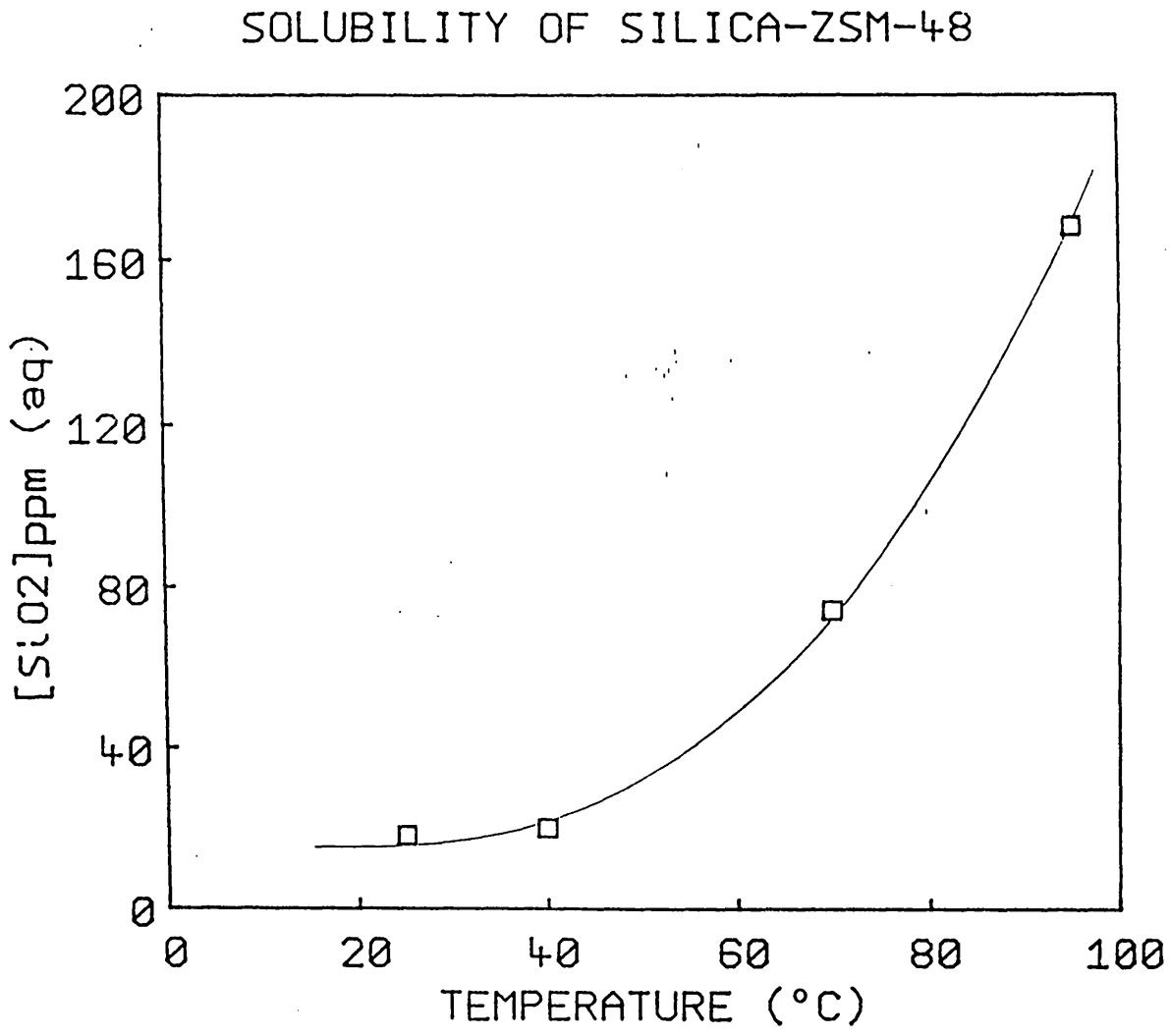

Figure 5.8 Solubility of H-silica-ZSM-48 in water

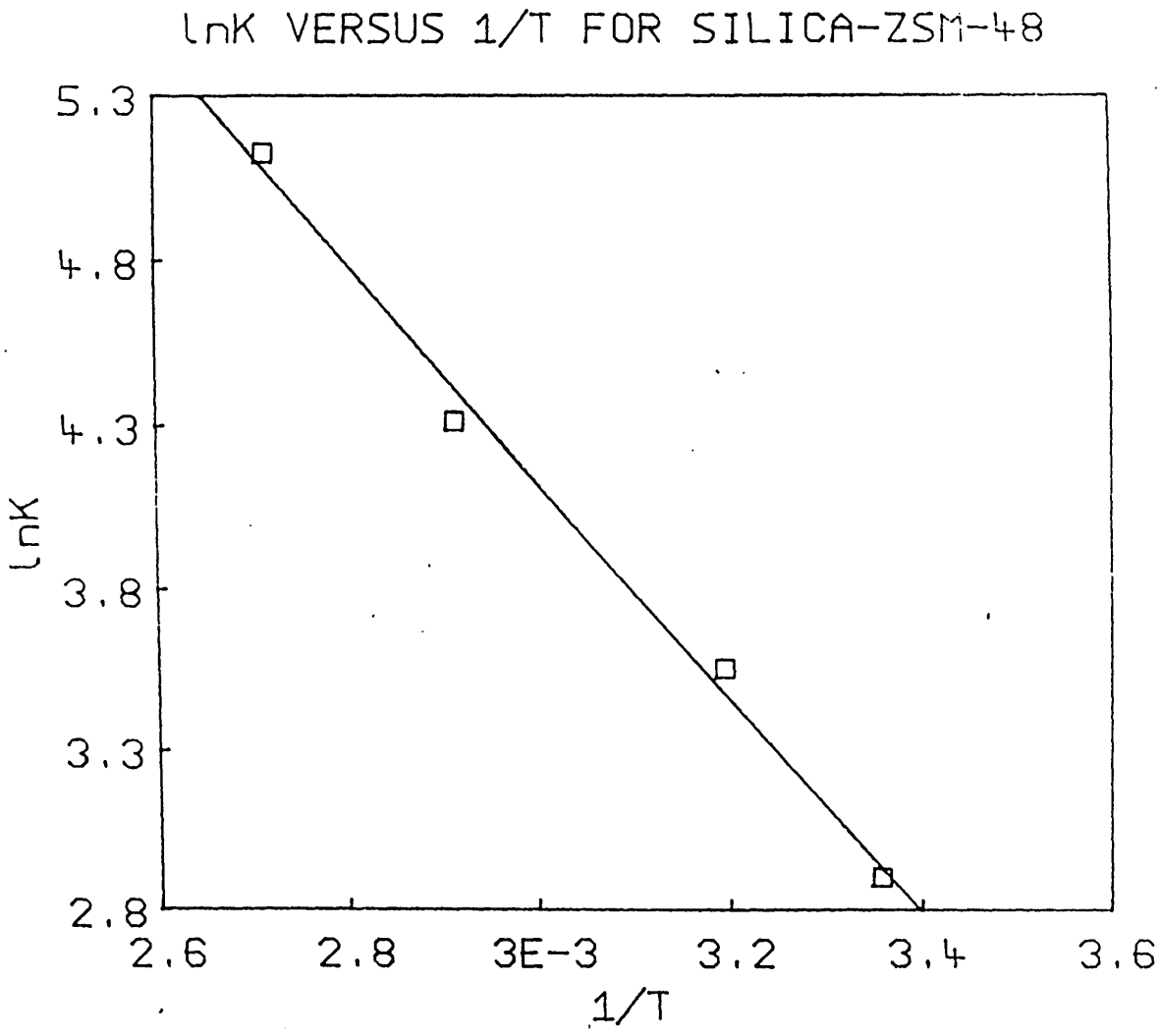

Figure 5.9 Van't Hoff plot for H-silica-ZSM-48

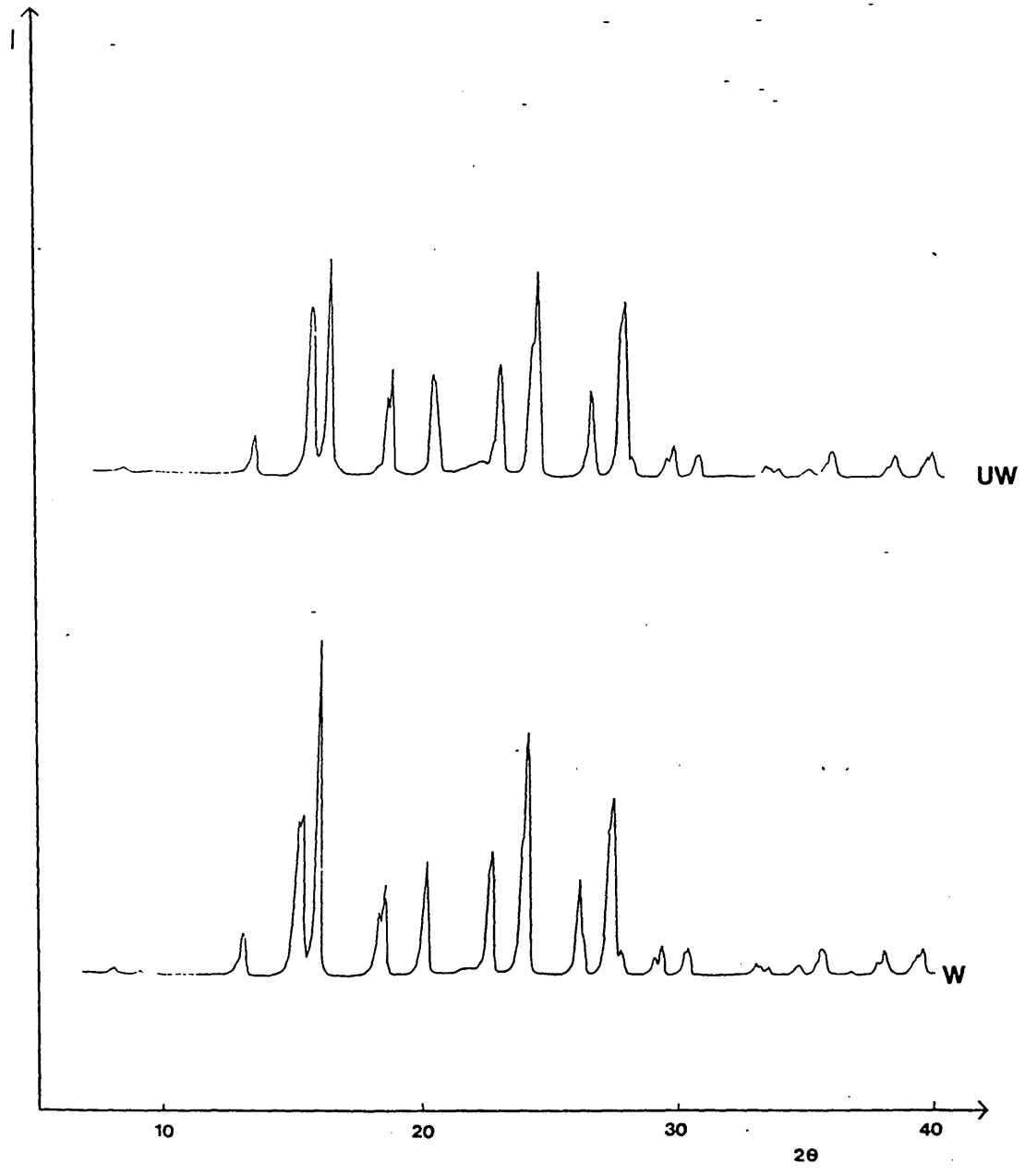

Figure 5.10 XRD patterns of untreated (UW) and treated (W) ZSM-39

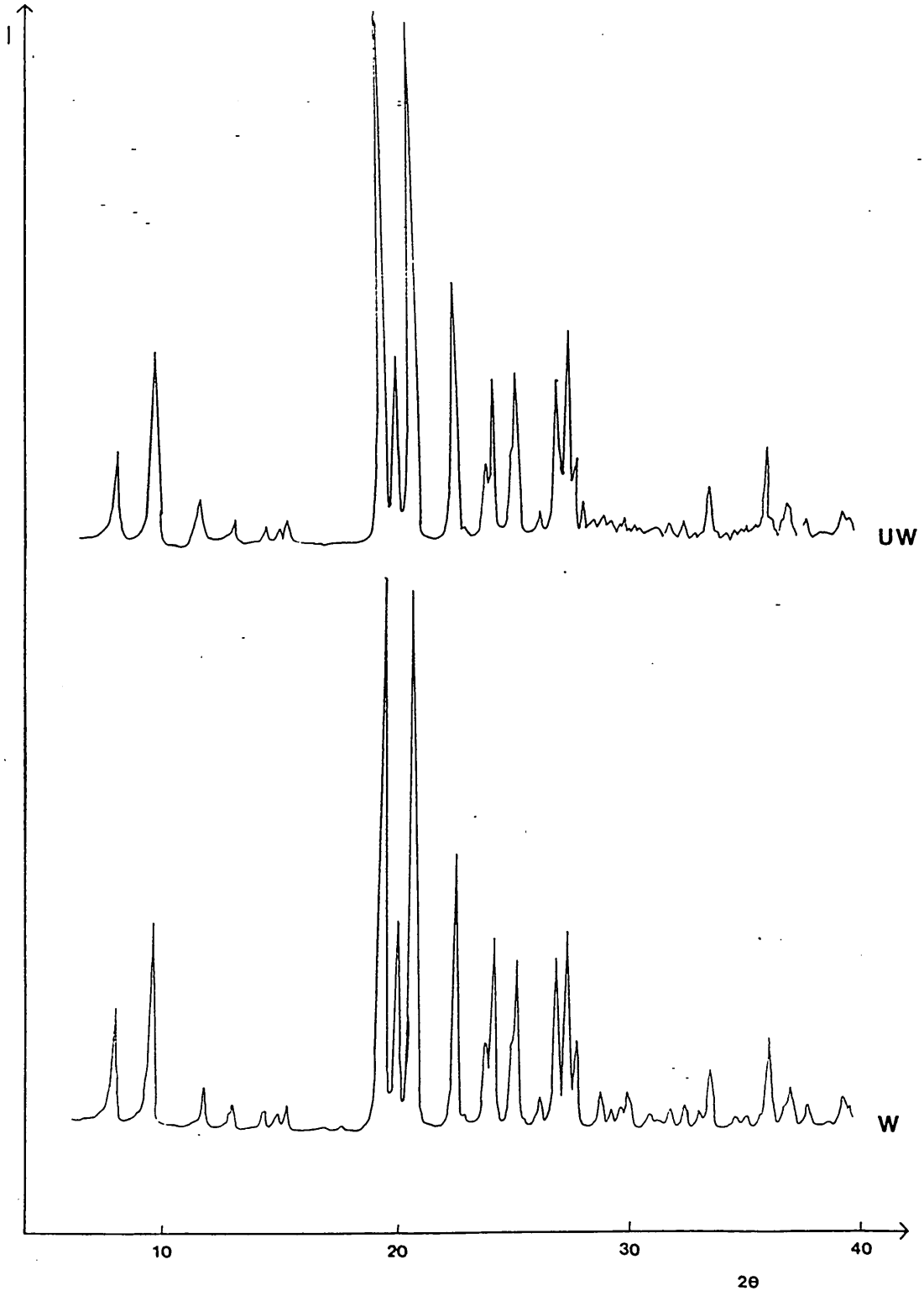

Figure 5.11 XRD patterns of untreated (UW) and treated (W) EU-4

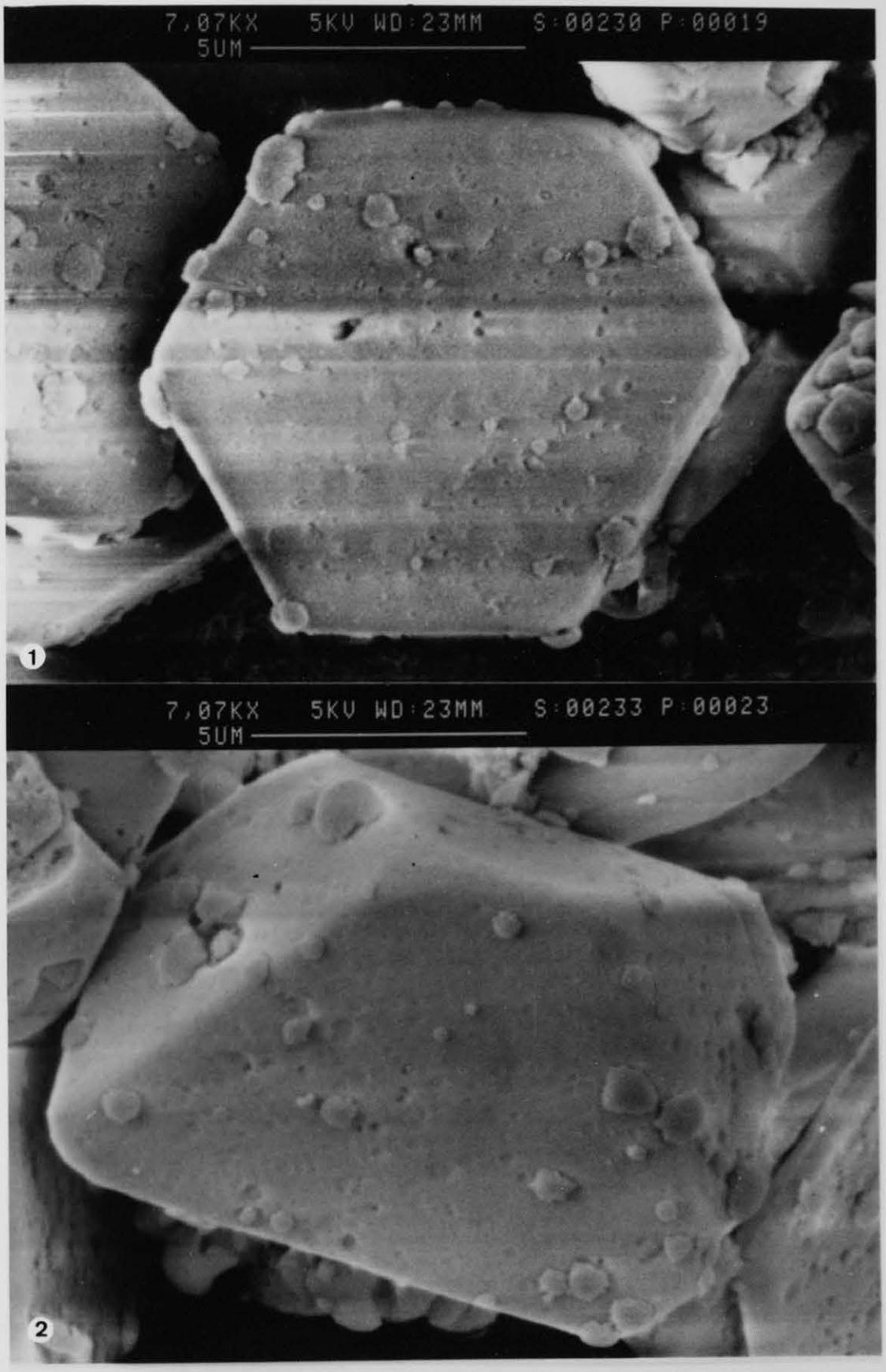
7,07KX 5KV WD:23MM S:00230 P:00019
5UM
1
7,07KX 5KV WD:23MM S:00233 P:00023
5UM
2

PLATE 5.2

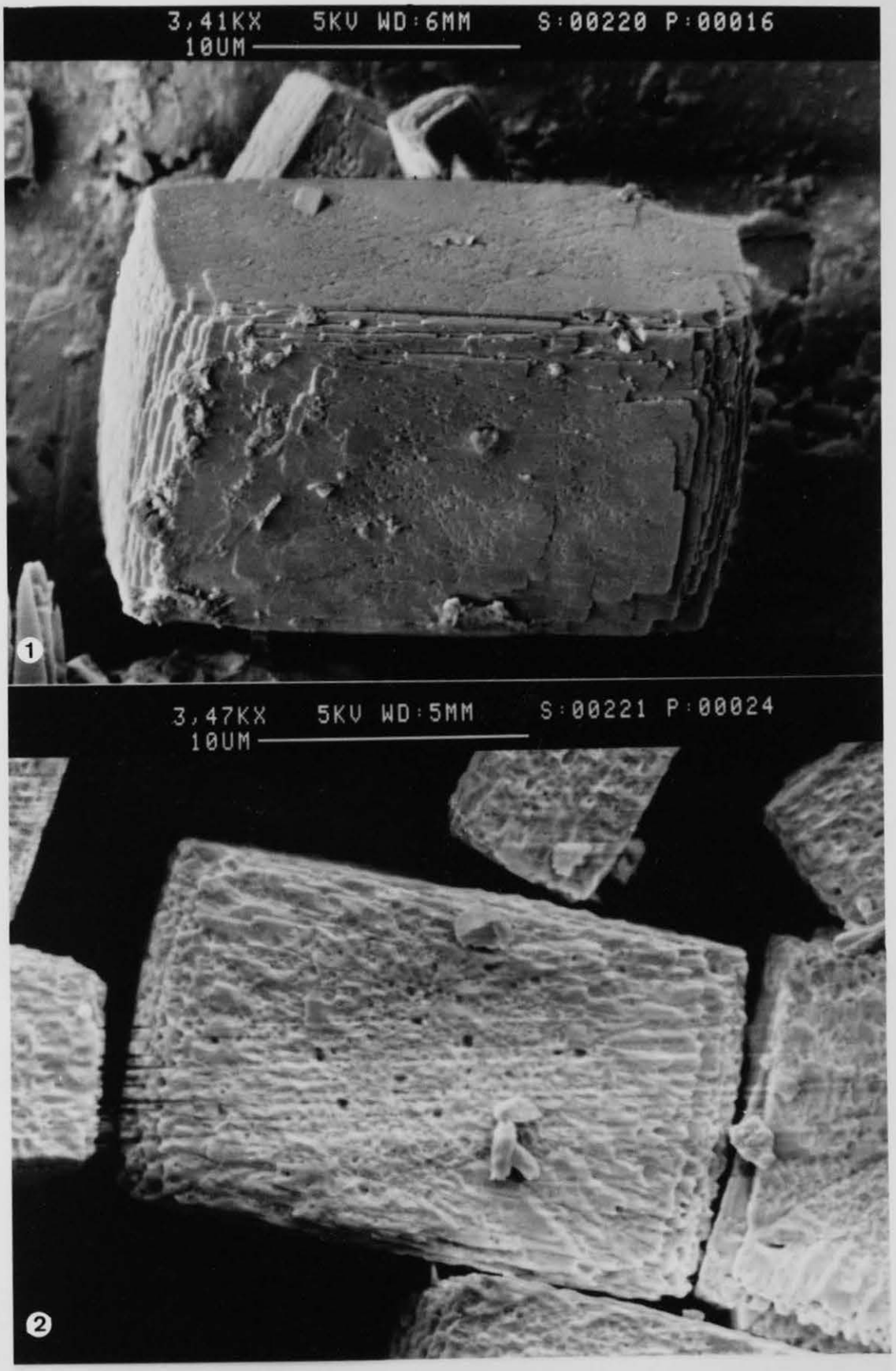
3,41KX 5KV WD:6MM S:00220 P:00016
10UM
1
3,47KX 5KV WD:5MM S:00221 P:00024
10UM
2

PLATE 5.3

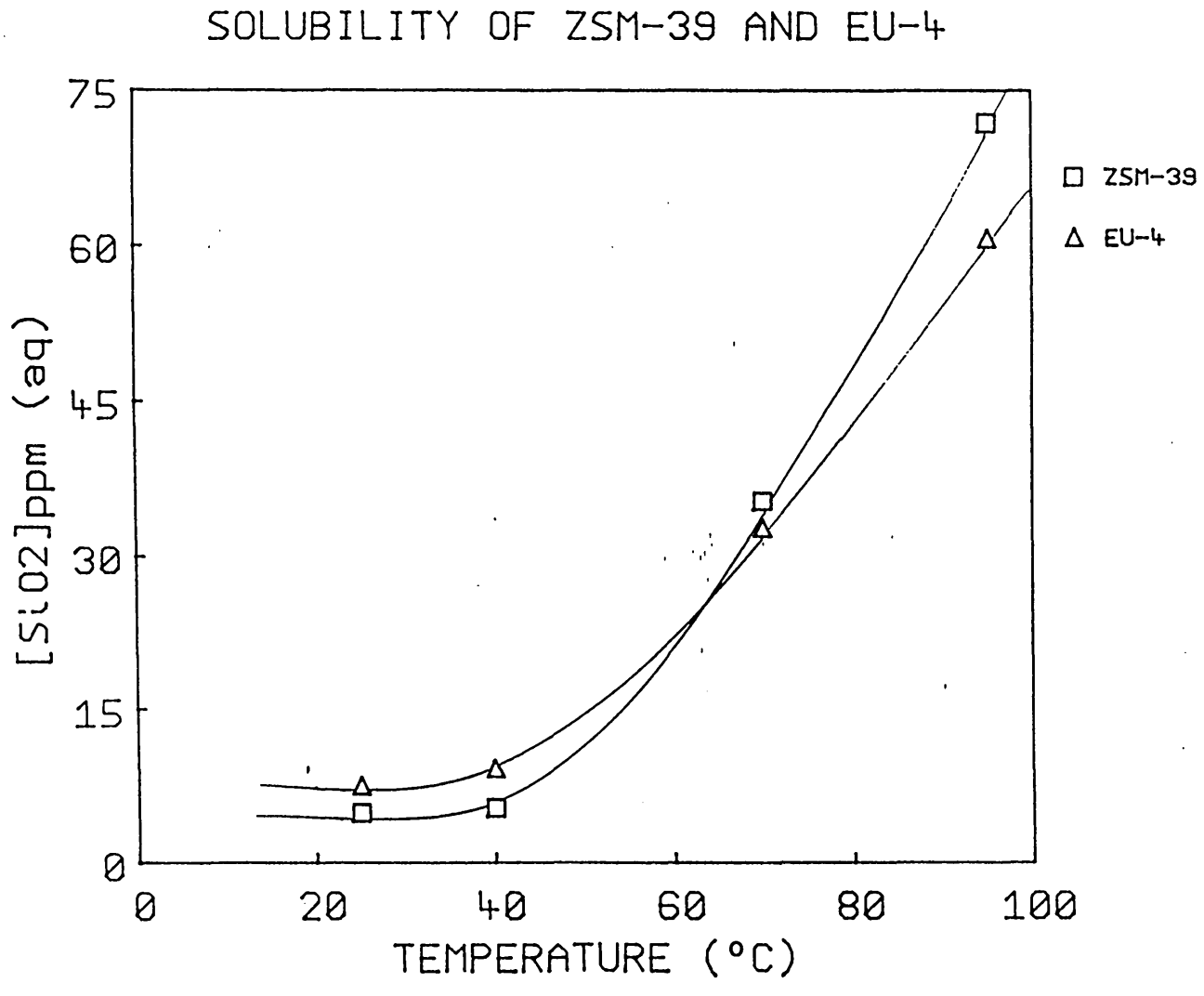

Figure 5.12 Solubility of ZSM-39 and EU-4 in water

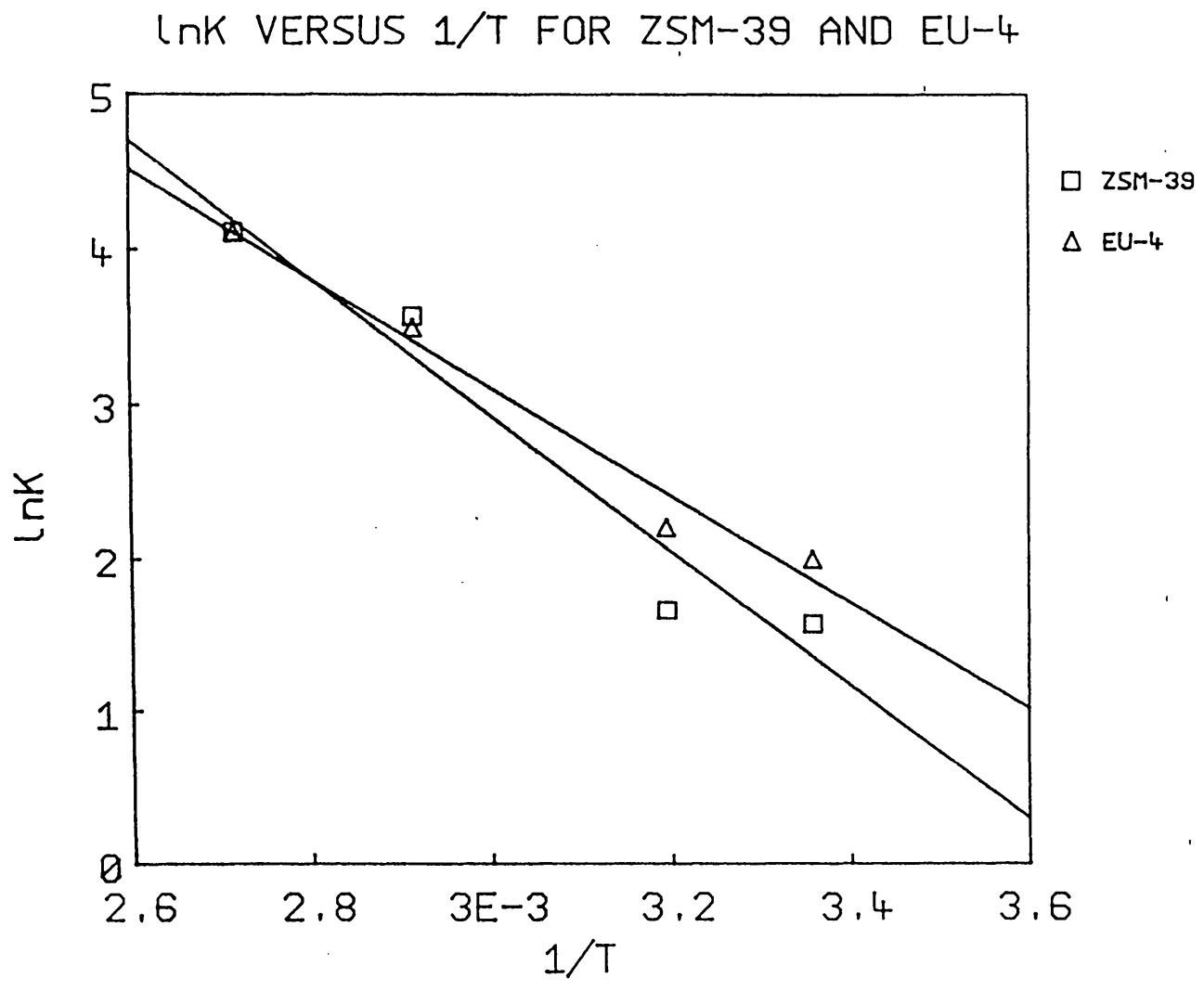

Figure 5.13 Van't Hoff plot for ZSM-39 and EU-4

5.4 Conclusion

The studies of the solubility of H-silicalite show that it is contaminated with amorphous silica. This may be residual material from the crystallisation or it may be generated by calcination. The presence of amorphous silica contaminants gives solubilities for H-silicalites which are too high when low L/S ratios are used. At very low L/S ratios the observed solubility is that of the amorphous material.

Since temperature increases solubility then the effect of amorphous silica will become less as the temperature is elevated. Solubility will be affected by broken framework siloxane bonds. If silanols are clustered within the silicalite framework then parts of the internal and external surface may dissolve to give solubility values somewhere between those for amorphous silica and crystalline H-silicalite. The model developed to account for the variation of observed solubility with L/S ratio is fairly simple, but in principle it can be further refined to take into account inhomogeneities in the solid phases and the different silicic acid species in the solution phase.

Uncalcined silicalites have solubilities which are less than for calcined ones. The presence of the template appears to stabilise the framework and hence reduce its solubility. The addition of either organic molecules that can stabilise the lattice or silicic acid to the aqueous phase may inhibit the dissolution of molecular sieves. Amorphous silica dissolves preferentially to crystalline silica, hence addition of amorphous silica should suppress dissolution of crystalline silicas. Framework damage will increase the hydrophilicity of silicalite and so decrease its organophilicity, and its capacity to sorb organic species from aqueous solution. Stabilisation of molecular sieves against dissolution is essential for their prolonged use in aqueous environments. It is noteworthy that the least soluble materials are the least hydrophilic and hence the best sorbents. It is also of interest that when a silica molecular sieve is loaded with sorbate it will be more resistant to

dissolution than when in its organic free state.

The heat of solution of H-silicalite was intermediate between those for ZSM-48 and ZSM-11. The ZSM-11 structure contains more 4-T atom rings, than ZSM-5, hence it is probably more strained, and this could account for its lower heat of solution and its higher solubility. Since silica molecular sieves are all composed of similar Si-O bonds, their solubilities are expected to be very similar and close to that of quartz. However the presence of structural strain or broken siloxane bonds should make silica molecular sieves more soluble than quartz. All of the pure silica materials investigated in the present study had solubilities at 25°C close to or larger than that observed for quartz (14.1 ppm). However silica molecular sieves stabilised by organic template were invariably less soluble than quartz.

Chapter 5 References

[1] R.K. Iler

"The Chemistry of Silica",

Wiley, New York, 1979, page 3.

[2] J.S. Falcone

"Soluble Silicates",

ACS Symposium Series, No. 194, 1982, page 73.

[3] S.A. Greenberg

J. Phys. Chem., 1957, **61**, 196.

[4] G.B. Alexander

J. Phys. Chem., 1957, **61**, 1563.

[5] T.M. El-Shamy, J. Lewins and R.W. Douglas

Glass Technology, 1972, **13**, 81.

[6] J.L. Guth, P. Caullet and R. Wey

Bull. Soc. Chim. Fr., 1974, **9-10**, 1758.

[7] J.L. Guth, P. Caullet and R. Wey

Bull. Soc. Chim. Fr., 1975, **9-10**, 2363.

[8] J.L. Guth, P. Caullet, P. Jacques and R. Wey

Bull. Soc. Chim. Fr., 1980, **3-4**, 121.

[9] J.L. Guth, P. Caullet and R. Wey

Bull. Soc. Chim. Fr., 1975, **11-12**, 2375.

[10] P. Caullet, J.L. Guth, A. Kalt, G. Nanse

and R. Wey

C. R. Ac. Sci. Paris (Ser D), 1978, **287**, 763.

[11] P. Caullet, J.L. Guth and R. Wey

C. R. Ac. Sci. Paris (Ser D), 1979, **288**, 1.

[12] P. Caullet, J.L. Guth and R. Wey

Bull. Mineral., 1980, **103**, 330.

[13] R.M. Barrer, J.W. Baynham, F.W. Bultitude

and W.M. Meier

J. Chem. Soc., 1959, 195.

[14] S.P. Zhdanov

Advan. Chem. Ser., 1971, **101**, 20.

[15] G.T. Kerr

J. Phys. Chem., 1966, **70**, 1047.

[16] G.H. Kuehl

Advan. Chem. Ser., 1971, **101**, 63.

[17] F.E. Schwochow and G.W. Heinze

Advan. Chem. Ser., 1971, **101**, 102.

[18] C.L. Angell and W.H. Flank

ACS Symposium Series, 1977, **40**, 194.

[19] A. Culfaz and L.B. Sand

Advan. Chem. Ser., 1973, **121**, 140.

[20] J.L. Guth, P. Caullet and R. Wey

"Proceedings of the Fifth International

Zeolite Association Conference", Naples, 1980, 30.

[21] H.E. Allen, S.H. Cho and T.A. Neubecker

Water Res., 1983, **17**, 1871.

[22] T.E. Cook, W.A. Cilley, A.C. Savitsky

and B.H. Wiers

Environ. Sci. Technol., 1982, **16**, 344.

[23] R.M. Dessau

U.S. Patent 4,272,288 (1981).

[24] R.M Barrer and E.V.T. Murphy

J. Chem. Soc. (A), 1970, 2506.

[25] T.P.J. Izod

European Patent Application, 13451 (1980).

[26] T.P.J. Izod

U.S. Patent 4,331,694 (1982).

[27] S. Kulprathipanja and R.W. Neuzil

U.S. Patent 4,319,928 (1982).

[28] S. Kulprathipanja and H.S. Bloch

U.S. Patent 4,333,768 (1982).

[29] S. Kulprathipanja and R.W. Neuzil

U.S. Patent 4,333,769 (1982).

[30] S. Kulprathipanja

U.S. Patent 4,431,456 (1984).

[31] S.G. Shilton

Fourth Year Report, Edinburgh University (1983).

[32] D. Hoebbel, A. Vargha, B. Fahlke

and G. Engelhardt

Z. anorg. allg. Chem., 1985, **521**, 61.

[33] R. K. Iler

"The Chemistry of Silica",

Wiley, New York, 1979, page 97.

[34] T.L. O'Connor

J. Phys. Chem., 1961, **65**, 1.

[35] V.W. Truesdale and C.J. Smith

Analyst, 1975, **100**, 203.

[36] V.W. Truesdale and C.J. Smith

Analyst, 1975, **100**, 797.

[37] K.A. Fanning and M.E.Q. Pilson

Analytical Chemistry, 1973, **45**, 136.

[38] N.K. Mitra, P.K.D. Poddar and R.G. Dastidar

Indian Ceram., 1983, **26**, 83.

[39] S. Kitahara

Rev. Phys. Chem. Japan, 1960, **30**, 131.

[40] L.S. Dent Glasser

"proceedings of the International Zeolite

Association Conference", Naples, 1980, 63.

[41] R.O. Gould, B.M. Lowe and N.A. MacGilp

J. Chem. Soc., Chem. Commun., 1974, 720.

[42] R.K. Harris, C.T.G. Knight and D.N. Smith

J. Chem. Soc., Chem. Commun., 1980, 726.

[43] D. Hoebbel, G. Garzo, G. Engelhardt and A. Till

Z. anorg. allg. Chem., 1979, **450**, 5.

[44] S.A. Greenberg

J. Phys. Chem., 1957, **61**, 960.

[45] B.M. Lowe

Zeolites, 1983, **3**, 300.

[46] J.L. Schlenker, F.G. Dwyer, E.E. Jenkins,

W.J. Rohrbaugh and G.T. Kokotailo

Nature, 1981, **294**, 340.

[47] P. Chu

U.S. Patent 4,397,827 (1981).

[48] A. Araya and B.M. Lowe

J. Catal., 1984, **85**, 135.

[49] J.L. Schlenker, W.J. Rohrbaugh, P. Chu,

E.W. Valyocsik and G.T. Kokotailo

Zeolites, 1985, **5**, 355.

[50] D.M. Bibby and L.M. Parker

Zeolites, 1983, **3**, 11.

[51] J.L. Casci, B.M. Lowe and T.V. Whittam

European Patent Application, 63436 (1982).

CHAPTER 6

THE HYDROTHERMAL STABILITY OF SILICALITE

6.1 Introduction

The solubility results described in Chapter 5 indicated that amorphous silica was present as an impurity in calcined TPA-silicalite (H-silicalite). The presence of amorphous silica is likely to affect the chemical and physical properties of the material, and it was therefore decided to carry out a detailed investigation. The properties chosen for study were:

(1) Thermal behaviour.

(2) Water sorption.

(3) X-ray powder diffraction pattern.

(4) Morphology.

Both the area and the peak position of the DTA exotherm for the combustion of the TPA template should be changed by the presence of amorphous silica, as it would restrict both the access of oxygen to the template and the outward diffusion of the decomposition products (1,2,3). This would occur if the amorphous material were present on the crystal surface or inside the crystal (e.g. at the channel intersections).

The water sorption behaviour of the H-silicalite (4) will be related in part to the amount of silanol rich amorphous silica present, either within the silicalite channel system or on its crystal surfaces. Crystal damage will also affect water uptake.

The presence of framework silanols (5,6,7) also affects the water sorption properties of silicalite. These affect the balance between hydrophobic and hydrophilic properties. Hunger et al (8) concluded from NMR studies that up to 8% of the lattice Si in highly siliceous ZSM-5 is present as Si-OH.

Silicalite undergoes a change from orthorhombic to monoclinic symmetry on calcination. Wu et al (9) indicated that water vapour may promote this change by relocation of residual sodium species.

More recently, it has been shown that the transition can occur in the absence of water and that this change is reversible (10). It seemed likely that because the transformation is dependent on quite small changes in conditions it could also be affected by the presence of amorphous material, especially if present within the crystals.

As described in Chapter 5.0 the presence of amorphous silica gives solubility values which depend on the liquid/solid (L/S) ratio and to obtain accurate solubilities for H-silicalite it is essential either to remove this amorphous silica or to work at very high L/S ratios. The only way in which amorphous silica can be readily removed is by selective dissolution in hot water. In this chapter the effect of various hydrothermal treatments on the properties of calcined TPA-silicalite are described.

6.2 The hydrothermal treatment of low pH 95°C silicalite products

6.2.1 Experimental

Each reaction product mentioned in Chapter 3.0, with the exception of material A4, was hydrothermally treated by the following method.

Particular masses of each product silicalite and water were weighed into a 1 litre polypropylene bottle, so that the resultant heterogeneous system always had a liquid/solid ratio of 200. A paddle was screwed to the top of each bottle and the vessels were inserted into the 95°C thermostat bath, as explained for silicalite synthesis (section 3.2). After 20 hours the solid phase of the heterogeneous system was filtered off hot on a Buchner funnel, washed with 500 ml distilled water at 95°C, then dried at 110°C for 2 hours in an oven. Millipore filter membranes (0.2um) were used. The solid phase was then reweighed into a 1 litre plastic bottle, along with the required mass of cold distilled water to gave the heterogeneous system a L/S of 200. The plastic bottle and stirrer were then reinserted into the thermostat bath as before. Each product was hydrothermally treated five times at 95°C for 20 hours at a L/S ratio of 200.

6.2.2 Preferred Orientation

The X-ray diffraction patterns of hydrothermally treated samples were run for comparison with their untreated counterparts. Each sample was run over the range 4 to 50 2θ on a sensitivity setting of 10^4.

To describe the treament applied to each sample a series of abbreviations were added in parentheses to the sample code. These abbreviations were as follows:-

UW - Unwashed (not hydrothermally treated)

W - Washed at 95°C (hydrothermally treated)

UC - Uncalcined

C - Calcined

If a sample, for example A2, had been hydrothermally treated, calcined then washed again its code would become A2 (W,C,W). Each sample was identified by this notation.

Examples of XRD patterns of the hydrothermally treated A1 (Figure 6.1), A3 (Figure 6.2) and A2 (Figure 6.3) materials are given in this sub-section.

Material A1 was the product from the reaction mixture:-

10Piperazine 2TPABr $20SiO_2$ $1000H_2O$

The reaction was stirred in a polypropylene bottle at 95°C until crystallisation was completed. When the XRD patterns of A1 (UW,UC) and A1 (W,UC) are compared, Figure 6.1, slight intensity increases in most peaks are observed. This indicates that the washed sample is more crystalline than the as-made material. The unresolved single peak at 24.5 2θ, which corresponds to the 313/133 (hkl) Bragg reflections in the theoretical XRD pattern (11), indicates that the material is in the expected orthorhombic form.

The XRD patterns of materials A1 (UW,C,W) and A1 (W,C,W) show predominant monoclinic symmetry, as evidenced by the splitting of the 313 and 133 Bragg lines into separate resolved peaks at about 24.5 2θ. Material A1 (W,C,W) is the more monoclinic, as can be deduced from the more distinct splitting of the 313 and 133 Bragg reflections. The low angle peaks showed an increase in intensity after calcination. Comparison of the XRD patterns of A1 (UW,C,W) and A1 (W,C,W) shows that the extra hydrothermal treatment prior to calcination leads to an increase in the low angle peak intensities. This indicates further removal of material from the structural voids within the framework after calcination. This effect of the hydrothermal treatment is dealt with in greater detail in Section 6.3.

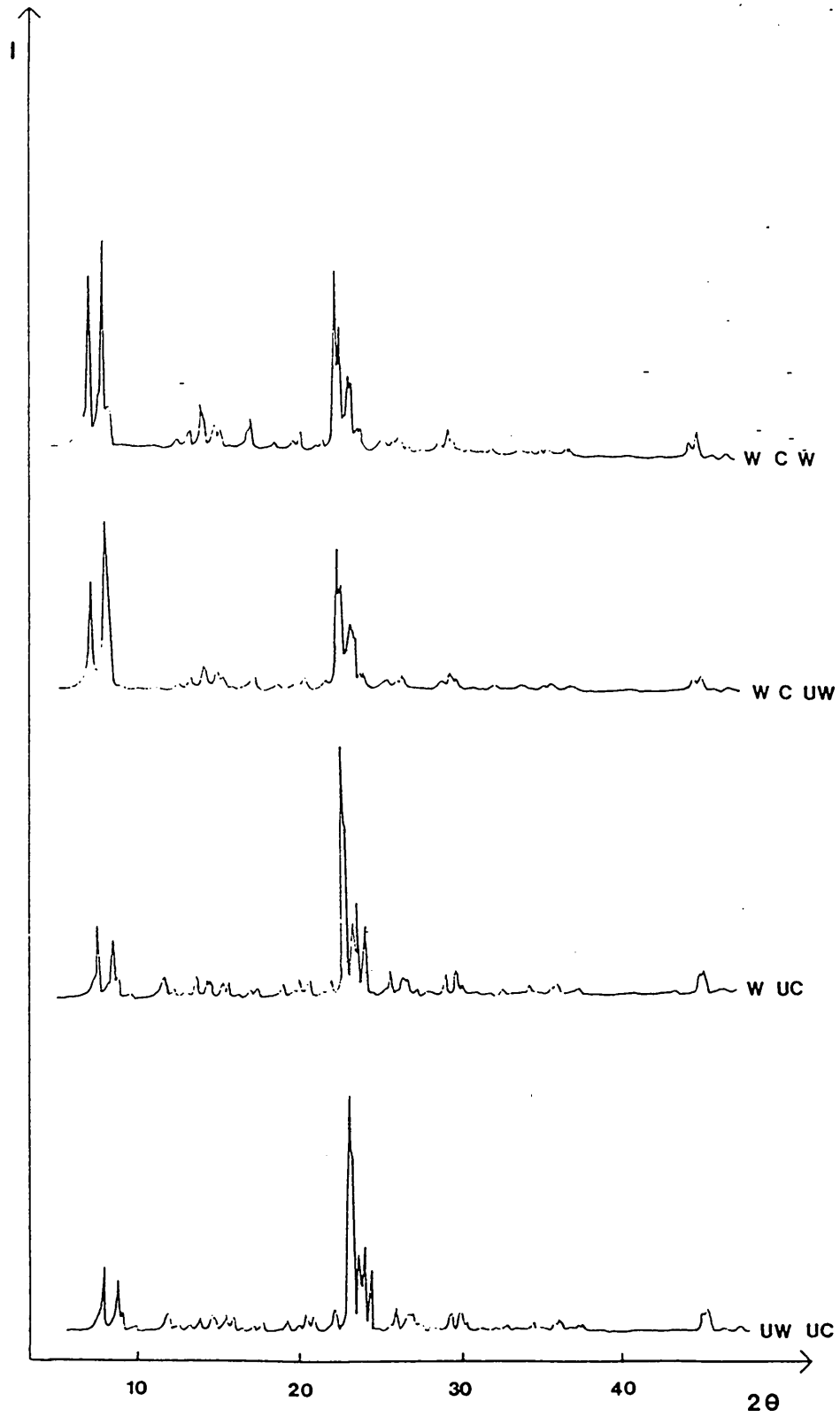

Figure 6.1 XRD patterns of treated Al silicalite samples

Only slight evidence for preferred orientation was observed in the XRD patterns of each A1 material. This indicates that the crystals have a squat morphology. This is confirmed by the electron micrographs in Section 3.3 [Plate 3.1].

Material A3 was synthesised at 95°C from the reaction mixture:-

8Piperazine 2Piperazine.diHCl 2TPABr $20SiO_2$ $1000H_2O$

The product was hydrothermally treated at 95°C as described for material A1.

The XRD patterns of the treated A3 series of materials are in Figure 6.2. All samples were in the orthorhombic form, with the exception of A3 (UW,C,W) which was partly monoclinic, as evidenced by the partial resolution of the 313 and 133 Bragg lines centred at around 24.5 2θ. Comparison of the XRD patterns of A1 (W,C,W) [Fig 6.1] and A3 (UW,C,W) [Fig 6.2] shows the contrast between the complete symmetrical resolution and partial splitting of the 313/133 (hkl) Bragg lines.

The XRD patterns of A3 (UW,UC) and A3 (W,UC) [Fig 6.2] were visually compared by overlaying them on a light box. It was noted that ten peaks decreased and twelve peaks increased in intensity when A3 was hydrothermally treated prior to calcination. Each of the peaks was indexed and assigned lattice indices (hkl). This was done by measuring the position in 2θ of each peak which changed in intensity after the hydrothermal treatment. The emergent peaks were then assigned lattice indices (hkl) by comparison with a theoretical powder pattern for orthorhombic (TPA)-silicalite in the literature (11). The resultant data are shown on the following tables in which the intensities are given as peak heights in cm.

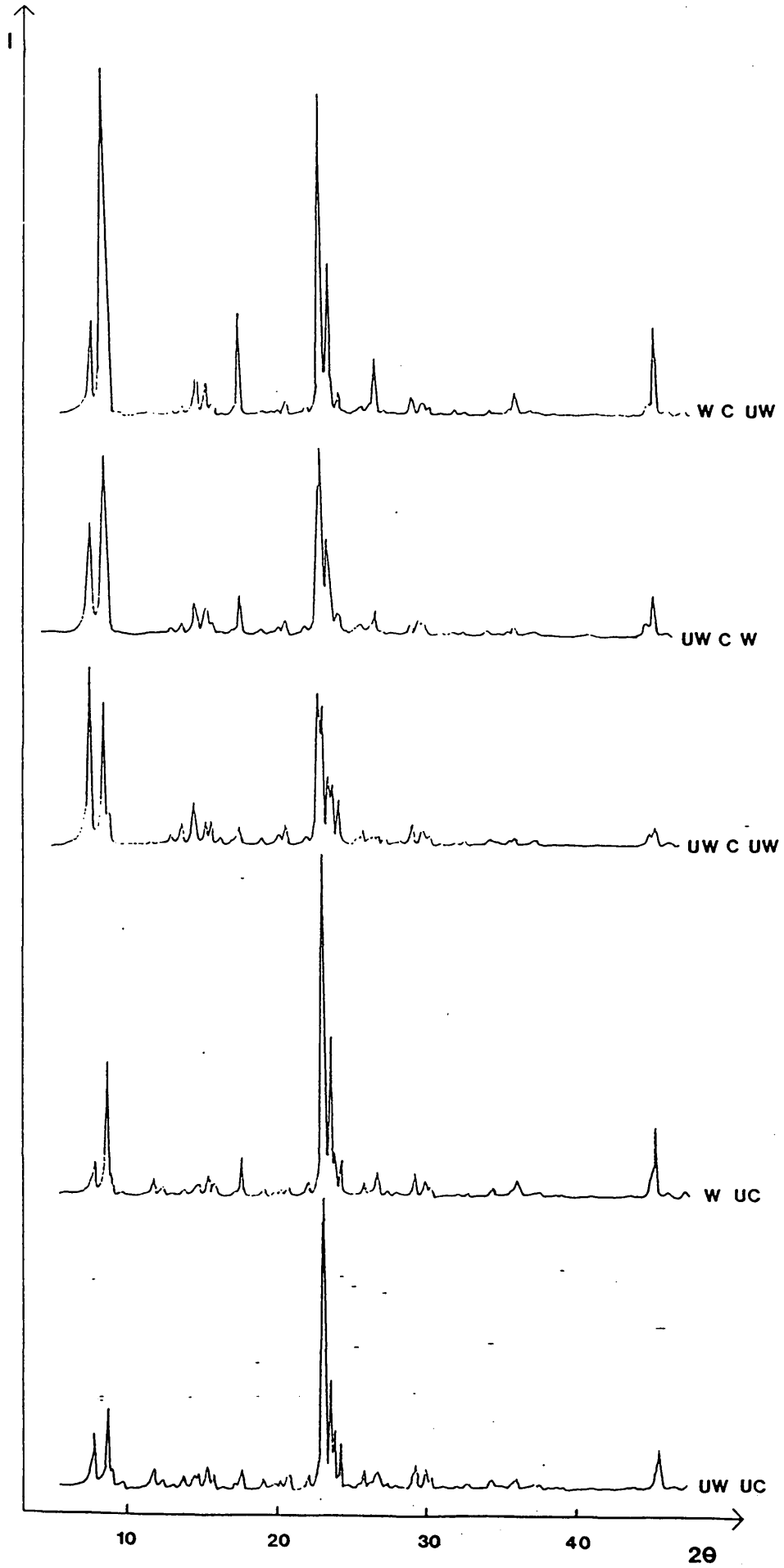

Figure 6.2 XRD patterns of treated A3 silicalite samples

Table 6.1 Comparison of XRDs of A3 (UW,UC) and (W,UC).

Peak Positions (2θ) (UW,UC)	(W,UC)	Intensity (cm) (UW,UC)	(W,UC)	Difference in I (%)
7.96	7.98	3.44	2.16	-37%
8.84	8.95	5.06	9.00	+78%
13.90	14.00	0.80	0.52	-35%
14.58	14.70	0.76	0.60	-21%
15.52	15.58	1.34	1.50	+22%
17.78	17.85	1.30	2.72	+109%
19.28	19.35	0.74	0.52	-29%
19.90	20.00	0.36	0.42	+16%
20.26	20.42	0.66	0.48	-27%
20.72	20.94	0.94	0.74	-21%
23.28	23.46	19.04	33.82	+77%
23.70	23.78	7.14	10.58	+48%
23.93	24.06	3.94	3.00	-23%
24.40	24.52	3.08	2.42	-21%
25.94	26.00	1.34	1.02	-23%
26.30	26.44	0.38	0.44	+15%
26.84	26.92	1.14	1.80	+57%
29.94	30.06	1.34	1.18	-11%
35.94	36.08	0.76	1.18	+55%
45.46	45.58	2.58	4.60	+78%
46.20	46.30	0.26	0.48	+84%
46.40	46.44	0.24	0.38	+58%

Table 6.2 Lattice Indices of A3 Emergent Peaks.

A3 (W,UC) Peak (2θ)	Intensity Increase (%)	Lattice Indices (hkl)	Literature Intensities (%) [11]
8.95	+78%	2 0 0	35.0%
		0 2 0	29.4%
15.58	+22%	3 1 1	1.4%
		1 3 1	10.8%
17.85	+109%	0 4 0	5.5%
		4 0 0	2.8%
23.46	+78%	3 3 2	3.5%
		5 0 1	100.0%
		0 5 1	78.4%
		4 3 1	2.1%
23.78	+48%	1 5 1	36.7%
26.96	+58%	0 0 4	1.9%
		4 0 3	4.2%
		3 5 1	0.7%
		6 0 0	1.8%
		0 6 0	2.4%
35.08	+55%	8 0 0	2.9%
		0 8 0	1.9%
		2 5 4	1.1%
		3 0 5	1.6%
		0 3 5	2.5%
45.58	+78%	8 0 4	5.7%
		0 8 4	3.5%
		10 0 0	6.2%
		0 10 0	9.4%
		4 8 3	3.5%
		1 8 4	1.8%
46.30	+85%	2 8 4	1.2%
46.44	+58%	4 3 6	3.6%

The major peaks with lattice indices h00 and 0k0 increased most in intensity, with the exception of the 501/051 peak at 23.46 2θ. When a Bragg reflection occurs, the intensity of the diffracted peak on a pattern is dependent on the amount of material in the particular crystal plane(s) which caused the reflection.

From the crystal data for orthorhombic silicalite/ZSM-5 $[(C_3H_7)_{16}N_4\ Si_{96}O_{192}(OH)_4]$ in the literature (11) a=20.096Å, b=19.949Å and c=13.428Å. Since the unit cell constants a and b are close then lines such as 200 and 020 (hkl) are often unresolved.

Calcination altered certain peak intensities and led to the resolution of the 10 0 0 and 0 10 0 lines centred around 45.5 2θ. The higher angle peak which corresponded to the 0 10 0 (hkl) reflection was far stronger in intensity than the 10 0 0 line. On calcination, lines indexed 0k0 became resolved and always occurred at a slightly higher angle than h00 peaks (where h=k). The 200/020 (hkl) peaks were always unresolved.

Table 6.3 compares the peak heights of XRD lines at 17.8 (040), 26.9 (060) and 45.5 (0 10 0) 2θ.

Table 6.3 Peak Intensities of A3 Samples.

Sample A3	Intensity (cm)		
	17.8 2θ 0 4 0&4 0 0	26.9 2θ 0 6 0&6 0 0	45.5 2θ 0 10 0&10 0 0
UW,UC	1.3	1.1	2.6
W,UC	2.7	1.8	4.5
UW,C,UW	1.5	1.2	1.3
UW,C,W	2.6	1.7	2.7
W,C,UW	6.8	3.9	5.9

The hydrothermal treatment appeared to increase the mass of material in the b-plane relative to the a- and c-planes. The same effect was observed for material A2, the XRD patterns of five A2 untreated and hydrothermally treated materials are shown in Figure 6.3.

The XRD patterns of the hydrothermally treated samples of A2 show exactly the same trends as for the A3 series of materials, but the effects are more pronounced. The major changes in XRD peaks are specific to a particular crystal plane, perpendicular to the b-axis. The crystals probably lay in the sample holder in a regular fashion. This would be possible if the crystals were in a flat or needle-like morphology. This effect is known as preferred orientation.

Scanning electron micrographs (SEM) of the materials A2 (UW,C,UW) and A2 (W,C,UW) are in Plate 6.1. These samples were chosen since they exhibited the most extreme effects observed in the XRD patterns. The morphology of crystals was uniform throughout the sample, however there was a wide variation in crystal size.

The SEM in Plate 6.1 show a pair of representative crystals from two A2 samples; their measurements are given in Table 6.4.

Table 6.4 Length/Depth ratio of Crystals in A2 Series.

Sample A2	Length (nm)	Depth (nm)	L/D ratio
UW,C,UW	3900	519	7.51
W,C,UW	3390	390	8.69

This shows that the hydrothermal treatment caused the crystals to

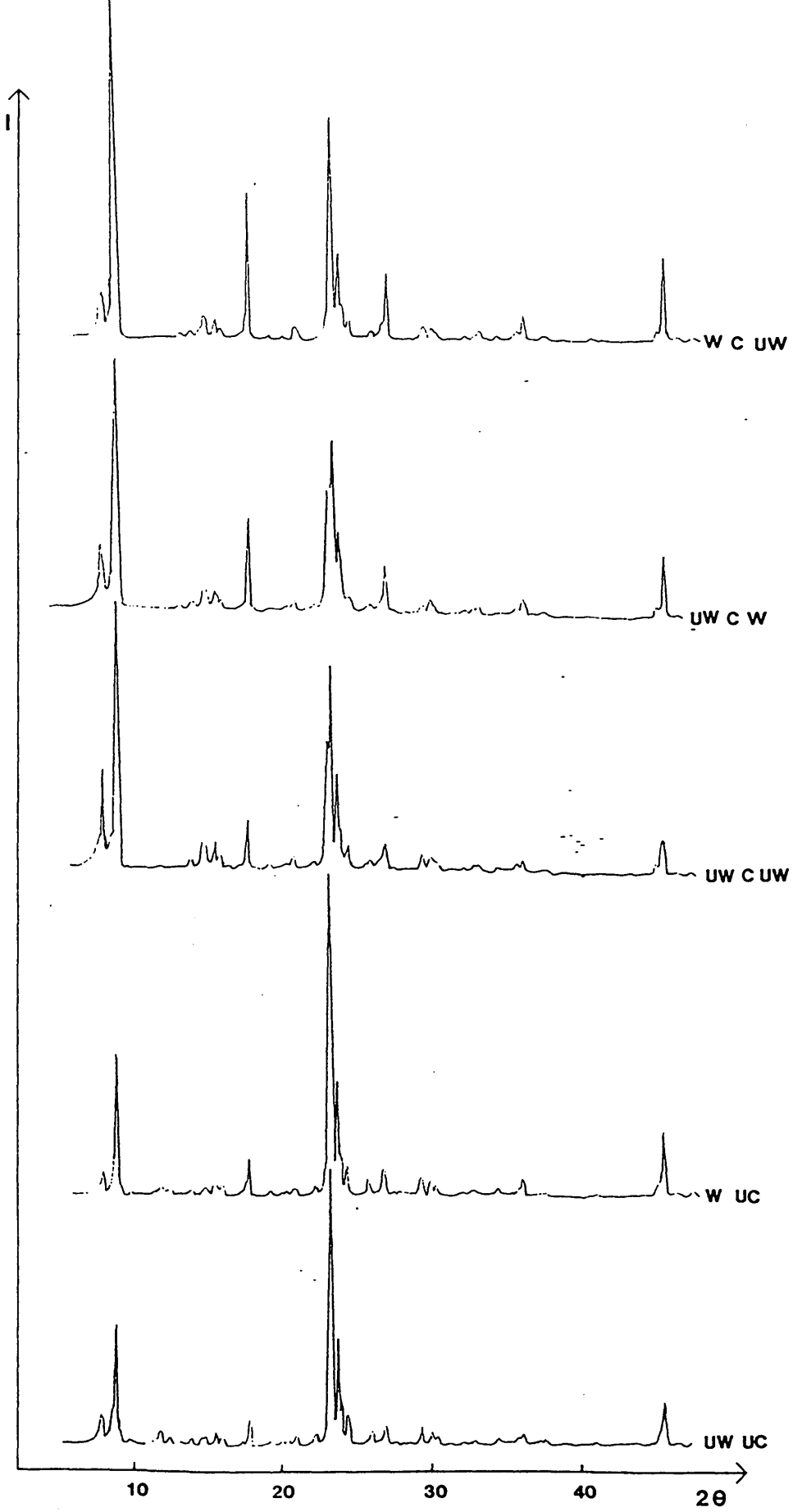

Figure 6.3 XRD patterns of treated A2 silicalite samples

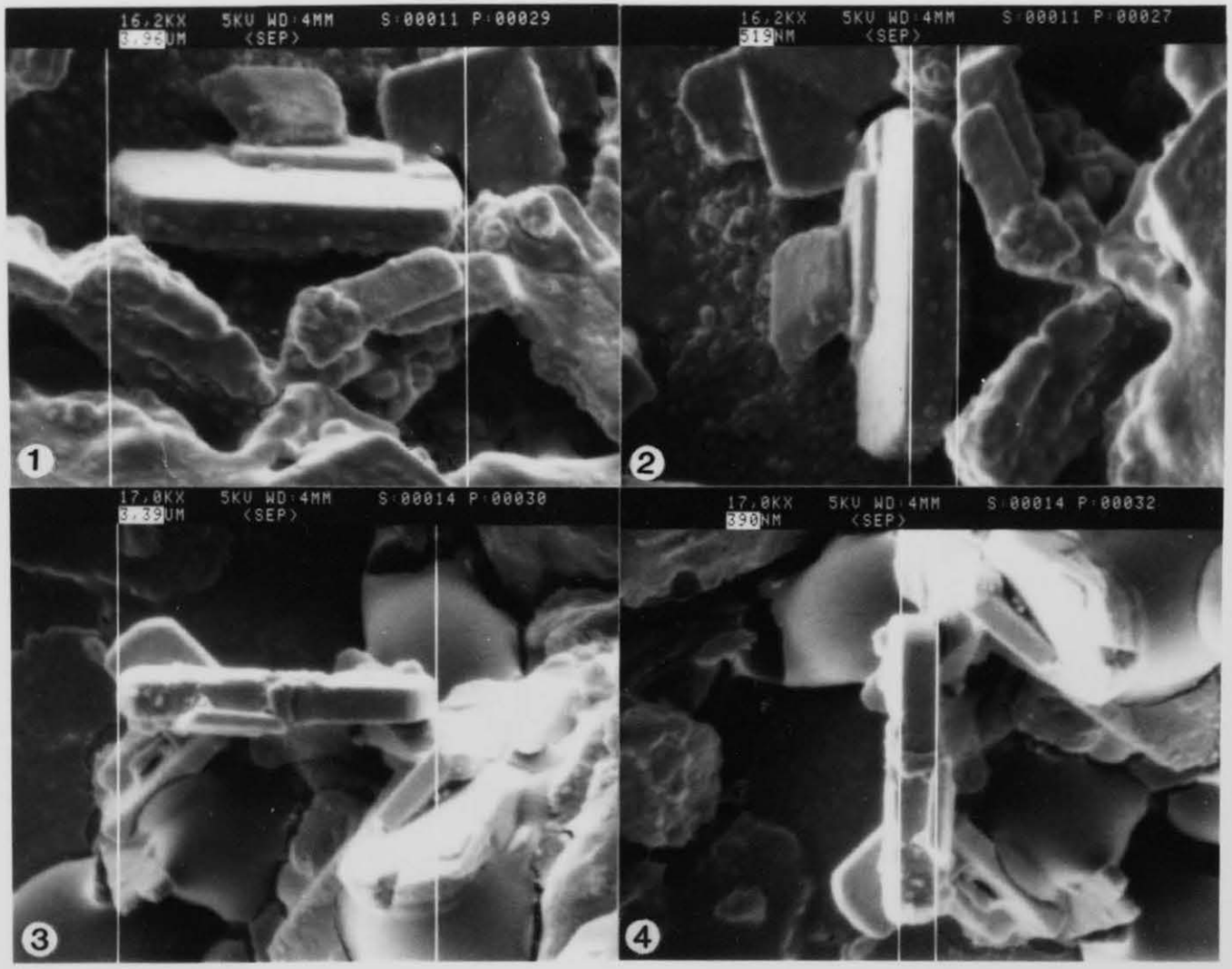
16.2KX 5KV WD:4MM S:00011 P:00029
3.96UM <SEP>
1
16.2KX 5KV WD:4MM S:00011 P:00027
519NM <SEP>
2
17.0KX 5KV WD:4MM S:00014 P:00030
3.39UM <SEP>
3
17.0KX 5KV WD:4MM S:00014 P:00032
390NM <SEP>
4

PLATE 6.1

become thinner, therefore dissolution of single silicalite crystals occurred predominantly in the one plane. The hydrothermal treatment also caused the removal of amorphous particles from the crystal surfaces and the break-up of aggregates. The formation of thinner crystals and the removal of aggregates is likely to promote preferred orientation. Thinner crystals will pack in a more regular manner, oriented in a particular plane within the sample holder. Removal of aggregates will also increase the number of plate-like crystals in the sample.

Plate-like crystals are far more likely to pack oriented in a certain plane than are cube-shaped ones. Morphology can thus dictate how crystals lie in a sample holder. For material A2 (W,C,UW) the plate-like crystals would stack one above the other. Therefore, during XRD, Bragg reflections will become artificially exaggerated in a certain plane (13,14). This was observed most in the XRD trace of A2 (W,C,UW) shown in Figure 6.3.

Studies on materials A3 and A2 showed that lines with 0k0 indices were exaggerated. The crystals were therefore oriented perpendicular to the b-plane when packed in the XRD sample holder.

Samples were submitted to ICI Chemicals and Polymers Limited at Wilton for XRD measurements. The square root intensity scale used for these XRD patterns enhances the intensity of the smaller peaks and the background. The XRD patterns are discussed in Section 6.2.5 and are shown in Figure 6.7, 6.8 and 6.9. The effects of preferred orientation were only very slightly present in these patterns. This is because the samples were rotated in the sample chamber; which should reduce the effects of preferred orientation. XRD effects are further discussed in Section 6.2.5.

6.2.3 Thermal Analysis

The DTA traces of hydrothermally treated uncalcined A1, A2, A3 and A5 were run and compared with those of the as-made materials.

Each DTA run was carried out under the same conditions (see Section 3.3). The heating rate was 1°C/minute, sensitivity was 50

and the chart speed was 0.5 mm/minute. The atmosphere was static air. TG traces were run at 10°C/minute, at 100% full scale deflection, with a chart recorder speed of 2 mm/minute. Flowing air, 15 ml/minute, was used. The DTA traces of each pair of materials are shown on Figure 6.4.

Peak areas were evaluated by tracing each TPA combustion exotherm onto pieces of paper, cutting them out and weighing them. Areas could then be calculated by the comparison of paper weights with the known weight of a known area of paper. The following data were obtained for each of the analysed materials:

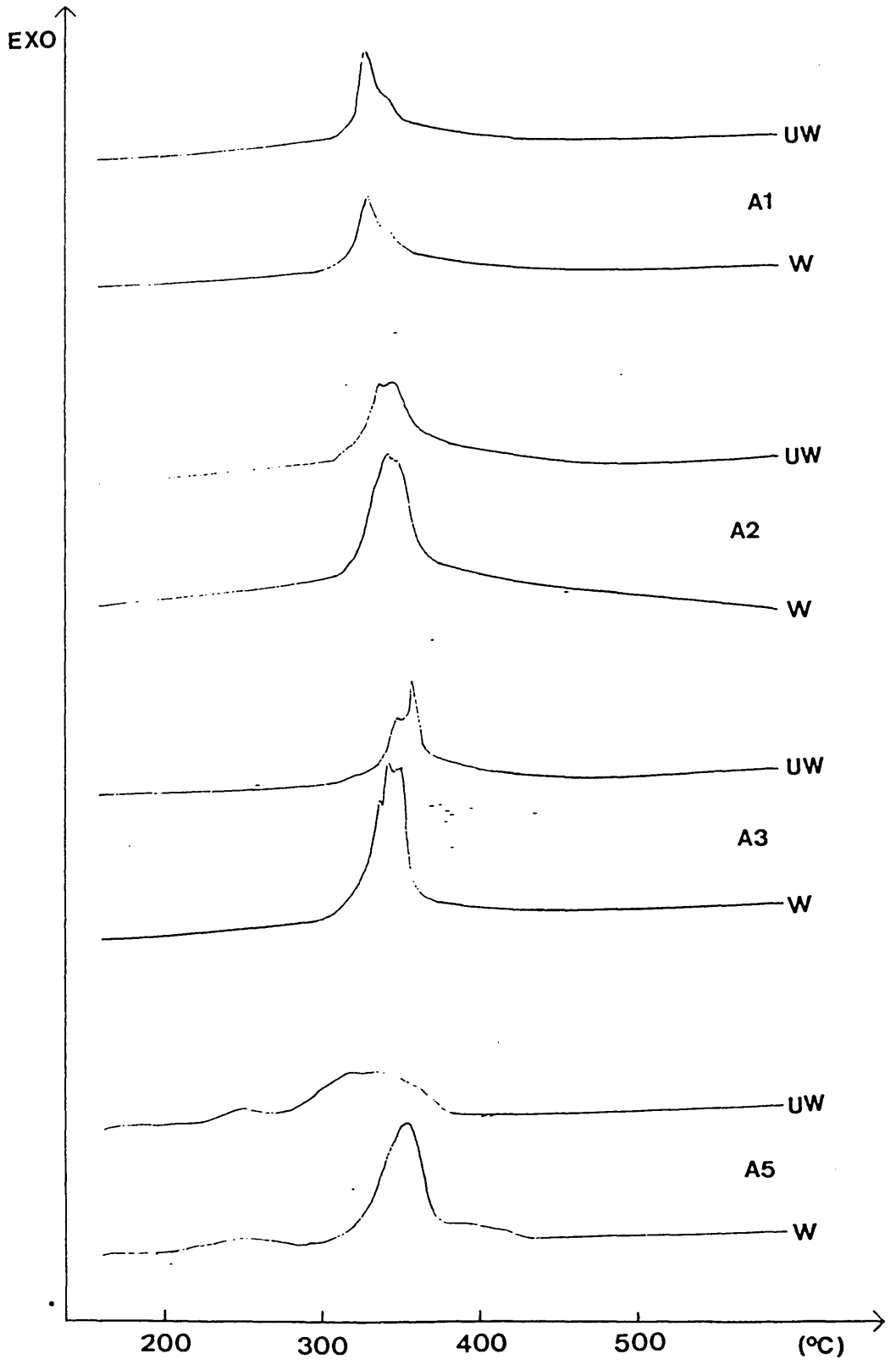

Figure 6.4 DTA traces of untreated (UW) and treated (W) TPA-silicalites

Table 6.5 Thermal Analysis data for materials A1, A2 and A3.

TG/ DTA Data	Samples A1 UW,UC	A1 W,UC	A2 UW,UC	A2 W,UC	A3 UW,UC	A3 W,UC
DTA main peak(s) [°C]	340	350	358 362	352 358	360 370	350 354 358 360
DTA peak area [cm^2]	4.11	4.10	5.79	8.12	3.91	7.13
DTA sample size [g]	0.044	0.042	0.040	0.041	0.040	0.042
TG sample size [mg]	4.32	4.34	7.92	5.40	5.45	6.24
TG weight loss [%]	14.0	12.2	13.0	14.8	12.8	13.6

Table 6.6 Thermal Analysis data for partially crystalline A5.

DTA/TG Data	Samples A5 UW,UC	W,UC
DTA Main Peak [°C]	264 330 350	286 364
DTA peak area [cm^2]	4.47	7.73
DTA sample size [g]	0.0413	0.0397
TG sample size [mg]	4.62	3.81
TG weight loss [%]	10.1	12.8

The splitting of the DTA peaks in the 350 and 360°C temperature range is believed to arise from oxygen starvation. The products of the oxidative degradation of the TPA must diffuse out through the intra and inter crystalline pores, and this slows down the rate at which oxygen reaches the TPA. Consequently the reaction slows down and less heat is given out. Once this has occurred it becomes easier for oxygen to reach the sample and the rate of the exothermic reaction increases. Under some circumstances the cycle may be repeated more than once (15).

For material A1 there was an increase of +10°C in the TPA exotherm peak position after the hydrothermal treatment (c.f. Figure 6.4). This was probably caused by the generation of amorphous silica which settled on the crystal surfaces. This would make access to the silicalite channels difficult and hence increase the time taken by oxygen to diffuse into the pore system, this in turn would slow down the oxidative degradation of the template. The hydrothermal treatment may also heal faults within the framework; this would also reduce the rate at which oxygen and decomposition products could diffuse into and out of the channel system. Generation of amorphous silica and lattice healing are both consistent with the increase in the DTA peak temperature. Little change was noted in the DTA peak area.

Materials A2, A3 and A5 all showed a decrease in the DTA exotherm temperature and an increase in peak area on hydrothermal treament. These observations are consistent with the removal of amorphous silica from the as-made products by the hydrothermal treatment. This results in a faster and cleaner combustion of TPA template since the amorphous material impedes the diffusion of oxygen into or decomposition products out of the silicalite channel system. The peak area therefore increases and the reaction occurs at lower temperatures.

The thermal gravimetry (TG) results for A2, A3 and A5 gave a larger weight loss due to template combustion after the hydrothermal treatment. This was also consistent with the removal of silica from the samples since this would increase the percentage of the sample

which was organic. This effect would also be consistent with cleaner TPA combustion. Figure 6.5 shows a typical TG trace for a silicalite sample. The expected weight loss for TPA combustion is 12.36%. The weight loss which was observed for the partially crystalline A5 was 10.1%. All the other weight losses were greater than 12.36%. Since the temperature range over which weight losses were observed was from room temperature to 1000°C the additional loss of sample mass will be due to water. Some loosely held water will come off at low temperatures. The loss of high temperature water is caused by the healing of silanol groups. There may also be some surface TPAOH. Little or no piperazine was occluded into the silicalite, see Chapter 3.0, so no second organic component was present.

The C, H and N analyses of the hydrothermally treated materials gave C/N values which were higher than for as-made materials, Table 6.7. This indicated cleaner carbon combustions occurred with the samples which had been hydrothermally treated.

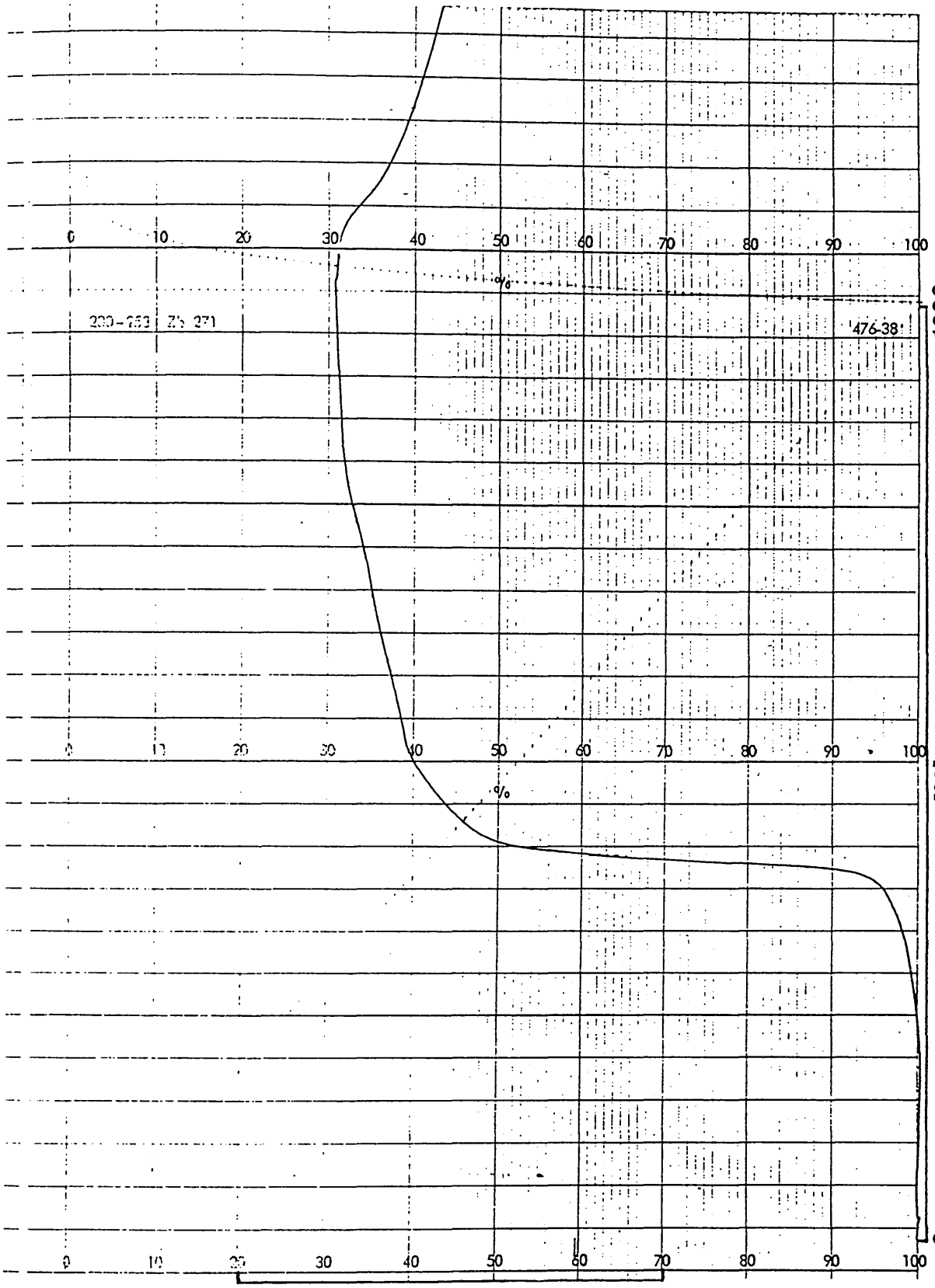

Figure 6.5 TG trace of a typical TPA-silicalite

Table 6.7 C/N ratios of TPA-silicalites.

TPA-silicalite	C/N ratio Untreated	C/N ratio Treated
A2	10.36	10.64
A3	9.28	9.79
A5	6.89	13.08

Hydrothermally treated A5 gave a C/N ratio greater than the ideal value of 12. The amount of nitrogen detected was about 60% of the expected value and may be due to an analytical error. The trend of increased C/N ratios after treatment is, however, quite clear.

6.2.4 13C MASNMR

Material A3 (UC,W<150°C>) was analysed by solid state ^{13}C magic angle spinning nuclear magnetic resonance (MASNMR). The spectrum showed that no decomposition of the TPA had occurred during the hydrothermal treatment. The only organic material present within the silicalite was TPA. The spectrum shown in Figure 6.6 should be compared with those in Section 3.3. The spectrum was in good agreement with that reported by other workers (12). The peak at 111.41ppm is a side band of the Cl resonance at 63.4ppm. The other peaks observed in the spectrum are characteristic of TPA.

6.2.5 X-ray Diffraction

The samples which exhibited preferred orientation were submitted to ICI for X-ray diffraction. The XRD patterns of the A2 series of materials derived by hydrothermal treatment are shown in Fig 6.7.

The patterns for A2 (UW,UC) and A2 (UW,C,UW) showed unsymmetrical doublets at 45-45.5 2θ. The higher angle 0 10 0 (hkl) peak was of greater intensity than the 10 0 0 peak. This implied that preferred orientation also occurred under the running conditions used at ICI. Each material was orthorhombic, as indicated by the unresolved singlet for the 313/133 reflections centred at 24.5 2θ. Unusually, in A2 (UW,C,UW) the 200/020 reflections were resolved and occurred at 8.71 and 8.81 2θ. This separation normally only occurred in

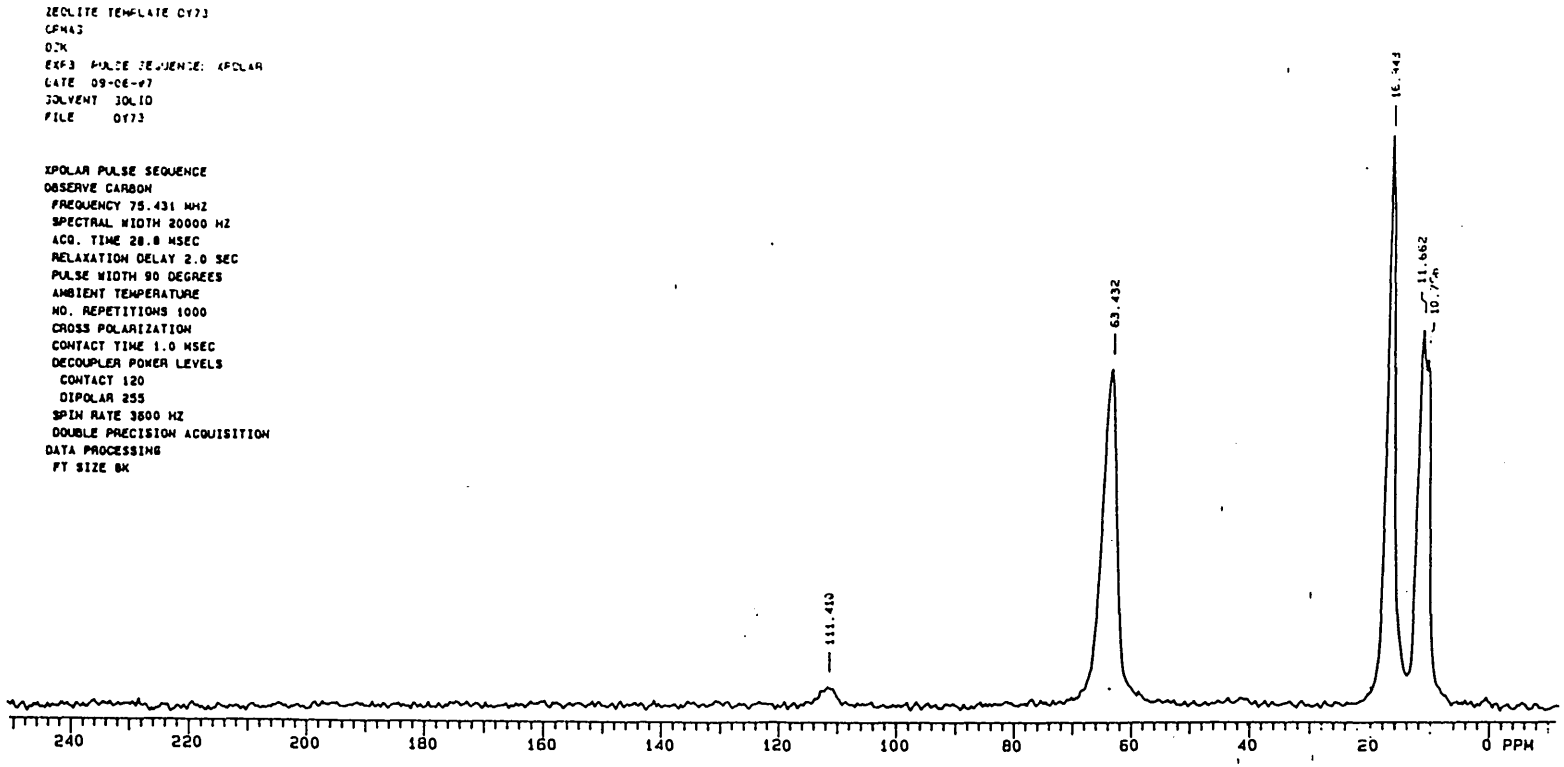

Figure 6.6 ^{13}C MASNMR spectrum of silicalite A3 (W,UC)

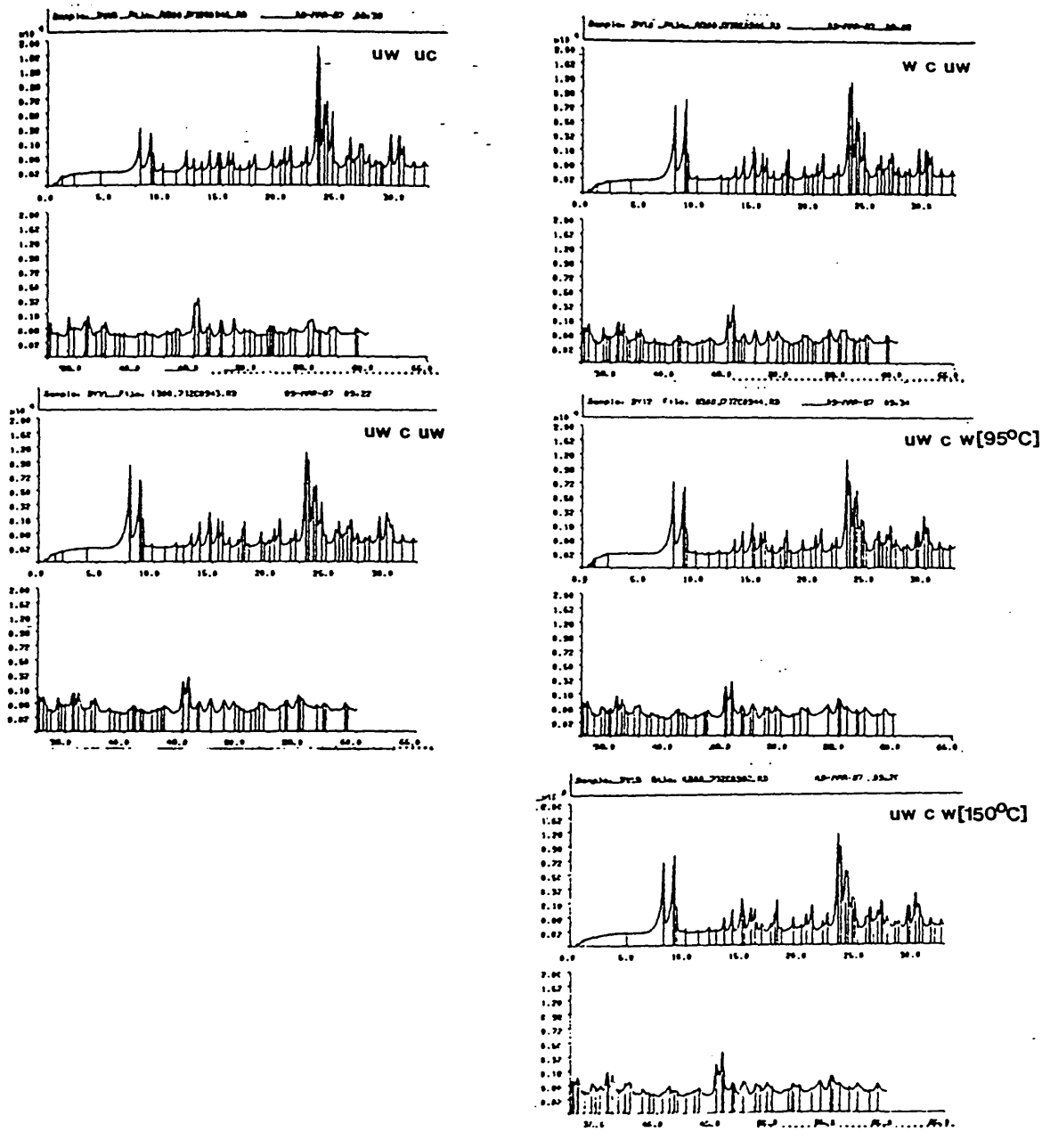

Figure 6.7 XRD patterns of treated silicalite A2 samples

monoclinic samples. Material A2 (W,C,UW) also continued to show orthorhombic symmetry and displayed a 0.11 2θ separation of the 200/020 reflections.

The final materials in the series were A2 (UW,C,W<95°C>) and A2 (UW,C,W<150°C>). The latter had been hydrothermally treated in an autoclave for three hours. Each material exhibited monoclinic symmetry, as demonstrated by the splitting of the 313/133 reflections.

The transition from orthorhombic to monoclinic symmetry arises from an increase in the difference between the unit cell parameters a and b. This increases the splitting between the h00 and 0k0 reflections, for silicalite/ZSM-5 h and k are even numbers for each symmetry.

It was observed that the splitting of the 200/020 reflections increased by 30% between orthorhombic A2 (UW,C,UW) and monoclinic A2 (UW,C,W <95°C>). The material treated with water at 150°C gave a pattern less monoclinic in character than the sample given the more prolonged 95°C hydrothermal treatment. The orthorhombic to monoclinic transition was found to be reversible; on recalcination the hydrothermally treated materials reverted to the orthorhombic form.

Whilst there was little change between the backgrounds of washed and unwashed uncalcined materials, there was a considerable change in the backgrounds of their calcined counterparts. This was also observed in many other cases.

Calcined and uncalcined A3 was hydrothermally treated in a 1 litre autoclave at 150°C and a L/S ratio of 500. The treatment time was 3 hours. The X-ray diffraction patterns of the materials are shown in Figure 6.8. The uncalcined treated material showed orthorhombic symmetry and the calcined treated sample exhibited monoclinic symmetry and resolution of the 200/020 reflections with a difference of 0.11 2θ. The as-made calcined orthorhombic material gave a 200/020 splitting of 0.08 2θ. There was some continued evidence of preferred orientation.

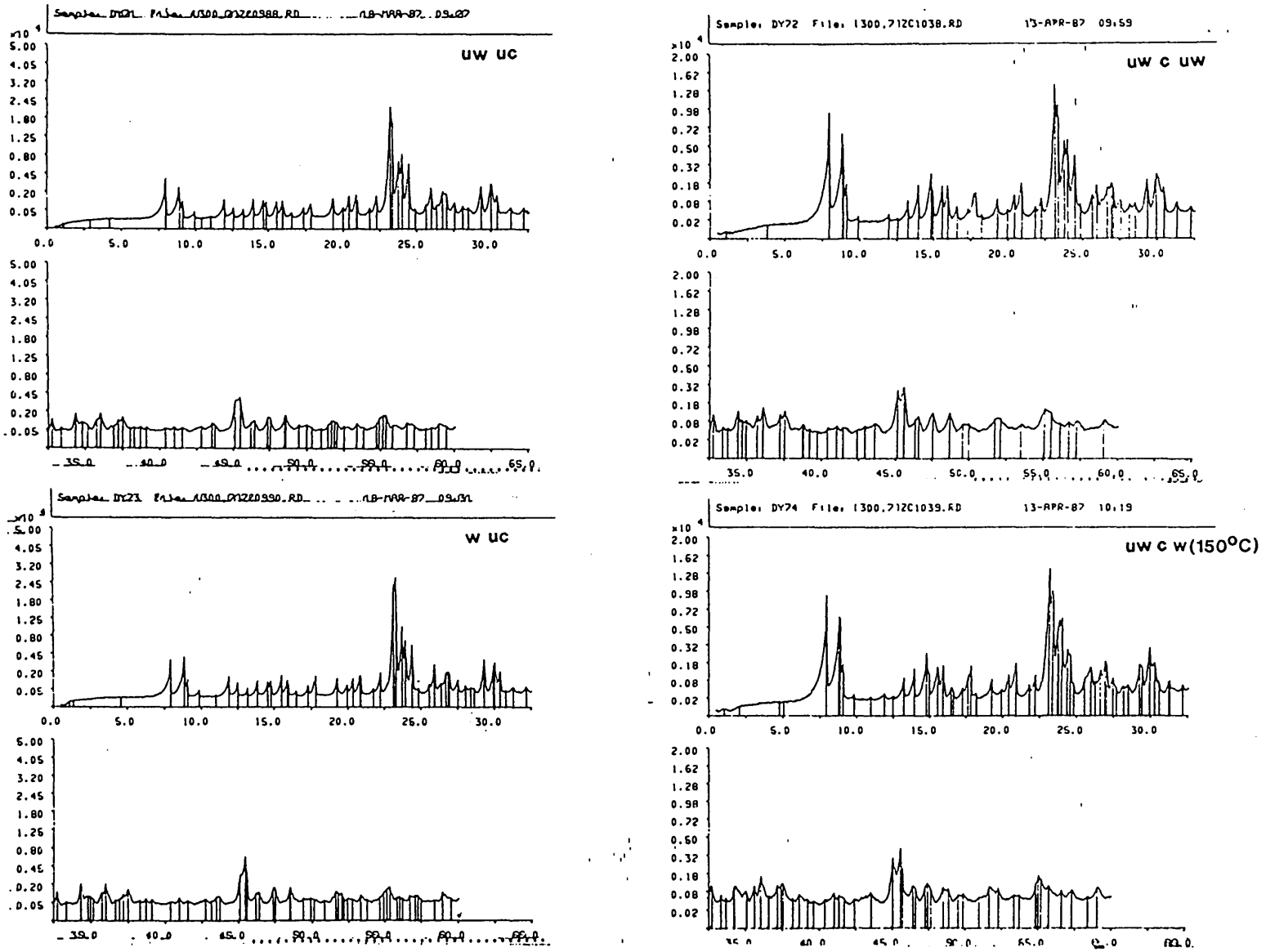

Figure 6.8 XRD patterns of treated silicalite A3 samples

The background of each XRD pattern at 25 2θ is given in Table 6.8.

Since the earlier solubility studies (Chapter 5.0) had been affected by the presence of amorphous silica in silicalite samples, the initial objective of the hydrothermal treatment had been to remove this impurity from the crystalline products. The results in Table 6.8 show that calcination leads to the production of amorphous material, and this can be reduced by hydrothermal treatment.

Table 6.8 Background (counts) A3 Materials.

Sample	XRD Background (counts)
A3 (UW,UC)	144
A3 (W<150°C>,UC)	142
A3 (UW,C,UW)	317
A3 (UW,C,W<150°C>)	266

Whilst there was little change in background between the washed and unwashed uncalcined materials, there was a considerable increase in background on calcination. This was also observed for other samples. The broad hump at 20-30 2θ is characteristic of amorphous material which in this case must be amorphous silica; hence the changes in background given in Table 6.8 must represent changes in the amount of amorphous silica in the samples.

Background intensities for the A2 series of materials are given in Table 6.9.

Table 6.9 XRD Background Intensity for A2 Materials

Sample	Background (counts)
A2 (UW,UC)	146
A2 (W<95°C>,C,UW)	172
A2 (UW,C,UW)	182
A2 (UW,C,W<95°C>)	199
A2 (UW,C,W<150°C>)	156

The decrease in XRD background intensity observed for A3 (UW,C,W<150°C>) and A2 (UW,C,W<150°C>), when compared with that of

their as-made calcined parent materials, showed some success in the removal of amorphous material. Samples washed five times at 95°C occasionally showed an increase in background and therefore amorphous contamination. Calcined materials heated with water in an autoclave at temperatures above 100°C and below 200°C always showed a decrease in background intensity. Each 95°C treatment was conducted in a 1 litre plastic bottle for 16 hours. This system was not as well sealed as an autoclave. During the hydrothermal treatment the concentration of silica in the solution phase reaches an equilibrium value controlled by the solid phase; for silicalite at 95°C this is about 150 ppm [SiO_2]. If the system was not perfectly sealed then evaporation of water would cause the solution phase to become supersaturated with aqueous silica and the SiO_2 concentration would exceed 150ppm. The solubility of amorphous silica is about 150ppm at 25°C (see Chapter 5.0), so when a solution saturated (or supersaturated) by dissolution of silicalite at 95°C is cooled to 25°C, precipitation of amorphous silica will occur. In the case of silicalite A2, because the filtration of the saturated solution through the millipore filter membranes was very slow it was possible for the temperature to fall sufficiently for deposition of amorphous silica. If evaporation occurred from the bottles the silica would stay in solution at this temperature since the solubility of amorphous silica (the first phase to precipitate) is ten times higher than that of crystalline silicalite. Thus the equilibrium solutions could become supersaturated relative to the crystalline solid phase present. Cooling of these supersaturated (with respect to silicalite) solutions would result in a greater amount of amorphous silica deposition at the filtration temperature. This effect is believed to be responsible for the increase in background observed for A2 (UW,C,W<95°C>).

The background difference between as-made products and their hydrothermally treated counterparts was always found to be small, relative to observed differences between the (UW,C,UW) and (UW,C,W) materials. This raised three questions. Was amorphous silica generated on calcination and subsequently removed on hydrothermal treatment? Was the amorphous silica present on the surface or in the

channels?, and if the amorphous silica was occluded into the silicalite channel system during crystallisation, did the presence of the template inhibit the dissolution of the contaminant from uncalcined materials? Uncalcined materials always have a lower solubility than calcined ones (see Chapter 5.0).

The XRD patterns of the partially crystalline A5 materials are shown in Figure 6.9. Some preferred orientation was still exhibited by the samples, despite the various treatments. Calcination of the as-made product resulted in the emergence of six extra peaks and a significant decrease in XRD background, from 231 to 149 counts. The extra peaks occurred at 33.15, 35.62, 40.83, 49.42, 53.99 and 54.09 2θ. The corresponding d-spacings are 2.70, 2.52, 2.21, 1.84, 1.70 and 1.69 Å. These d-spacings were checked against those of known crystalline inorganic phases, and found to correspond to iron oxide, Fe_2O_3. This phase was generated by the calcination, which caused amorphous iron oxide present as an impurity in the silicalite to become crystalline. This could account, at least in part, for the reduction in background intensity. The prolonged hydrothermal treatment at 95°C wash removed the Fe_2O_3, as was observed by XRD. The sample A5 (UW,C,W<95°C>) was a paler brown than the rusty brown coloured A5 (UW,C,UW) parent material. Surpisingly, sample A5 (UW,C,W<150°C>) continued to show lines for crystalline Fe_2O_3 in its XRD. The explanation for this apparent anomaly appears to be related to the type of filter paper used to separate the solid from solution phase after hydrothermal treatment. A wide-pore Whatman GF/F filter (glass fibre) paper had been used after the 95°C hydrothermal treatment of calcined A5. This allowed the microcrystalline Fe_2O_3 to pass through with solution during the filtration. This did not occur with the finer millipore filter membranes which were used in the filtration of the material treated at 150°C.

In the DTA studies of the hydrothermally treated materials, it was observed that the exotherm for A1 (UW,UC) occurred at a temperature 10°C lower than that observed for A1 (W<95°C>,UC). This observation can be correlated with the XRD background intensities of the two materials, which were 159 and 169 counts respectively. It appears that the presence of amorphous material obstructs the

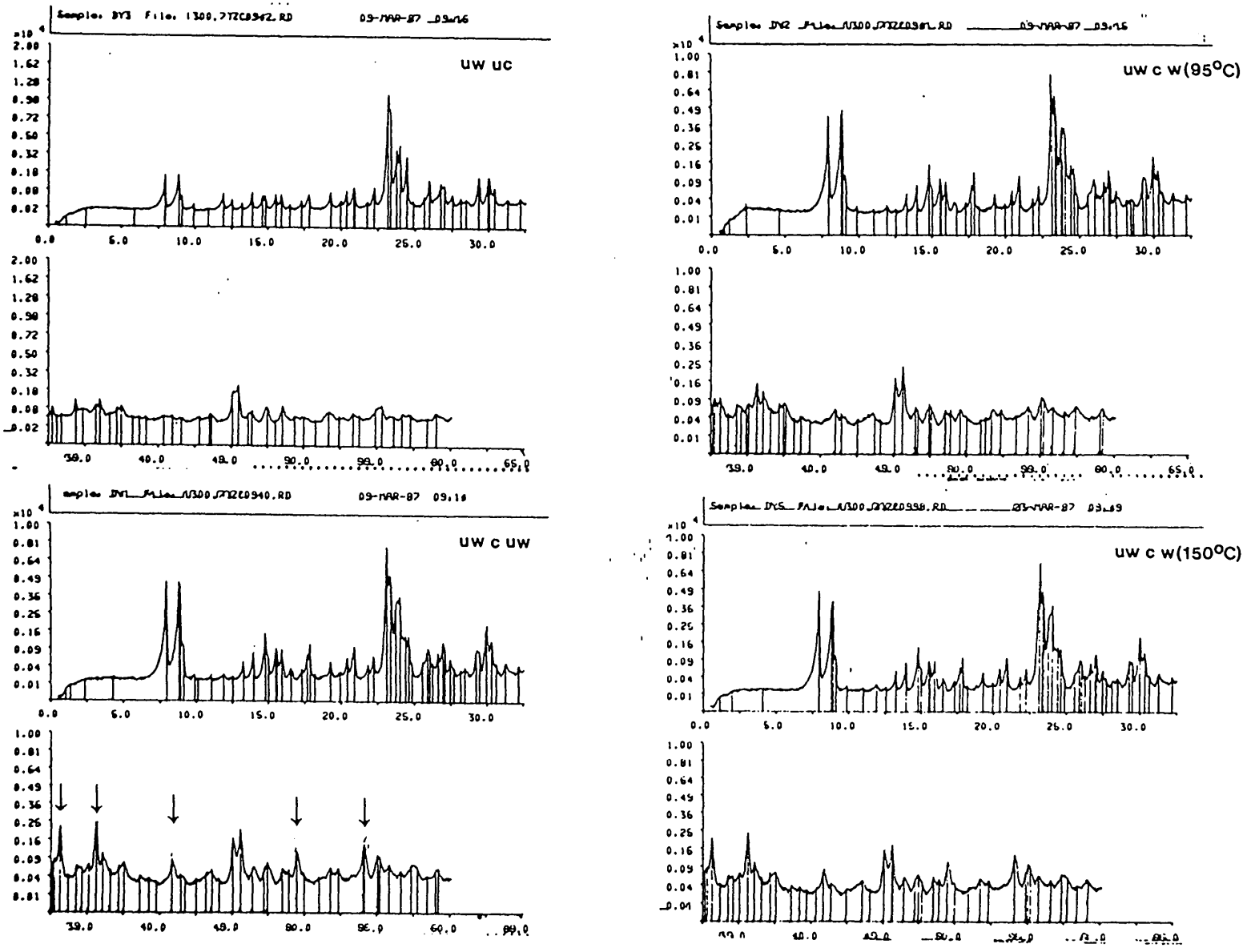

Figure 6.9 XRD patterns of treated silicalite A5 samples

diffusion of oxygen for the TPA template combustion and consequently the exotherm occurs at the higher temperature for the material with the higher content of amorphous material.

6.2.6 Conclusion

Many effects of the hydrothermal treatment were observed in these initial studies. Increased preferred orientation during XRD studies of washed materials indicated dissolution of the faces parallel to the b-plane. This was shown to be correct by SEM. Hydrothermally treated uncalcined materials generally gave larger DTA peak areas, for TPA template combustion, than their as-made parent samples. This indicated some removal of amorphous silica from the crystalline silicalite products, XRD background studies yielded further evidence for this effect. The ^{13}C MASNMR of a (TPA)-silicalite indicated the TPA template did not decompose during the hydrothermal treatment.

A greater change in XRD background was observed when calcined rather than uncalcined products were washed. This indicated that amorphous impurities were not solely confined to the crystal surface. The TPA template appeared to inhibit the removal of amorphous material from within the silicalite channels. The amorphous material could either be occluded into the pores of the silicalite framework during crystallisation or could be generated on calcination.

The hydrothermal treatment also promoted the transition from orthorhombic to monoclinic symmetry. This was shown to be reversible on calcination.

6.3 A HYDROTHERMAL STABILITY STUDY OF A SPECIFIC H-SILICALITE

6.3.1 Introduction

The results contained in Section 6.2 indicated that a more detailed study of a single silicalite sample would be worthwhile, and that particular attention should be paid to the following:

(1) Removal of amorphous silica.

(2) The morphology of the silicalite crystals.

(3) Water sorption.

(4) The crystal symmetry of the silicalite.

The key experimental factors that affected the characteristics of treated materials were identified from the preliminary studies as:

(1) The temperature of the treatment.

(2) The length of time at the treatment temperature.

(3) The number of treatments.

(4) The liquid/solid ratio.

It was planned to vary all of these in a systematic nature. Calcined silicalite was chosen for this study, as uncalcined materials were earlier found to be resistent to the removal of amorphous silica and to symmetry changes.

6.3.2 Experimental

The silicalite (S1) was synthesised at 95°C from a reaction mixture composition:

10Piperazine 2TPABr $20SiO_2$ $1000H_2O$

The preparation was stirred and took about six weeks to reach

100% crystallinity. During the crystallisation the pH decreased by 0.4 units. The product was calcined for 16 hours at 550°C to remove the TPA template and then heated to 800°C for an hour to remove piperazine and any residual carbon from the pore system.

A standard hydrothermal treatment time of 3 hours and temperatures of 95, 150, 180 and 230°C were chosen. The 95°C treatment was performed in a polypropylene bottle, treatments at temperatures above 100°C were conducted in a 1 litre autoclave. The solvent used was demineralised water. The liquid/solid ratio was held at 200, except for a second treatment at 230°C which was performed at a L/S ratio of 500. Samples were hydrothermally treated once only. Separation of the solid and liquid phases was performed with millipore filter membranes and microfiltration apparatus at 95°C. This temperature was considered high enough for the deposition of amorphous silica to be avoided.

Samples were dried at 110°C for 2 hours and examined by X-ray powder diffraction and scanning electron microscopy. Their water sorption capacities at fixed water activities were also determined.

6.3.3 Removal of Amorphous Material

Calcined samples of material S1 were hydrothermally treated at various temperatures, as explained in the previous section. The resultant materials were submitted to ICI Chemicals and Polymers Limited at Wilton for examination by X-ray powder diffraction. The samples were run consecutively, under exactly the same conditions, so that valid comparisons can be made between the patterns. XRD traces are in Figures 6.10-15.

The XRD intensities are plotted on a square root scale, which enhances the smaller diffraction peaks and background intensity. The samples were coded as follows:

S1 (UW C W<x°C>)

The above code indicates that the as-made product was calcined then hydrothermally treated at x°C. The XRD background intensities

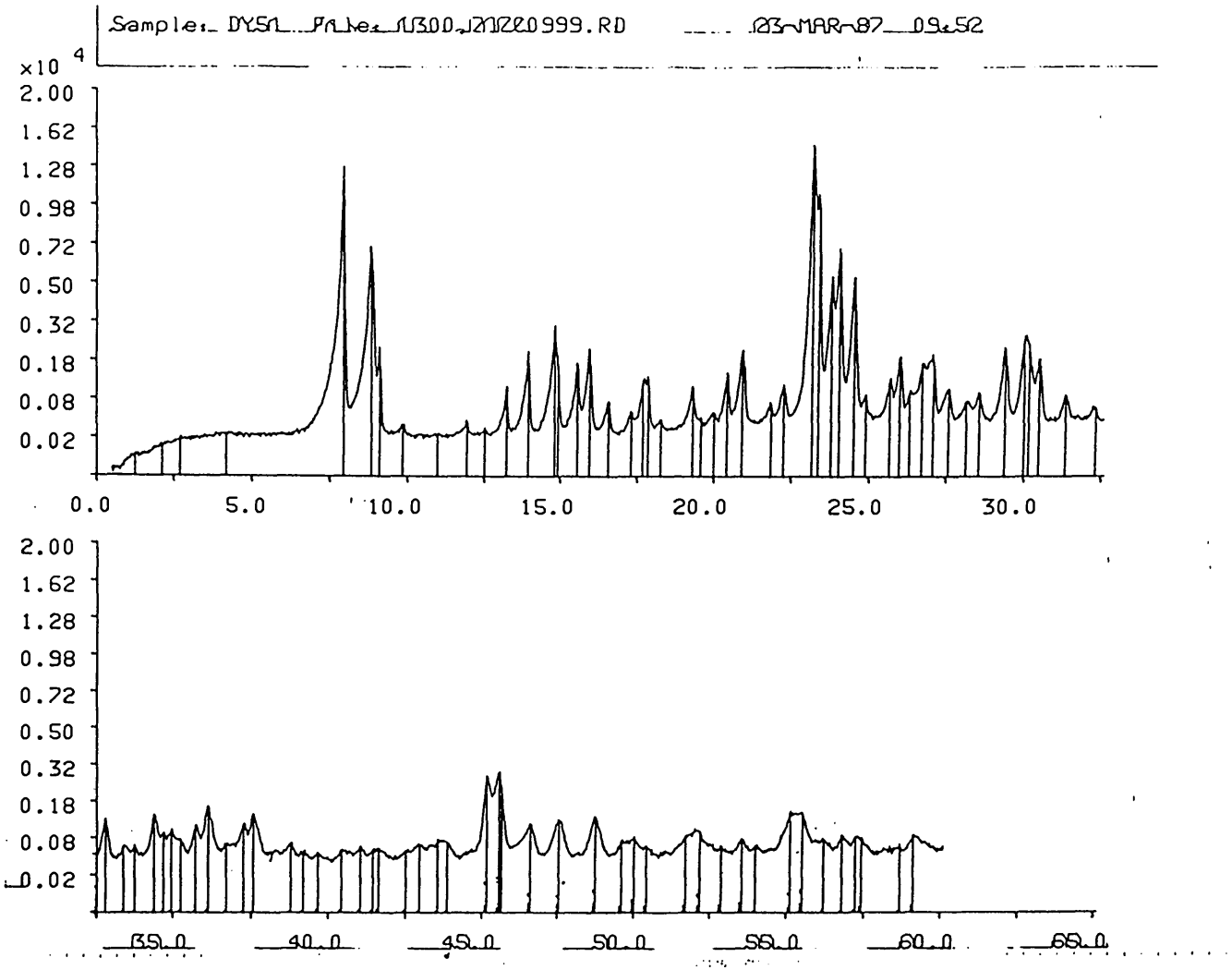

Figure 6.10 XRD pattern of S1 (UW C UW)

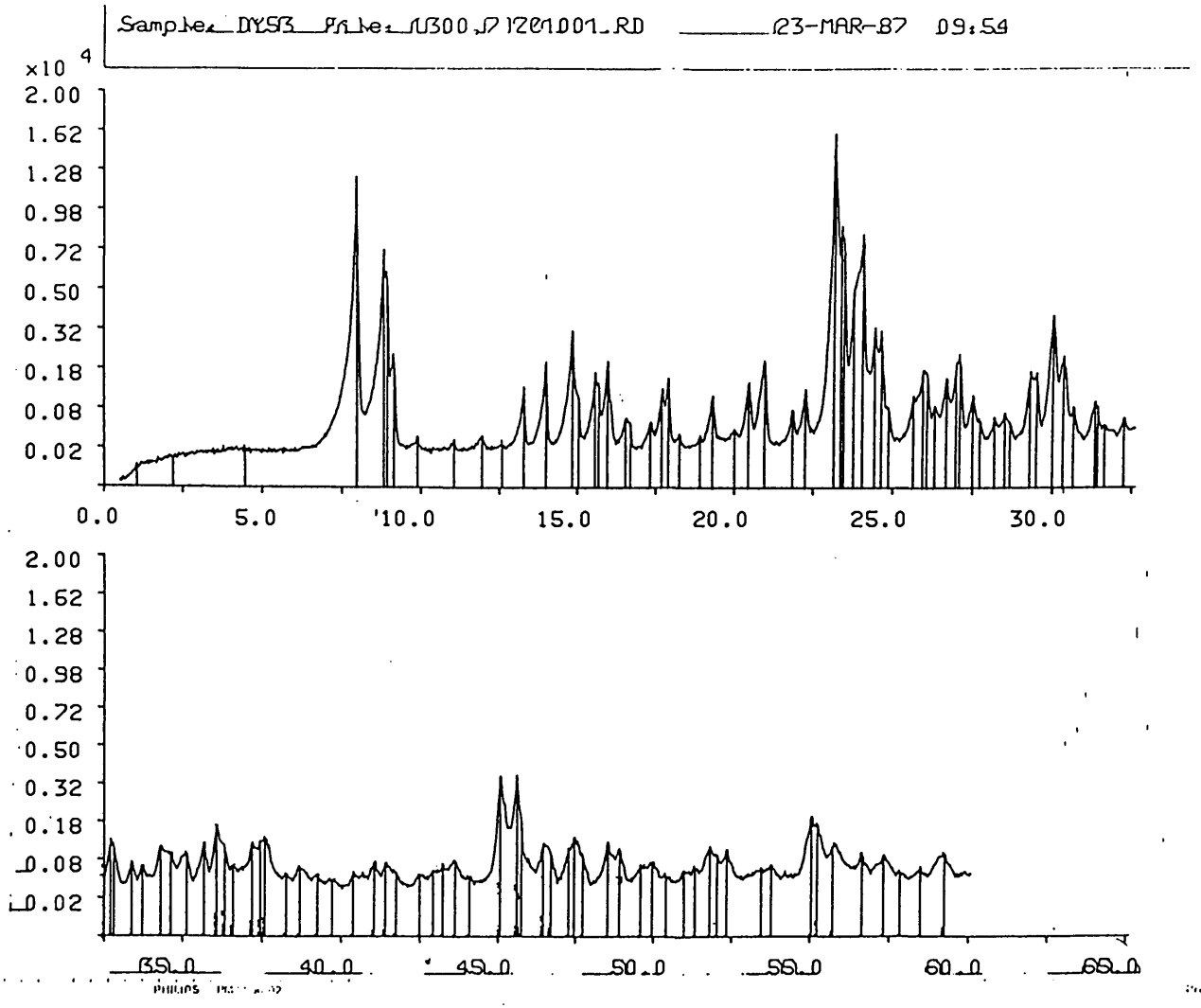

Figure 6.11 XRD pattern of S1 (UW C W<95°C>)

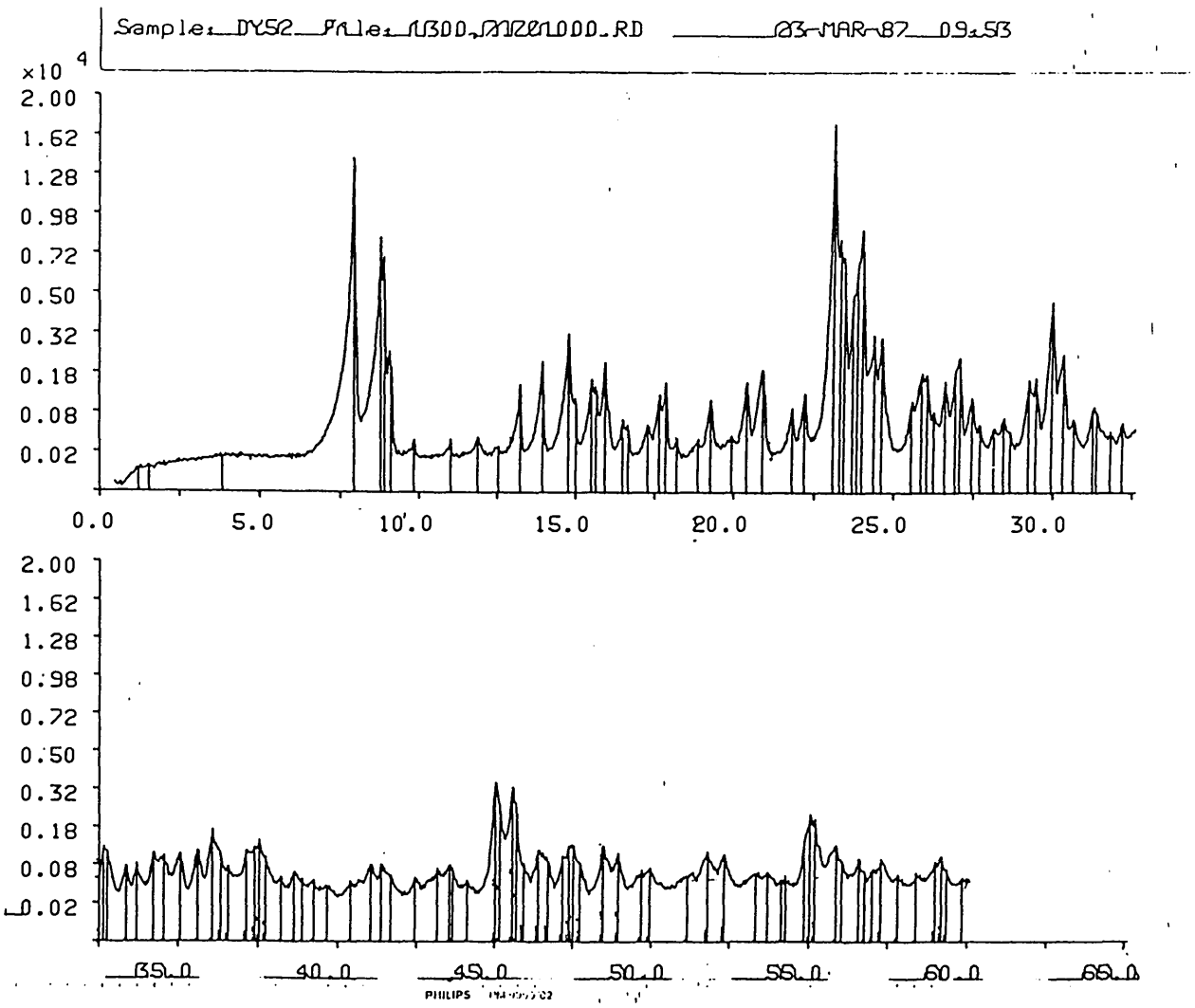

Figure 6.12 XRD pattern of S1 (UW C W<150°C>)

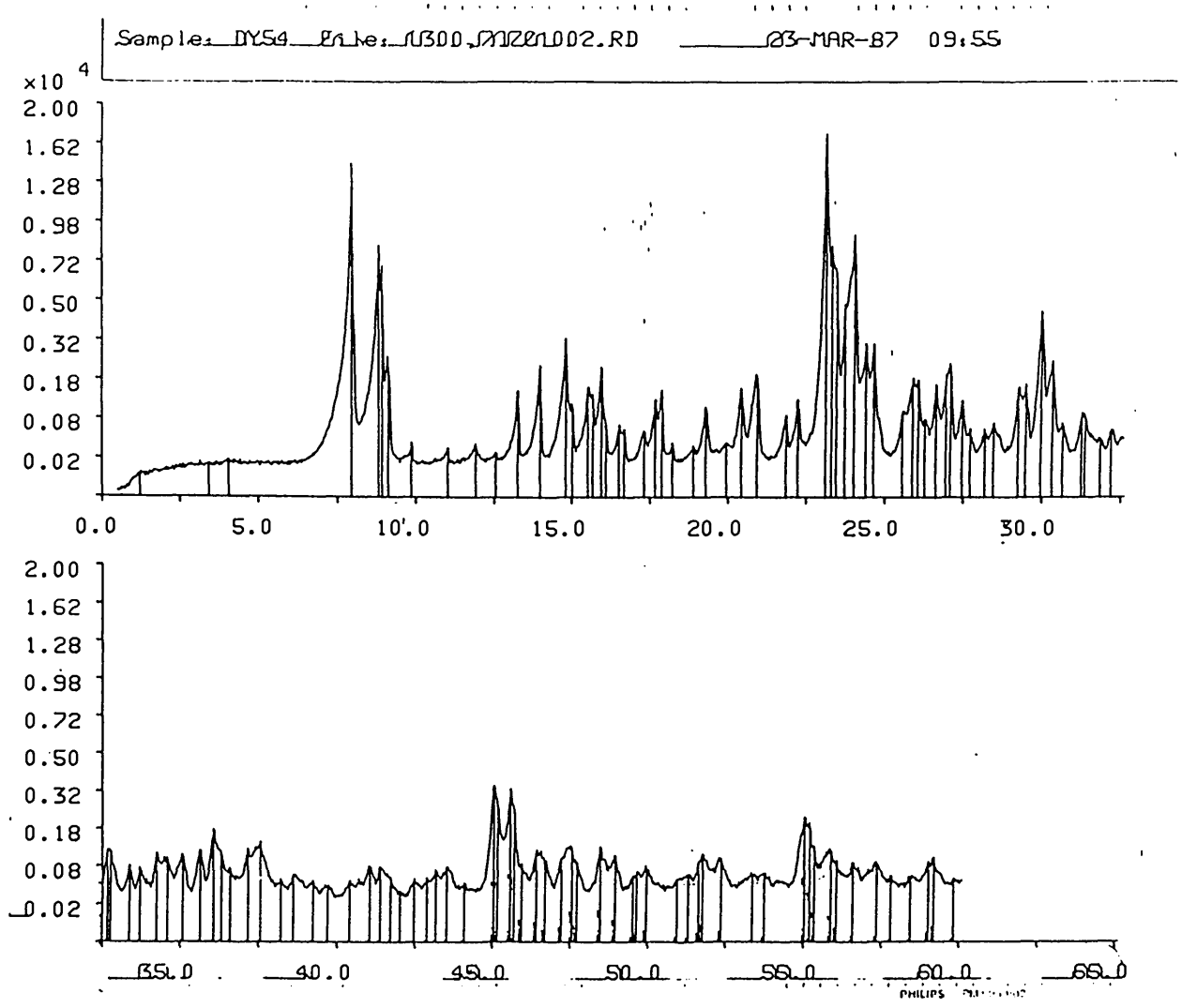

Figure 6.13 XRD pattern of S1 (UW C W<180°C>)

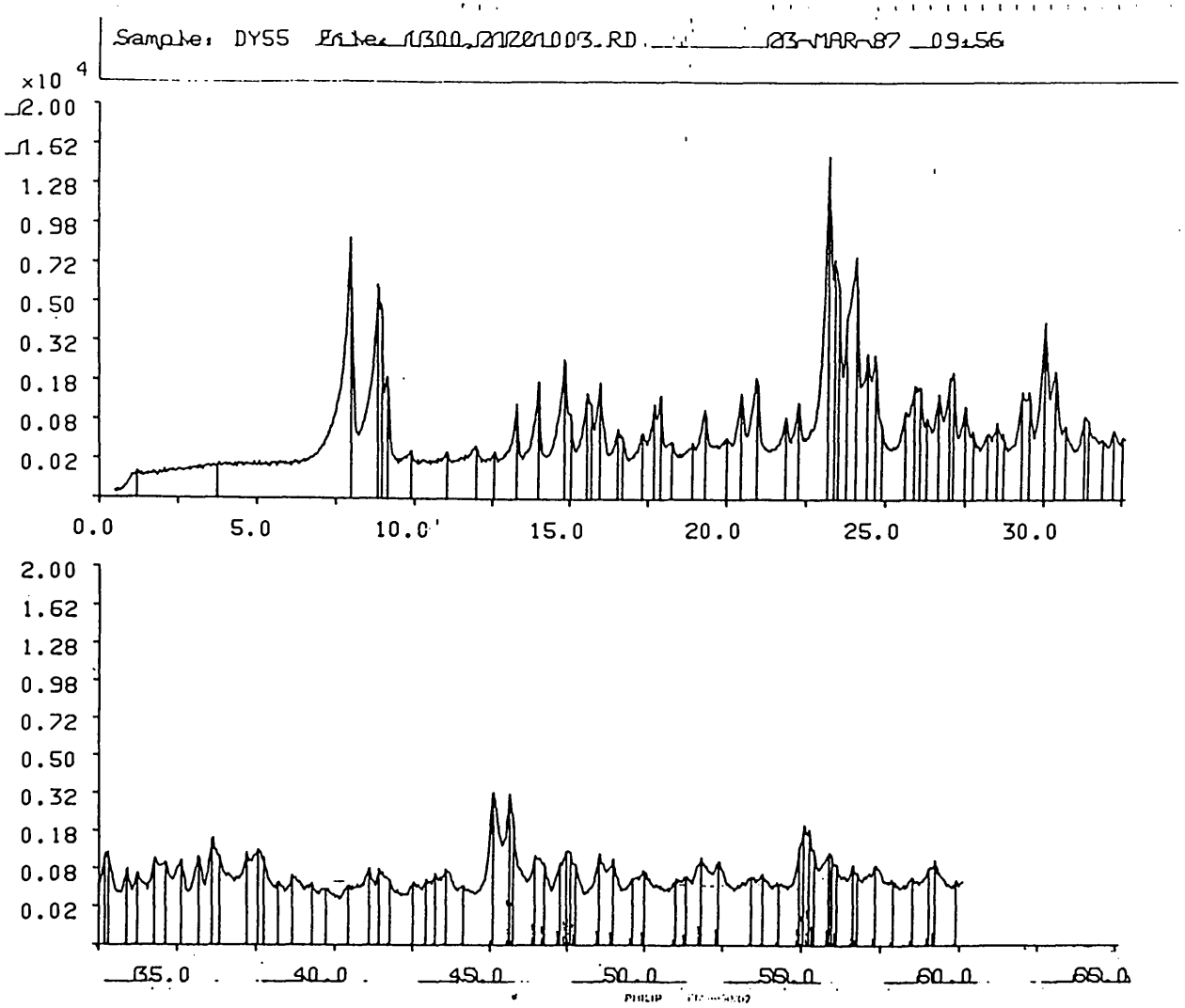

Figure 6.14 XRD pattern of S1 (UW C W<230°C>)

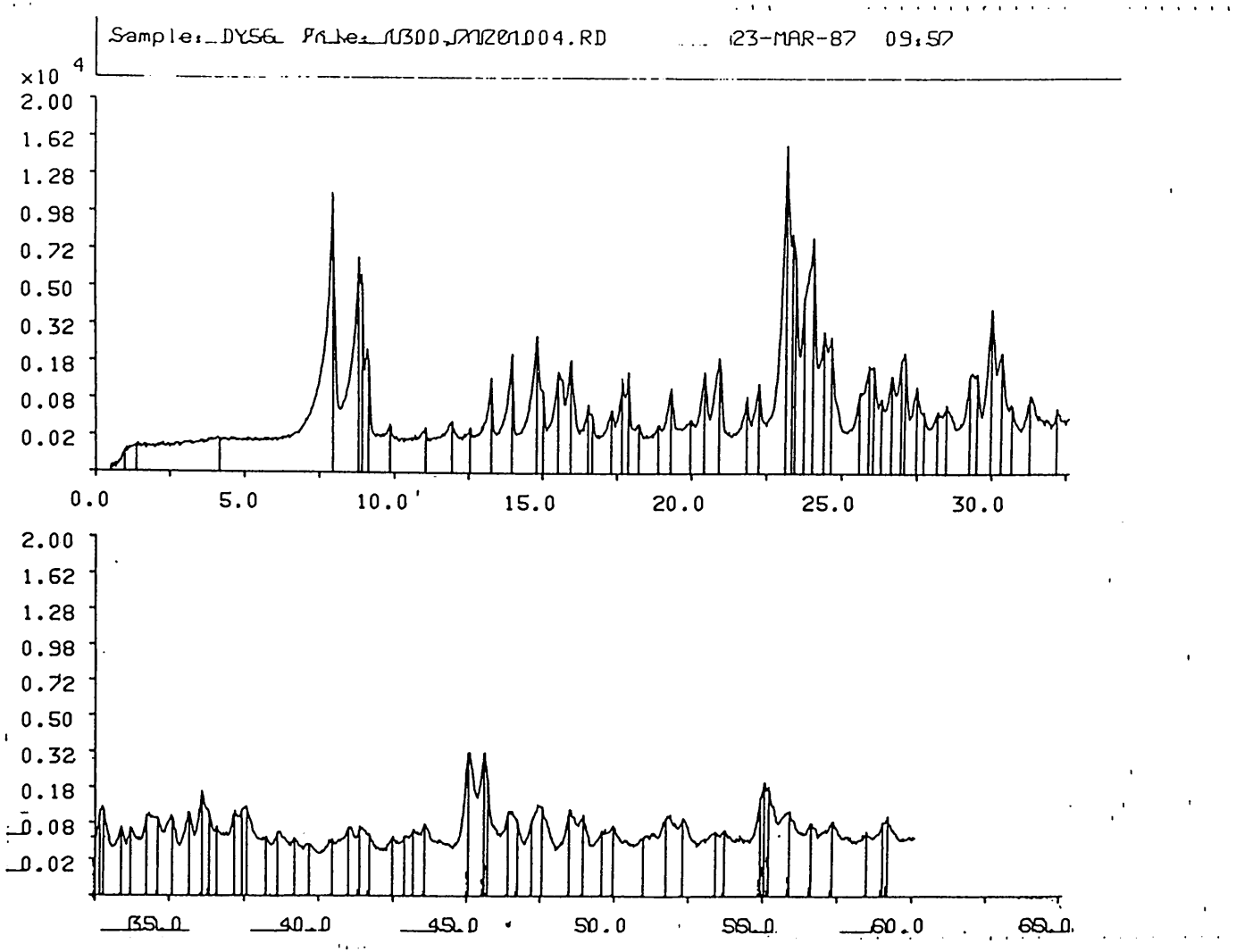

Figure 6.15 XRD pattern of S1 (UW C W<230°C, L/S=500>)

for each sample are given in Table 6.10.

Table 6.10 Background intensities of Sl materials.

Sample Sl	XRD Background (counts)
UW,C,UW	231
UW,C,W<95°C>	174
UW,C,W<150°C>	151
UW,C,W<180°C>	146
UW,C,W<230°C,L/S=200>	154
UW,C,W<230°C,L/S=500>	161

The initial calcined material had the highest background intensity (231 counts) but this was reduced by each hydrothermal treatment and was least (146 counts) after that at 180°C. This effect was sufficiently large to be observed visually by comparison of the XRD patterns. The 230°C hydrothermally treated sample at L/S=200 showed a slight increase in XRD background. The autoclave had to cool to about 95°C before its load was discharged for filtration of the solid phase. The equilibrium concentration of aqueous silica at 230°C in the silicalite/water system will be sufficiently high that cooling to 95°C would result in the redeposition of amorphous silica. Since there was less solid phase in the L/S=500 system it would be expected that the effect of redeposition would be more pronounced, as was observed.

The XRD background intensity (counts) is plotted against hydrothermal treatment temperature (°C) in Figure 6.16. In this plot the point for 25°C is for material Sl (UW,C,UW).

Earlier studies indicated there was little reduction in background intensity when as-made (i.e. uncalcined) silicalites were hydrothermally treated. Nevertheless differences between the DTA peak areas of as-made materials and their hydrothermally treated counterparts were often observed. This indicates that only trace amounts of amorphous impurity need be removed to significantly improve template combustion.

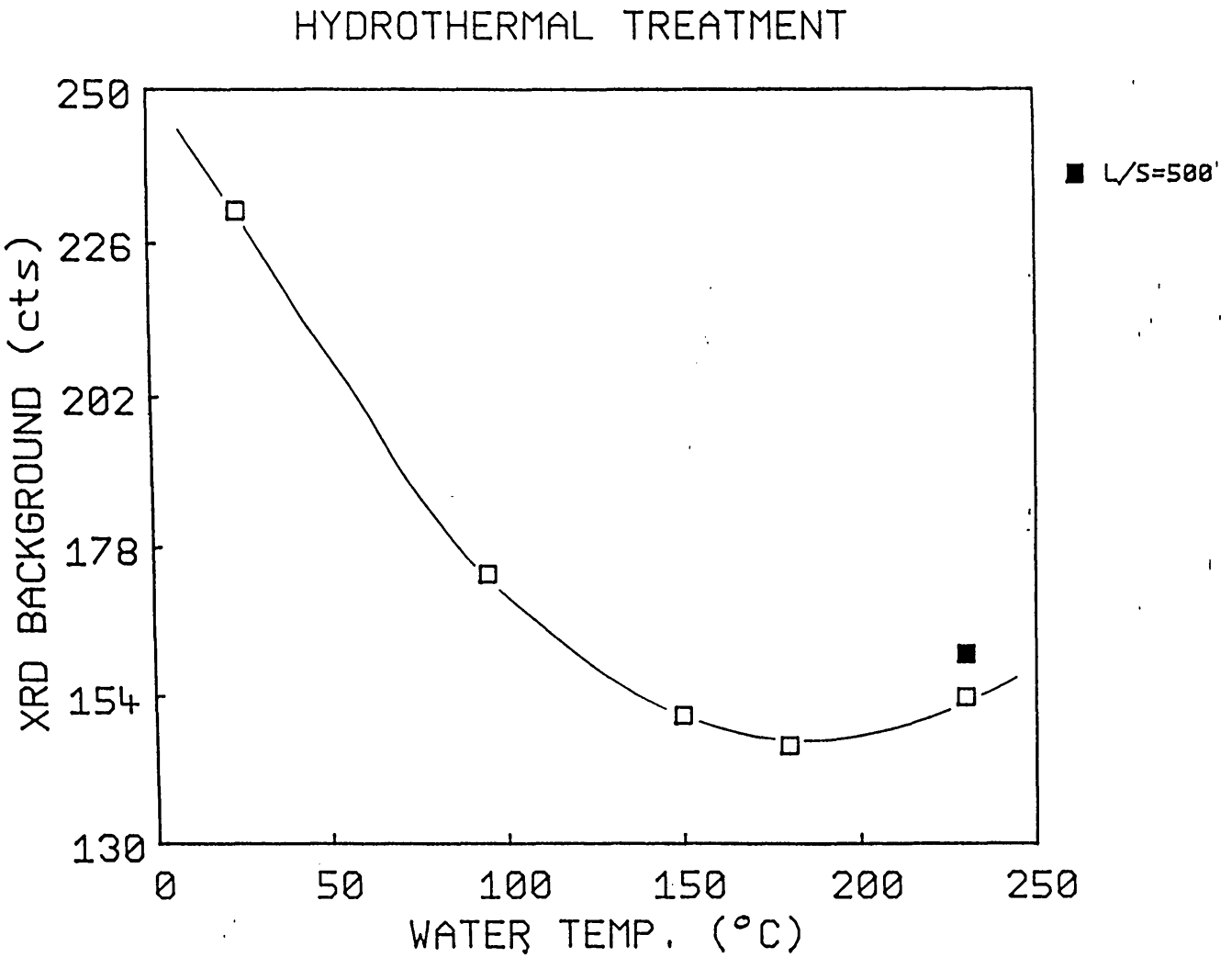

Figure 6.16 XRD background of treated silicalite samples

Table 6.11 Background (counts) as-made versus

washed uncalcined materials.

Material	Treatment T (°C)	Background (counts) UW,UC	W,UC
A1	95	159	169
A3	150	144	142
W1	150	135	149
X1	150	142	151

As can be seen from Table 6.11 the change in background intensity was always less than 10%. The lowest background intensity for uncalcined materials was about 140 counts. When TPA-silicalite samples were calcined an increase in background intensity was usually observed, as can be seen in Table 6.12.

Table 6.12 Background (counts) of uncalcined versus

calcined materials.

Material	XRD Background (counts) Pre-calcination	Post-calcination
A1 (W<95°C>,UC)	169	222
A3 (UW,UC)	144	204
A2 (UW,UC)	146	182

For the three examples the increase in background intensity on calcination ranged between 40 and 60 counts. Hydrothermal treatment of calcined S1 (UW,C,UW) at 180°C reduced the XRD background from 231 to 146 counts, a decrease of 85 counts to a level similar to that of an unwashed as-made material (144 counts).

These experiments established that amorphous silica is usually generated by the calcination, and that synthesis products also contain traces of amorphous silica left over from the reaction mixture. Another possible source of amorphous silica are trace amounts of layered structured silicates (e.g. piperazine silicate) which collapse to amorphous material on calcination. Solubility

studies indicated the presence of about 2% amorphous silica in calcined silicalite samples synthesised at 95°C. Only 2% of an extra crystalline phase in a product 98% silicalite would be very difficult to detect. The diffraction peaks of the crystalline impurity would be dwarfed in comparison with those of the silicalite, which might even mask any extra impurity lines. In practice, no extra reflections were observed in the XRD traces of as-made products.

In calcined silicalite, the amorphous silica impurity will exist at either of two sites, externally on crystal surfaces or internally within the three dimensional channel system. Scanning electron microscopy indicated that very little amorphous silica was present on the crystal surfaces of Sl (UW,C,UW), hence the amorphous silica is likely to be present within the silicalite framework (see Plate 6.2). Amorphous characteristics exhibited by impure samples may not be from a distinct phase. It has been reported that up to 8% of the lattice Si in highly siliceous ZSM-5 is present as Si-OH. Clusters of silanols may show characteristics of amorphous material. The silanol groups may be generated by calcination of the TPA-silicalite precursor.

In the XRD patterns of silicalite and ZSM-5 there are two peaks centred around approximately 7.92 and 8.81 2θ, each of which arises from two normally unresolved reflections. The 7.92 2θ line has lattice indices 101/011 (hkl) and the 8.81 2θ peak is indexed 200/020 (hkl). Each peak should be resolved, but the near identity of the a and b parameters of the orthorhombic unit cell makes it difficult to observe the splitting. Both peaks greatly increase in intensity when the organic TPA template is removed from the silicalite channel system during calcination.

Table 6.13 Low Angle Peak Areas (counts)

with Calcination.

Sample A1	XRD peak area (counts) 7.90 2θ peak	8.81 2θ peak
W<95°C>,UC	3994	2381
W<95°C>,C,UW	12928	7327

The 101&011 and 200&020 (hkl) peak intensities are reduced by the presence of organic material in the zig-zag channel system in silicalite and its removal increases the low angle peak areas. On the other hand if the silicalite channel system was loaded with amorphous silica then if this was removed by the hydrothermal treatment the intensity of the 101/011 and 200/020 (hkl) peaks should increase.

The sum of the areas of the 101&011 and 200&020 (hkl) peaks for S1 after various hydrothermal treatments are given in Table 6.14.

Table 6.14 Low Angle Peak Areas and

Hydrothermal Treatment.

Sample S1	101/011+200/020 area (cts)
UW,C,UW	18818
UW,C,W<95°C>	23221
UW,C,W<150°C>	26908
UW,C,W<180°C>	26893
UW,C,W<230°C,L/S=200>	21594
UW,C,W<230°C,L/S=500>	18041

These values are plotted against treatment temperature in Figure 6.17. The graph shows a maximum between 150 and 180°C. This coincides with the minimum observed in the plot of background intensity against hydrothermal treatment temperature shown in Figure 6.16. The results indicate that amorphous silica was removed from the silicalite channel system rather than from the external crystal surfaces. The results show that amorphous impurity can be removed by hydrothermal treatment for 3 hours over a range of temperatures.

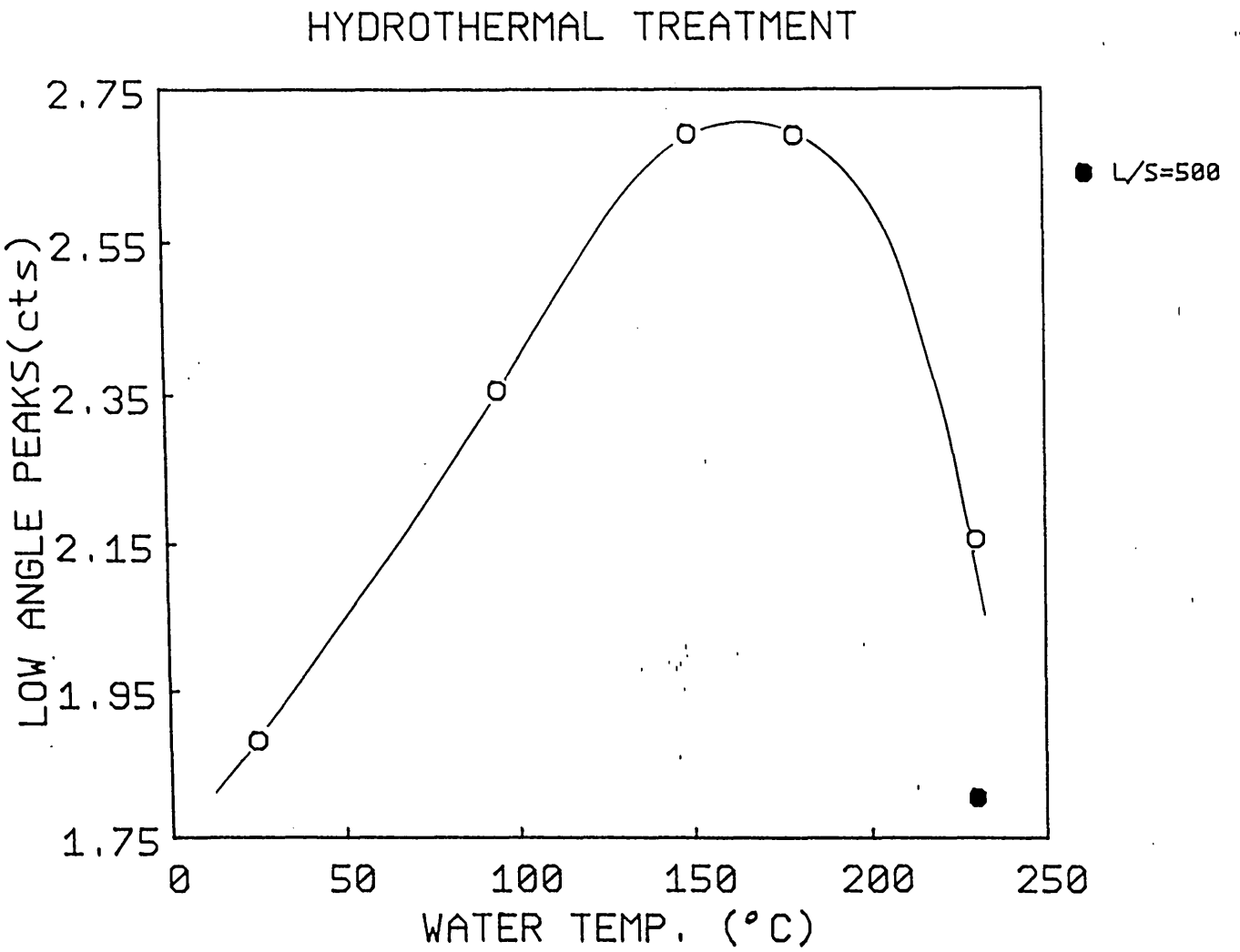

Figure 6.17 Low angle peak areas and hydrothermal treatment

An initial study of the water sorption of the materials was conducted by equilibration over a saturated NaCl solution at 25°C. Small portions of each sample were placed in glass vials over the saturated NaCl solution in a dessicator. This was evacuated for ten minutes with a Buchner pump and then placed in a 25°C thermostat bath for seven days. The samples were then analysed for their water uptake by thermal gravimetry (TG). The results are shown in Figure 6.18.

The as-made calcined material sorbed 5.4% water; this was reduced to 3.6% after the 95°C treatment and was reduced further by the treatments at 150 and 180°C. The minimum value that could be achieved is estimated from the graph to be 2.1%. Water sorption capacity was increased by each of the 230°C treatments. This is believed to be due to the deposition of amorphous silanol rich silica on cooling of the mixture in the autoclave prior to discharge. Some of the water uptake could also be due to the generation of hydrophilic silanol groups during the hydrothermal partial dissolution process of the crystals at the high temperature.

The decrease in water uptake to a minimum of 2.1% corresponds with the removal of amorphous silica from the silicalite channel system by the hydrothermal treatment. The hydrothermal treatment may also result in the healing of the crystal framework. Dissolution of the crystalline silicalite would be stabilised by the dissolution of the amorphous silica impurity in the calcined H-silicalite. The temperature treatment may heal silanols associated with broken siloxane bonds in the H-silicalite framework.

6.3.4 SEM Study of Crystal Dissolution in Water

The samples in the S1 series of hydrothermally treated materials were examined in ICI Chemicals and Polymers Limited at Wilton by scanning electron microscopy (SEM). Material S1 (UW,C,W<230°C,L/S=500) was examined with the Cambridge Instrument Stereoscan S90B SEM in the Edinburgh University Science Faculty Electron Microscope Unit. Prints of the samples are shown in Plates 6.2-6.8. The materials were assigned the following codes.

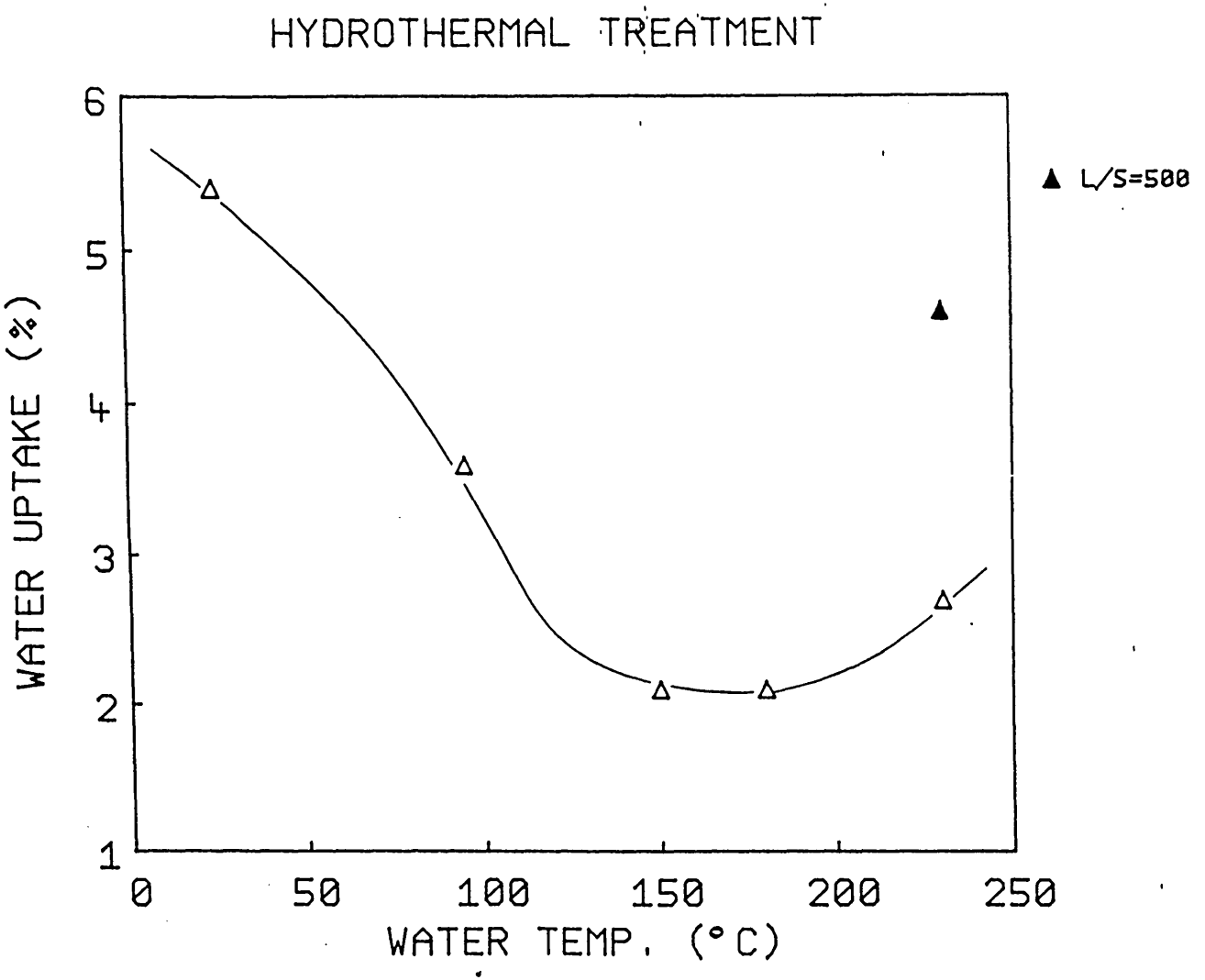

Figure 6.18 Water uptake and hydrothermal treatment

Table 6.15 SEM Sample Codes for S1 Materials.

Material S1	Sample Code	Plate
UW,C,UW	DY51	6.2-3
UW,C,W<95°C>	DY53	6.4
UW,C,W<150°C>	DY52	6.5
UW,C,W<180°C>	DY54	6.6
UW,C,W<230°C>	DY55	6.7
W<230°C,L/S=500>	DY56	6.8

The liquid to solid ratio (L/S) was 200 in each hydrothermal treatment, unless otherwise stated in the table.

The scanning electron micrographs of DY-51 showed that the initial product contained mostly twinned crystals. Very little amorphous material could be seen, and that which was present appeared to be associated with certain crystal faces. The SEM of DY-53 showed some external amorphous silica and initial attack at the cross lozenge of the twin. Continued attack at the intersection and surface pitting was observed in the SEM of DY-52. The SEM of DY-54 shows penetration of the twinned crystal surface at the cross lozenge and internal dissolution of the material. Further evidence for this process is given in the SEM of DY-55, which provides clear evidence that once the crystal surface had been penetrated the twinned crystals dissolve from inside, and that the remaining external surface stays intact. In the SEM of DY-56 it can be clearly seen that the twinned crystals have fallen apart, leaving shell-like fragments in various states of dissolution. In contrast, the single crystals showed few signs of dissolution, and are clearly much more resistant to hydrothermal attack.

In the earlier solubility studies (Chapter 5.0) it was observed that ZSM-5 had a lower solubility than silicalite. This indicates that the presence of aluminium depresses the solubility of materials of similar structure, and it also suggests that they will have a lower dissolution rate. The Si/Al ratio of the initial silicalite was 511.43. In the present case, once the amorphous material has been removed then penetration of the surface by dissolution at the weakest point, in the case of twins the cross lozenge, takes place

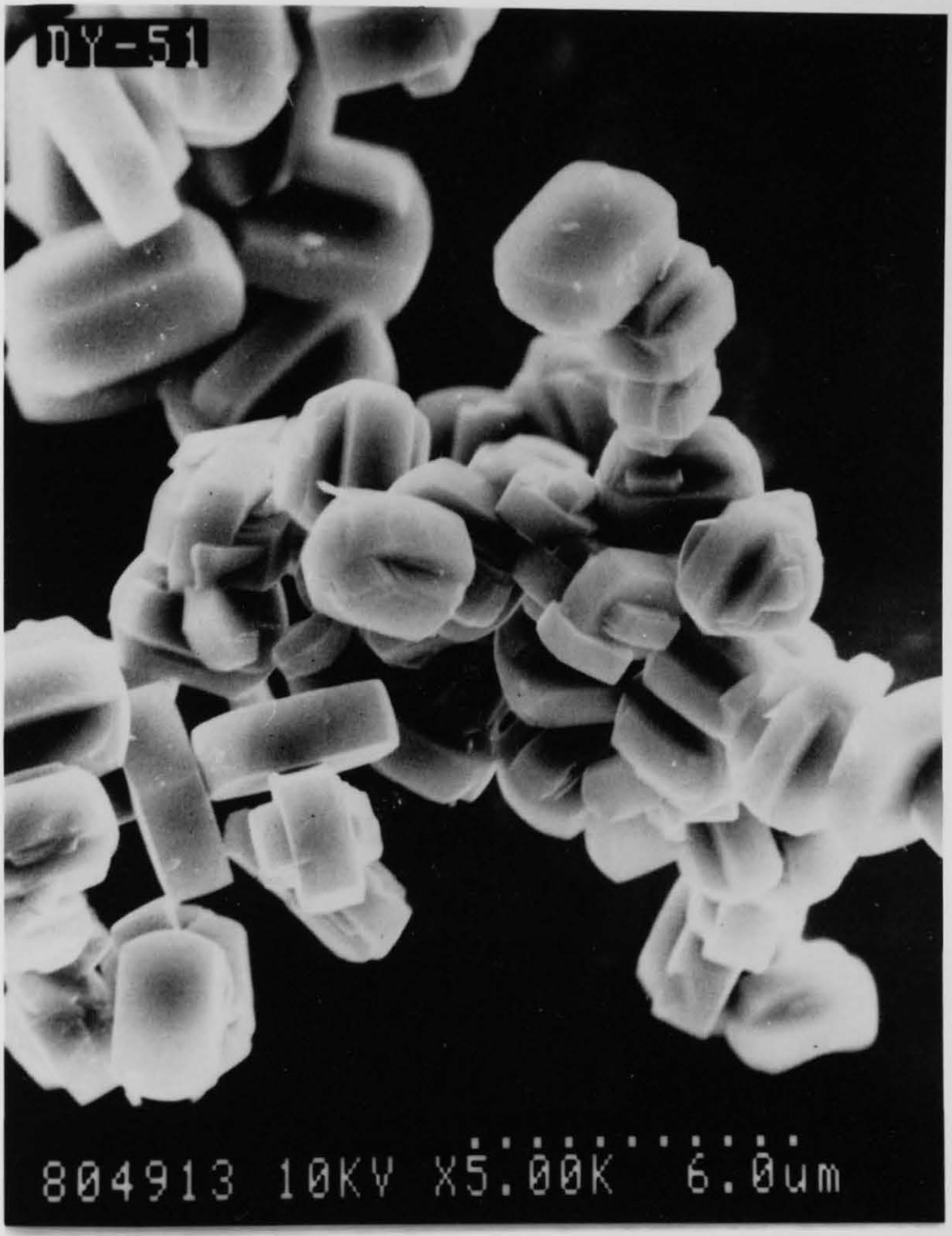

PLATE 6.2

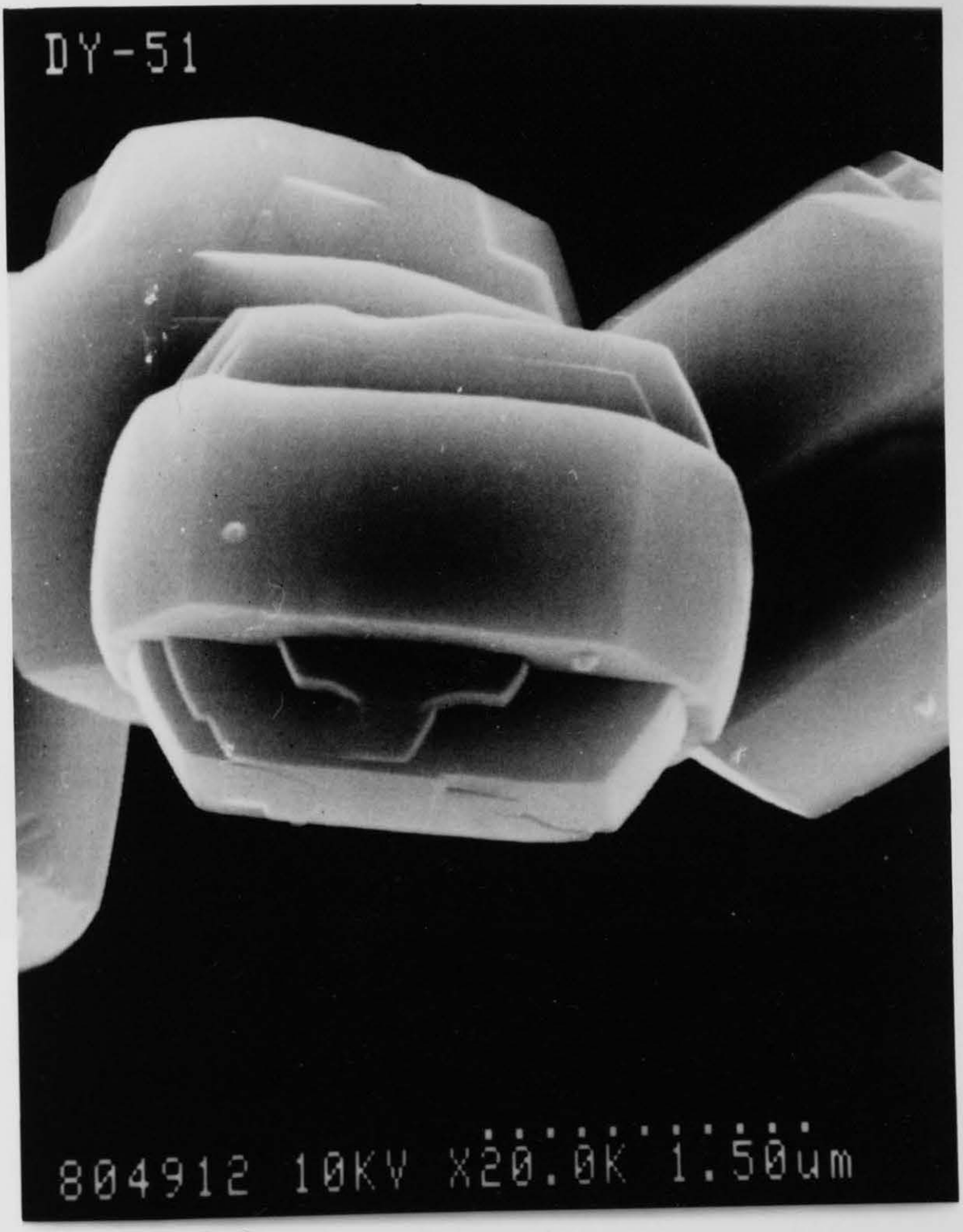

PLATE 6.3

PLATE 6.4

PLATE 6.5

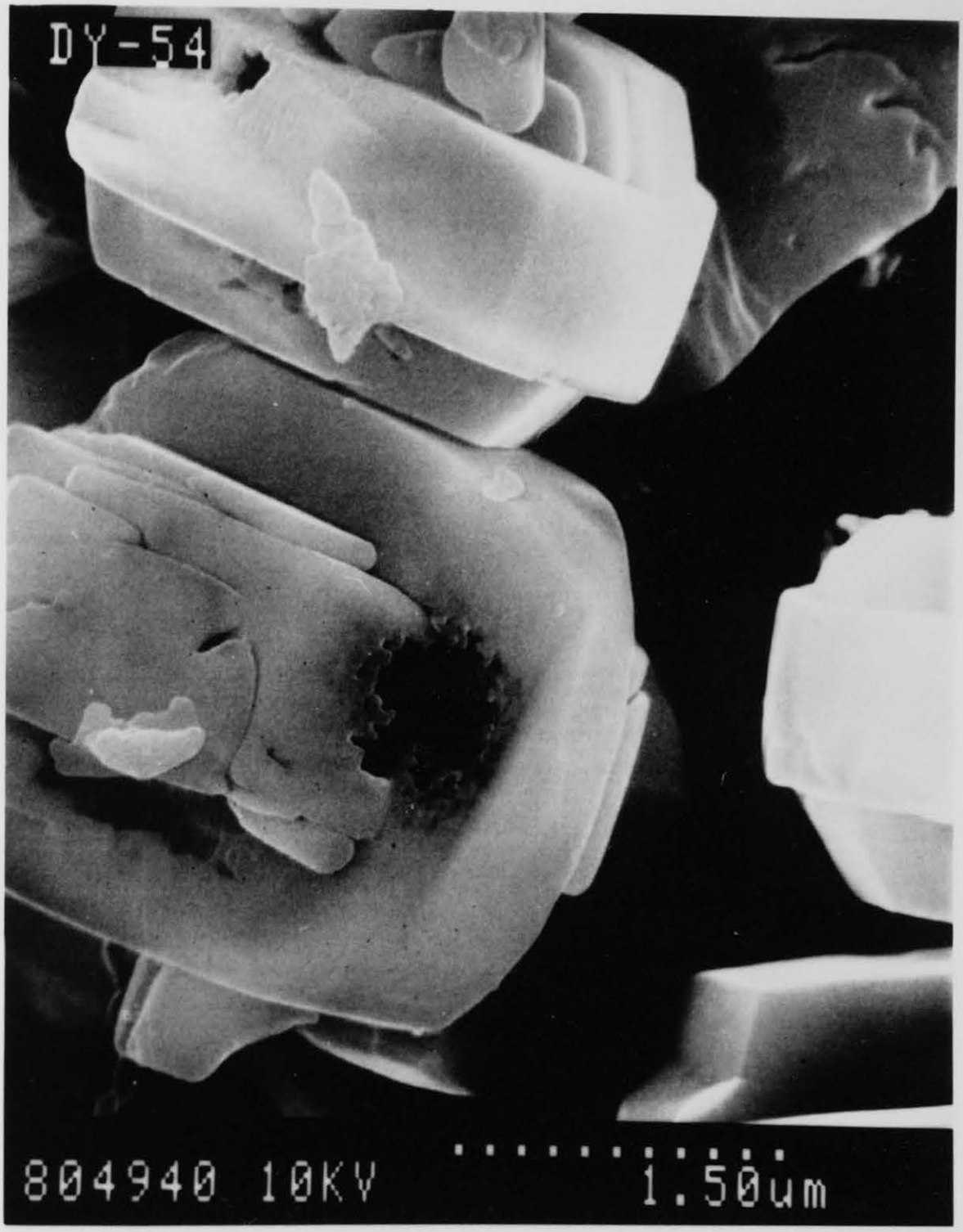

PLATE 6.6

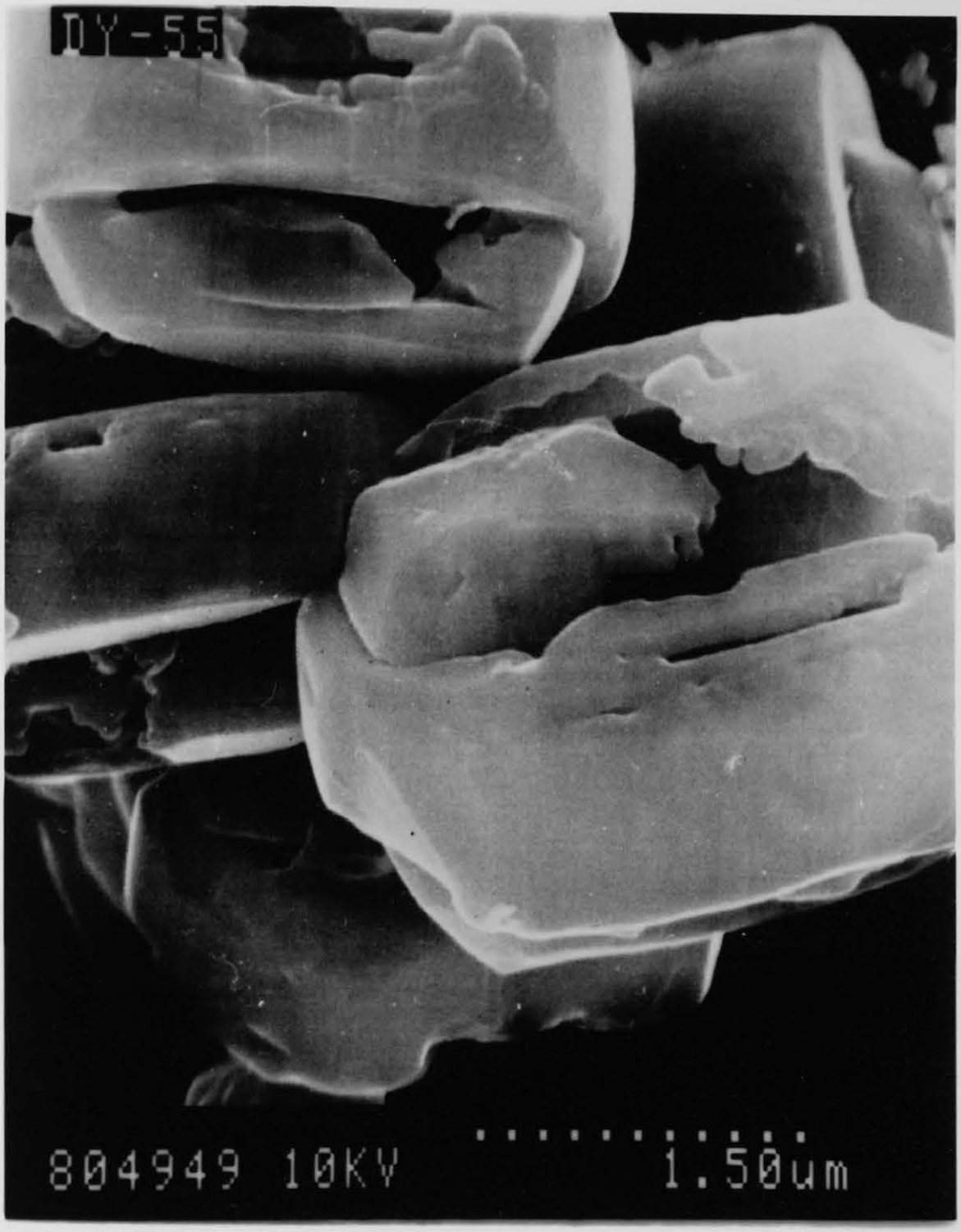

PLATE 6.7

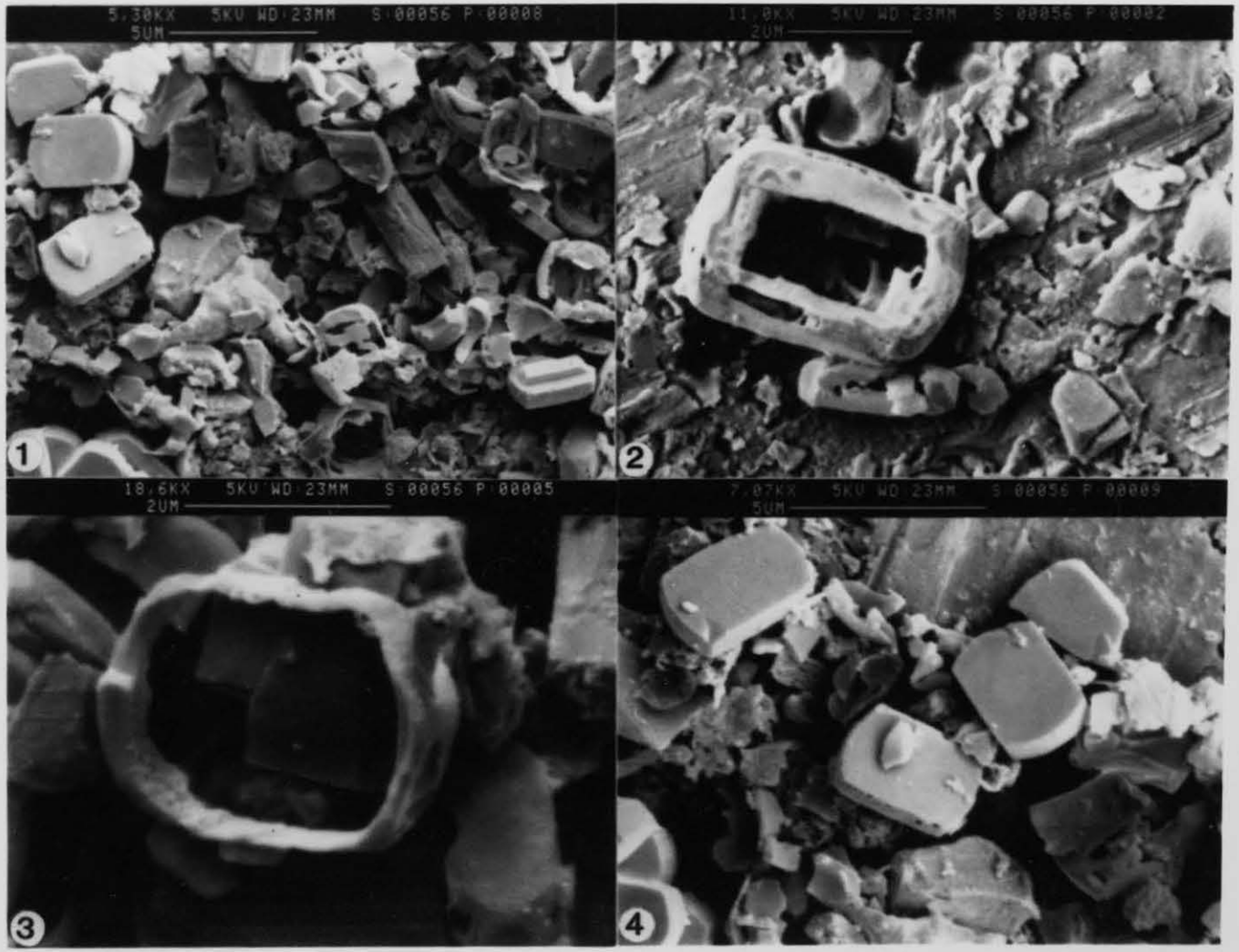
5.30KX 5KV WD:23MM S:00056 P:00008
5UM
1
11.0KX 5KV WD 23MM S 00056 F 00002
2UM
2
18.6KX 5KV WD:23MM S:00056 P:00005
2UM
3
7.07KX 5KV WD 23MM S 00056 F 00009
5UM
4

PLATE 6.8

and preferential dissolution of the bulk of the crystal relative to the surface occurs. It has been reported that up to 8% of lattice Si is present as silanols (8). These may be generated by calcination (16), along with an amorphous phase, which is confirmed by the XRD background and water sorption studies. The presence of internal silanols will promote dissolution from inside twinned crystals. The generation of silanol groups is part of the dissolution process.

The single crystals had no such weak point so their dissolution is much slower than that of the twinned crystals. This explains the presence of fragmented twins and complete single crystals in sample DY56. This implies that single crystals could be separated from mixtures with twinned crystals by selective dissolution.

This has implications for zeolite catalysts. Molecular traffic control (MTC) is reported to play an important role in the product selectivity in catalytic conversion over ZSM-5 (17). In the case of ZSM-5, reactant molecules preferentially enter the catalyst through one channel system, possibly the straight channels, and the products leave by the sinusoidal channels. This prevents counterdiffusional limitations in catalytic conversions. Since twinned crystals will have each channel type perpendicular to each other then this will cause counterdiffusion of reactant and product molecules. This will decrease catalytic activity and change product selectivity. If this is correct it should be advantageous to use untwinned crystals in catalytic applications.

6.3.5 Orthorhombic/Monoclinic Symmetry Change

Wu et al reported that the XRD patterns of samples of as-synthesised ZSM-5 were consistent with idealized orthorhombic symmetry (9). If the product was calcined and ion-exchanged then monoclinic symmetry was observed. This transition was shown to be reversible and was thought not to reflect a change in framework topology.

All of the hydrothermally treated H-silicalites examined in the current study exhibited monoclinic symmetry whereas the untreated calcined H-silicalite was always in the orthorhombic form.

The theoretical XRD powder pattern (11) of orthorhombic silicalite has the following peaks between 23.0 and 23.4 2θ.

Table 6.16 Theoretical orthorhombic TPA-silicalite

peaks between 23.0 - 23.4 2θ.

Peak Position (2θ)	I(rel)	h k l
23.04	3.5	3 3 2
23.10	100.0	5 0 1
23.16	2.1	4 3 1
23.26	78.4	0 5 1

Experimentally, two peaks were observed in this region of the XRD pattern of the orthorhombic as-synthesised H-silicalite [S1 (UW C UW), Figure 6.10]. The 5 0 1 (hkl) line was observed at 23.08 2θ, its I(rel) value was 100%. The 0 5 1 (hkl) line occurred at 23.29 2θ and had an I(rel) value of 66.29%. The observed experimental values were within 0.03 2θ of the theoretical values noted above.

Unit cell parameters were calculated from the observed h 0 0, 0 k 0 and 0 0 1 line positions for the orthorhombic S1 (UW,C,UW) material. The values were a=20.095, b=19.905 and c=13.397 Å.

The powder pattern d-spacings were then calculated with the program DSPACE on Edinburgh University's EMAS computing system. The theoretical positions of the 5 0 1 and 0 5 1 (hkl) lines were 23.08 and 23.29 2θ. These values correspond exactly to those observed in the experimental XRD powder pattern.

The hydrothermally treated H-silicalite samples were observed to be in the monoclinic form and three peaks were noted in the 23.0 to 23.4 2θ region of their XRD patterns. The sample S1 (UW,C,W<150°C>), Figure 6.12, gave the best example of the resolution of the three reflections in this region at 23.03, 23.22 and 23.37 2θ. The unit cell parameters for the monoclinic material were calculated as a=20.150, b=19.901 and c=13.392 Å from the experimentally observed XRD pattern. The alpha value was taken to be 90.5°, as reported in the literature (9). The theoretical XRD

pattern was generated with the DSPACE program. This simulation gave 23.03 2θ for the position of the 5 0 1 (hkl) line and 23.35 2θ for that of the the 0 5 1 line. This corresponds well with two lines in the experimental XRD. The observed Bragg line at 23.22 2θ was not present in the experimental powder patterns of orthorhombic silicalite. The reported calculated line intensity at 23.16 2θ for orthorhombic silicalite is 2.1% (9); indexed 431 (hkl). The calculated XRD pattern generated by program DSPACE for the monoclinic form gave lines indexed as 4 3 1 (hkl) at 23.16 2θ and 3 4 1 (hkl) at 23.24 2θ.

Other effects were noted in the transition from orthorhombic to monoclinic symmetry. The 313/133 (hkl) lines centred around 24.5 2θ became resolved, as did the 806 and 086 (hkl) lines at 54.95 and 55.12 2θ. In the XRD patterns reported by Hay and Jaeger (10) for silicalite the separation between the 051 and 501 was less obvious in the monoclinic pattern than in the orthorhombic one. This was also observed in the present work but the lack of resolution of the 051 reflection appears to be due to the emergence of an unresolved 341/431 peak of the monoclinic silicalite. This was observed in the XRD traces of several hydrothermally treated silicalite samples, either as a distinct peak or a shoulder. The print-out which accompanied the XRD patterns listed the following line intensities.

Table 6.17 Observed monoclinic H-silicalite

peaks between 23.0 - 23.4 2θ.

Peak Position (2θ)	Peak Indices (hkl)	I[rel] (%)
23.03	501	100.0
23.22	431/341	46.8
23.37	051	37.5

In the orthorhombic silicalite sample the intensity of the 501 peak was 100% whilst the intensity of the 051 line was 66.29%. This is consistent with the I(rel) value of 78.4% in the literature (11) for the 051 reflection.

The extra peak at 23.22 2θ observed in the XRD pattern of the monoclinic silicalite is due to the 341/431 reflections. This was probably observed because the material was a good example of monoclinic symmetry and was highly crystalline. It is believed that the removal of amorphous material from the zeolite channels by the hydrothermal treatment was responsible for the high crystallinity of the silicalite and produced a particularly well developed example of monoclinic symmetry.

6.3.6 Water Sorption

The results in Section 6.3.3 indicated materials became more hydrophobic as amorphous silica was removed by the hydrothermal treatment . The water uptakes reported in that section were measued by thermal gravimetry after the silicalite samples were equilibrated over a saturated solution of sodium chloride at 25°C. These measurements were therefore restricted to a single water activity. In order to extend these measurements to a range of water activities measurements were also carried out by an isopiestic technique. The aim of the work was to obtain further information on the relationship between water uptake and:

(1) The removal of amorphous material from the samples.

(2) Crystal damage.

It was believed that an increase in vapour pressure would cause a greater amount of water to become associated with silanol groups of the amorphous silica and the damaged crystals, and that more water would be sorbed in the zeolite void space. To provide the constant vapour pressure required for these studies saturated salt solutions were used. The vapour pressure of the saturated salt solutions used in the present work are given in Table 6.18.

Table 6.18 Water activity of Saturated Salt

Solutions at 25°C.

Salt	a=P/Po
LiCl	0.1105
$MgCl_2$	0.3300
NaBr	0.5770
NaCl	0.7528
KCl	0.8426
$BaCl_2$	0.9019

The experimental method was as follows. Twelve glass vials were weighed to five decimal places. Hydrothermally treated H-silicalites from the S1 series were weighed into pairs of vials. These were then placed in a metal block with recesses for each container. A saturated solution of NaCl in a petri dish was placed in the bottom of a dessicator and a circular piece of metal gauze was put in the dessicator to support the metal block. The top of the dessicator was then fitted and the dessicator evacuated on a Buchner pump for ten minutes. The dessicator was placed in a water bath at 25°C. An equilibration time of one week was allowed. Samples of each H-silicalite were then removed one by one from the dessicator for thermal gravimetric analysis, to determine their uptake of water from the vapour phase. The weights of the equilibrated material in the duplicate vials were then determined. The weight of anhydrous solid in each of the duplicate vials could be calculated. The samples were then re-equilibrated over the other saturated salt solutions (Table 6.18) from the highest to the lowest vapour pressure. One week was allowed for each equilibration, after which the vials were removed from the dessicator and immediately recapped and weighed. The percentage increase in weight relative to the initial weight of anhydrous H-silicalite was then calculated. Water sorption isotherms were then plotted for each hydrothermally treated material and for the as-made calcined H-silicalite. These are shown in Figure 6.19.

It can be seen from Figure 6.19 that the as made calcined silicalite has by far the highest water uptake at low vapour pressures. This is considered to be due to the presence of

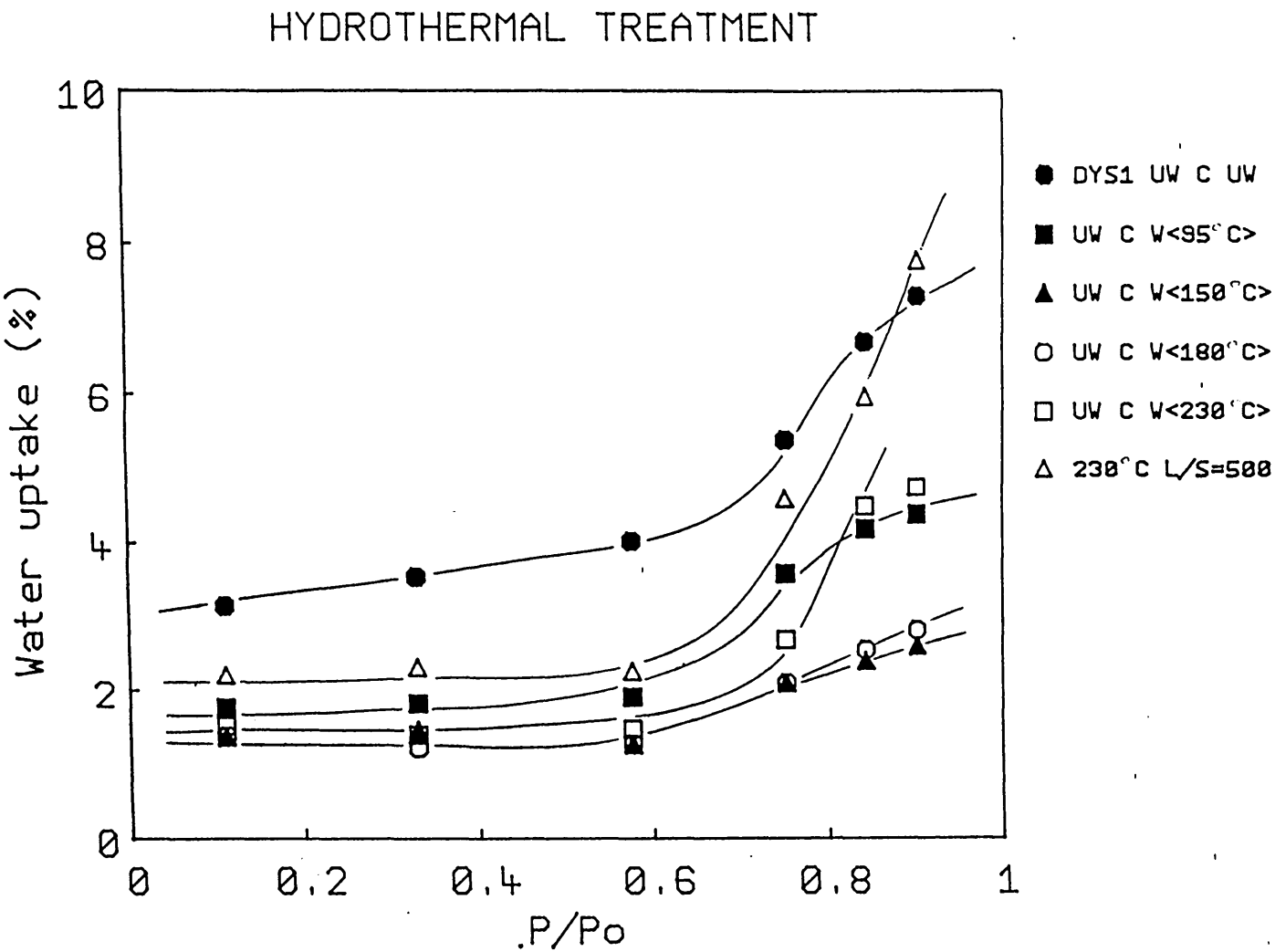

Figure 6.19 Water uptake isotherms of treated silicalite samples

contamination of the material by amorphous silica. This could be generated by the calcination, or alternatively it could be residual amorphous silica from the synthesis mixture. The hydrothermal treatment reduced the water uptake by the removal of amorphous silica (see Section 6.3.3) and perhaps also by the healing of internal silanols. The effect is most marked for the samples treated at 150 and 180°C; for these the water uptake is low even at high water activities and there is little, if any, capillary condensation. The highest water uptake at high water activity occurred with the sample treated at 230°C (L/S=500). The SEM of this material, given in Section 6.3.4, indicated that crystals were either single, shell-like or fragmented. This sample must have a high surface area, and probably has the most dissolution generated silanol groups. It is interesting that at low water activities this material did not have the highest water uptake; only at high water activities where capillary condensation can occur does its uptake exceed that of the as made untreated material. This indicates that the latter has the highest water capacity, and that the highly fragmented and partially dissolved material is most susceptible to capillary condensation.

6.3.7 Conclusion

These studies have shown that the specific sample of H-silicalite chosen for detailed study was contaminated with amorphous silica, which could be selectively removed by hydrothermal treatment. The increase in intensity of the 101&011 and 200&020 (hkl) low angle peaks upon the hydrothermal treatment indicated that some of this amorphous material was lodged in the silicalite channels.

The hydrothermal treatment was also found to lead to the dissolution of the silicalite crystals; this too was a selective process with twinned crystals being dissolved in preference to untwinned ones. Thus, at least in principle, a method of preparing a sample of single crystals from a mixture with twinned crystals has been discovered.

The mechanism by which the twinned crystals dissolved is of particular interest. Dissolution commenced at the intersection of

the two crystals, which is therefore the weakest point and the most susceptible to dissolution. It then continued from the inside of the crystals, leaving the outer skin intact. It is surmised that the outer skin is aluminium rich and that internal dissolution was promoted by silanol groups that were generated by the calcination.

It is interesting to speculate whether the single crystals also dissolve from the inside. This is possible in principle as monomeric silicic acid could be transported through the channel system and into solution. However even this monomeric species would be a tight fit in the channels and its diffusion would be slow. A TEM (Transmission Electron Microscopy) study might determine whether the single crystals were hollow.

When orthorhombic material was hydrothermally treated the resultant sample took on monoclinic symmetry. Three peaks were observed experimentally between 23.0 to 23.4 2θ. These reflections correspond to the 501, 431/341 and 051 lines. In both the theoretical and experimental XRD powder patterns of orthorhombic silicalite/ZSM-5 only the 501 and 051 reflections were observed. The emergence of an extra line at 23.22 2θ in the experimental XRD of monoclinic silicalite, which was of greater intensity than the 051 peak, has not been previously reported.

Chapter 6 References

[1] Z.G. Gabelica, J.B. Nagy, P. Bodart and A. Nastro

Thermochimica Acta, 1985, **93**, 749

[2] V.R. Choudary and S.G. Pataskar

Thermochimica Acta, 1986, **97**, 1

[3] A.N. Kotasthane, V.P. Shiralker

Thermochimica Acta, 1986, **102**, 37

[4] C.G. Pope

Journal of Colloid and Interface Science, 1987,

116 (1), 221

[5] H. Pfeifer, D. Freude and M. Hunger

Zeolites, 1985, **5**, 273

[6] G. Engelhardt, B. Fahlke, M. Maegi and E. Lippmaa

Z. Phys. Chem. (Leipzig), 1985, **266**, 239

[7] G.L. Woolery, L.B. Alemany, R.M. Dessau

and A.W. Chester

Zeolites, 1986, **6**, 14

[8] M. Hunger, J. Kaerger, H. Pfeifer, J. Caro,

B. Zidobrowius, M. Bulow and R. Mostowicz

J. Chem. Soc., Faraday Trans. I, 1987, **83**, 3459

[9] E.L. Wu, S.L. Lawton, D.H. Olson,

A.C. Rohrman,Jr. and G.T. Kokotailo

J. Phys. Chem., 1979, **83**, 2777

[10] D.G. Hay and H. Jaeger

J. Chem. Soc., Chem. Commun., 1984, 1433

[11] R. von Ballmoos

"Collection of Simulated XRD Powder

Patterns for Zeolites", published by

the Structure Commission of the

International Zeolite Association

(1984), page 74.

[12] G. Boxhoorn, R.A. van Santen, W.A. van Erp,

G.R. Hays, R. Huis, D. Clague.

J. Chem. Soc., Chem. Commun., 1982, 264.

[13] S.G. Fegan

PhD Thesis (1985), page 299.

[14] L.S. Dent Glasser,

"Crystallography and its Applications", Van

Nostrand Reinhold, New York, 1977, pages 125 and 136.

[15] K.R. Franklin and B.M. Lowe

Thermochimica Acta, 1988, **127**, 319.

[16] J. Gordon

Personal Communication.

[17] E.G. Derouane and Z. Gabelica

J. Catal., 1980, **65**, 486.

CHAPTER 7

THE HYDROTHERMAL STABILITY OF ZSM-5

7.1 Introduction

The synthesis of ZSM-5 was discussed in Chapter 1 and the methods used in the present work were described in Chapter 4. Several workers have discussed the relationship between the catalytic properties of ZSM-5 and its synthesis and sorption behaviour (1-3). Studies have also been conducted on the relationship between acidity and catalytic cracking activity of high silica zeolites (4,5,6), diffusion characteristics (7) and shape selectivity (8,9,10). However, little research has been published on the effect of hydrothermal treatment on catalytic activity. The steam stability of samples of H-ZSM-5 which contained alkaline earth metals has been studied in relation to methanol conversion to higher hydrocarbons (11). The effects of hydrothermal treatment on the catalytic properties of super high silica zeolites has also been studied. The results showed that for n-hexane conversion, cracking activity decreased but selectivity towards aromatic products increased after treatment (12). This decrease in activity is probably due to the loss of tetrahedral aluminium from the zeolite framework and its relocation on the zeolite surface as octahedral aluminium. This can be thought of as zeolite dissolution. It is probable that silicon is also lost from the framework during hydrothermal treatment, but the catalytic consequences will be less apparent than those arising from aluminium dissolution.

There is uneven distribution of aluminium within ZSM-5 crystals. Zoning of aluminium in ZSM-5 has been studied by von Ballmoos and Meier (13). Derouane et al showed that Si/Al ratios tend to be higher in the bulk of a ZSM-5 crystal than at its surface (14). Bibby et al indicated that the aluminium content of ZSM-5 affects its orthorhombic to monoclinic symmetry change and that this provided a technique for the determination of framework aluminium in ZSM-5 (15). This technique uses splitting of the X-ray diffraction peaks at 45.0 and 45.5 2θ as a measure of the aluminium content of the framework. This has an advantage over bulk analysis in that the observations are specific to the zeolite framework and do not include aluminium present as amorphous impurities. However it is important that the

samples used for calibration are free from non-framework aluminium, including amorphous impurities in the zeolite channels which cannot be detected by scanning electron microscopy. The presence of siliceous amorphous impurities in the channel system of silicalite was discussed in Chapter 6.

The effect of hydrothermal treatment on ZSM-5 will be very sensitive to the presence of template species. Aluminium at the channel intersections will be stabilised by the presence of tetrapropylammonium (TPA) ions. These ions will also obstruct the access of water to the aluminium sites. When the TPA ions are removed by calcination, there is ready access for water molecules and the catalytic behaviour is likely to be influenced by hydrothermal treatment. If internal amorphous material is removed by the hydrothermal treatment then the diffusion of organic reactants and products within the ZSM-5 framework will become more efficient. The molecular traffic control within the zeolite channel system will be affected, and this may have consequences for selectivity (16).

Hydrothermal treatment need not reduce the catalytic activity of ZSM-5. Sendoda and Ono (17) showed that steaming enhanced the catalytic activity of ZSM-5 for the cracking of propane. The optimum steaming temperature for hexane cracking over ZSM-5 was found to be 550°C; this is higher than that (400°C) which gave the highest concentration of acidic hydroxyl groups (18,19) in the catalyst. It was suggested that stronger acid sites may be formed when the zeolite is partially dehydroxylated (20). In a study of mordenite, Mirodatos and Barthomeuf (21) suggested that hydroxyl groups interacted with dislodged aluminium species which enhanced their acid strength. Further studies showed that activity depended on a balance between framework and non-framework aluminium (17,22). It should be noted that in the work summarised here (17-21) hydrothermal treatment implies treatment of the heated zeolite with steam, whereas in the present work hydrothermal treatment denotes the action of liquid water under autogenous pressure. This, unlike steam treatment, allows the dissolution of the lattice.

The results in this chapter deal with the hydrothermal treatment

of some of the ZSM-5 samples which were crystallised at 95 and 150°C; as described in Chapter 4. The catalytic isomerism of but-1-ene (23,24) was chosen as a test reaction to monitor the effect of the hydrothermal treatment temperature on catalyst selectivity and activity. The aim of the study was to find evidence of amorphous impurities in the precursor TPA-ZSM-5 samples and in calcined H-ZSM-5. Catalytic product selectivity changes, caused by the hydrothermal treatments, may indicate a variation in the position of active sites within the ZSM-5 framework. Particular attention was paid to cis- and trans-but-2-ene product selectivities and the rate of conversion of initial but-1-ene by the catalytic reaction. The TPA template is located at the channel intersections (25) and DTA results from Chapter 4 showed that aluminium was associated with TPA at these sites. Removal of aluminium from these sites during the hydrothermal treatments should be stabilised by the presence of TPA in ZSM-5 precursors. The selective dealumination of hydrothermally treated uncalcined TPA-ZSM-5 may show changes in catalytic product selectivities if different transition states are preferred at different framework aluminium sites. The treatment should result in a decrease in framework aluminium, which may result in a reduction in catalytic activity. This effect should be partly offset by the removal of amorphous material from the catalysts, as this will improve the diffusion of organic species in the ZSM-5 channel system.

7.2 Experimental

The samples of ZSM-5 were hydrothermally treated in either their TPA-precursor or calcined hydrogen forms. The preparation of the samples is described in Chapter 4.

Chosen masses of the zeolites and water were weighed into a 1 litre polypropylene bottle. The liquid/solid mass ratio (L/S) of each system was 200. For the 95°C treatments, a stirrer cap was screwed onto the top of the bottle, which was then placed in a 95°C water bath. The equipment is described in Chapter 2.0. Treatments at temperatures above 95°C were carried out in either a 1 litre or a 500 ml autoclave. The materials were weighed out as indicated above and poured into the autoclave vessel. The autoclave was immediately assembled and switched on.

Six different samples of TPA-ZSM-5 were hydrothermally treated at 95°C for 16 hours. The effects of this treatment were examined by comparison of their differential thermal analysis traces. Two samples of H-ZSM-5 were treated. One was treated at 150°C over a range of times. The other was hydrothermally washed for 3 hours over a range of temperatures.

All the materials were analysed by XRD and bulk analysis (by atomic absorption spectrophotometry (AAS)). Differential thermal analysis was used, but only for uncalcined materials. Samples were run at a heating rate of 5°C/minute from room temperature up to 1000°C in a static air atmosphere. To determine the peak areas, the peaks were traced, cut out and weighed.

Three samples of the treated H-ZSM-5 were equilibrated over a saturated solution of sodium chloride and their water uptakes subsequently measured by thermal gravimetry. The materials were run at a heating rate of 10°C/minute from room temperature to 1000oC in a 15ml/minute flow of air.

An elemental profile of the crystal surfaces of the treated H-ZSM-5 samples was obtained by X-ray photoelectron spectroscopy

(XPS). The H-ZSM-5 samples which were used as catalysts were examined by scanning electron microscopy (SEM). The catalytic isomerism of but-1-ene was used to monitor the effect of hydrothermal treatment on catalyst activity and product selectivity. The catalytic rig used a system in which the reactant and product gases were repeatedly cycled over the same catalyst (see Chapter 2).

7.3 Results

7.3.1 Uncalcined ZSM-5

Six samples of uncalcined TPA-ZSM-5 with different Si/Al ratios together with a sample of TPA-silicalite, were hydrothermally treated at 95°C and analysed by XRD, DTA and bulk analysis, as described in section 7.2.

The XRD patterns showed little difference between the treated and untreated materials. All samples retained their orthorhombic symmetry. As an example, the X-ray powder patterns of a TPA-ZSM-5 and of its hydrothermally treated counterpart are shown in Figures 7.1 and 7.2. The DTA of the samples showed that the hydrothermal treatment decreased the temperature of the exotherm for the oxidative degradation of the TPA ion. The DTA traces of each parent and treated material are shown in Figures 7.3 to 7.9. The splitting of the major exotherm is believed to arise from oxygen starvation consequent on the use of relatively large samples (about 40mg). The exotherm temperatures were established by the method described in Chapter 4. Bulk analysis data were supplied by ICI Chemicals and Polymers Limited.

The DTA peak positions and the Si/Al ratios evaluated from the bulk analysis data are given in Table 7.1. The sample codes are the same as those given in Chapter 4.0. Material B1 is a TPA-silicalite.

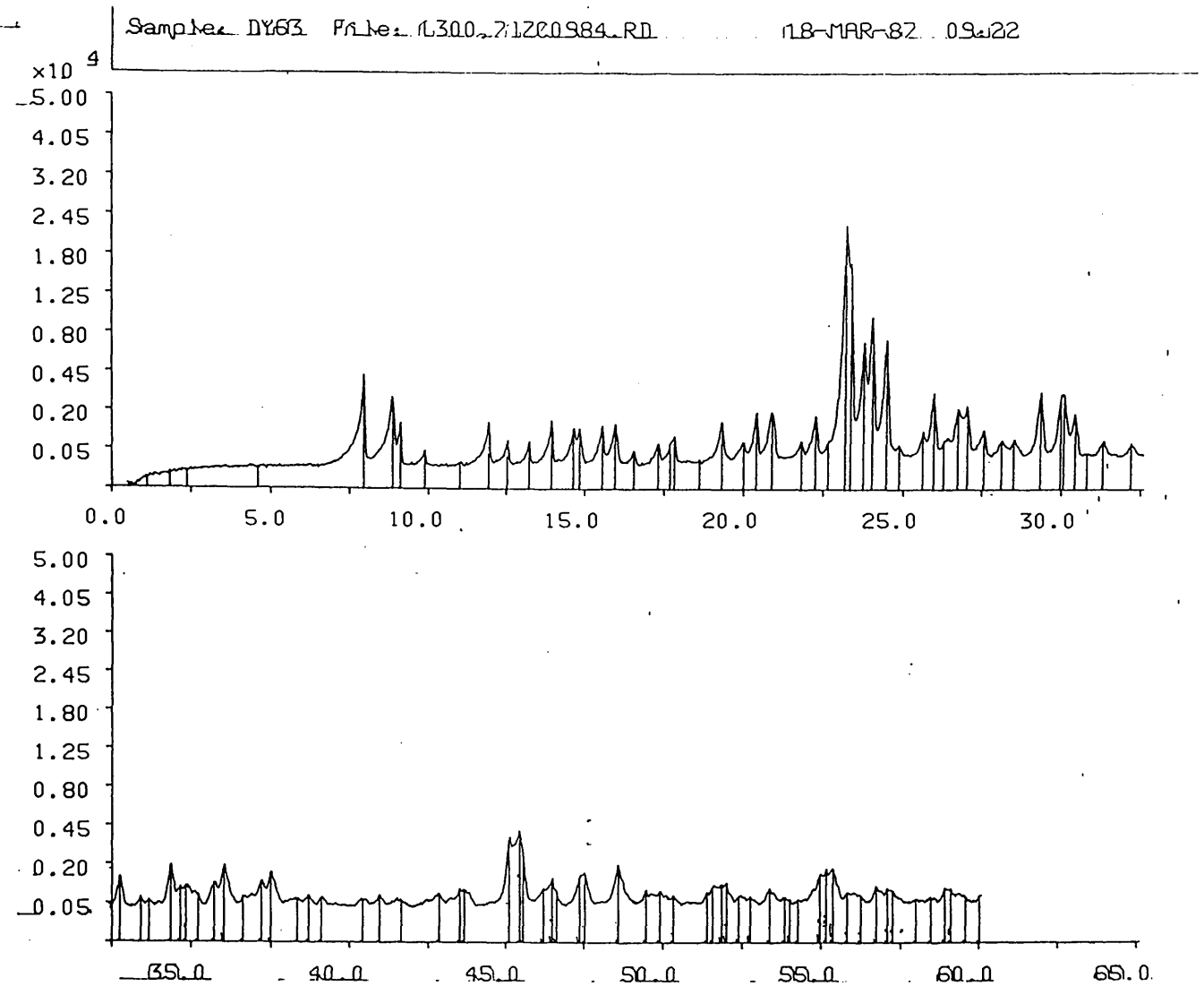

Figure 7.1 XRD pattern of uncalcined TPA-ZSM-5 (E3)

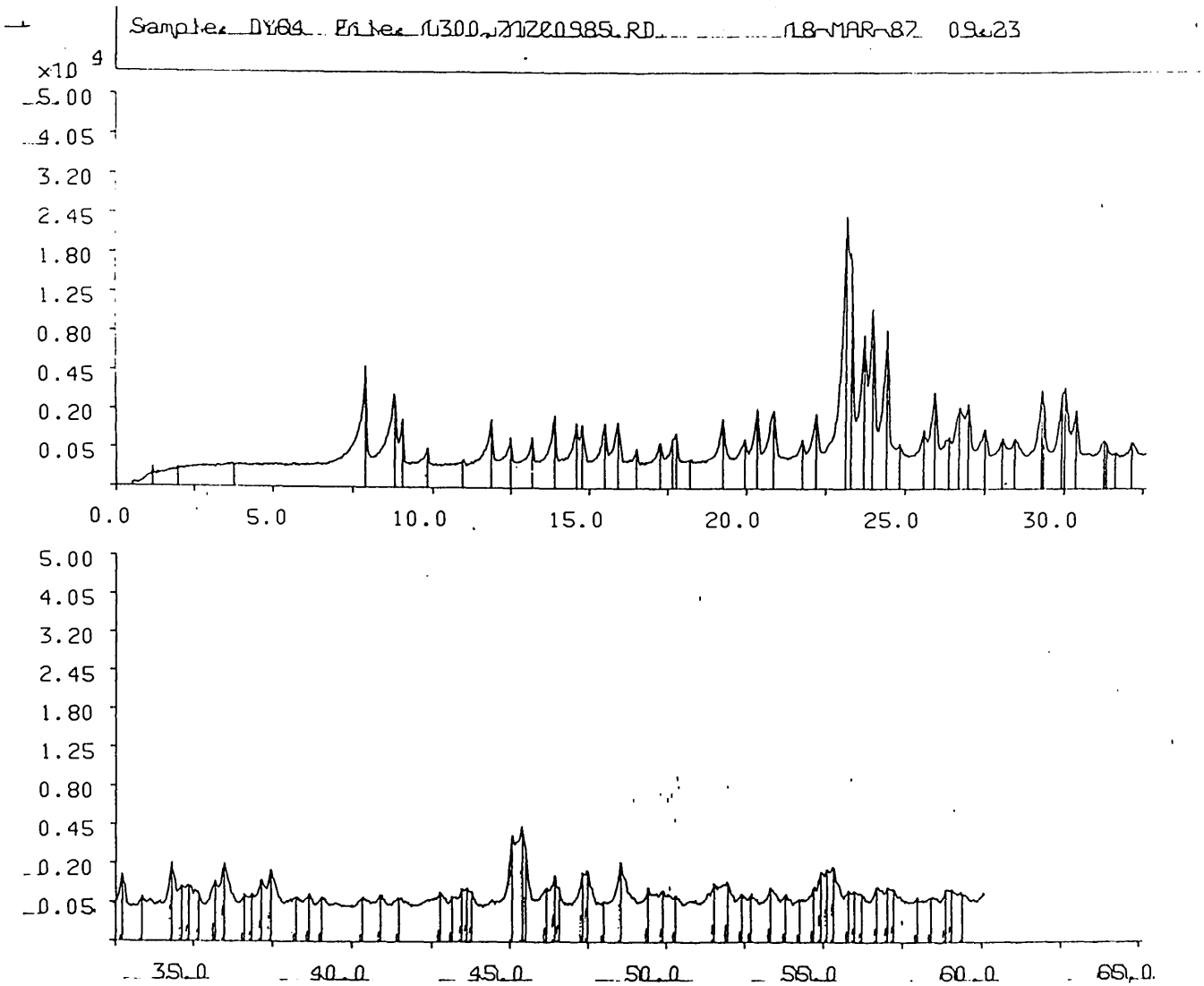

Figure 7.2 XRD pattern of hydrothermally treated (95°C) uncalcined TPA-ZSM-5 (E3)

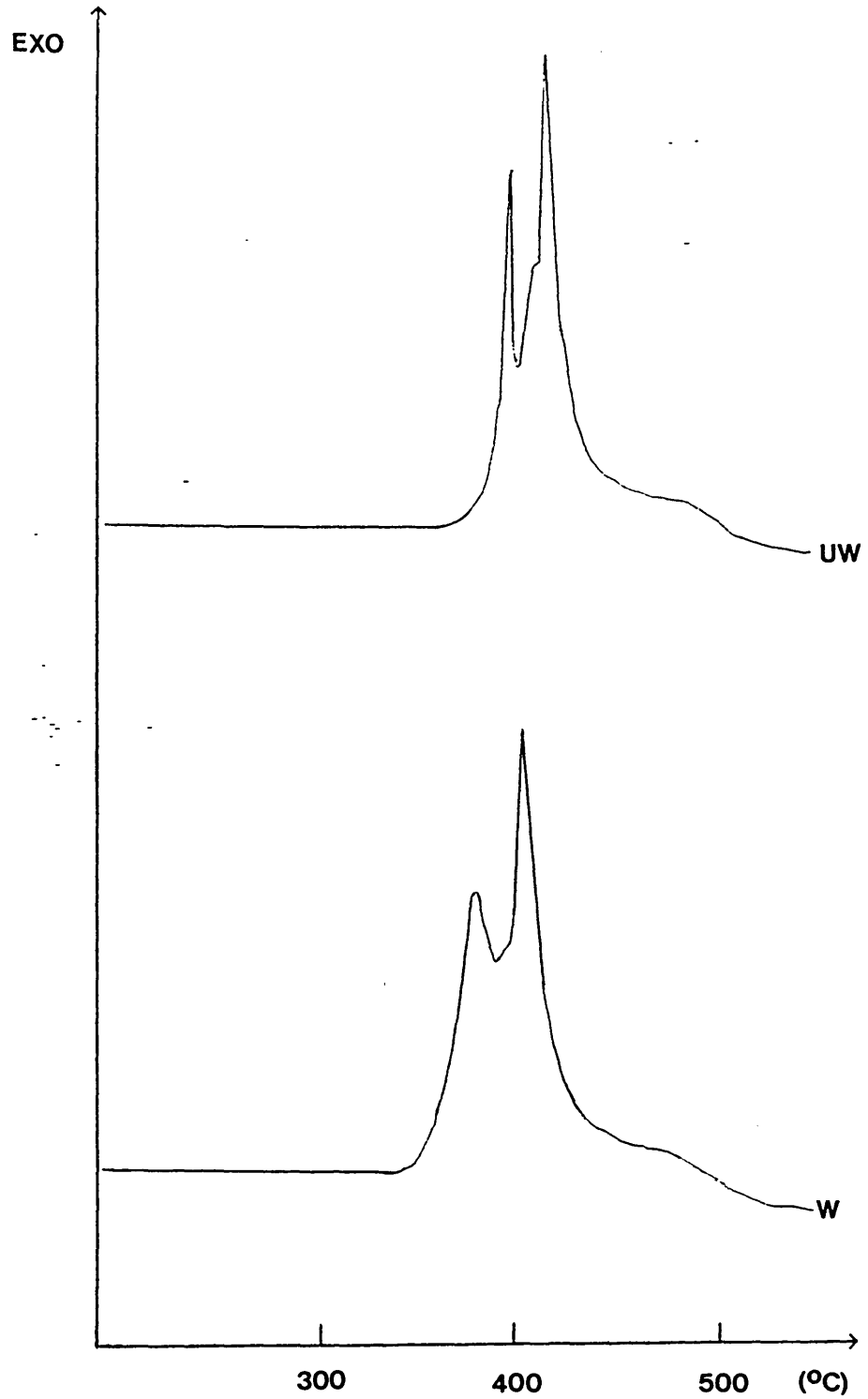

Figure 7.3 DTA traces of treated (W) and untreated (UW) samples of uncalcined TPA-ZSM-5 (E1)

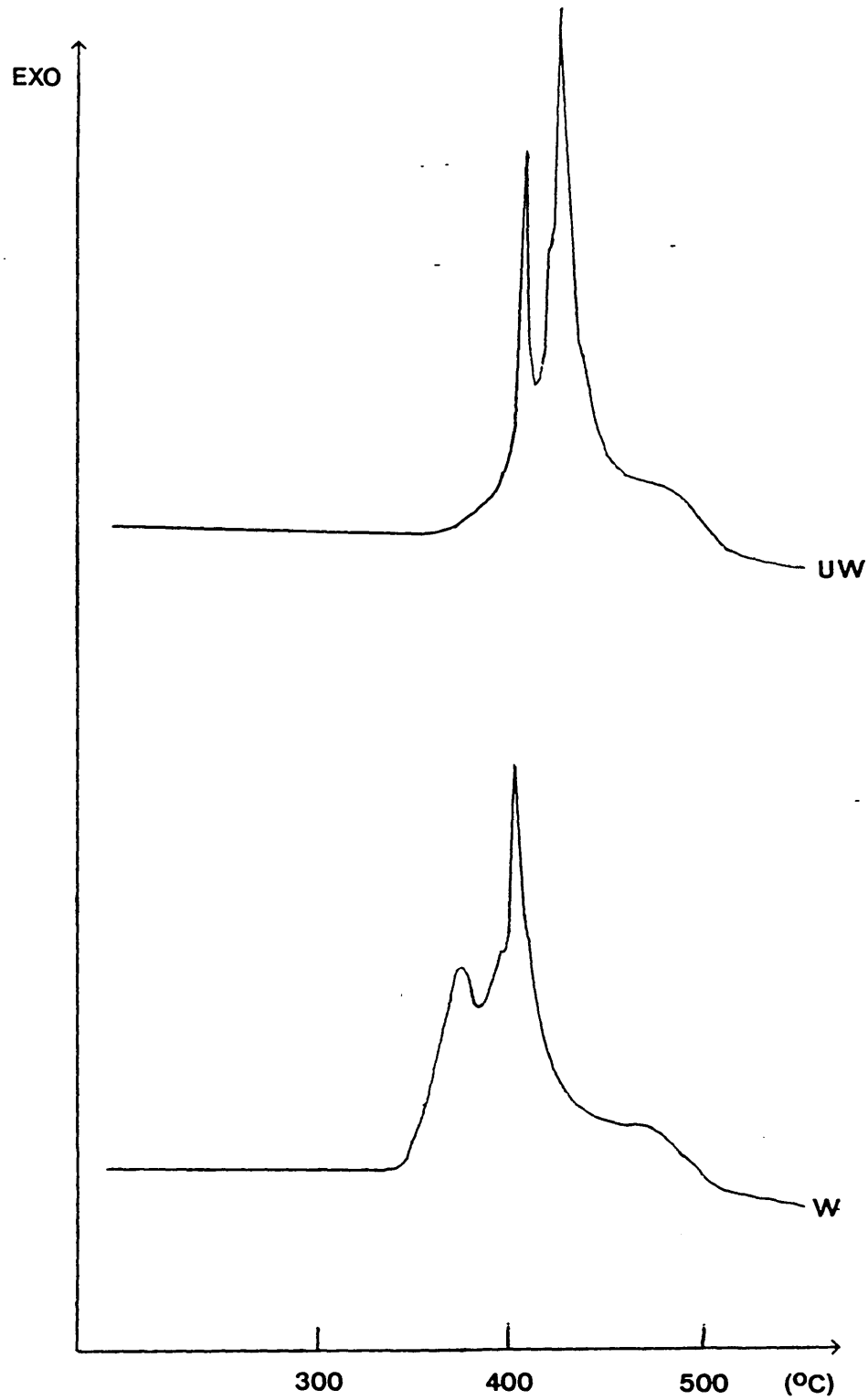

Figure 7.4 DTA traces of treated (W) and untreated (UW) samples of uncalcined TPA-ZSM-5 (E2)

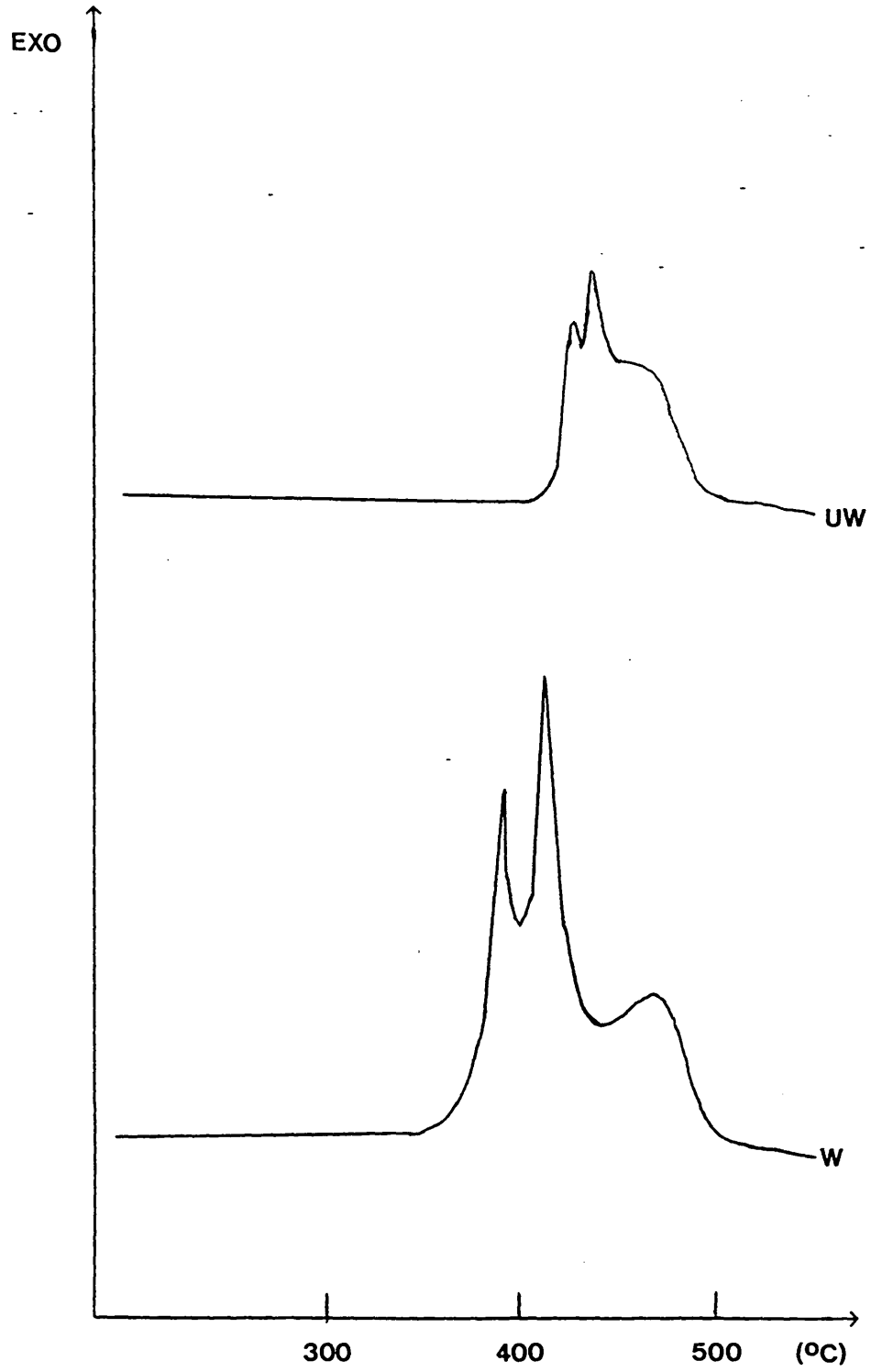

Figure 7.5 DTA traces of treated (W) and untreated (UW) samples of uncalcined TPA-ZSM-5 (E3)

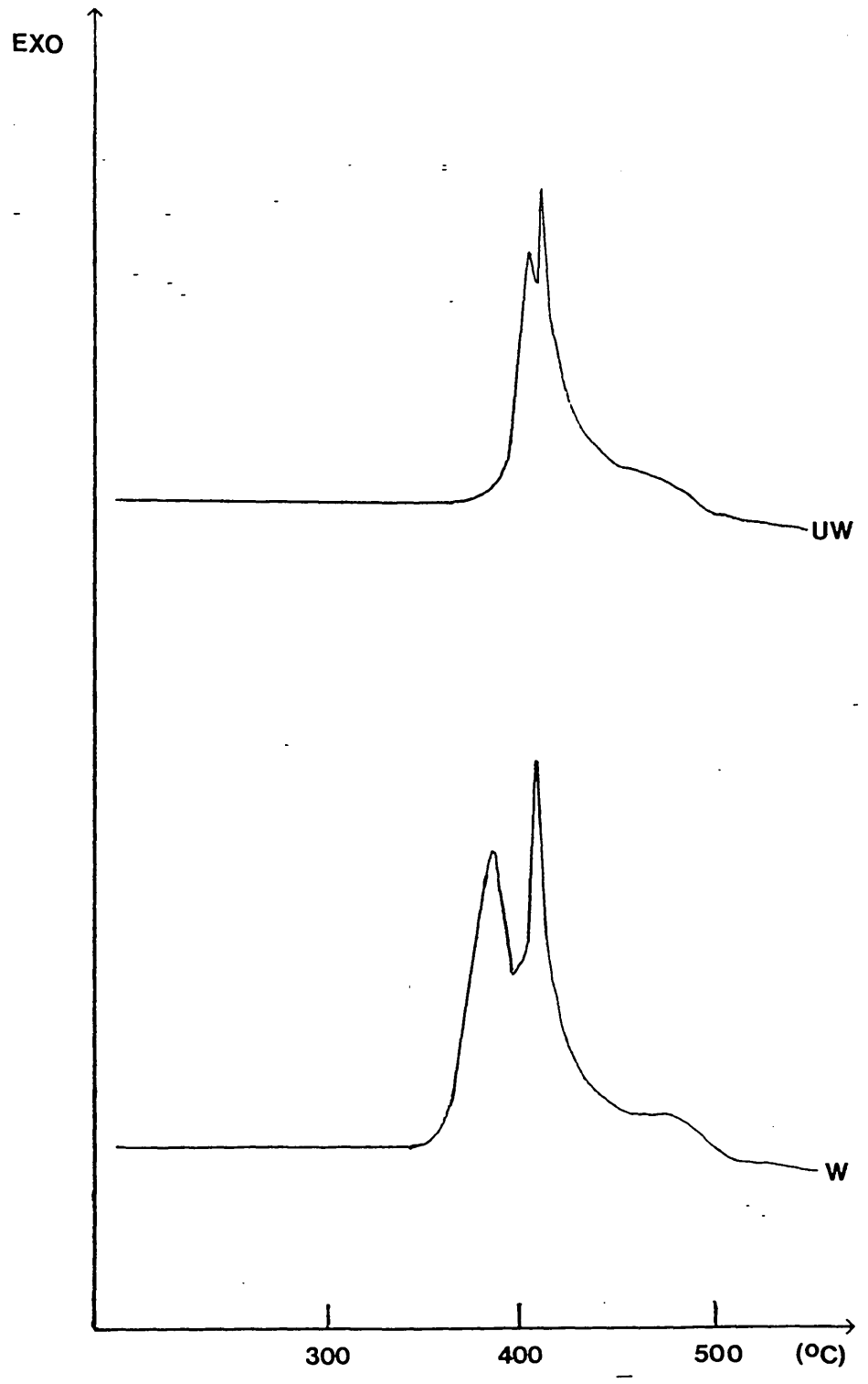

Figure 7.6 DTA traces of treated (W) and untreated (UW) samples of uncalcined TPA-ZSM-5 (C3)

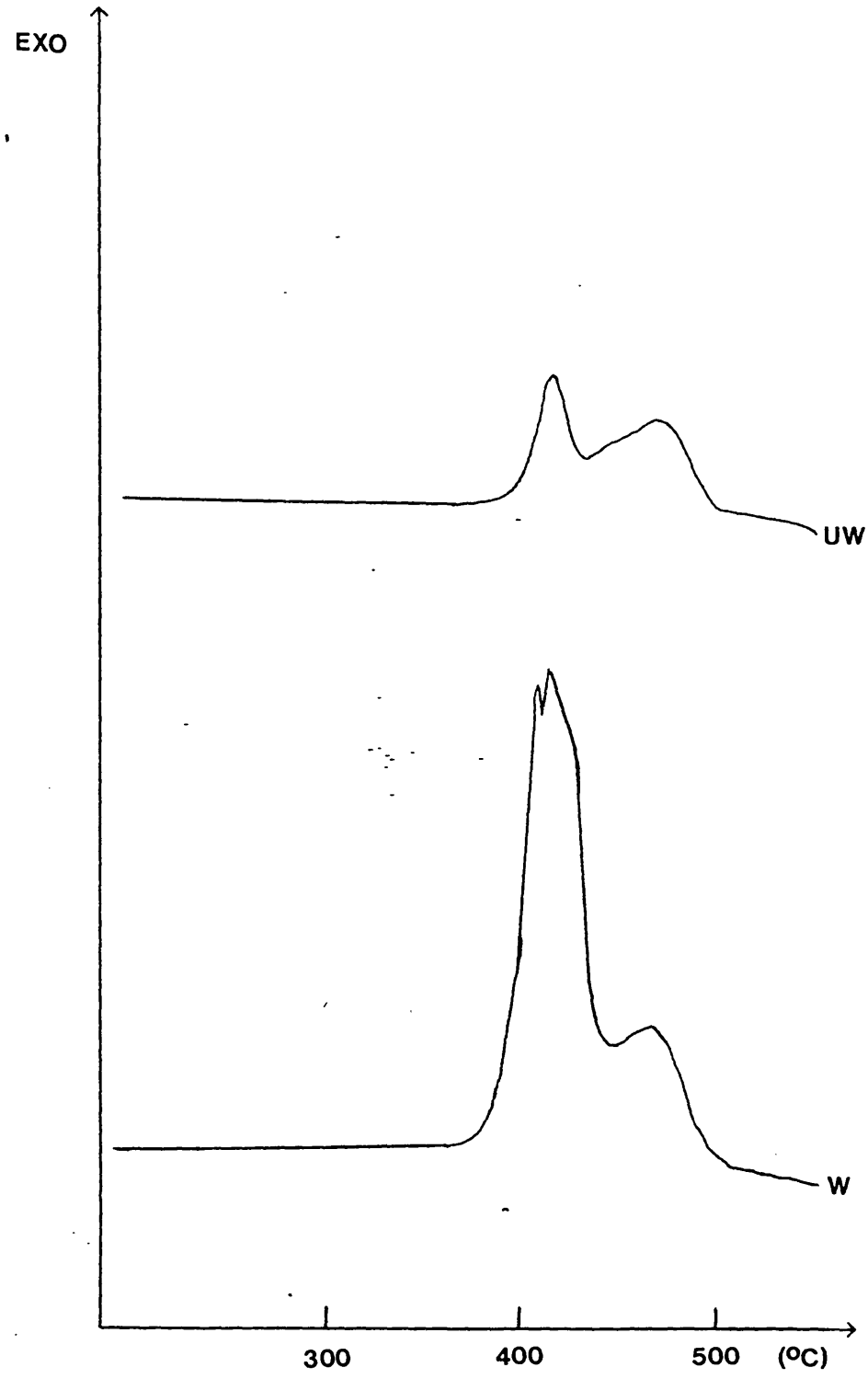

Figure 7.7 DTA traces of treated (W) and untreated (UW) samples of uncalcined TPA-ZSM-5 (C4)

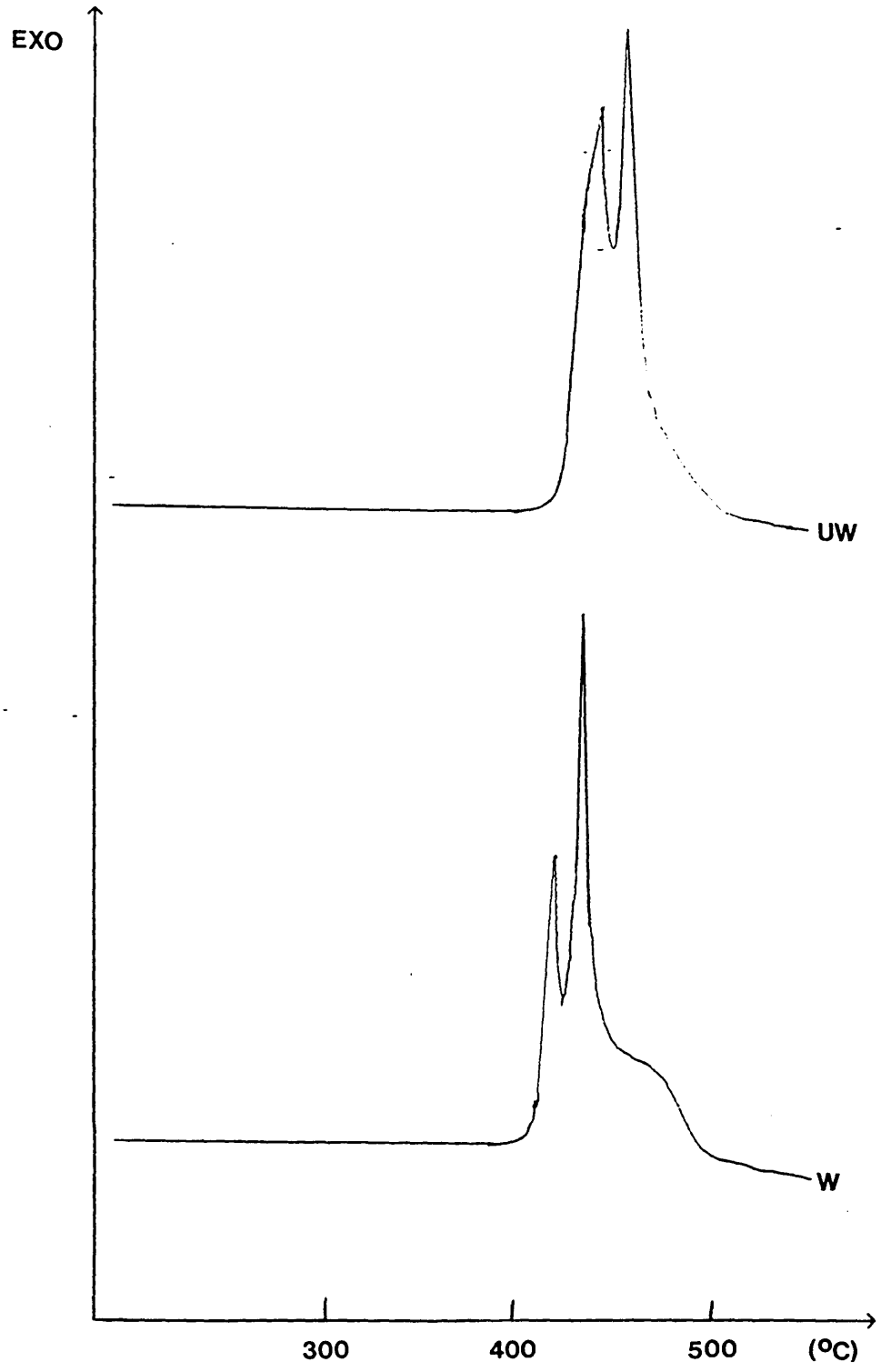

Figure 7.8 DTA traces of treated (W) and untreated (UW) samples of uncalcined TPA-ZSM-5 (D3)

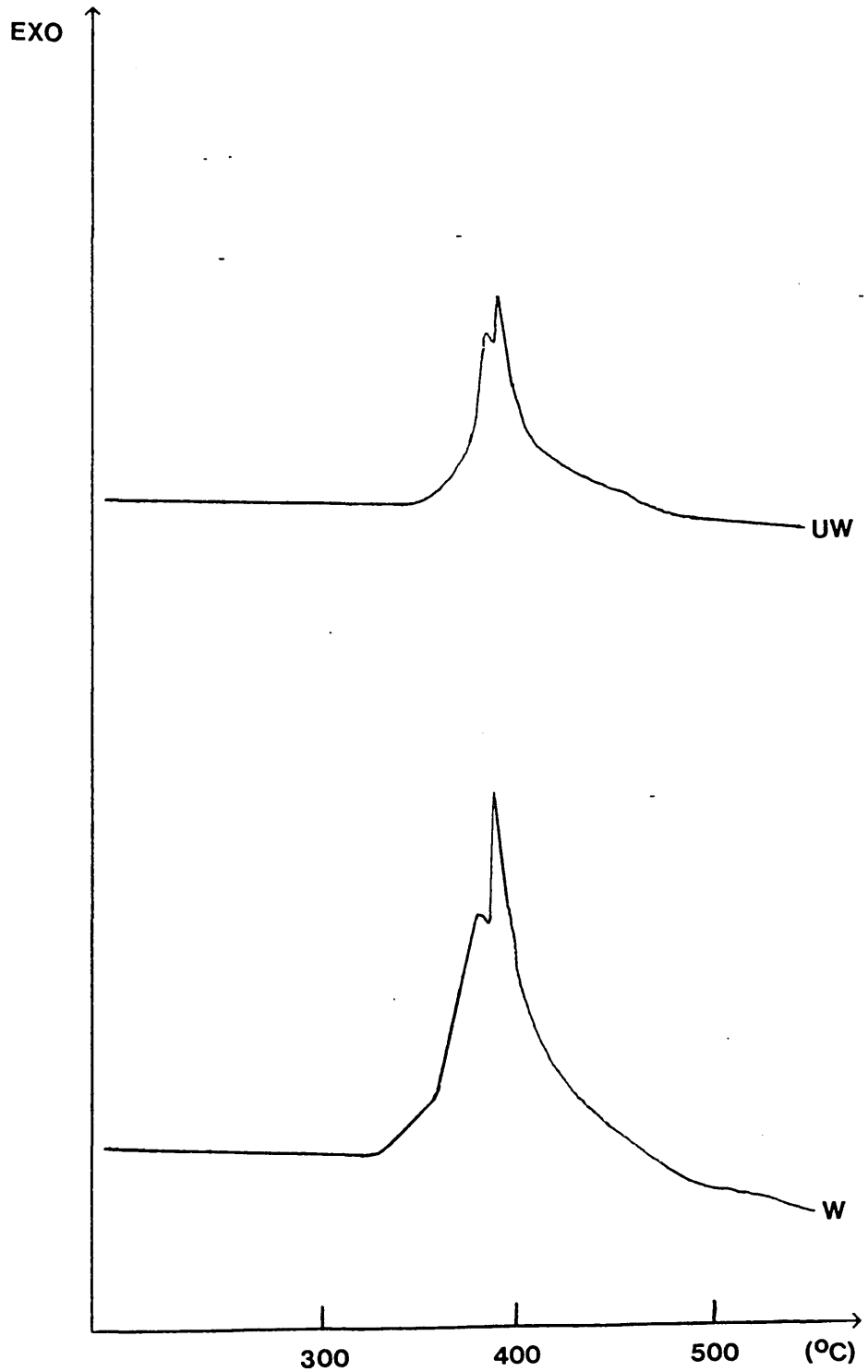

Figure 7.9 DTA traces of treated (W) and untreated (UW) samples of uncalcined TPA-silicalite (B1)

Table 7.1 DTA data for TPA-ZSM-5.

	Untreated		Treated		
Code	Si/Al ratio	DTA peak position (°C)	Si/Al ratio	DTA peak position (°C)	Change in DTA peak Area (%)
E1	862.5	388	882.5	383	+34.6
E2	207.5	404	211.2	388	+6.1
E3	52.4	426	66.7	394	+131.3
C3	64.9	402	78.6	385	+61.5
C4	29.5	406	27.5	404	+221.4
D3	72.3	434	80.0	427	-14.3
B1	1193.3	380	1511.4	380	+112.6

Increases in the TPA decomposition/combustion exotherm peak areas were observed for all but one of the samples, even though the sample sizes were approximately equal in all experiments. This shows that removal of the template was more exothermic for the treated samples and suggests that air could reach the TPA ions more easily. There was a cleaner combustion of the template from the ZSM-5 framework after the hydrothermal treatment. This may have been caused by the removal of amorphous aluminosilicate species from the crystal surfaces. The results in Chapter 6 indicated that the XRD background was reduced as amorphous material was removed by hydrothermal treatment. The XRD background of the initial TPA-ZSM-5 C4 was 146 counts. This was reduced to 135 counts after hydrothermal treatment at 150°C, which implied that amorphous material had been removed. This was also apparent from the scanning electron micrographs of ZSM-5 sample C4; see Plate 7.1. Plates 4.1-4.4 in Chapter 4 showed little evidence of amorphous surface material, except in the case of product C4. For this material (C4) the removal of amorphous material was demonstrated by SEM and it is noteworthy that it shows the largest increase in DTA exotherm area, +221.4%. The removal of the amorphous material makes it easier for oxygen to diffuse into the zeolite channel system and enhances the combustion of the TPA. Conversely, diffusion of TPA decomposition/combustion products to the surface will be enhanced. The improved diffusion characteristics lead to cleaner combustion of the template, which results in the larger area of TPA combustion exotherms for most of

the hydrothermally treated materials. An important consequence is that the cleaner combustion may reduce the formation of residual coke in the channel system.

TPA-ZSM-5 D3 was the only material which showed a decrease in the area of its TPA combustion exotherm (-14.3%). This is significant as D3 was the only hydrothermally treated material which was crystallised at 150°C. It is known that TPA-silicalites crystallised at 150°C are less prone to amorphous contamination than those synthesised at 95°C (26). The DTA result for D3 suggests that this also applies to TPA-ZSM-5 and that there was little residual amorphous material in this sample.

The changes in the DTA exothermic peak areas caused by the hydrothermal treatments were irregular. This indicated variable levels of amorphous contamination in the precursor TPA-ZSM-5 products. On average the exothermic peak temperature position was reduced by the hydrothermal treatment by 11°C.

7.3.2 Calcined H-ZSM-5

Two ZSM-5 products were calcined and hydrothermally treated. The first material (E3) was crystallised at 95°C from a reaction mixture prepared from piperazine, tetrapropylammonium bromide, amorphous silica, aluminium nitrate and water. Its bulk Si/Al ratio was 42.5. The second ZSM-5 (C4) was made with a different source of aluminium (aluminium sulphate), but its preparation was otherwise identical. Its bulk Si/Al ratio was 29.5. Further details of the synthesis and characterisation of these materials are given in Chapter 4. The materials were calcined at 550°C for 16 hours then at 800°C for 1 hour.

7.3.2.1 Results for H-ZSM-5 (E3)

The first material to be hydrothermally treated was that crystallised from the reaction mixture which contained aluminium nitrate (E3). A constant hydrothermal wash temperature of 150°C was chosen but the times of the washes were varied between 3 and 66 hours. Four samples of the original calcined H-ZSM-5 were treated.

(Note: the term wash is used to denote treatment with water as described in section 7.2).

The XRD patterns of the untreated and treated materials are shown in Figures 7.10 to 7.14. Most of the materials were predominantly orthorhombic but one showed mostly monoclinic symmetry (E3, Figure 7.12). There was no clear trend. The TPA-ZSM-5 was calcined in two batches, one a week before its hydrothermal treatment and the second portion only one day prior to treatment. The H-ZSM-5 which was treated one week after calcination was mainly monoclinic, as judged from the resolution of the 133/313 (hkl) Bragg reflections centred at 24.5 2θ (Figure 7.12). The material which was calcined one day before treatment was orthorhombic after each treatment. This suggests either that one of the calcinations led to a greater dealumination than the other (increased dealumination would result in a faster transition to monoclinic symmetry (31)), or that the week at ambient temperature after calcination and before treatment was sufficient for the symmetry change to take place (see Table 7.2 for details). Bulk analysis data for the samples were supplied by ICI Chemicals and Polymers Limited, and the Si/Al ratios are given in Table 7.2.

Table 7.2 Bulk Si/Al ratios for H-ZSM-5 (E3)

treated with water at 150°C.

ZSM-5 Treatment Time (hours:mins)	Si/Al Ratio	Crystal Symmetry
0:00	42.5	Orthorhombic
3:40	48.9	Orthorhombic
5:10	84.4	Monoclinic
16:00	55.6	Orthorhombic
66:28	54.8	Orthorhombic

The Si/Al results show that in general the extent of dealumination increases with treatment time. The Si/Al ratio increased from an initial value of 42.5 to around 55 after 66 hours. The initial dealumination appeared to be rapid, and may have been from non-framework sites; perhaps an alumina rich amorphous impurity.

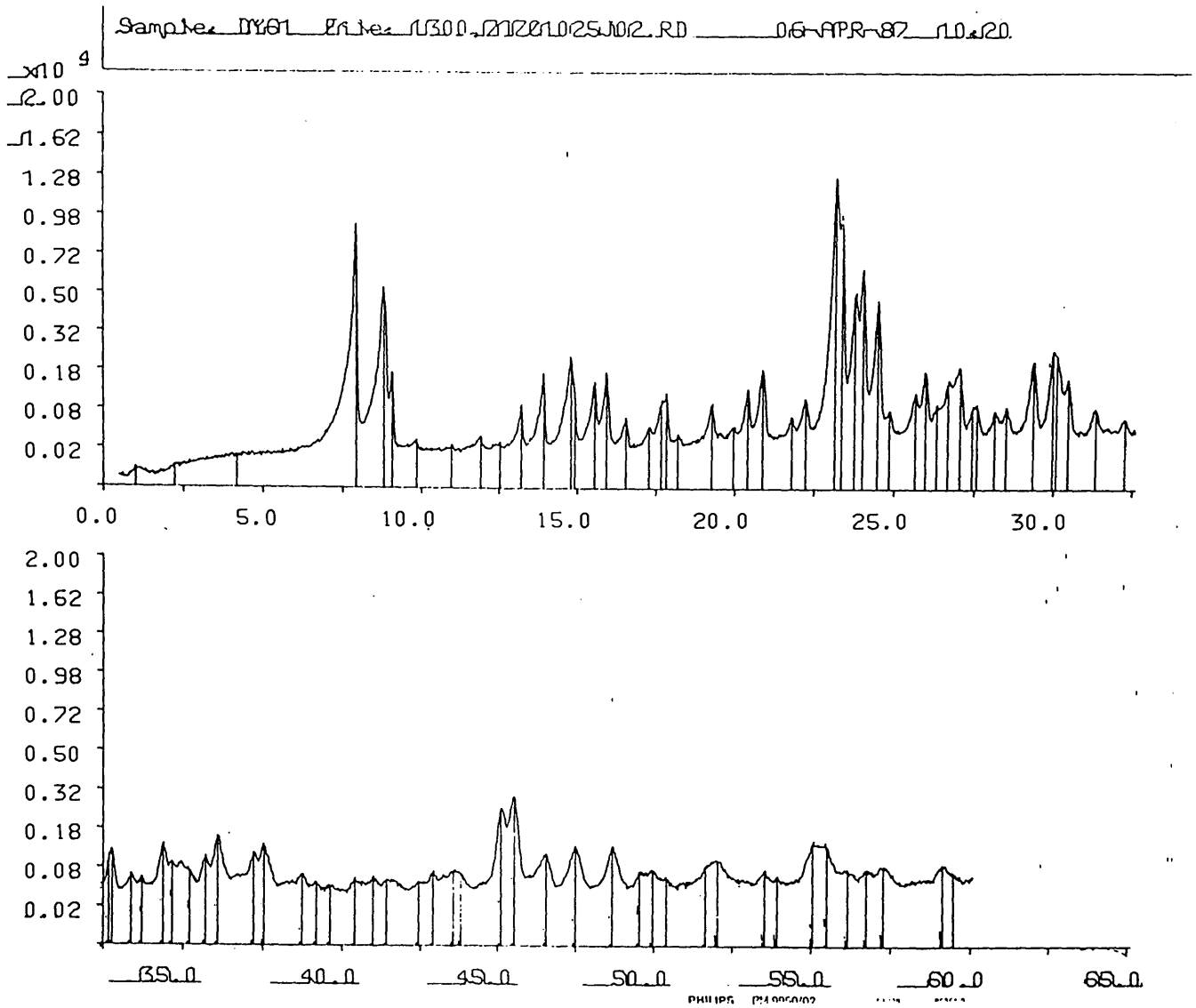

Figure 7.10 XRD pattern for untreated calcined ZSM-5 (E3)

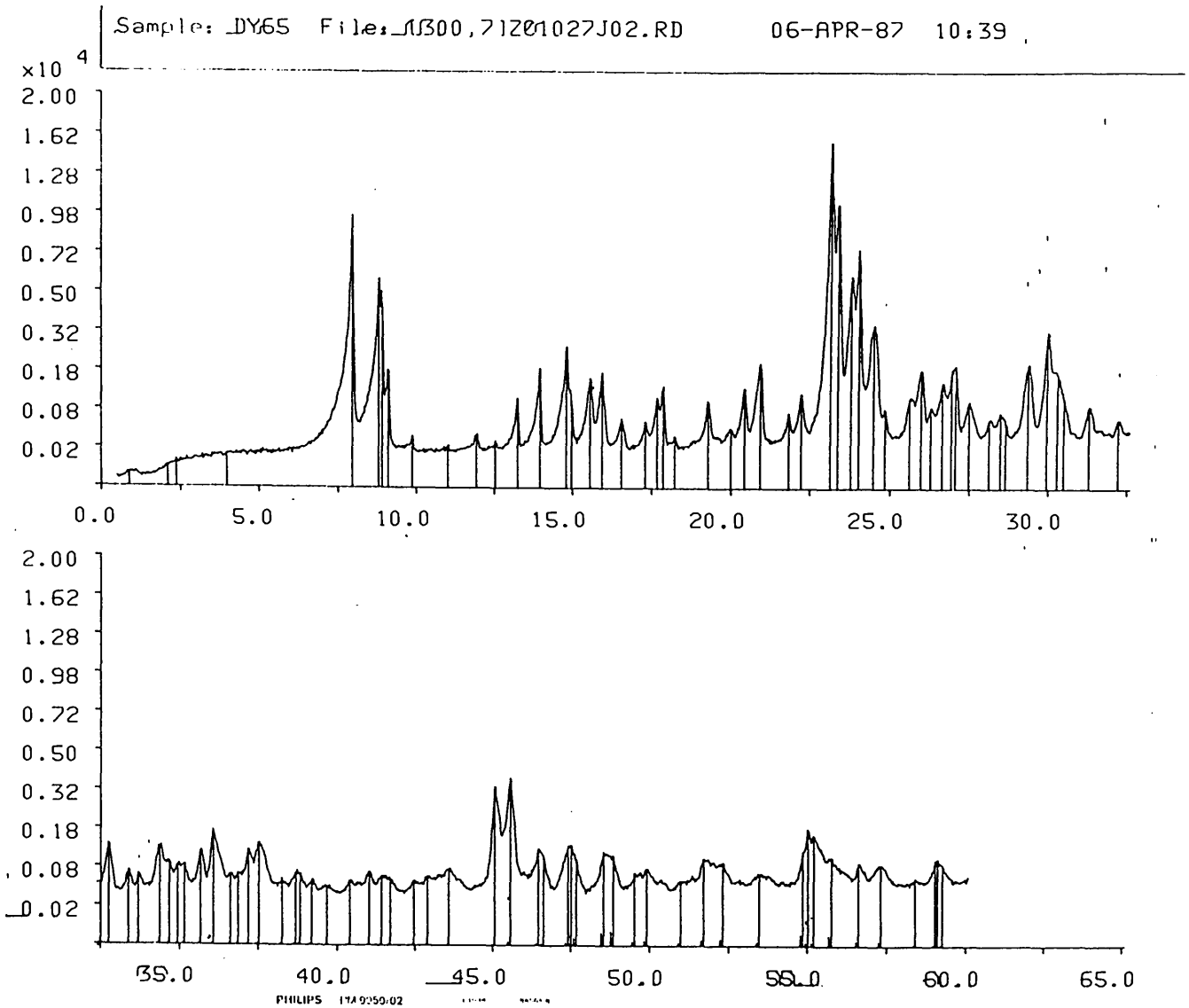

Figure 7.11 XRD pattern for calcined ZSM-5 (E3) treated for 3 hours 40 minutes at 150°C

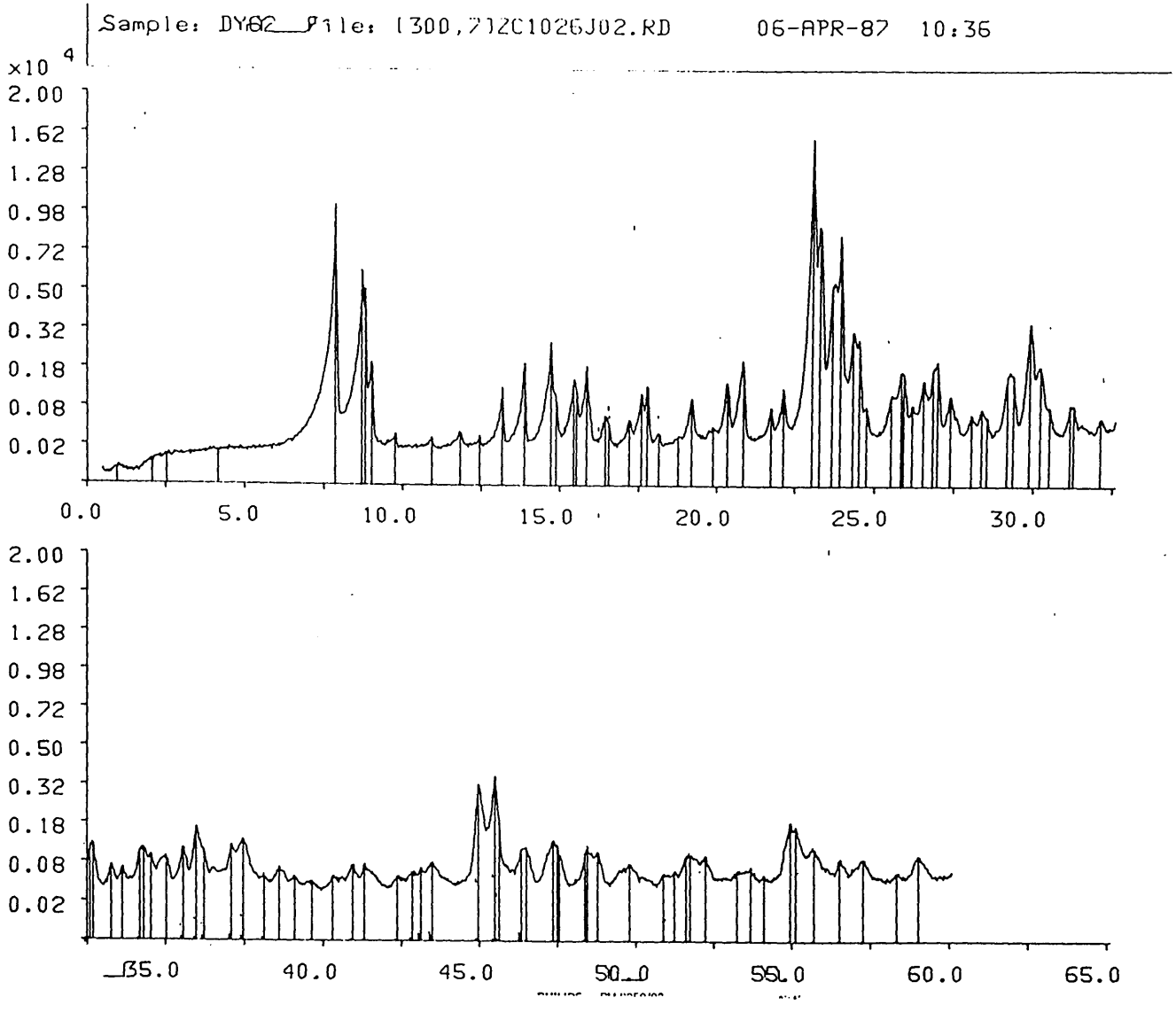

Figure 7.12 XRD pattern for calcined ZSM-5 (E3) treated for 5 hours 10 minutes at 150°C

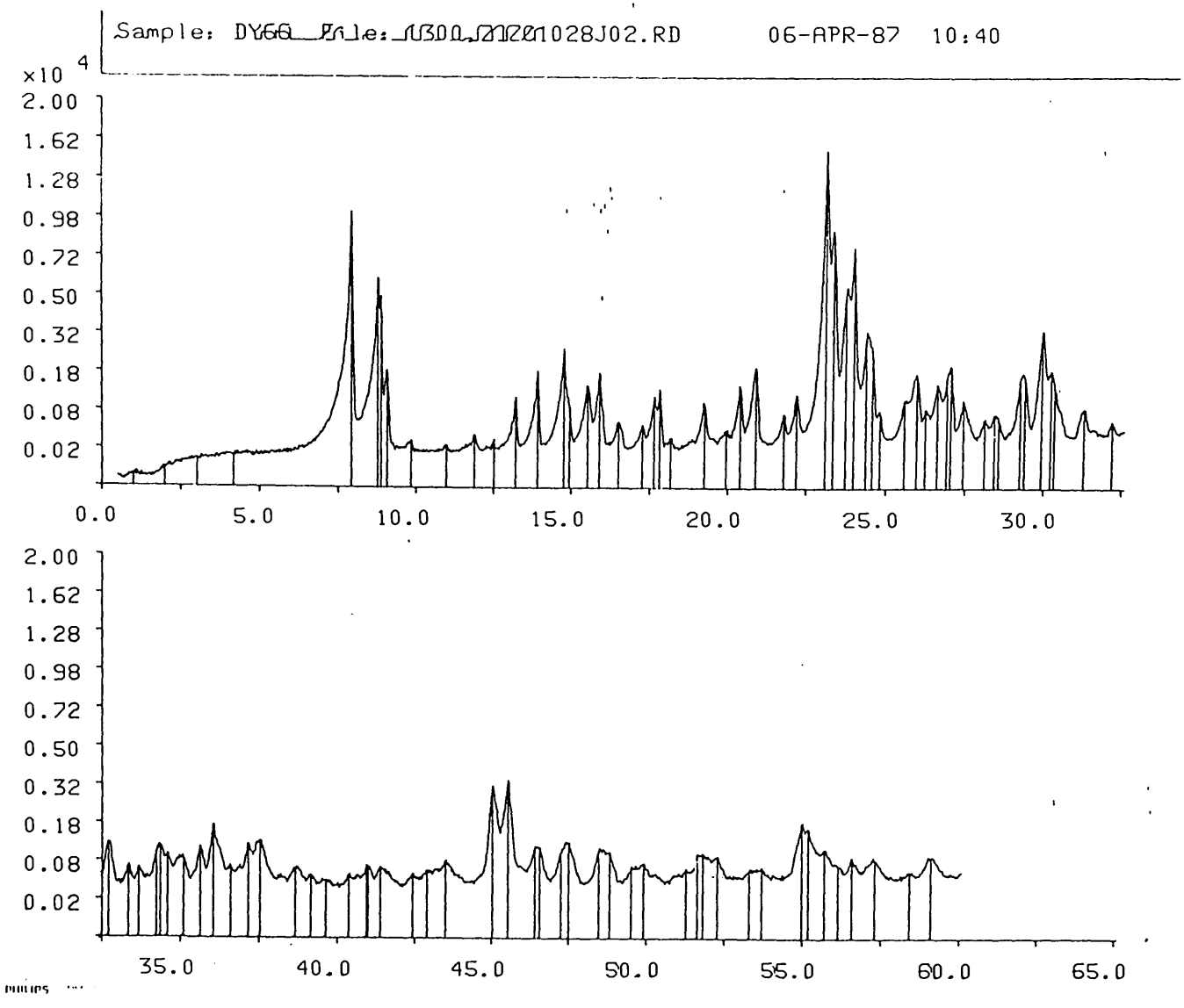

Figure 7.13 XRD pattern for calcined ZSM-5 (E3) treated for 16 hours at 150°C

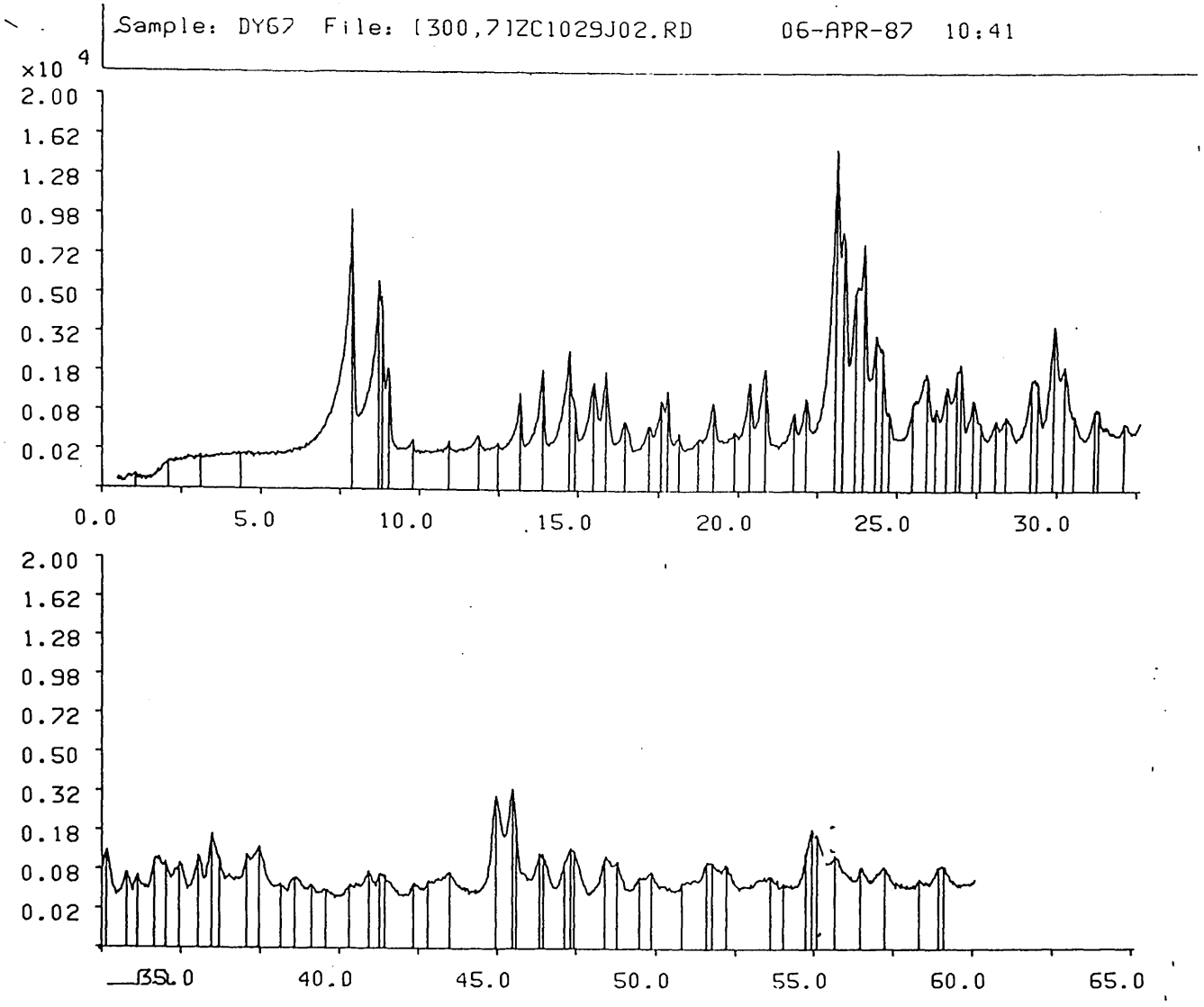

Figure 7.14 XRD pattern for calcined ZSM-5 (E3) treated for 66 hours 28 minutes at 150°C

XPS studies of the surface showed a similar trend. The data are given in Table 7.3. This technique gives an elemental analysis for the first two unit cell thicknesses of the ZSM-5 crystal surfaces. It is immediately apparent that this surface layer is considerably more aluminous than the bulk crystal. Similar accumulation of aluminium in the surface has been observed by other workers (13) and almost certainly arises during the synthesis. It has been suggested (13) that the more aluminous gel particles are the last to depolymerise during the synthesis, and hence the last species to be incorporated into the zeolite crystals.

Table 7.3 Si/Al ratios for the crystal surfaces

of hydrothermally treated H-ZSM-5 (E3).

ZSM-5 Treatment Time (hours:mins)	Si/Al Ratio
0:00	10.2
3:40	14.2
5:10	14.9
16:00	12.7
66:28	14.5

The results in Tables 7.2 and 7.3 are plotted in Figure 7.15, which shows the dealumination of the bulk zeolite and its crystal surface with treatment time. When equilibrium is reached between the solid ZSM-5 and the aqueous silica and alumina species in solution then dissolution of the framework should stop. The greatest loss of aluminium occurred during the first 3 hours of treatment, and it seems likely that equilibrium is reached thereafter.

The only H-ZSM-5 which showed monoclinic unit cell symmetry, Figure 7.12, had the highest bulk Si/Al ratio (84.4). As can be seen from Table 7.2 and Figure 7.15 the Si/Al ratio is quite different to those of the other samples. However it is consistent with the monoclinic symmetry, as the transition occurs more easily for material with a low aluminium content; for example it was readily observed when silicalite was hydrothermally treated at 95°C (section 6.3).

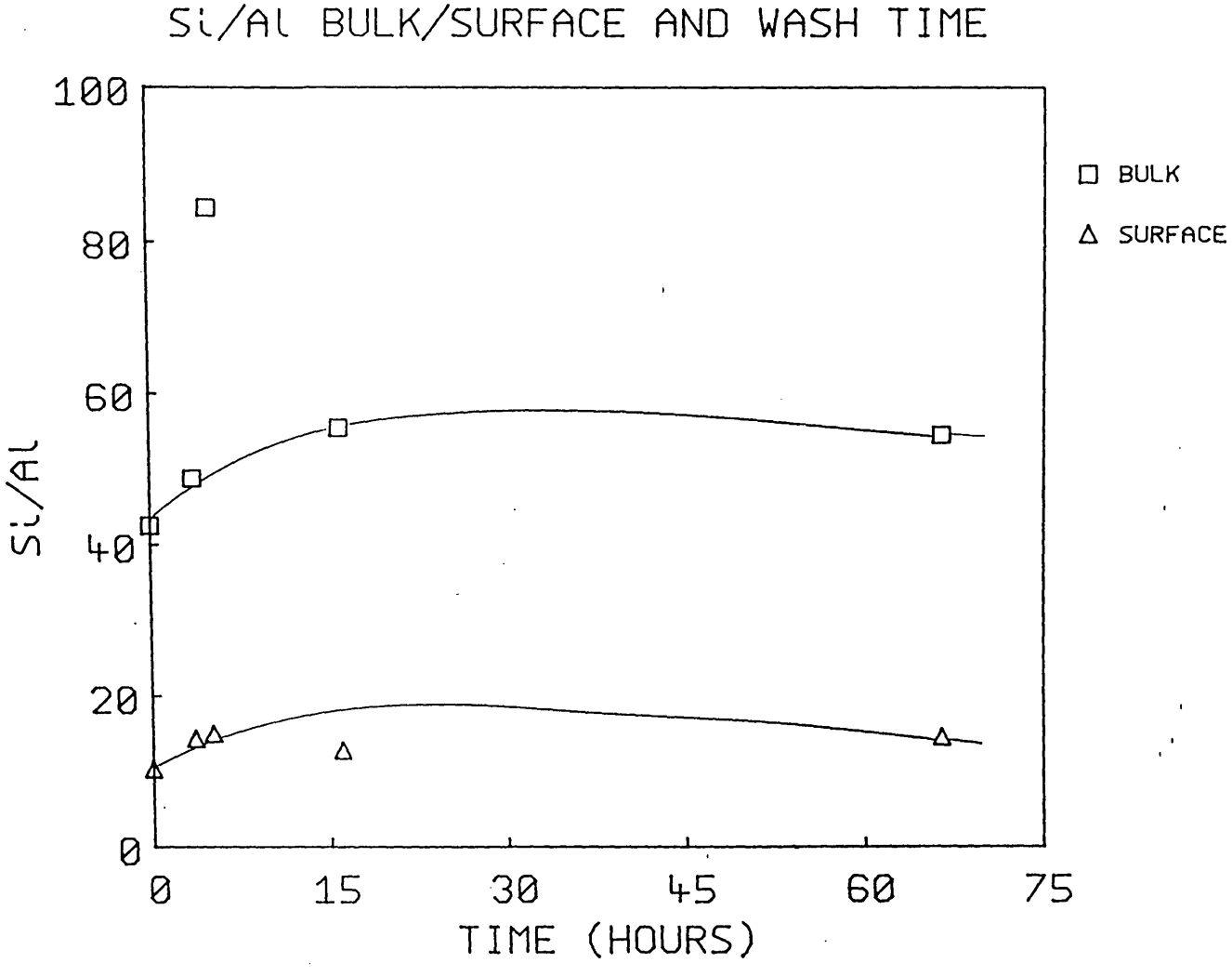

Figure 7.15 Bulk and surface Si/Al ratios for calcined H-ZSM-5 (E3) hydrothermally treated at 150°C for different times

7.3.2.2 Results for H-ZSM-5 (C4)

The hydrothermal treatment of a second sample of H-ZSM-5 was conducted under a different regime. The wash time was restricted to 3 hours (except for one treatment), but the temperatures were varied.

The XRD patterns of the treated materials are shown in Figures 7.16 to 7.20. A portion of the uncalcined sample (C4) was also washed with water at 180°C. XRD traces of the as-made, washed uncalcined and washed calcined materials are in Figures 7.21 to 7.23.

The as-made calcined material, Figure 7.16, was in the expected orthorhombic crystal symmetry. The XRD trace for the material treated at 90°C for 25 hours is shown in Figure 7.17. This had predominantly monoclinic symmetry. The samples of H-ZSM-5 (C4) treated with water for 3 hours at 120 and 150°C were mainly orthorhombic. These results suggest that treatment time had a major influence on the symmetry transition, the longer time favouring the monoclinic form. The H-ZSM-5 washed at 180°C (Figure 7.20) was monoclinic as indicated by the resolution of the 133/313 (hkl) Bragg reflections centred at 24.5 2θ. The uncalcined materials, Figures 7.21 and 7.22, were orthorhombic. The ZSM-5 which was washed prior to calcination (Figure 7.23) was also orthorhombic.

Bulk analysis and XPS results for the treated H-ZSM-5 samples were supplied by ICI Chemicals and Polymers Limited, Si/Al ratios were evaluated from the results. The bulk analysis data are in Table 7.4.

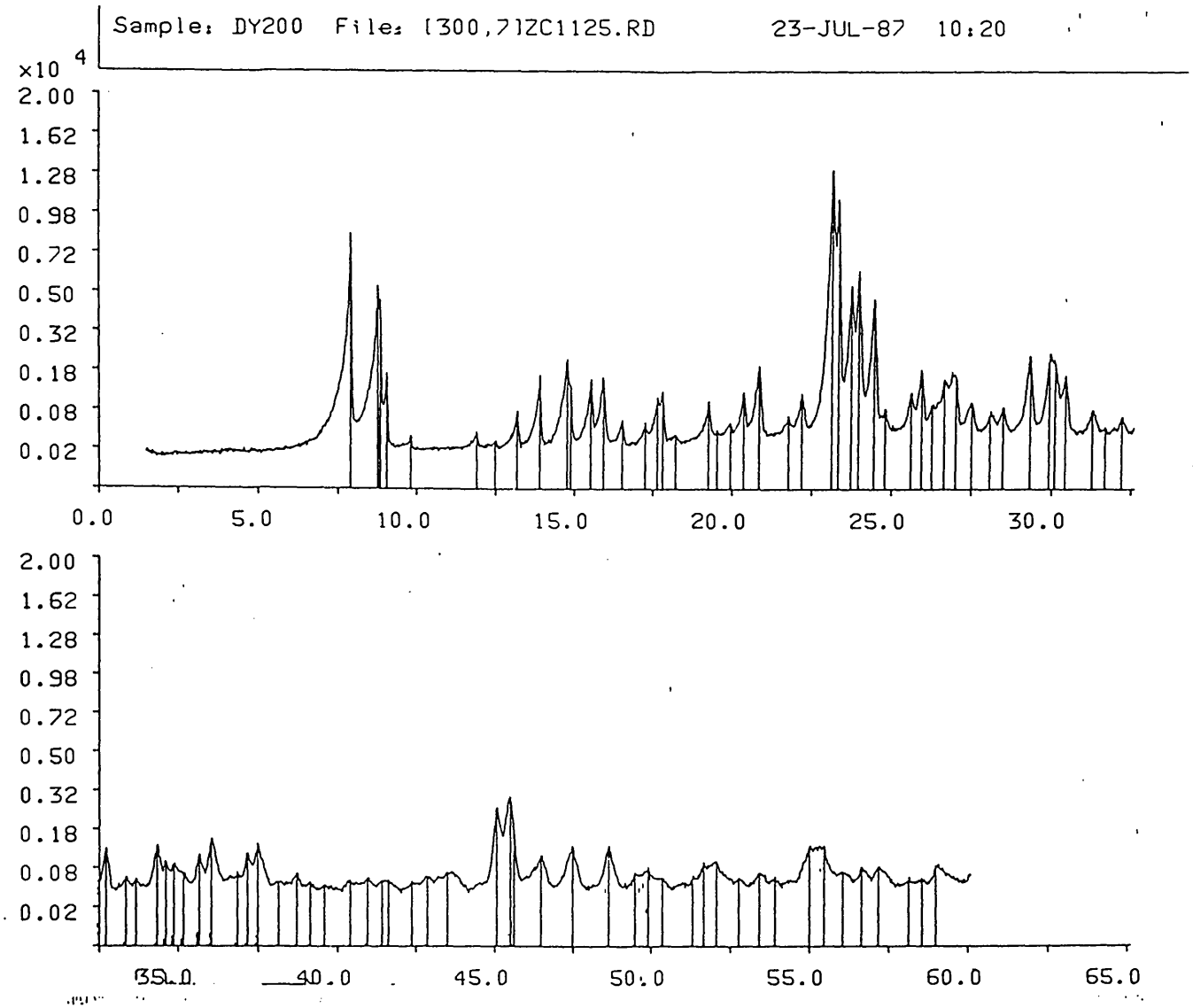

Figure 7.16 XRD pattern for 'as made' calcined H-ZSM-5 (C4)

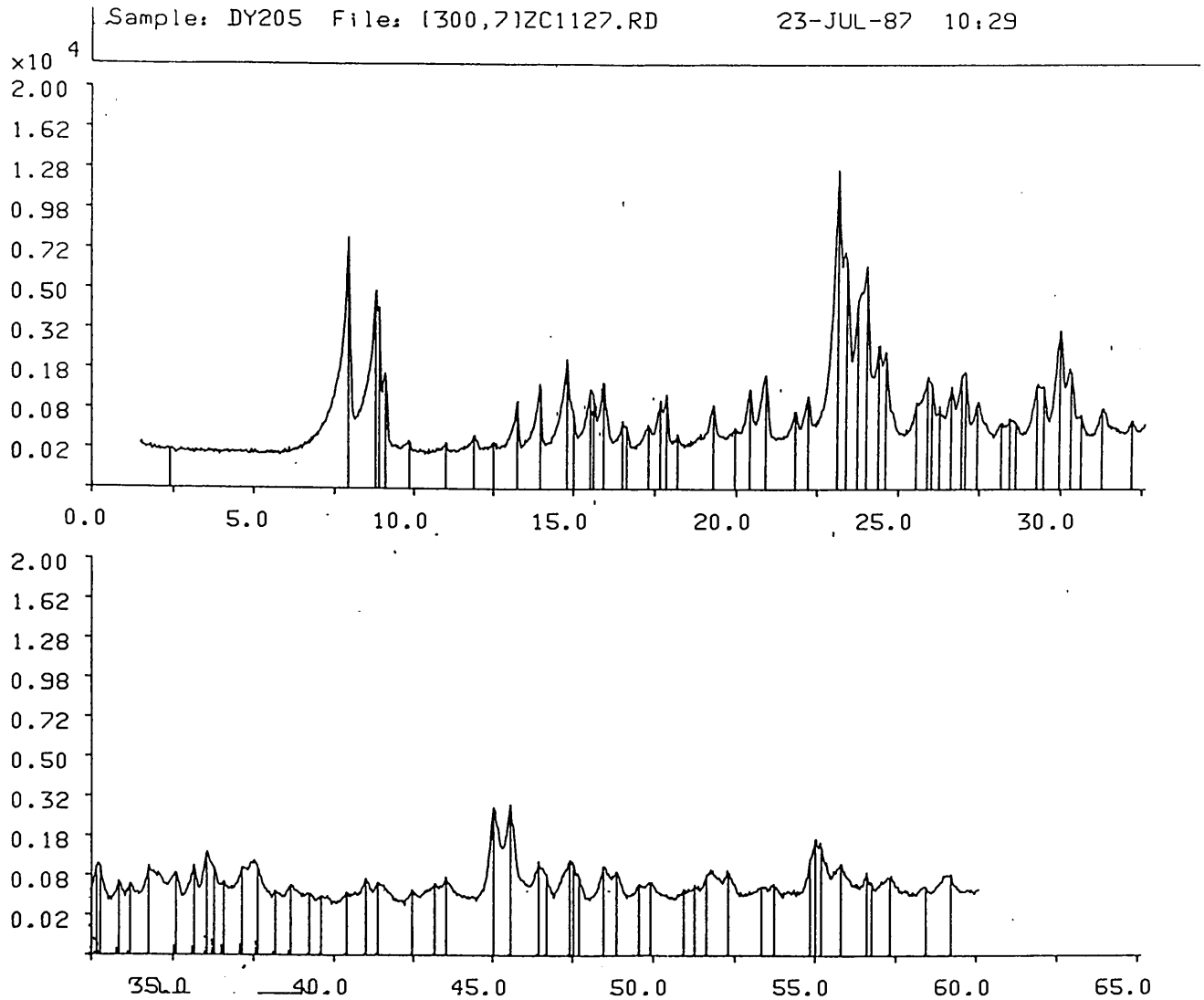

Figure 7.17 XRD pattern for H-ZSM-5 (C4) treated at 90°C for 25 hours

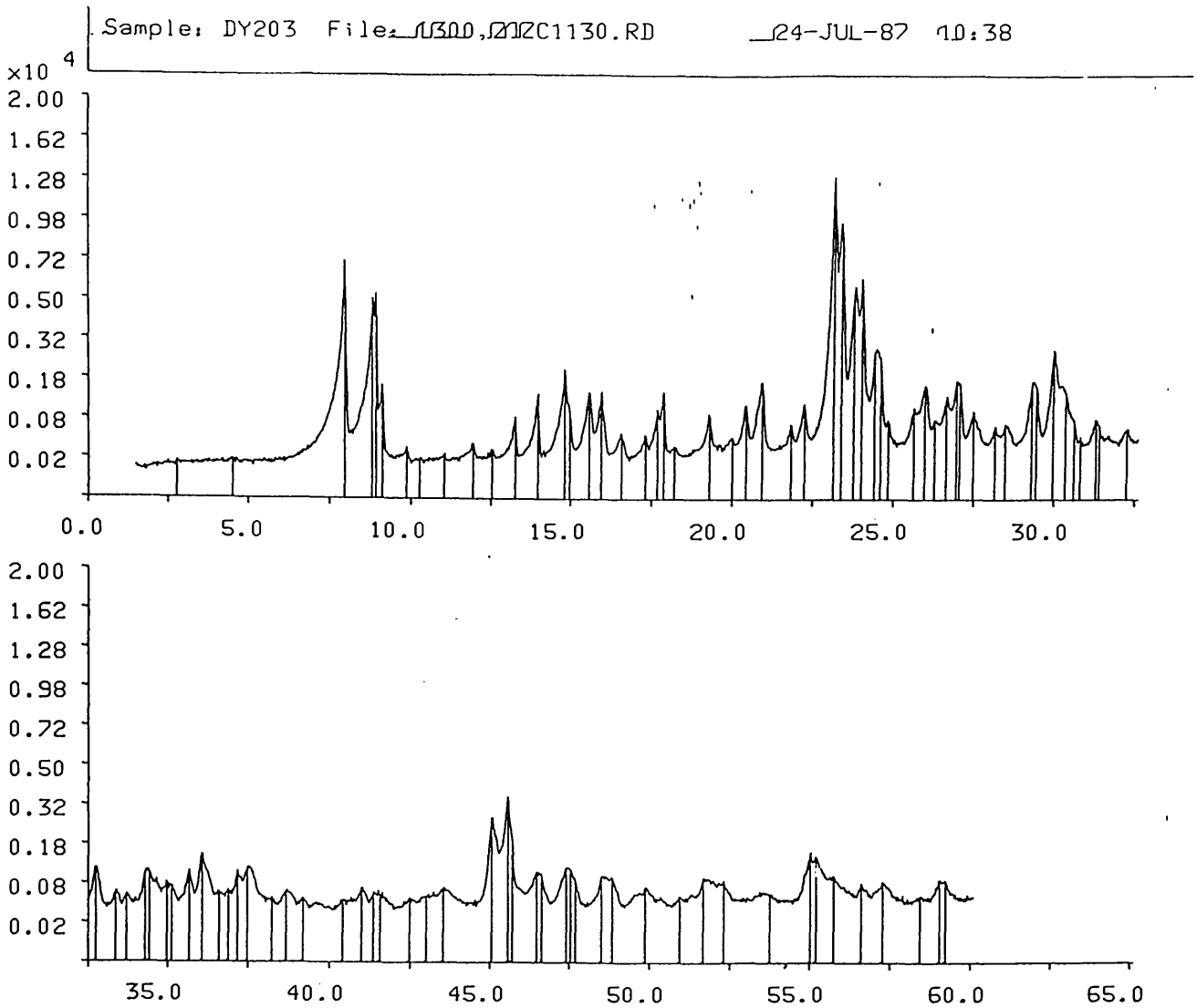

Figure 7.18 XRD pattern for H-ZSM-5 (C4) treated at 120°C for 3 hours

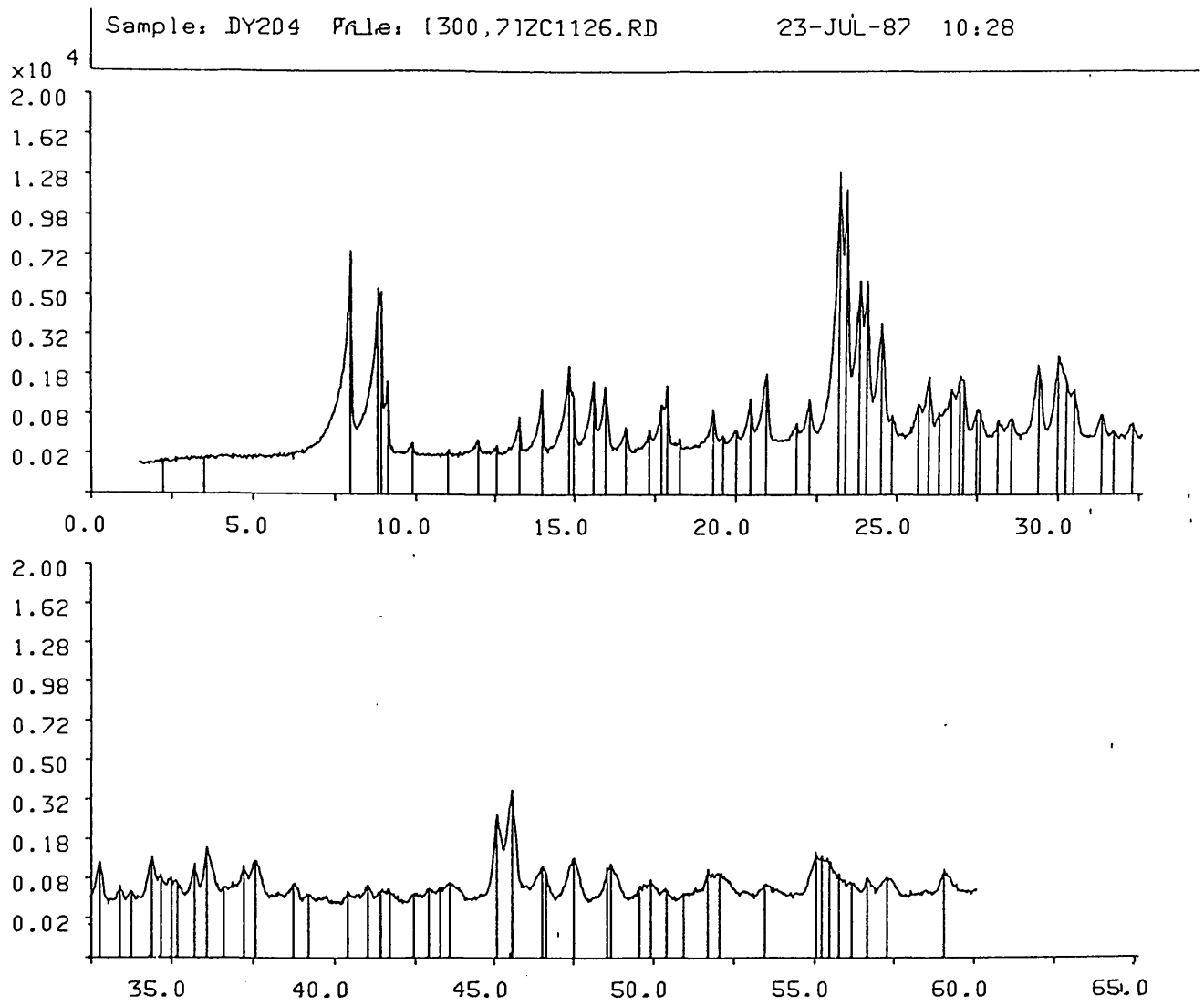

Figure 7.19 XRD pattern for H-ZSM-5 (C4) treated at 150°C for 3 hours

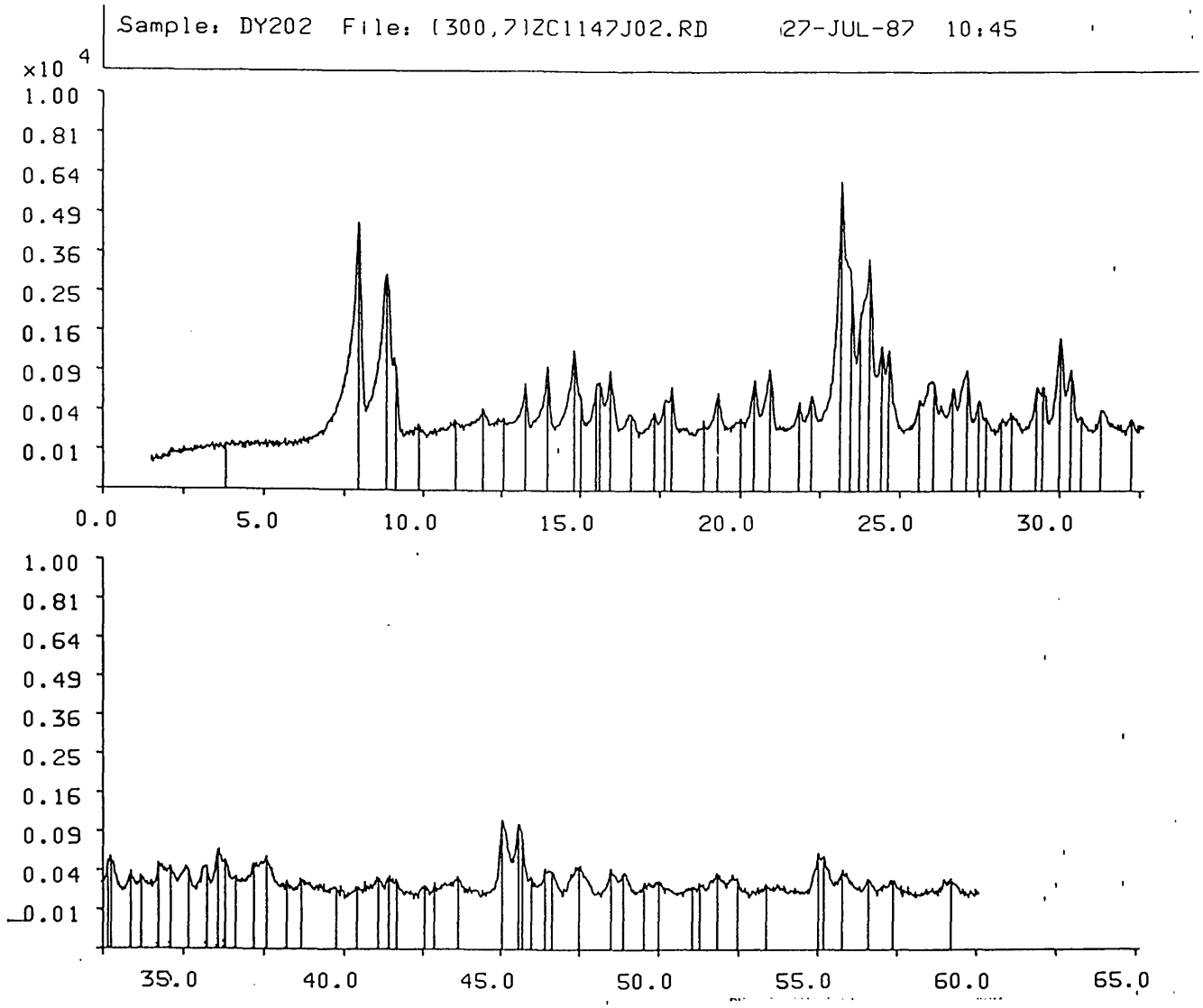

Figure 7.20 XRD pattern for H-ZSM-5 (C4) treated at 180°C for 3 hours

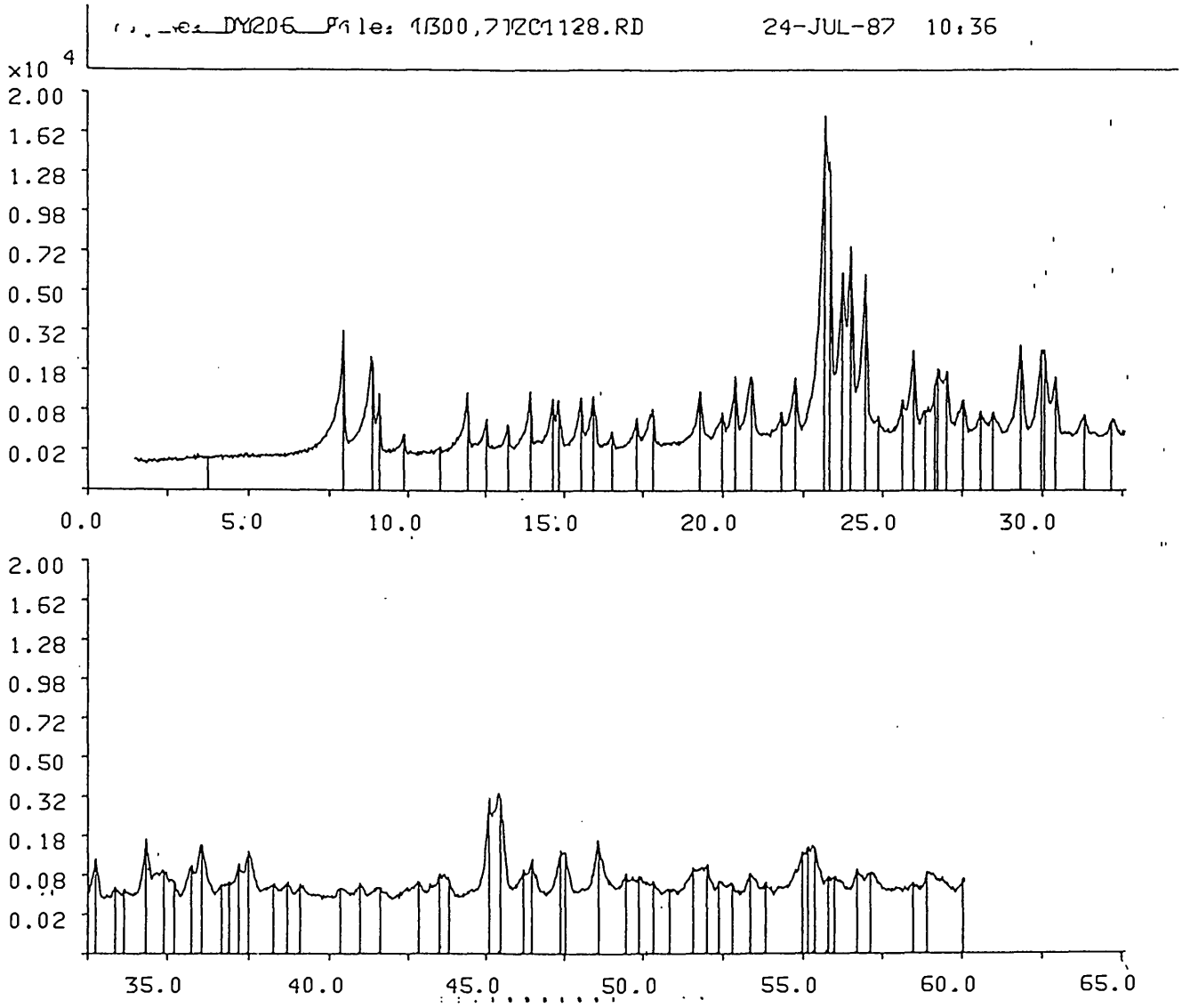

Figure 7.21 XRD pattern for untreated uncalcined TPA-ZSM-5 (C4)

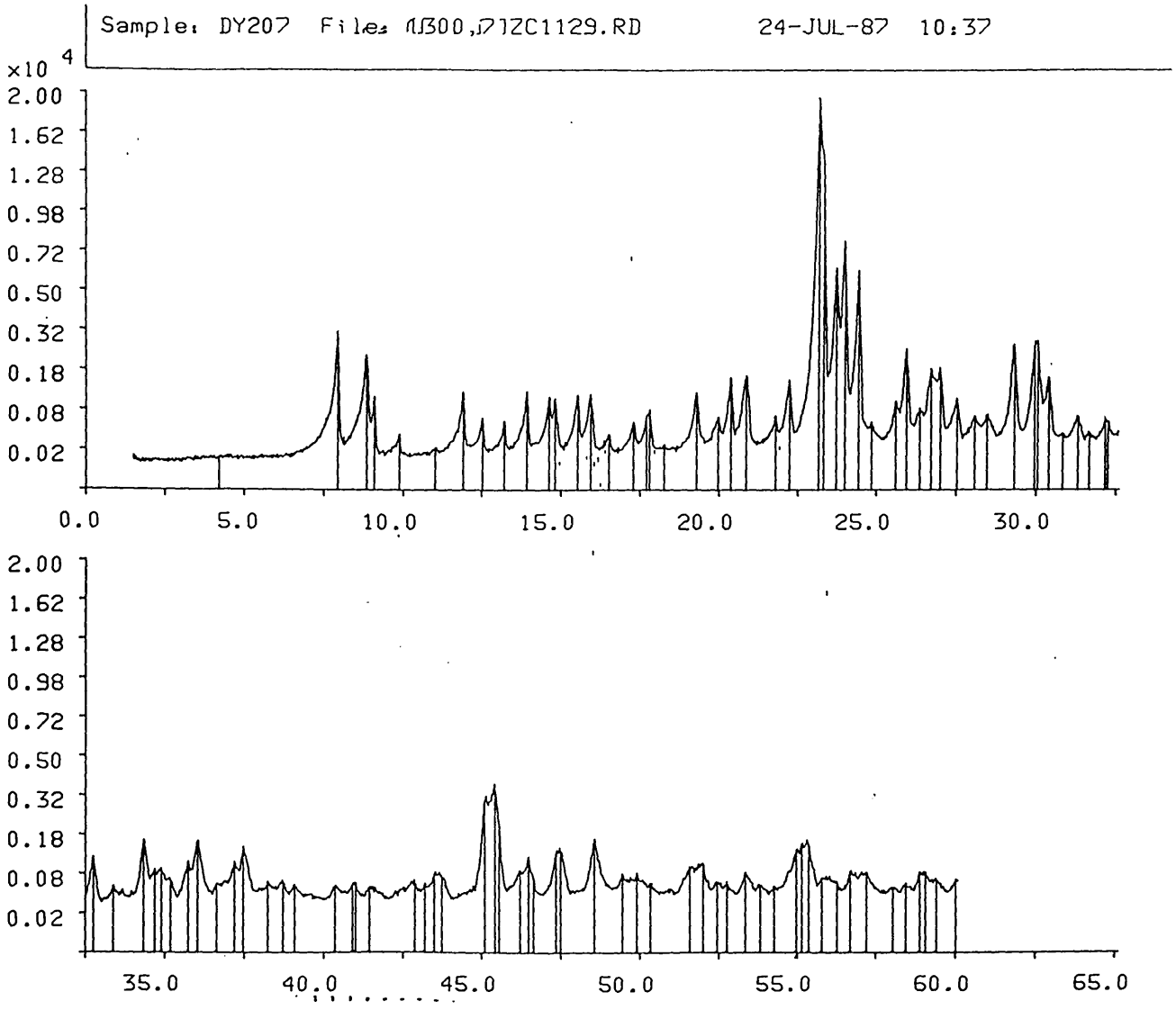

Figure 7.22 XRD pattern for uncalcined TPA-ZSM-5 (C4) treated at 180°C for **15** hours

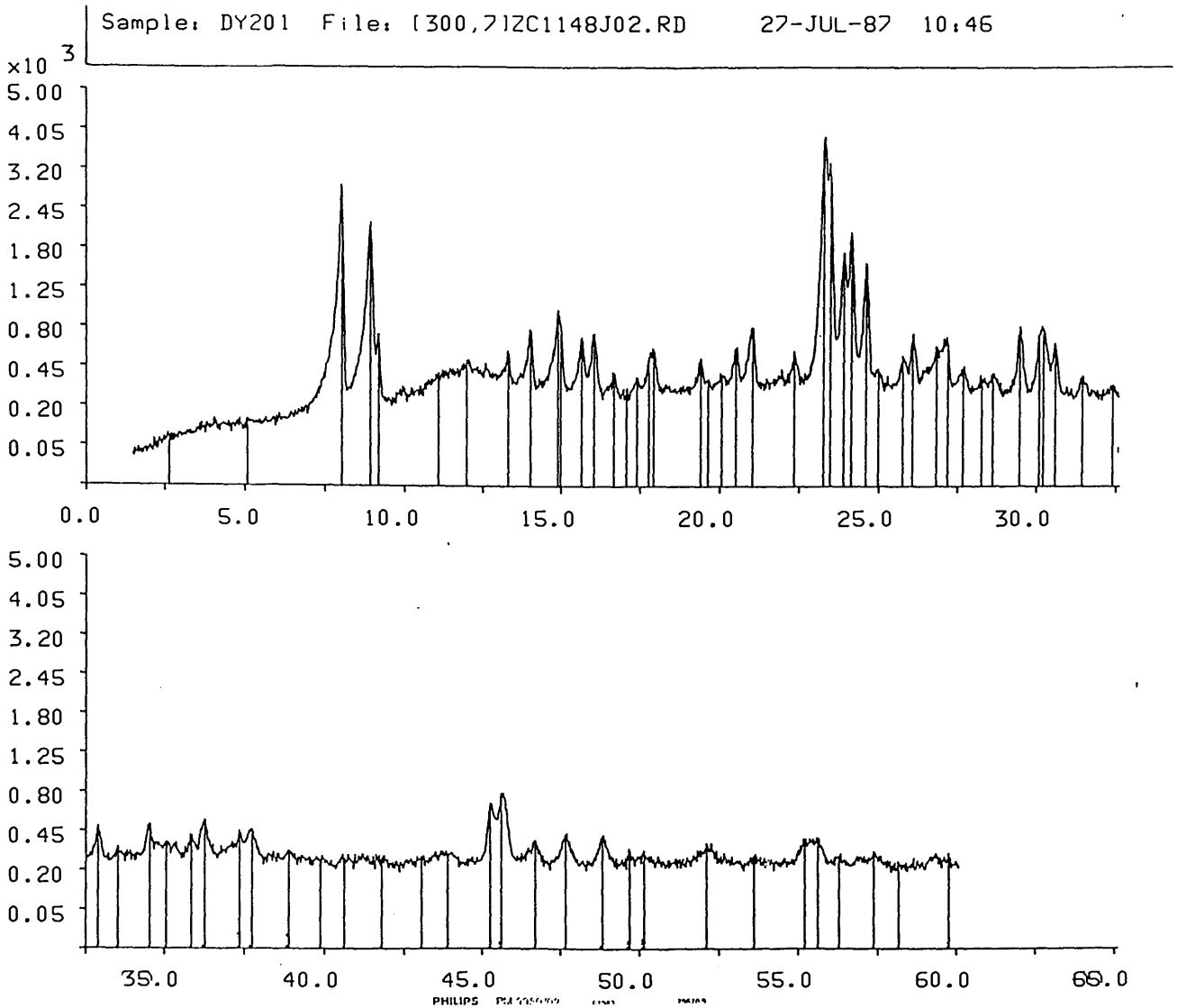

Figure 7.23 XRD pattern for H-ZSM-5 (C4) treated at 180°C for 15 hours before calcination

Table 7.4 Si/Al ratios for H-ZSM-5 (C4) hydrothermally treated at different temperatures.

ZSM-5 Hydrothermal Treatment T (°C) and time (hours)	Si/Al Ratio	Crystal Symmetry
25	29.5	Orthorhombic
90 (25h)	26.7	Monoclinic
120 (3h)	25.4	Orthorhombic
150 (3h)	25.0	Orthorhombic
180 (3h)	25.1	Monoclinic

The material treated at 25°C (Table 7.4 and Figure 7.24) is the 'as made' calcined material which was simply washed on the Buchner funnel in the usual manner.

The Si/Al ratios of the treated H-ZSM-5 samples decreased with hydrothermal treatment temperature, from a maximum of 29.5 to a minimum of about 25. The samples became more aluminous as the wash temperatures increased; this shows that in this case silica was selectively dissolved from the framework. The initial rapid removal of silica was probably due to the preferential dissolution of amorphous impurities. The XRD background of the initial H-ZSM-5 was 282 counts and that of the material treated at 150°C was 161 counts. This confirms that amorphous aluminosilicate was removed. This is also supported by SEM results (see Plate 7.1) and is discussed later. It is noteworthy that short treatment times or low treatment temperature decrease the bulk Si/Al ratio, whereas prolonged treatments at 150°C (Table 7.2) increase the Si/Al ratio. This suggests that in the early stages silica species dissolve in preference to aluminous ones, but that with time aluminium species dissolve until equilibrium is reached. However, it should be noted that Tables 7.2 and 7.4 refer to different samples of H-ZSM-5 and this rather than relative dissolution rates could be the origin of the contrasting behaviour.

XPS (X-ray photoelectron spectroscopy) analytical data were also supplied by ICI Chemicals and Polymers Limited for this series of materials. The calculated Si/Al ratios are given in Table 7.5.

Table 7.5 XPS Si/Al ratios for

samples of H-ZSM-5 (C4).

ZSM-5 Hydrothermal Treatment T (°C) and time (hours)	Si/Al Ratio
25	6.1
90 (25h)	4.9
120 (3h)	4.0
150 (3h)	4.7

There was insufficient of the H-ZSM-5 sample treated at 180°C for XPS analysis. The data in Tables 7.4 and 7.5 are plotted, see Figure 7.24. The XPS data follow the same trend as the bulk analysis results, the Si/Al ratios at the H-ZSM-5 crystal surfaces decrease as the hydrothermal treatment temperature is increased. This is opposite to the behaviour observed in the time study (section 7.3.2.1), in which the H-ZSM-5 samples became increasing dealuminated with treatment time. This suggests that in the temperature study insufficient time was allowed for the dissolution equilibrium between the solid and liquid phase to be established, and that silica appeared to dissolve from the H-ZSM-5 samples first. However it should be noted that the time and temperature studies were carried out with different samples of H-ZSM-5. The time study used preparation E3 which had an initial Si/Al ratio of 42.5 and the temperature study used C4 which had an initial Si/Al ratio of 29.5. Furthermore, E3 was prepared with aluminium nitrate and C4 with aluminium sulphate and it is possible that this may have caused the incorporation of aluminium into the zeolite framework to occur in different ways.

Plate 7.1 shows scanning electron micrograph (SEM) prints of four samples of H-ZSM-5 (C4), identified in Table 7.6.

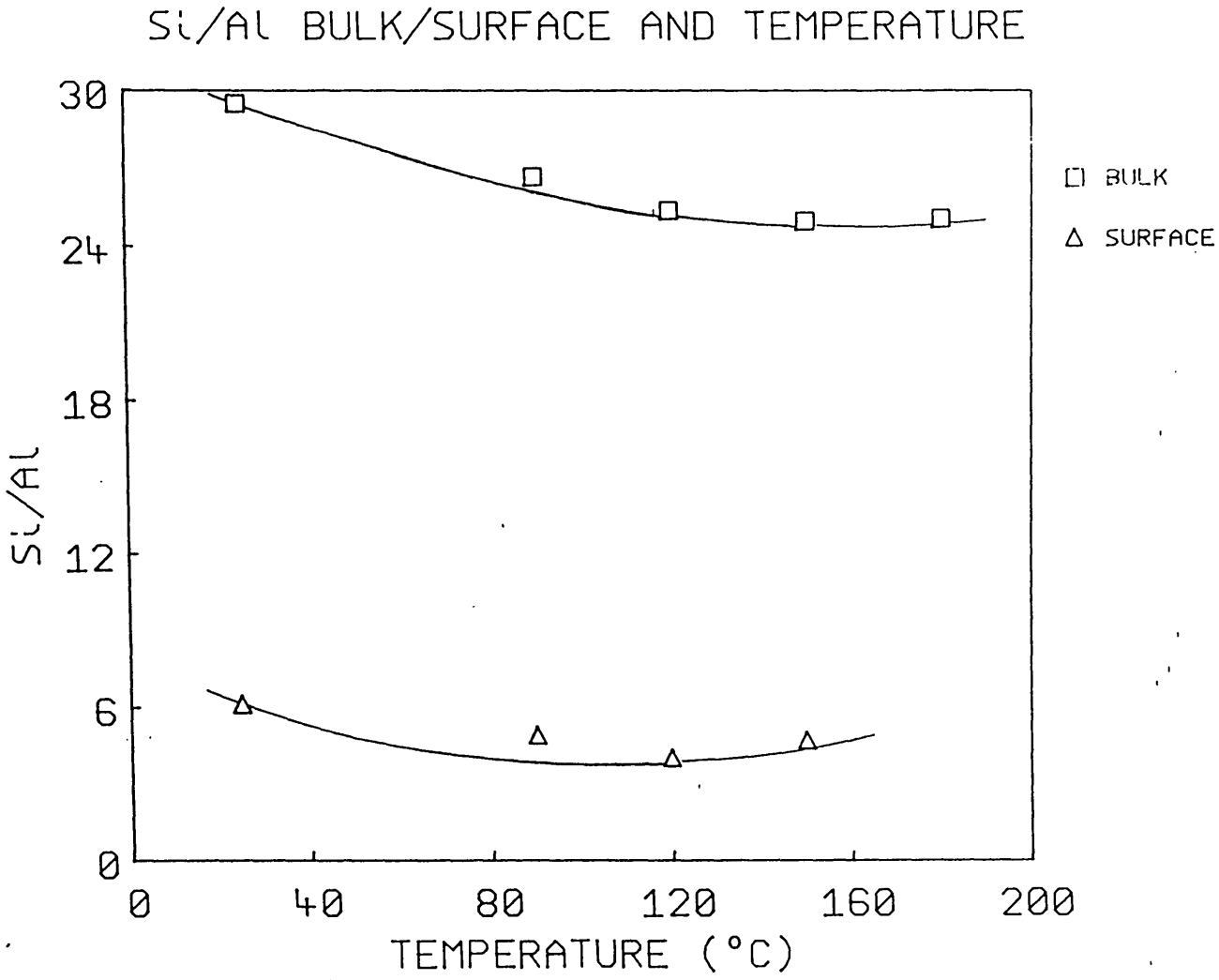

Figure 7.24 Dependence of Si/Al ratios on treatment temperature

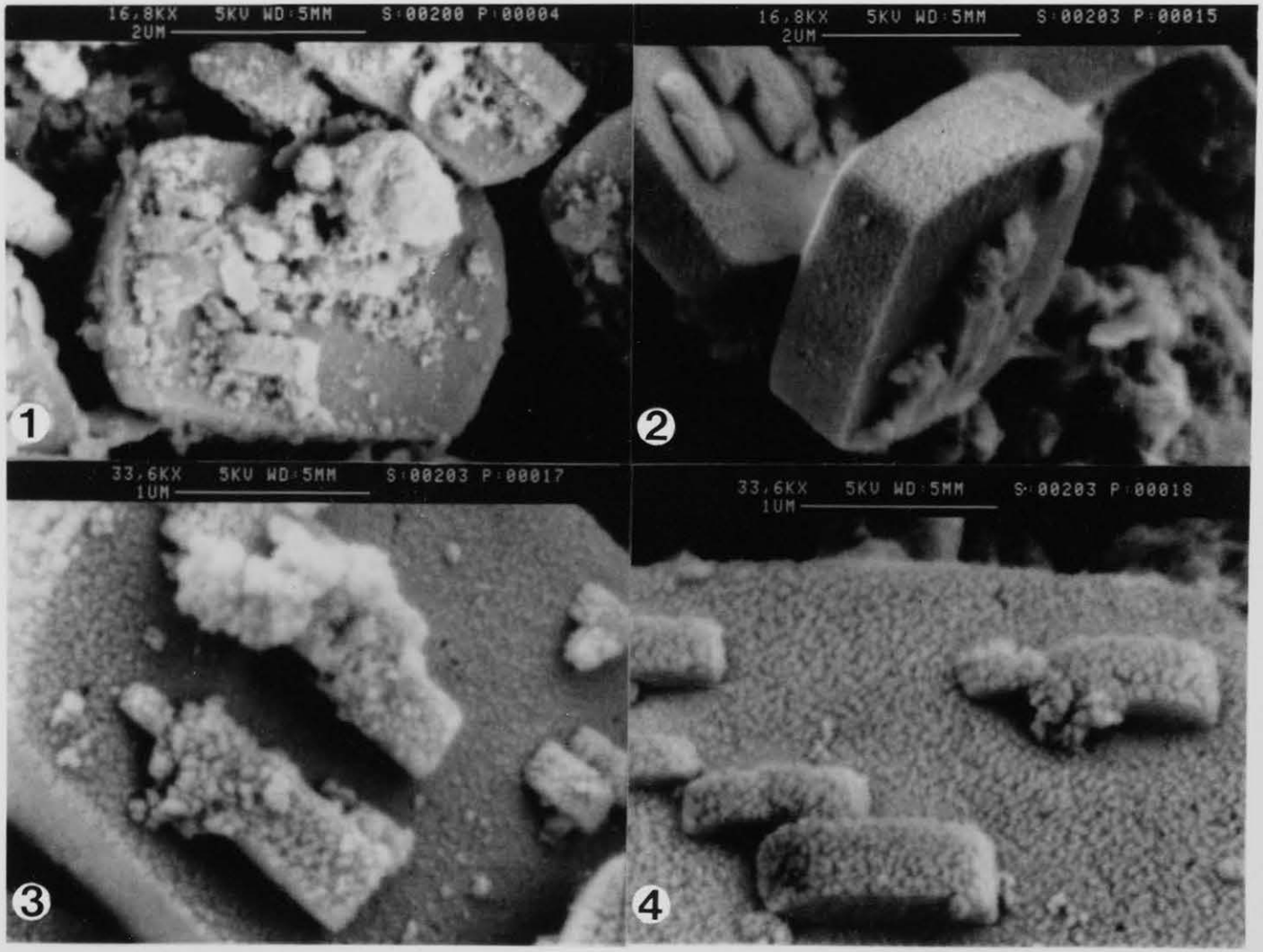
16,8KX 5KV WD:5MM S:00200 P:00004
2UM
1
16,8KX 5KV WD:5MM S:00203 P:00015
2UM
2
33,6KX 5KV WD:5MM S:00203 P:00017
1UM
3
33,6KX 5KV WD:5MM S:00203 P:00018
1UM
4

PLATE 7.1

Table 7.6 SEM of hydrothermally treated H-ZSM-5 (C4).

ZSM-5 Sample	Print Number
UW,C,UW	1
UW,C,W<120°C, 3h>	2
UW,C,W<150°C, 3h>	3
UW,C,W<180°C, 3h>	4

ZSM-5 sample codes are defined in section 6.3.3. Print 1 is for the untreated initial material, there is clear evidence of amorphous impurities on the crystal surfaces. This is easily removed by low temperature hydrothermal treatment (Print 2). Prints 3 and 4 show the granularity of the crystal surfaces after hydrothermal treatment at 150 and 180°C. This effect was not observed with silicalite (section 6.3.4) and hence is likely to be related to the presence of aluminium. A granular effect may result from the gold sputter coating of samples, however the magnification was not sufficiently high for this to be observed. As the hydrothermal treatment temperature is increased the crystal surfaces became more aluminous and their granularity also increases. The most probable explanation is that areas of the surface which are silica rich may dissolve selectively. The solubility studies described in Chapter 5.0 showed that the presence of aluminium in ZSM-5 suppressed its solubility relative to silicalite. Only if the hydrothermal treatment times were prolonged was dealumination of the surface and bulk of the crystals observed.

The thermal gravimetry traces of the water uptakes of the initial H-ZSM-5 (C4) and its daughter materials treated at 150°C and 180°C are shown in Figure 7.25. The materials each displayed a major weight loss up to 130°C, which corresponds to the loss of loosely bound water. A second weight loss was observed in the TG trace of the H-ZSM-5 hydrothermally treated at 150°C. This occurred at about 450°C; the inflection is arrowed in Figure 7.25. This weight loss is probably associated with the removal of hydroxyl groups. These are likely to be those associated with the catalytically active Bronsted sites (17).

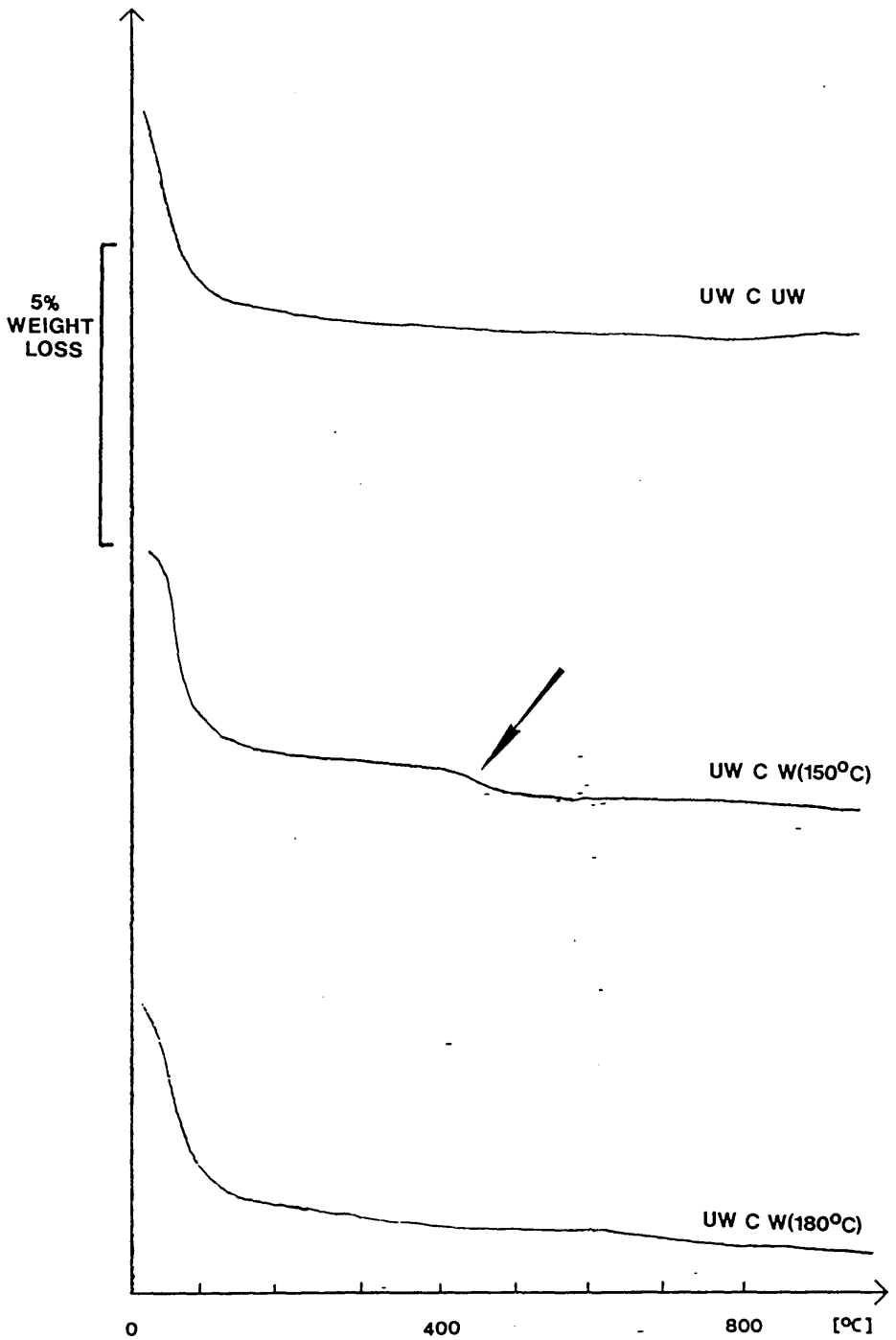

Figure 7.25 TG traces for treated H-ZSM-5 (C4) samples

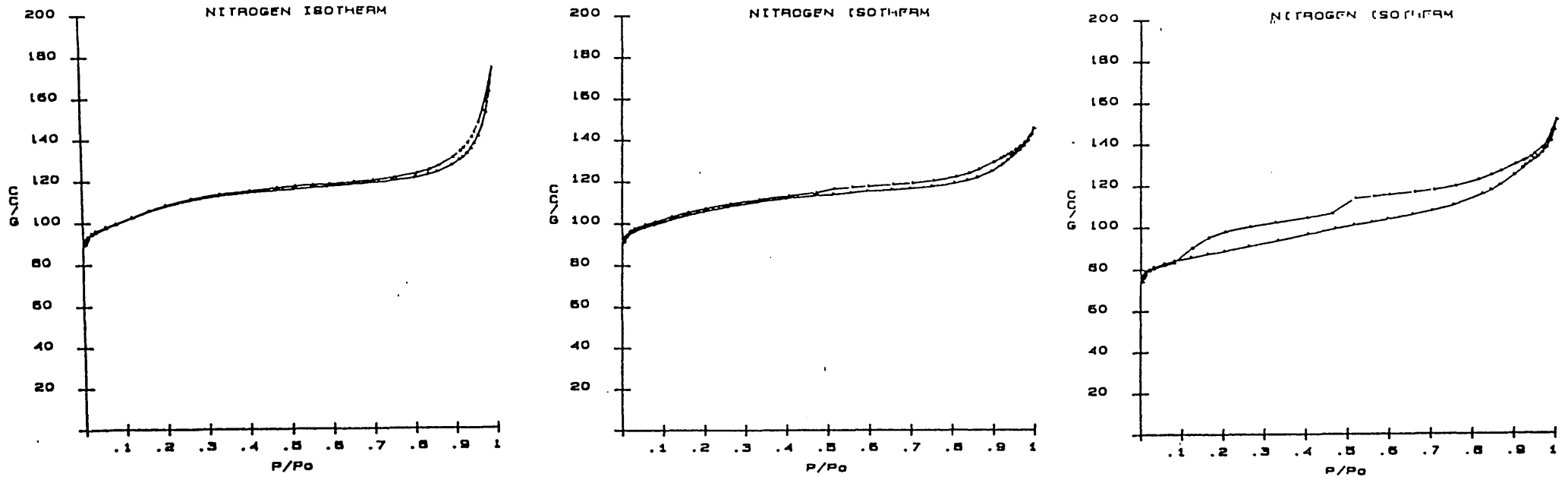

Figure 7.26 Nitrogen sorption isotherms for H-ZSM-5 (C4) samples

Figure 7.26 shows nitrogen sorption isotherms obtained for samples ZSM-5 (C4) treated in different ways. These isotherms were obtained by the micromeritics group at ICI Chemical and Polymers Limited at Runcorn. The exact interpretation of the isotherms must be somewhat speculative, however differences between the isotherms are quite marked and must arise purely from the hydrothermal treatment. The isotherm denoted as A in Figure 7.26 is for a sample of ZSM-5 (C4) which has been calcined but not hydrothermally treated; there is minimal hysteresis, but marked capillary condensation as P/P_o tends to 1. This may be related to small quantities of amorphous material on the zeolite surface (see SEM, Plate 7.1 Print 1). Figure 7.26 B shows the isotherm for a sample of ZSM-5 (C4) which was hydrothermally treated (for 15 hours at 180°C) before calcination. It appears that this has reduced the extent of capillary condensation, possibly because the amorphous material has been removed, and slightly increased the amount of hysteresis. This may indicate that the hydrothermal treatment has had some effect on the zeolite crystals (Plate 4.1). Figure 7.26 C shows the isotherm for ZSM-5 (C4) which was hydrothermally treated (for 3 hours at 180°C) after calcination. It is clear that this hydrothermal treatment has had a marked effect on the shape of the isotherm and on the extent of the hysteresis. The latter indicates that there has been a pronounced increase in the mesopore capacity of the zeolite. Comparison with the other isotherms shows that the micropore volume is much reduced. (Mathematical analysis of the curves by experts in ICI gave a micropore volume of $0.166 cm^3 g^{-1}$ for the untreated material and 0.163 and $0.108 cm^3 g^{-1}$ for the treated ones.)

Thus it appears that hydrothermal treatment after calcination has a marked effect on the pore structure, increasing the mesopore capacity and reducing the micropore volume. This is consistent with internal dissolution of the zeolite crystals (see Chapter 6). The scanning electron micrographs of the hydrothermally treated calcined materials (Plate 7.1) do not show evidence of internal dissolution but the surfaces of the crystals are pitted. This is in marked contrast to the other two materials which have smooth crystal surfaces, and provides further evidence that calcined materials are

much more soluble than their precursors.

7.3.3 Catalytic Isomerism of But-1-ene

But-1-ene isomerism has been used as a test reaction for oxide catalysts (27). The reaction is normally first order in but-1-ene and gives a mixture of cis-but-2-ene and trans-but-2-ene. The cis-/trans- product ratios give information on the reaction mechanism. An initial cis-/trans- ratio of less than one is indicative of an acid catalysed mechanism (28). Such a reaction mechanism involves the secondary butyl carbenium ion, Figure 7.27. The C_1, C_2 and C_3 atoms all lie in the one plane, which is presumed parallel to the catalyst surface, but rotation about the C_2-C_3 bond is inhibited by steric interaction between the methyl group and the surface whereas rotation about the C_1-C_2 bond may occur more readily. The secondary butyl carbenium ion is formed by the addition of a proton to the C_1 of but-1-ene. Loss of either hydrogen on C_3 subsequently gives but-2-ene. Loss of H_a tends to cause the formation of cis-but-2-ene and loss of H_b tends to lead to the formation of the trans- isomer. Cis-/trans- ratios close to unity are often observed for acid catalysts, this is perhaps not surprising as the two C_3-H bonds are energetically near identical.

For ZSM-5, initial cis-/trans- ratios of about 0.7 are usually observed (29), ratios tend to rise to about unity as the isomerism progresses. Catalysts gradually become poisoned as reaction time increases. This is believed to be due to preferential adsorption of but-2-ene and its subsequent polymerisation to give organic species which are unable to leave the ZSM-5 channel system. Further decomposition gives carbon rich material referred to as coke. These residues may themselves be catalytically active. When active catalysts are used for a prolonged time thermodynamic equilibrium is established between the reactants and the products. At 125°C the equilibrium cis-/trans- ratio is 0.45, and the amount of but-1-ene at equilibrium is 7.95%.

The materials were dried at 110°C for 2 hours then pelletted and crushed to 40-60 mesh (275-400um). The small pellets were heated at

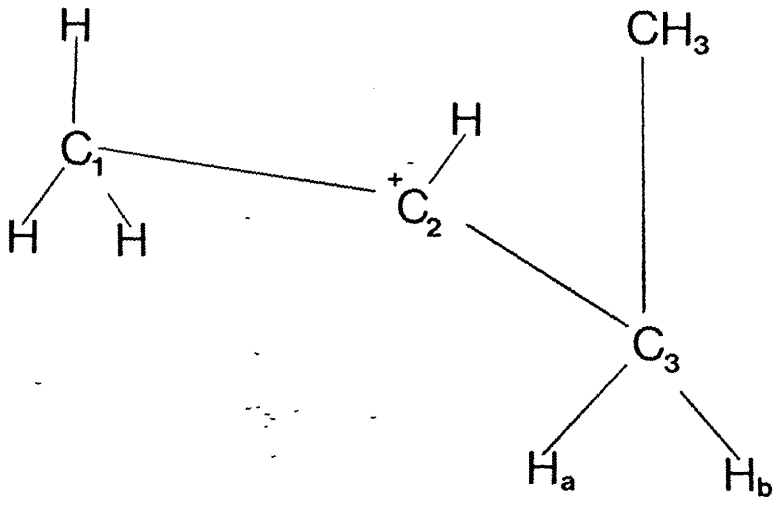

Figure 7.27 Butene carbenium ion

400°C overnight in air then at 450°C for 1 hour under vacuum. The catalytic isomerism of but-1-ene over the treated ZSM-5 catalysts was then studied at 125°C. Each catalytic run lasted for 3 hours. The details of the catalytic rig are in Chapter 2.

The H-ZSM-5 was ideal for the study. It did not require acid-exchange to remove alkali metal cations (such procedures, commonly used in catalyst preparation, are themselves hydrothermal treatments and may affect the catalyst in other ways, for example selective dissolution besides ion-exchange).

The aim of the catalytic investigation was to detect changes in H-ZSM-5 activity or selectivity consequent on the hydrothermal treatment.

The plots showing the % composition of the isomer mixture with time are presented in Figures 7.28 to 7.34. Further catalytic data are given in Tables 7.7 to 7.9. In these each catalyst is described by the abbreviations used throughout this thesis, namely C=calcined and W=hydrothermally treated (washed). The treatment temperature and duration is given in brackets after each W. Calcinations were performed at 550°C for 16 hours then at 800°C for 1 hour.

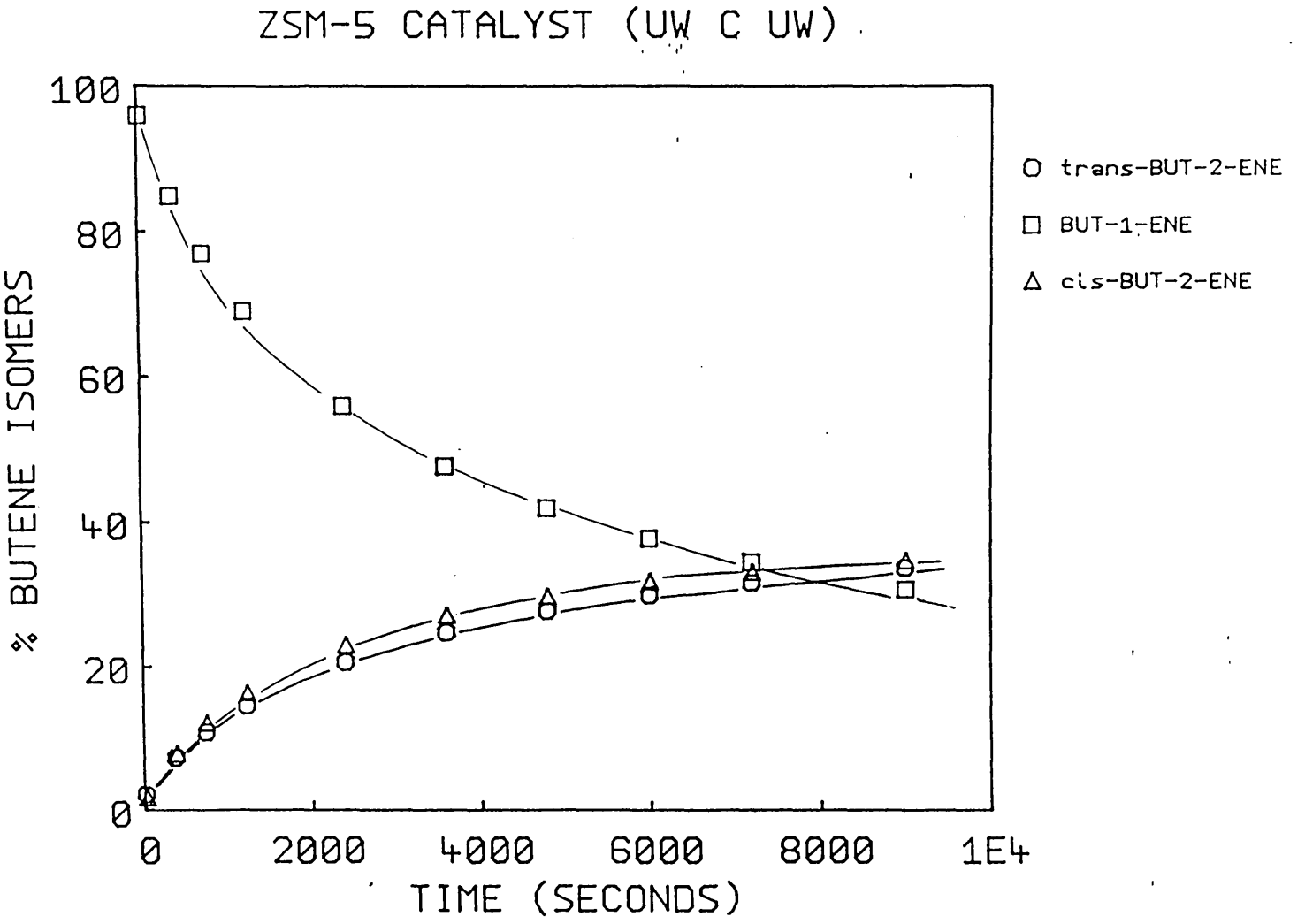

Figure 7.28 Isomerisation results obtained with H-ZSM-5 (C4), (UW C UW)

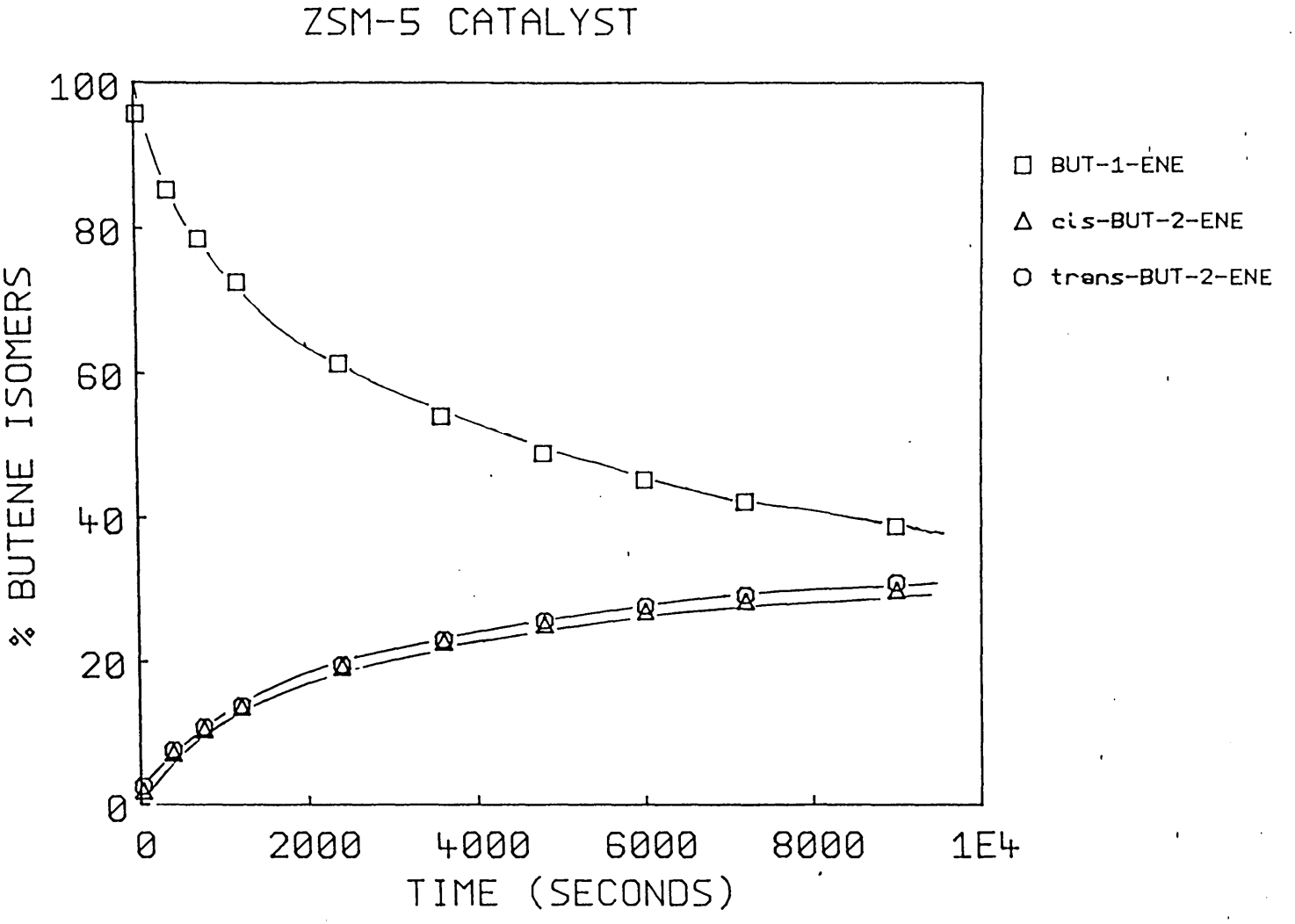

Figure 7.29 Isomerisation results obtained with H-ZSM-5 (C4), (UW C W<120°C>)

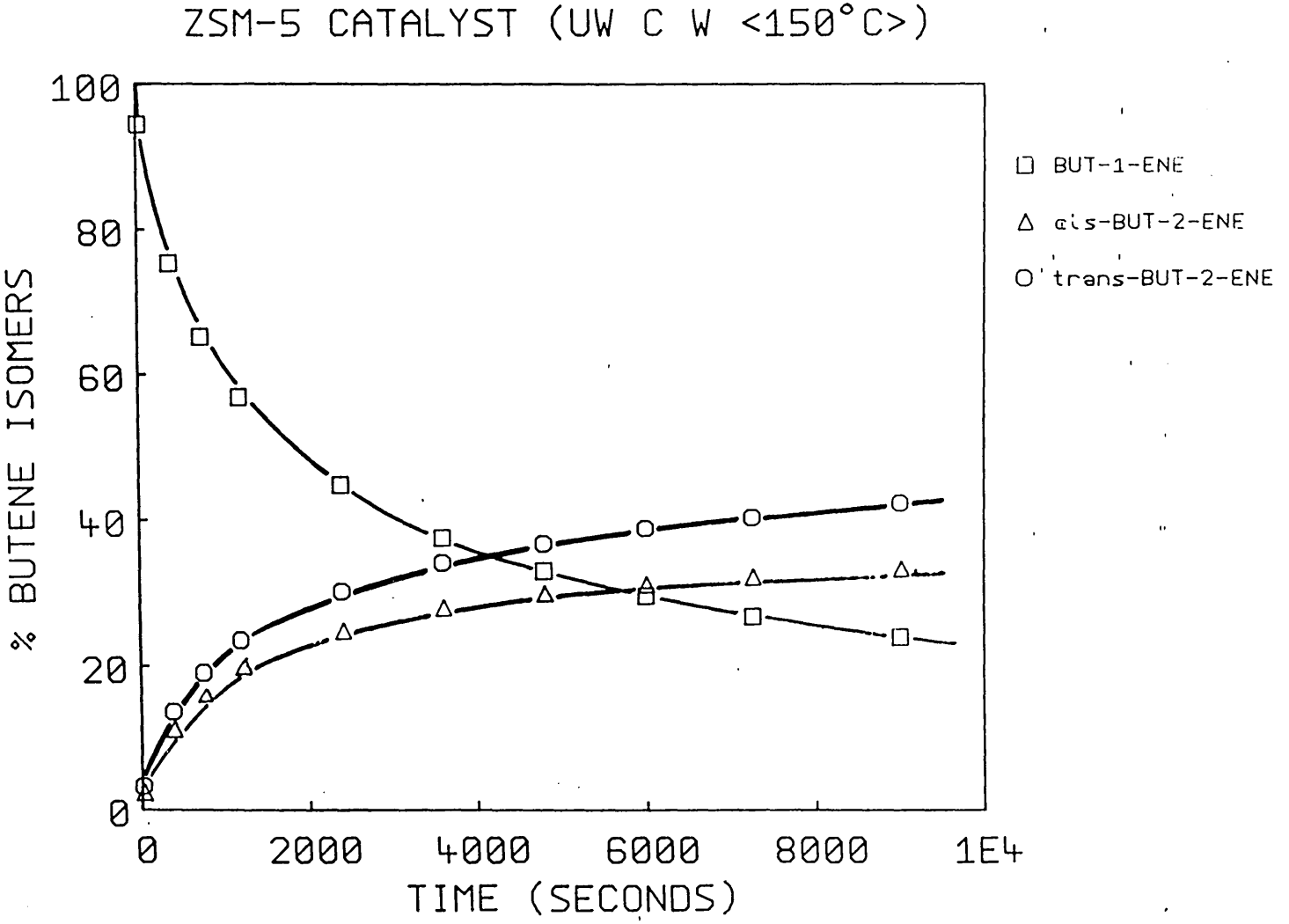

Figure 7.30 Isomerisation results obtained with H-ZSM-5 (C4), (UW C W<150°C>)

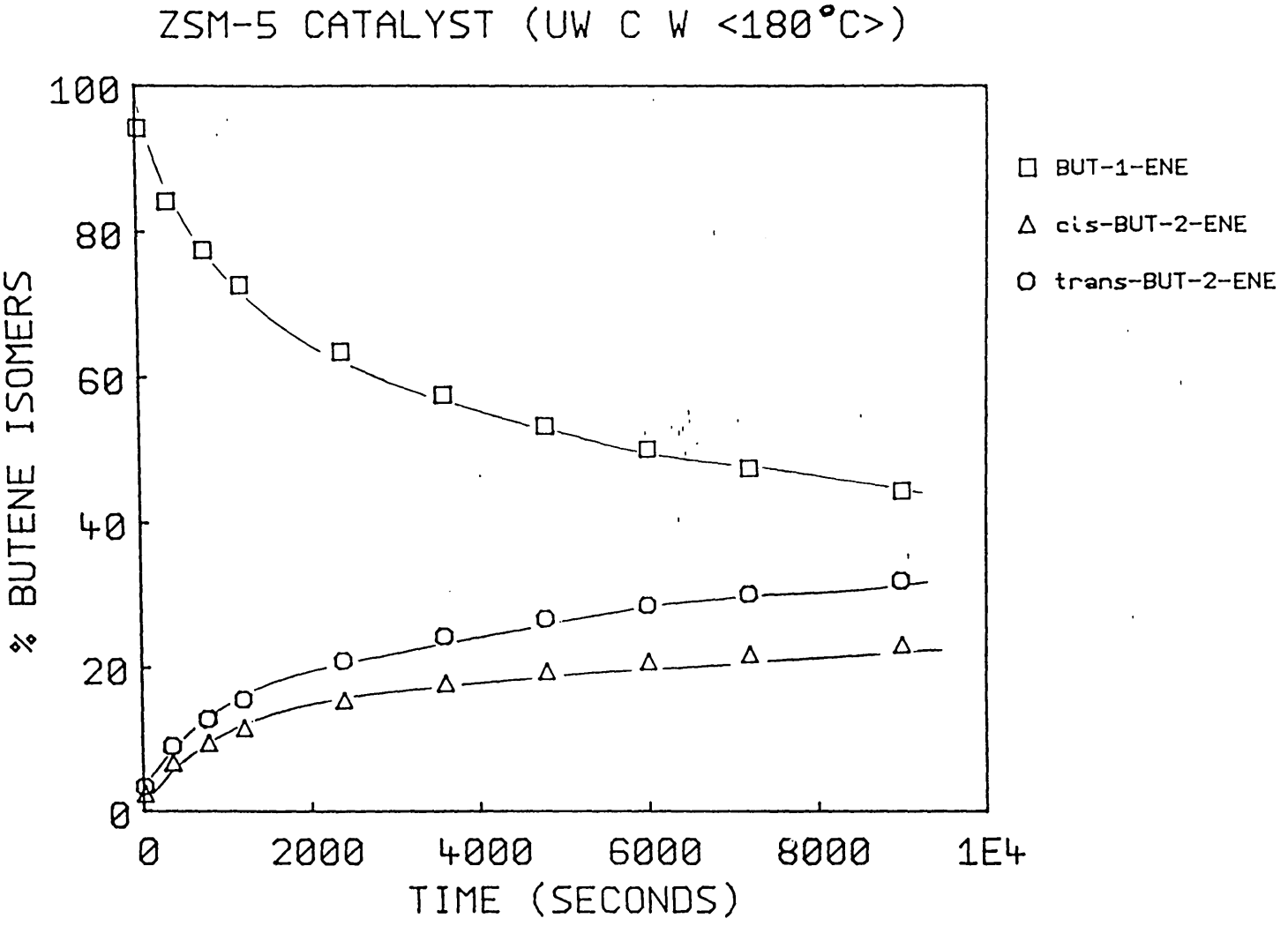

Figure 7.31 Isomerisation results obtained with H-ZSM-5 (C4), (UW C W<180°C>)

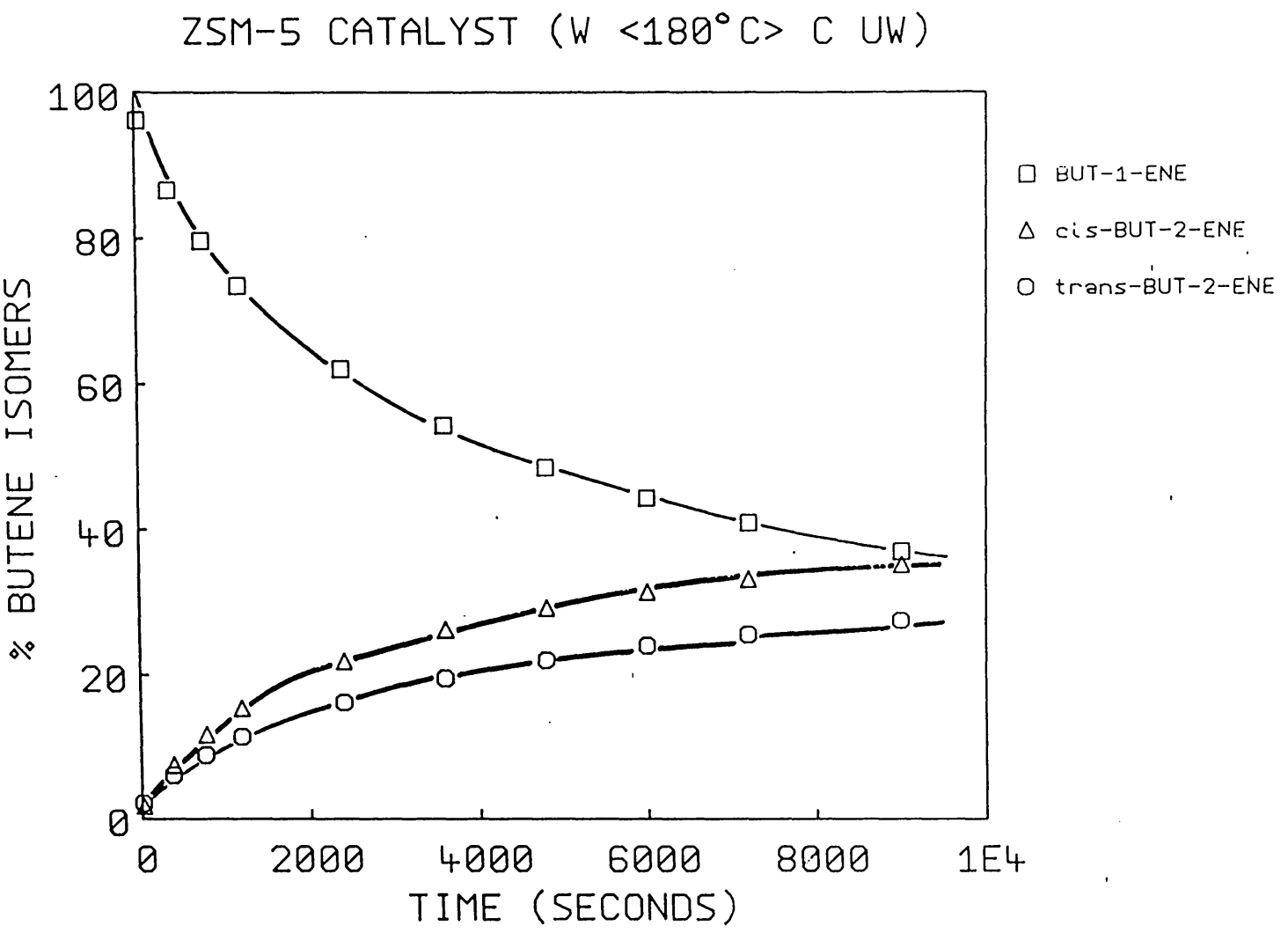

Figure 7.32 Isomerisation results obtained with H-ZSM-5 (C4), (W<180°C> C UW)

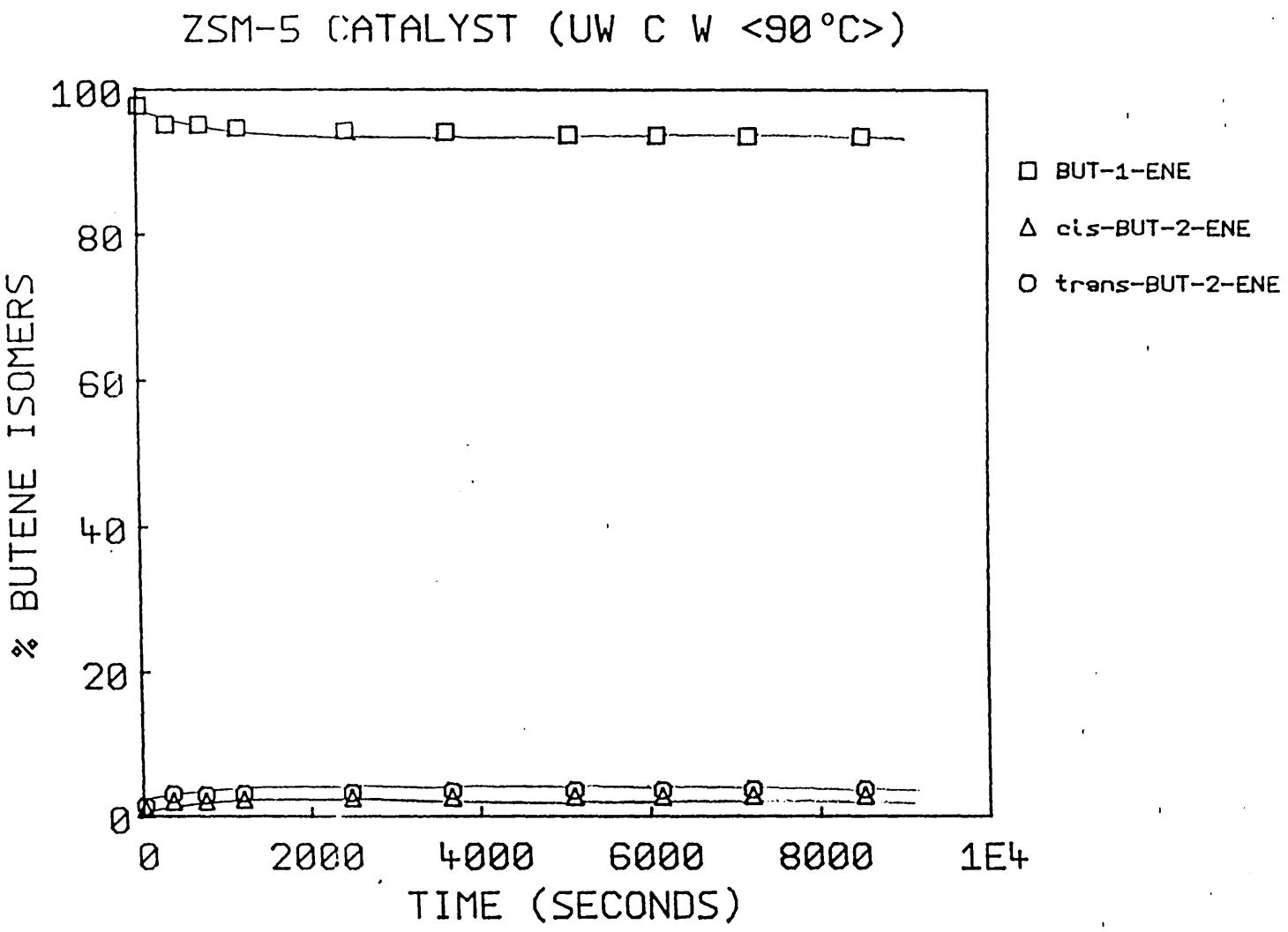

Figure 7.33 Isomerisation results obtained with H-ZSM-5 (C4), (UW C W<90°C>)

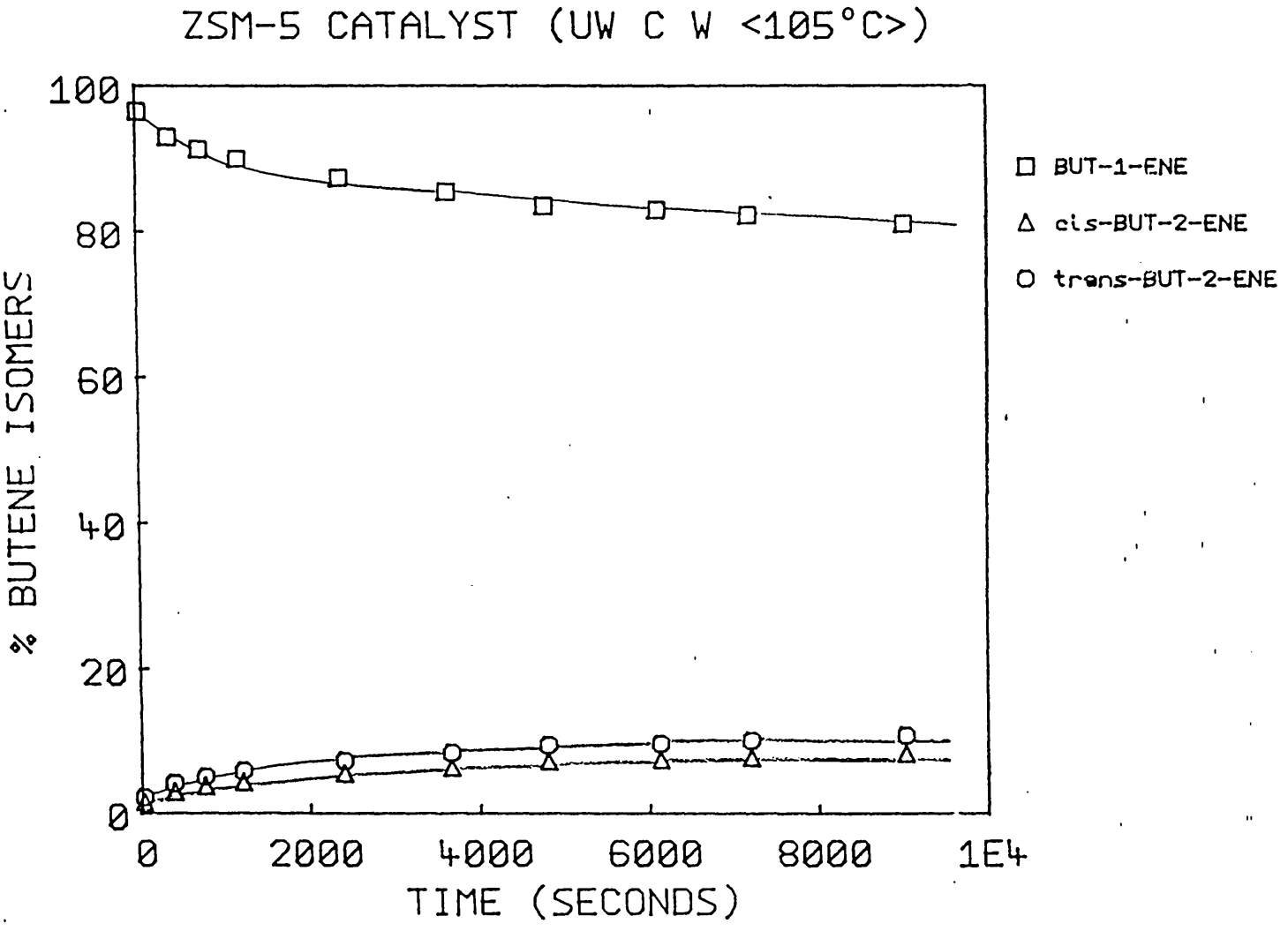

Figure 7.34 Isomerisation results obtained with H-ZSM-5 (C4), (UW C W<105°C>)

Table 7.7 Details of catalyst, weight used

and initial but-1-ene pressure.

H-ZSM-5 (C4) Treatment	Weight ZSM-5 (g)	But-1-ene P (Torr)
C,UW	0.0390	291.9
C,W<120°C, 3h>	0.0425	294.0
C,W<150°C, 3h>	0.0448	282.7
C,W<180°C, 3h>	0.0440	300.8
W<180°C, 15h>,C	0.0389	296.2
C,W<90°C, 25h>	0.0411	293.4
C,W<105°C, 17h>	0.0426	303.5

Table 7.8 Results obtained after 3 hours at 125°C.

H-ZSM-5 (C4) Catalyst	% But-1-ene	% Cis-but-2-ene	% Trans-but-2-ene
C,UW	31.04	34.95	34.01
C,W<120°C>	39.05	29.91	31.03
C,W<150°C>	24.08	33.42	42.50
C,W<180°C>	44.64	23.19	32.17
W<180°C>,C	37.24	35.18	27.58
C,W<90°C>	93.52	2.78	3.70
C,W<105°C>	80.95	8.23	10.82
Equilibrium Values	7.95	28.61	63.45

It is apparent from these results that the most active catalyst was that obtained by hydrothermal treatment at 150°C. The low temperature treatments (95, 105 and 120°C) appear to make the catalyst less active. Likewise, catalyst treatment at 180°C appears to reduce its activity.

Table 7.9 Initial (30 seconds) and Final (3 hours)

cis-/trans- ratios and initial conversion rates

Treated ZSM-5 Catalyst	cis-/trans- ratio after 30 seconds	Initial Rate ($s^{-1}g^{-1}$)	cis-/trans- ratio after 3 hours
C,UW	0.80	0.036	1.03
C,W<120°C>	0.74	0.033	0.96
C,W<150°C>	0.70	0.046	0.79
C,W<180°C>	0.69	0.047	0.72
W<180°C>,C	0.77	0.036	1.28
C,W<90°C>	0.62	0.018	0.75
C,W<105°C>	0.68	0.033	0.76

The thermodynamic equilibrium cis-/trans- ratio is 0.45. The but-1-ene to cis- and trans-but-2-ene conversion is a first order reaction.

The initial cis-/trans- ratio (after 30 seconds) was 0.80 for the 'as made' calcined catalyst. This was reduced to 0.74, 0.70 and 0.69 after 3 hour hydrothermal treatments at 120, 150 and 180°C respectively. The prolonged hydrothermal treatments at lower temperatures further reduced the cis-/trans- ratio to 0.62 (90°C for 25 hours) and 0.68 (105°C for 17 hours). The initial conversion rates, for which there should be little effect on the catalyst by coking, were calculated from the conversion data (after 30 seconds) for each reaction. The initial reaction rates showed that the isomerism was enhanced, in the early stages, by hydrothermal treatment of calcined ZSM-5 samples at 150 and 180°C. There was no change in the initial reaction rate between the 'as made' calcined (untreated) H-ZSM-5 and the material treated at 180°C prior to calcination. The hydrothermal treatments at 90, 105 and 120°C each reduced the initial reaction rates. However the initial rates of the catalytic reactions over the H-ZSM-5 samples hydrothermally treated at 150 and 180°C are consistant with the removal of amorphous material from the crystal surfaces. This will improve the diffusion of reactant and product butene molecules within the catalyst and should therefore enhance catalytic activity. It should also delay the onset of coking within the catalyst, since the butene molecules

will enter and leave without their diffusion being inhibited by the amorphous aluminosilicate material on the crystal surfaces. This is the probable explanation for the high activity shown by the H-ZSM-5 which had been hydrothermally treated at 150°C. This high activity may also be due to the formation of Bronsted acid sites by the hydrothermal treatment. Evidence for this was obtained from thermal gravimetric analysis (Figure 7.25) and it is important to note that this sample was the only one to show loss of water at 450°C.

The cis-/trans- ratio varied with reaction time, as shown in Figure 7.35. This may be an effect of coking but it is certainly affected by the hydrothermal treatment. The cis-/trans- ratios of the hydrothermally treated materials after 3 hours ranged from 0.72 to 0.96 and were in all cases lower than that (1.03) of the untreated material. The only higher value was that (1.28) obtained for the sample which was hydrothermally treated before calcination. Amongst the samples which were treated after calcination no clear systematic trend could be observed. The highest value (0.96) was obtained for the material treated at 120°C and the lowest value (0.72) for that treated at 180°C. However it is significant that the H-ZSM-5 samples which were washed at 120, 150 and 180°C were hydrothermally treated for 3 hours. The catalysts treated at 90 and 105°C were treated for 17 and 25 hours respectively, by which time they may have been in equilibrium with the solution phase. The activities of these catalysts were significantly reduced by their hydrothermal treatments (see Figures 7.33 and 7.34).

Plots of $\ln(x-x_e)$, where x is the but-1-ene concentration and x_e is the thermodynamic equilibrium value, against time are shown in Figure 7.36. For a first order reaction these should be linear, but in the present case each plot was curved. It is possible that this is a consequence of two competing first order reactions taking place at different sites within the framework. The overall catalytic observations tend to support this hypothesis. The catalytically active sites at the channel intersections are probably cis-but-2-ene selective, and those at non-intersection sites trans-but-2-ene selective. However further work and proper mathematical analysis of the kinetics would be required to confirm this hypothesis.

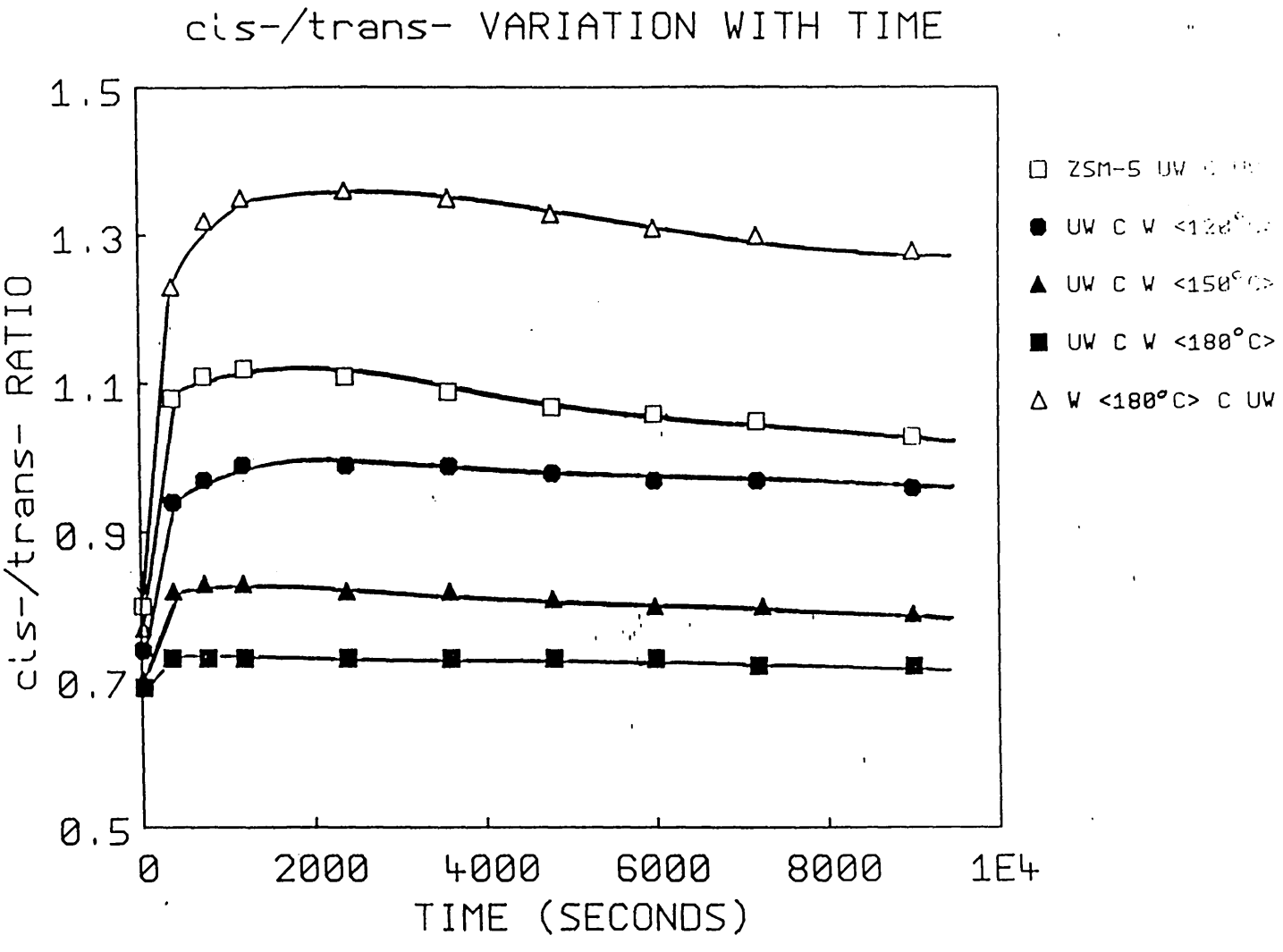

Figure 7.35 cis-/trans- ratios obtained for H-ZSM-5 (C4) treated in different ways

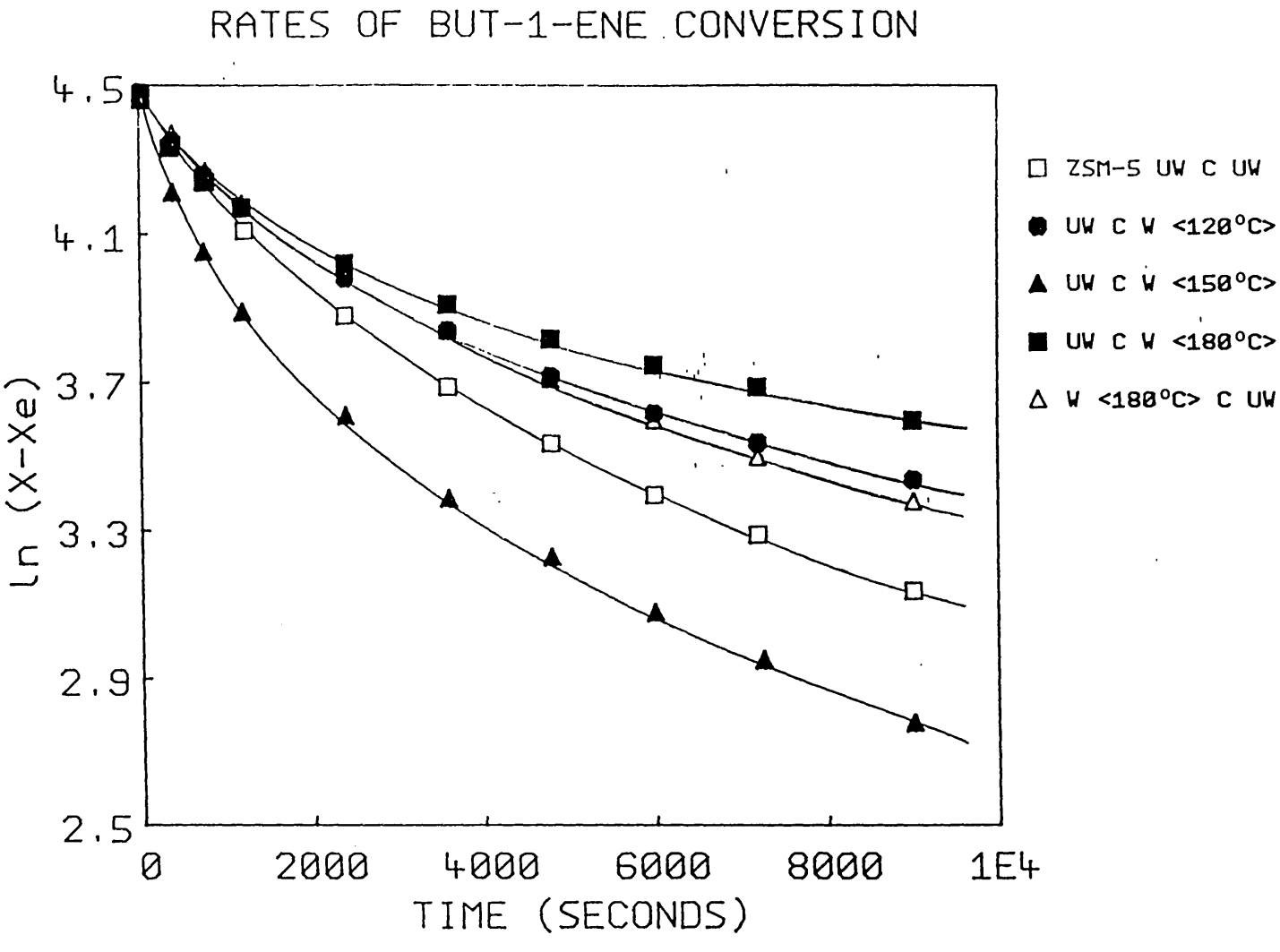

Figure 7.36 First order plots for H-ZSM-5 (C4) treated in different ways

Conversely, Sendoda and Ono (17) showed that dislodged aluminium species, caused by steaming, promoted the catalytic activity of ZSM-5 for propane conversion. The observation of the cis-/trans-selectivity changes and the peak in catalytic activity for the ZSM-5 treated at 150°C may also be due to the relocation of aluminium species caused by the hydrothermal treatment. However this does not appear likely as it is believed that the chief effect of the hydrothermal treatment was to remove amorphous impurities from the calcined zeolite.

7.4 Conclusions

Hydrothermal treatment of samples of TPA-ZSM-5 crystallised at 95°C showed that they were contaminated with amorphous aluminosilicate residues. When these were removed by treatment with hot water, a cleaner combustion of the TPA template was observed. This was evidenced by an increase in the DTA peak area. A TPA-ZSM-5 crystallised at 150°C did not show this effect; this is consistent with the observation that ZSM-5 synthesised at 150°C tends to contain less amorphous aluminosilicate material.

The amorphous material could be removed from uncalcined and calcined materials. The hydrothermal treatment at 150°C with time led to dealumination of H-ZSM-5. When the treatment time was restricted to 3 hours, the hydrothermally treated materials became more aluminous as the wash temperature was increased.

The hydrothermal treatment was found to modify the catalytic behaviour of H-ZSM-5 for butene isomerisation, particularly its product selectivity, and this may have applications for other isomerisation processes.

Chapter 7 References

[1] G.T. Kerr

Catal. Rev.-Sci. Eng.,

1981, **23(1&2)**, 281.

[2] J.R. Anderson, K. Foger, T. Mole,

R.A. Rajadhyaksha and J.V. Sanders

J. Catal., 1979, **58**, 114.

[3] H.-J. Doelle, J. Heering and L. Riekert

J. Catal., 1981, **71**, 27.

[4] A.L. Klyachko, G.I. Kapustin,

T.R. Brueva and A.M. Rubinstein

Zeolites, 1987, **7**, 119.

[5] F. V. Shamovski

React. Kinet. Catal. Lett., 1982,

21 (3), 327.

[6] V.S. Nayak and V.R. Choudhary

J. Catal., 1983, **81**, 26.

[7] E.G. Derouane

"Intercalation Chemistry", 1982,

(Academic Press), page 101.

[8] S.M. Csicsery

Zeolites, 1984, **4**, 202.

[9] P.A. Jacobs, J.A. Martens, J. Weitkamp

and H.K. Beyer

J. Chem. Soc. Faraday Trans. 1, 1982, 354.

[10] C. Clement

Pet. Tech., 1986, **328**, 32.

[11] K. Fujisawa, T. Sano, K. Suzuki, H. Okado,

K. Kawamura, Y. Kohtoku, S. Shin,

H. Hagiwara and H. Takaya.

Bull. Chem. Soc. Jpn., 1987, **60**, 791.

[12] Ya. S. Yakhyaev, S.N. Khadzhiev,

T.M. Gairbekov and S.E. Spiridonov

React. Kinet. Catal. Lett., 1986,

30 (2), 263.

[13] R. von Ballmoos and W.M. Meier

Nature, 1981, **289**, 782.

[14] E.G. Derouane, J.P. Gilson, Z. Gabelica,

C. Mousty-Desbuquoit and J. Verbist

J. Catal., 1981, **71**, 447.

[15] D.M. Bibby, L.P. Aldridge and N.B. Milestone

J. Catal., 1981, **72**, 373.

[16] E.G. Derouane and Z. Gabelica

J. Catal., 1980, **65**, 486.

[17] Y. Sendoda and Y. Ono

Zeolites, 1988, **8**, 101.

[18] Y. Ono and J. Turkevich

Adv. Catal., 1969, **20**, 135.

[19] Y. Ono and J. Turkevich

Adv. Chem. Ser., 1971, **102**, 315.

[20] P.D. Hopkins

J. Catal, 1968, **12**, 325.

[21] D. Barthomeuf and C. Mirodatos

J. Chem. Soc., Chem. Commun., 1981, 39.

[22] A.G. Ashton

"Catalysis by Acids and Bases",

Elsevier, Amsterdam, 1985, page 135.

[23] Z.V. Gryaznova, M.M. Ermilova

and K.A. Baskunjan

"Proceedings of the Symposium on the

Mechanisms of Hydrocarbon Reactions",

1973, 389.

[24] S. Tsuchiya, S. Ito, S. Namba

and T. Yashima

Zeolites, 1983, **3**, 193.

[25] J.B. Nagy, Z. Gabelica and E.G. Derouane

Zeolites, 1983, **3**, 43.

[26] K.R. Franklin and B.M. Lowe

Thermochimica Acta, 1988, **127**, 319.

[27] J. Goldwasser, J. Englehardt and W.K. Hall

J. Catal., 1981, **71**, 1014.

[28] I.R. Shannon, C. Kemball and H.F. Leach

"Chemisorption and Catalysis", Institute

of Petroleum, London, 1971, page 46.

[29] I.D. Harrison, H.F. Leach and D.A. Whan

Zeolites, 1987, **7**, 21.

[30] I.D. Harrison, H.F. Leach and D.A. Whan

Zeolites, 1987,**7**, 28.

[31] E.L. Wu, S.L. Lawton, D.H. Olson,

A.C. Rohrman Jr. and G.T. Kokotailo

J. Phys. Chem., 1979, **83**, 2777.

CHAPTER 8

CONCLUSIONS AND

FUTURE WORK

8.1 Conclusions

The silicalite synthesis results showed that the suppression of the reaction mixture pH led to longer crystallisation times and product crystals of plate-like morphology. Flat or needle-like crystals resulted in preferred orientation effects in the X-ray powder diffraction patterns. Surprisingly the suppression of the reaction mixture pH did not result in the synthesis of larger crystals, which could have been due to secondary nucleation, as evidenced by the wide crystal size distribution. This may have been caused by temperature and concentration oscillations consequent on 'topping up' of the reaction vessels. The use of a sealed system, e.g. an autoclave, should prevent secondary nucleation since there would be no evaporation from the reaction mixture, and hence no need to add water during the crystallisation. In principle, the low pH syntheses should yield larger crystals.

The silicalite samples were synthesised from alkali metal free reaction mixtures, piperazine was used as an organic base and tetrapropylammonium as the MFI structure directing template. Attempts were made to crystallise ZSM-5 from similar reaction mixtures by the incorporation of a source of aluminium. Aluminium sulphate (at 95°C and 150°C synthesis temperatures) or aluminium nitrate (95°C only) were used and the quality of the ZSM-5 products was gauged by differential thermal analysis. The higher the peak temperature of the DTA major exotherm, for the TPA decomposition/combustion, the greater the incorporation of aluminium into the ZSM-5 channel system. However the exact relationship is unknown. Scanning electron microscopy showed that the greater the incorporation of aluminium into the ZSM-5 product the smaller the crystals; this suggests that the presence of aluminium in the intermediate gel promotes nucleation. The ZSM-5 products synthesised at 150°C with aluminium sulphate had most aluminium incorporated into their frameworks. At 95°C the reaction mixtures which contained aluminium nitrate were shown to yield a higher quality product than those crystallised in the presence of aluminium sulphate. Aluminium nitrate appears to be a more active source of aluminium for ZSM-5

crystallisation. The use of aluminium salts in conjunction with an organic base gave products which were alkali metal free. This removes the acid-exchange step, which is normally required before the zeolite can be used as a catalyst. The ZSM-5 products which are crystallised by this method only require calcination prior to use as catalysts. However the amount of aluminium in the ZSM-5 frameworks may only be about one tenth of the possible 4 per 96 T-atom unit cell. In contrast the external crystal surfaces are relatively rich in aluminium.

Solubility studies indicated that calcined silicalite contained small amounts of amorphous silica impurities. This was demonstrated by the fact that the observed amount of silica in solution at equilibrium varied with the liquid/solid ratio of the solubility system. Low L/S ratios yielded observed solubility values akin to those for the true solubility of amorphous silica, whereas high L/S ratios gave observed solubility values in line with those expected for a crystalline silica. These observations could form the basis of a simple method for the detection of amorphous silica impurities in calcined H-silicalite. This assumes that the crystalline silicalite and amorphous silica contaminant are two homogeneous phases, which they are not. The amorphous silica could be in someway attached to or incorporated in the crystals. The surface of a growing crystal, for example, may be partially amorphous. However the amorphous silica impurity levels were estimated at about 1%. These results indicated either that there was incomplete crystallisation of product from the reaction mixture or that amorphous material was generated during calcination. ZSM-5, with a Si/Al ratio of 60, was shown to have a lower solubility than the silicalite, even though the materials have the same framework structure. The presence of small amounts of aluminium appears to suppress the dissolution of silica from the framework. The solubilities of silica-ZSM-11, silica-ZSM-39, silica-ZSM-48 and EU-4 were also studied. The results for silica-ZSM-11 suggest that as the number of 4-T atom rings in high silica zeolites increases they become more soluble. Thus it appears that solubility is related to structural strain. Uncalcined materials had a lower solubility than calcined ones; this reflects

the stabilising effect of the organic template.

Hydrothermal treatment of uncalcined silicalite samples produced little change in their characteristics. The only significant changes were those observed in their DTA traces. Washed materials generally gave TPA decomposition/combustion peaks of greater area than those of their untreated counterparts. This is consistent with the removal of residual amorphous impurities from the 'as made' products. Hydrothermal treatment of calcined silicalite changed its properties in several ways. The transition from orthorhombic to monoclinic symmetry was promoted. A decrease in the XRD background was also observed; this is ascribed to the removal of post-calcination amorphous silica impurities and the healing of internal clusters of silanol defects. The water uptake of calcined materials was decreased by hydrothermal treatments up to 180°C, which indicates that amorphous impurity removal and silanol healing events probably took place. Twinned crystals were shown to dissolve internally once their external surface had been penetrated at the cross-lozenge. Single crystals which cannot be dissolved by this mechanism were found to be more resistant to dissolution than twinned ones. This appears to provide a method for the separation of single crystals from a mixture of single and twinned ones. It is of course possible that internal dissolution of single crystals may occur, but no evidence for this was obtained.

Hydrothermal treatment of uncalcined (TPA, piperazine)-ZSM-5 led to increases in the peak area of the major exotherm. This indicates that the removal of amorphous aluminosilicate impurities from the 'as made' products had occurred and this allowed either oxygen to diffuse more easily into the ZSM-5 channel system or the TPA decomposition products to diffuse faster to crystal surfaces for combustion. Both should make the removal of TPA more exothermic and hence give a larger DTA peak area. A TPA-ZSM-5 sample which was crystallised at 150°C showed a slight decrease in the area of its DTA exotherm after it was hydrothermally treated. This indicates that TPA-ZSM-5 crystallised at this higher temperature is less prone to amorphous aluminosilicate contamination then materials synthesised at 95°C. Decreases in exothermic peak positions (by about 11°C) were

generally observed; this may also indicate the removal of framework aluminium associated with the TPA template at the channel intersections. The hydrothermal treatment of calcined H-ZSM-5 (C4) led to little observable crystal dissolution (SEM), less well resolved monoclinic XRD traces than for silicalite and significant removal of amorphous impurities from the crystal surfaces. Samples of hydrothermally treated H-ZSM-5 were shown to become dealuminated when they were washed at 150°C for various lengths of time, but when they were treated for 3 hours at various temperatures they became relatively more aluminous. Silica appeared to dissolve preferentially from the H-ZSM-5 framework in the early stages of hydrothermal treatment.

A series of hydrothermally treated ZSM-5 samples were tested as catalysts for the catalytic isomerism of but-1-ene to cis- and trans-but-2-ene. The as-made calcined ZSM-5 gave a cis-/trans- ratio of 1 after a catalytic run time of 3 hours. When the material was washed at 180°C after calcination the cis-/trans- ratio after 3 hours fell to 0.7. Treatment at 180°C prior to calcination led to a cis-/trans- ratio of 1.3 after 3 hours. The initial cis-/trans- ratios, after 30 seconds, showed a similar trend to those after 3 hours; but only between a range of 0.69 and 0.80. Thus it is quite clear that hydrothermal treatment can have a pronounced effect on catalyst selectivity. The most likely explanation is that the hydrothermal treatment effects the formation of coke in the zeolite channel system and hence influences the diffusion of reactant and product butenes in the catalyst. The H-ZSM-5 (C4) which was treated at 150°C for 3 hours was the most catalytically active sample. This was probably due to the complete removal of amorphous material from its framework which would enhance the diffusion of butene molecules within the catalyst. This may also have a beneficial effect on catalyst coking, since butene molecules will be able to enter and leave the ZSM-5 framework more easily. Bulk analysis data showed that the ZSM-5 samples obtained after the three hour hydrothermal treatments became more aluminous with increasing treatment temperature. This indicates the preferential dissolution of silica, relative to alumina, from the ZSM-5 framework. Although clear trends

were observed for selectivity, there were irregular differences in catalytic activity. Catalysts which were treated over a prolonged period at low temperatures were poisoned, and it is probable that their tetrahedral framework aluminium atoms relocated as octahedral species in the zeolite channels. The changes in catalytic selectivity may also be due to the presence of two types of active site within the zeolite. The sites (type A) at channel intersections will be cis-but-2-ene selective since there is more room for its transition state at this position in the framework. There will be less room for the cis-but-2-ene transition state at non-intersection aluminium sites (type B). These sites are likely to be relatively trans- selective. The presence of the TPA template will stabilise type A sites to hydrothermal treatment but lead to removal of type B sites. Calcination will most likely damage the framework at channel intersections, so that aluminium at type A sites will be dissolved earlier than at type B positions. This would account for the changes in product selectivity but it is at present somewhat speculative and further experimental work would be required to confirm it.

8.2 Future Work

The hydrothermal treatment promoted the transition from orthorhombic to monoclinic symmetry. An extra peak emerged with the change in symmetry and the improvement in the crystallinity of the silicalite. This was indexed 4 3 1/3 4 1 (hkl). Such a peak should not be observed for orthorhombic silicalite but was observed for the monoclinic material. The appearance of this peak and the resolution of the 313/133 reflections centred at 24.5 2θ were both dependent on the highly crystalline nature of the material produced by the hydrothermal treatment. The H-silicalite hydrothermally treated at 150°C appeared to be an excellent standard which might well repay examination by ^{29}Si MASNMR. It seems possible that it might yield hitherto unresolved peaks.

The solubility results indicated the presence of amorphous impurities in calcined silicalite. The hydrothermal stability studies produced further evidence that amorphous material was located internally and that there were silanol groups located within the silicalite channel system. This amorphous hydrophilic material will have two effects on the uptake of organic species from the aqueous environment. Internal amorphous material will inhibit the diffusion of organic molecules into the silicalite framework and reduce the available pore volume. The presence of internal silanol groups will increase the water uptake of the samples, so increasing their hydrophilicity and decreasing their organophilicity. The H-silicalite samples which were treated with water at temperatures of 150 and 180°C showed a decrease in water uptake greater than 50%, when compared with their 'as made' calcined parent material. Hydrothermally treated materials should then be more organophilic. Studies of uptake of organic species over hydrothermally treated silicalite samples should confirm this. The healing of the framework by the hydrothermal treatment could be confirmed by IR spectroscopy since healing should reduce the intensity of the silanol stretching peak.

Some of the amorphous silica and internal silanol groups were

probably generated by the calcination. A slower heating rate may cause less framework damage during this process, reducing the formation of amorphous silica and silanol groups.

Solubility studies showed that amorphous silica dissolved to give higher equilibrium aqueous silica concentrations than did crystalline H-silicalite. When silicalite is used to sorb organic species from aqueous solution it is inevitable that it will slowly dissolve. In a continuous process the solid silicalite will never reach equilibrium with the aqueous silica in solution, thus even though it has a low solubility it will gradually dissolve away. This could be prevented by saturating the aqueous phase with monomeric silicic acid, possibly generated by cheap amorphous silica. This would not only prolong the working life of the silicalite but should also inhibit framework attack and the formation of silanol groups. It would also be an inexpensive solution to the dissolution problem.

Further catalytic studies over hydrothermally treated H-ZSM-5 samples should also be undertaken. In the studies outlined in Chapter 7, a catalyst was hydrothermally treated whilst the TPA template was still present within the channels. The material was then calcined and used for the isomerism of but-1-ene. The catalytic reaction was cis-but-2-ene selective. Since cis- is larger than trans-but-2-ene and the typical cis-/trans- ratio for ZSM-5 is about 1 it is possible that there are two active catalytic sites within the framework; one at the channel intersections and one elsewhere in the framework. The results suggest that if this is so the aluminium at the intersection is stabilised by the TPA whereas non-TPA associated aluminium is selectively removed. Conversely the hydrothermal treatment may cause a different rate of coke formation on the catalysts, which itself would affect product selectivity. The sorption properties of the chosen H-ZSM-5 samples (C4) in this study were also affected by the hydrothermal treatment. These effects should be studied for commercially important applications such as toluene disproportionation or xylene isomerism. If the hydrothermal treatment of TPA-ZSM-5 did selectively dealuminate the framework and leave aluminium at channel intersections, where there is more space for transition states, then the treated zeolite would be expected to

give the larger catalytic products such as ortho-xylene.

There is a great deal of scope for the further study of hydrothermally treated materials, either as molecular sieves or as catalysts.

Courses, Lecture Series and Conferences

Courses

Fortran 77 Computing Course

ERCC Scribe Course

Lecture Series

Molecular Electronics

Least Squares Methods

Medicinal Chemistry

Industrial Chemistry

Solving and Refining Crystal Structures

Signal Processing

Seminars/Conferences

Research group and departmental seminars were attended.

Attended British Zeolite Association Conferences in 1985, 1986 and 1988.